Study of Heavy Mesons using Effective Theories and Potential Model

A thesis presented for the degree of

Doctor of Philosophy

By

Ritu Garg

(Reg. No.: 901912003)

Under the guidance of

Dr. Alka Upadhyay

THAPAR INSTITUTE
OF ENGINEERING & TECHNOLOGY
(Deemed to be University)

Department of Physics and Material Science

Thapar Institute of Engineering & Technology

Patiala (India)

2024

CERTIFICATE

This is to certify that the thesis titled "**Study of Heavy Mesons using Effective Theories and Potential Model**", submitted by **Ms. Ritu Garg**, for the fulfillment of the requirements for the award of the Degree of Doctor of Philosophy in the Department of Physics and Material Science, Thapar Institute of Engineering and Technology, Patiala, is a record of the candidate's own work carried out by her under my supervision. The matter presented in this thesis has not been submitted in part or full for the award of any degree in any other university or institute.

Supervisor
Dr. Alka Upadhyay
Professor
Department of Physics and Material Science
Thapar Institute of Engineering and Technology (TIET)
Patiala - 147004
Punjab (India)

Dedicated to My Family, My Strongest Support.

Acknowledgements

Thank you God *for all your blessings to me. For the strength you give me each day and for all the people around me who make life more meaningful. At this moment, I am writing these words in the completion of this thesis. So, I hereby express my gratitude for some very important people through these small letters.*

At this moment of submission of my thesis, I would like to express my sincere gratitude and obligation to my esteemed supervisor, Dr. Alka Upadhyay, Professor, Department of Physics and Material Science, Thapar Institute of Engineering and Technology, Patiala. I am very grateful for her continuous support, motivation, and confidence in me. Her guidance helped me in all the time of research and writing of this thesis. Thank you for believing in me and encouraging my research.

Besides my advisor, I would like to thank the rest of my thesis committee members, Dr. Manoj Kumar Sharma, Dr. Sunil Devi, and Dr. Mukesh Singh, for their insightful comments and encouragement, and for the hard question, which encouraged me to widen my research from various perspectives.

I wish to express sincere and humble gratitude to Prof. Kulvir Singh, Head, Department of Physics and Material Science, TIET, Patiala, for providing me with the necessary facilities in the department. My sincere thanks also go to all the staff of the School for their help and kind support. My sincere thanks also go to Prof. N. Tejo Prakash, present Dean of Research and Sponsored Projects and Prof. Bhupendrakumar Chudasama, present Associate Dean, Research and Sponsored Projects TIET, Patiala, for providing the grants to attend the conferences and necessary resources to accomplish my research work.

I am happy to acknowledge the help and cooperation given to me by Kundan Kumar Vishwakarma and my fellow labmates Ankush Sharma, Preeti, and Rashmi Garg for the stimulating discussions and suggestions at various points of my research program.

Lastly, most importantly, I feel an immense admiration and humble obligation for my family, my husband, my constant source of happiness. Words that I know are rather insufficient to convey my sincerest regard to my parents, whose moral encouragement, countless blessings, everlasting desire, and untiring struggle brought

me here. God is generous enough to bless me with unforgettable persons for their endless love, best wishes, and moral support to achieve this goal successfully.

Publications

Publications from this thesis work

1. **Ritu Garg**, Alka Upadhyay, Masses and decay widths for radially excited $n = 3$ S-wave bottom mesons, Eur. Phys. J. Plus, **137**, no.7, 828 (2022), doi:10.1140/epjp/s13360-022-03043-5 (Impact: 3.758).

2. **Ritu Garg**, Alka Upadhyay, Study of F-wave bottom mesons in heavy quark effective theory, Prog. Theor. Exp. Phys, **2022**, no.9, 093B08 (2022), doi:10.1093/ptep/ptac113 (Impact: 8.3)(**Editor's choice paper**).

3. **Ritu Garg**, Kundan Kumar, Alka Upadhyay, Radially excited (n = 3) charm mesons in heavy quark effective theory, Prog. Theor. Exp. Phys, **2022**, no.4, 043B06 (2022), doi:10.1093/ptep/ptac048 (Impact: 8.3).

4. **Ritu Garg**, Pallavi Gupta, Alka Upadhyay, Placing of the recently observed bottom strange states $B_{sJ}(6063)$ and $B_{sJ}(6114)$ in bottom spectra, Prog. Theor. Exp. Phys, **2023**, no.7, 073B03 (2023), doi:10.1093/ptep/ptad080 (Impact: 8.3).

5. **Ritu Garg**, K.K Vishwakarma, Alka Upadhyay, Bottomonia in quark-antiquark confining potential,(communicated).

International / National conferences and Workshop

1. **Ritu Garg**, Kundan Kumar and Alka Upadhyay, Mass spectrum and decay widths for excited ($n = 2$) D- wave bottom meson family, volume 65, Page no. 535-536, DAE symposium on Nuclear Physics, 2021.

2. **Ritu Garg** and Alka Upadhyay, Masses of radially excited P-wave strange bottom meson ($n = 3$) and Regge trajectories in HQET, in DAE symposium on High Energy Physics, 2022.

3. Kundan Kumar, **Ritu Garg** and Alka Upadhyay, S-wave charm and bottom baryons in HQET, in DAE symposium on High Energy Physics, 2022.

4. **Ritu Garg**, Kundan Kumar, Preeti and Alka Upadhyay, Masses of radially excited P-wave bottom meson ($n = 3$) in HQET, Workshop on Hadron Physics, 2023.

Abstract

The work presented in the thesis is carried out to investigate recently observed heavy mesons using heavy quark effective theory and phenomenological potential model. Since the momentous discovery of heavy quarks, namely the charm (c) and bottom (b) quarks, there has been a notable and focused interest in investigating the properties of heavy hadrons. Different experimental facilities like LHCb, BABAR, BESIII, FOCUS, SLAC, Belle, CDF, etc., have been on a discovery spree for stimulating the spectrum of heavy mesons. Consequently, it becomes essential to employ appropriate theoretical methodologies in order to attain a profound comprehension of these mesons. Several theoretical models, such as the Heavy Quark Effective Theory (HQET), potential models, lattice Quantum Chromodynamics (QCD), and QCD sum rules, are present in the literature for the in-depth exploration of these heavy mesons. In the past few years, HQET has emerged out as a successful model for studying the properties of heavy-light mesons. In this thesis, we intend to study the basic properties like masses, strong decays, branching ratios, and splittings for the newly observed heavy-light mesons in both the charm and bottom sectors. By this study, we will be able to fill the charm and bottom spectra up to F-wave and P-wave mesons for radial quantum numbers $n = 2$ and $n = 3$, respectively. Also, to understand quark-antiquark interactions and their dynamics, we have explored bottomonia in the framework of the phenomenological potential model. This thesis is organized into six chapters, a transient outline of which is given below:

- **Chapter 1** gives a brief discussion of theoretical and experimental aspects related to the study of bound states of quarks, which interact through the exchange of gluons. Here, we have categorized bound state hadrons into two primary groups: Baryons, which are composed of qqq structure, and mesons, having $q\bar{q}$ configuration. The primary focus of this thesis is on the investigation of mesons, particularly heavy mesons, which come in low-energy regimes. For high-energy interactions, the strong coupling constant is small; thus, perturbative techniques are a viable option, while, the inclusion of heavy quarks invokes low-energy interactions, thus treated non-perturbatively. We conduct a brief review of various non-perturbative approaches commonly found in the

literature, such as potential models, lattice QCD, effective theories, and QCD sum rules. The major focus is given to effective field theories. Unlike other phenomenological models, these theories construct Lagrangian based on QCD symmetries, and interaction terms are organized systematically by some expansion parameters. We particularly highlight the fundamental concepts behind effective theories, with a specific focus on heavy quark effective theory and potential model. The heavy quark effective theory explored two essential symmetries in QCD: one in the limit of infinite heavy quark mass ($m_Q \to \infty$, where $Q = c, b$) and the other in the chiral limit of light quark masses ($m_q \to 0$, where $q = u, d, s$). The potential models are based on the concept that potential can describe the interaction of quarks and antiquarks. Although interquark interaction is a non-abelian and non-linear theory, it is complicated and still poorly understood. But, with the help of the potential model, we can grasp interquark interaction to some extent. Some of the potential models are mentioned and discussed in this chapter.

- In **Chapter 2**, we give details of the HQET framework used in the thesis to study the heavy-light charm and bottom mesons. We start by exploring the concept of heavy quark $SU(2N_H)$ spin and flavor symmetry, which serve as the origin of heavy quark effective theory. We present a general notation $nL_{s_l}J^P$ for any heavy-light state for its quantum numbers. In particular, J^P notations for the S-wave ground state and low-lying excited P-wave states are mentioned. We also define how the static nature of the heavy quark, classifies the states into doublets, which are represented by some covariant effective fields like H_a, S_a, T_a^μ, etc. We proceed to write the effective general Lagrangian for heavy-light system in the inverse powers of $1/m_Q$, by embodying the heavy quark symmetry in the QCD Lagrangian. This results in the modification of the QCD Feynman rules in the limit $m_Q \to \infty$. The leading order term of this Lagrangian will preserve the heavy quark symmetries while the higher orders will break these symmetries. This chapter also provides a short introduction to the chiral perturbation theory, which describes the low-energy interactions between the higher excited heavy-light charm and bottom mesons and their ground state S-wave mesons by the emission of goldstone bosons

π, η, K. Effective chiral Lagrangians at the leading order describing the interactions among different doublets help in calculating the two-body strong decay widths. The strong decay widths formulae dependent on the initial and final meson masses, their strong coupling constants, pion decay constant, energy scale Λ, mass, and momentum of light pseudo-scalar mesons are listed in this chapter.

- In **Chapter 3**, by exploring heavy quark effective theory (HQET), we use theoretical available data for bottom mesons to analyze the masses and decays for $n = 3$ charm mesons. Then, mass results of $n = 3$ charm meson are used as input to calculate masses of $n = 3$ bottom mesons. For a better understanding of bottom mesons, we further extend mass calculations for F-wave states. From the predicted masses, we studied ground state strong decay modes in terms of couplings. Comparing the decays with available total decay widths, we provide upper bounds on the associated couplings. We also plot Regge trajectories for our predicted data in planes (J, M^2) and (n_r, M^2) and estimated higher masses ($n = 4$) by fixing Regge slopes and intercepts. These Regge trajectories and branching ratio are used to clarify $D_2^*(3000)$ state's J^P as 1^3F_2 state. In addition to this, values of coupling constants $\tilde{g}_{HH}$, $\tilde{\tilde{g}}_{HH}$, $\tilde{\tilde{g}}_{SH}$, $\tilde{\tilde{g}}_{TH}$ are estimated with heavy quark symmetry by using Pearson chi-square test with multivariate normal distribution.

- In **Chapter 4**, we have employed HQET to give the spin-parity quantum numbers for recently observed bottom strange states $B_{sJ}(6063)$ and $B_{sJ}(6114)$ by LHCb collaborations. By exploring flavour independent parameters $\Delta_F^{(c)} = \Delta_F^{(b)}$ and $\lambda_F^{(c)} = \lambda_F^{(b)}$ appearing in HQET Lagrangian, we calculated masses of experimentally missing bottom strange meson states $2S, 1P, 1D$. The parameter Δ_F appears in HQET Lagrangian and gives the spin averaged mass splitting between excited state doublets (F) and ground state doublets (H). Another parameter λ_F comes from first-order corrections in HQET Lagrangian and gives hyperfine splittings. We have also analyzed these bottom strange masses by taking $1/m_Q$ corrections which lead modifications of parameter terms as $\Delta_F^{(b)} = \Delta_F^{(c)} + \delta\Delta_F$ and $\lambda_F^{(b)} = \lambda_F^{(c)}\delta\lambda_F$. Further, we have analyzed their two-body decays, couplings, and branching ratios via the emission of light pseudoscalar mesons. Based on predicted masses and decay widths, we tentatively identified the states $B_{sJ}(6063)$ as 2^3S_1 and $B_{sJ}(6114)$ as 1^3D_1. Our predictions may provide crucial information for future experimental studies.

- In **Chapter 5**, we comprehensively explore bottomonia mass spectra and their decay properties by solving the non-relativistic Schrodinger wave equation numerically with approximate quark-antiquark potential form. We also incorporate spin-dependent terms - spin-spin, spin-orbit, and tensor terms to remove mass degeneracy and to obtain excited states $(nS, nP, nD, nF, n = 1, 2, 3, 4, 5)$ mass spectra. By using Van Royen - Weisskopf formula, we investigate leptonic decay constants, di-leptonic, di-gamma, tri-gamma, di-gluon decay widths and also incorporate first-order radiative corrections. We also computed radiative transition widths, which give a better insight into the non-perturbative aspects of QCD. The present results for mass spectroscopy and decay properties are in tune with available experimental values and other theoretical prediction

- **Chapter 6**, summarizes the work carried out in this thesis. A brief account of the results obtained and the conclusion so drawn is discussed, and a possible extension of this work from a future perspective is outlined.

Contents

List of Figures

List of Tables

Chapter 1

Introduction

The field of particle physics involves exploring the nature of fundamental particles and the fundamental forces that govern their interactions. It seeks to understand the smallest constituents of matter and the nature of the universe at its most fundamental level. The field of particle physics emerged in the early 20^{th} century with the discovery of subatomic particles such as electrons, protons, and neutrons. Over time, scientists realized that these particles were not elementary but were composed of even smaller building blocks known as quarks.

However, the actual journey of particle physics commenced with the discovery of electrons. In 1897, J.J Thomson invented a subatomic particle known as an "electron" in a cathode ray tube experiment[1]. At that time, the prevailing theory was that atoms were indivisible and the basic constituents of matter. The Discovery of electrons was the first to provide evidence for the existence of subatomic particles and challenged the prevailing notion of indivisible atoms. In 1911, Rutherford discovered the nucleus in an alpha particle scattering experiment [2]. Till the middle of the 20th century, protons, neutrons, and electrons were supposed to be fundamental building blocks of matter. But in 1956, analysis of the spectrum of beta particles in the beta decay process gave evidence of the presence of very light and neutral particles called neutrinos, which provoked the era of quarks and leptons [3]. The first appearance of the point-like substructure of hadron was found in deep inelastic scattering experiment at Stanford Linear Accelerator Center (SLAC) in 1968 and identified as quarks later on [4–6].

At present, quarks and leptons are marked as fundamental constituents of atoms.

From the literature, we can see how the study of fundamental particles transformed with time. So, particle physics studies basically: i) dynamics of fundamental constituents of matter and ii) searching new elementary building blocks of matter. To unravel the internal structure of matter, we have to break the matter into its constituents. For that process, we need to accelerate them at high energies. That is why particle physics is also called high-energy physics.

1.1 Standard Model

Standard Model was developed by physicists Steven Weinberg, Abdus Salam, and Sheldon Glashow in the 1970s that assembles fundamental constituents - quarks and leptons as well as their interactions in terms of fundamental forces- Strong, electromagnetic, and weak interactions [7–9]. To date, six different flavors of quarks have been experimentally observed and confirmed. These quarks are - up, down, charm, strange, top, and bottom. These are cataloged in three different generations (families) with respect to their experimental observations. Also, there are six types of leptons, and they are classified into three different families- Electron family, muon family, and tau family. An electron and an electron neutrino comprise the Electron family. Similarly, the muon family includes muon and muon neutrino, while the tau family consists of tau and tau neutrino. This theoretical framework comprises a total of 24 fermions, 12 vector bosons, and four scalar particles that interact to produce a plethora of composite subatomic entities. At present time, only three generations of quarks and leptons have been identified and confirmed experimentally. However, the curious nature of human beings toward searching for more generations provokes them to continuously try high-energy accelerators. All stable matter in the world is formed from particles of the first generation. However, particles belong to second and third generations, being heavy decay to lightest particles (first generation). The standard model is gauge quantum field theory, which describes local gauge symmetry.

$$SU(3)_c \times SU(2)_L \times U(1)_Y \tag{1.1}$$

where $SU(3)_c$ is gauge group represents strong interactions of quarks. The subscript "c" stands for "color," which is an abstract property introduced to describe the behavior of quarks under the strong force. The symmetry group $SU(2)_L$ describes weak interactions, while $U(1)_Y$ influences all particles that possess a hypercharge quantum number Y. $SU(3)_c$ gauge group exhibits an exact symmetry, while $SU(2)_L \times U(1)_Y$ is spontaneously broken down by the Higgs doublets, which give mass to $W^{\pm}$, Z^0. So, each group specifies a gauge interaction and meditates via gauge bosons for all three interactions. Gluons, photons, $W^{\pm}$, and Z bosons are gauge bosons that are intermediates for fundamental interactions. Gluons carry strong interactions, while photons are the mediator for electromagnetic interactions. The intermediates $W^{\pm}$ and Z bosons are associated with weak interactions. Higgs bosons were the theoretical discovery of "Peter Higgs" in 1964, which is a key element of the standard model. Later in 2012, this particle was confirmed by "ATLAS" and "CMS" experimental facilities at CERN's large hadron collider [10, 11]. Table 1.1 shows fundamental constituents assembled in the standard model.

Table 1.1: Fundamental particles in the Standard Model with their total angular momentum (J) and their parity (P).

Fundamental constituents	Particles	J	P
Leptons	$(e^-, \nu_e), (\mu^-, \nu_\mu), (\tau^-, \nu_\tau)$	1/2	-
Quarks	$(u, d),\ (c, s),\ (t, b)$	1/2	+
Gauge Bosons	$g,\ \gamma,\ W^{\pm},\ Z^0$	1	-
Higgs Boson	H	0	+

The standard model provides many accurate predictions of fundamental particles, which are later identified through experimental measurement. Even this model proposed the existence of particles that were not detected experimentally till then. Instead of many remarkable and precise predictions, the standard model is still lacking [12]. There are many fundamental phenomena like general relativity, gravity, dark energy, neutrino oscillations, and matter-antimatter asymmetry, the unification of forces that are not explained or fitted in this model. To answer the above issues, many new ideas are proposed that demand "new physics" at high energy scales. Ongoing research aims to extend the model, seeking new theoretical frameworks such as supersymmetry, string theory, and other beyond the standard model theories to address these open questions and advance our understanding of the fundamental nature of the universe. Grand unified theory (GUT) is the theory that describes the unification of three forces as a big task for experimentalists nowadays. Beyond GUT, there lie supersymmetry and theory of everything.

1.2 Quark Model

Quark Model was formulated by two theoreticians, George Zweig, and Murray Gell-Mann, in 1964 [13, 14]. This model explains the classification of hadrons in terms of quantum numbers i.e isospin, charge, hypercharge, strangeness, baryon number, spin, etc. The hypothesis of this model included eightfold SU(3) symmetry, which classified hadrons into octets and decuplets corresponding to their quantum numbers i.e charge and strangeness. In the picture of quark model, mesons are composed of quark-antiquark pairs whereas, baryons are composed of three quarks. The quarks carry fractional charges 2/3, $-1/3$ in units of e and obey Fermi statistics. The other characteristics of quarks with their quantum number are mentioned in Table 1.2.

The electric charge Q of the quark is connected with two other quantum numbers of quarks (baryon number and strangeness) and is given by the relation, which is known as the Gell-Mann-Nishijima formula [16, 17]:

$$Q = I_3 + \frac{\mathcal{B} + S}{2} \tag{1.2}$$

This formula is modified and generalized with the discovery of charm, top, and bottom quarks. The generalized formula is:

$$Q = I_3 + \frac{Y}{2}$$

, here Y is hypercharge expressed as

$$Y = \mathcal{B} + S - \left(\frac{C - B + T}{3}\right). \tag{1.3}$$

Where $\mathcal{B}, S, C, B, T$ denotes baryon numbers, strangeness, charmness, bottomness, and topness are quantum numbers of quark, respectively.

In 1964, a particle Δ^{++} consists of three quarks predicted by O.W Greenberg, which violates Pauli exclusion principle. To solve this issue, a new quantum number of quarks - color charge is introduced [18]. Color charges are of three types - Red, Blue, and Green. Quarks can carry red, green, and blue color charges, while

Table 1.2: The properties of six quark flavors, along with their associated quantum numbers, are detailed, with their respective masses taken from the Particle Data Group (PDG). Notably, the quark masses of u, d, and s are expressed in MeV units and c, b and t are running masses in GeV within the $\overline{MS}$ scheme, evaluated at a scale of approx 2 GeV. The top quark mass results from DO and CDF experiments at Tevatron at Fermilab [15, 16].

.

Properties of quarks	Up (u)	Down (d)	Strange (s)	Charm (c)	Bottom (b)	Top (t)
Baryon Number($\mathcal{B}$)	1/3	1/3	1/3	1/3	1/3	1/3
Mass (M)	2.16	4.70	93.4	1.27	4.18	172.69
Electric charge (e)	2/3	-1/3	-1/3	2/3	-1/3	2/3
Strangeness (S)	0	0	-1	0	0	0
Charmness (C)	0	0	0	1	0	0
Bottomness (B)	0	0	0	0	-1	0
Topness (T)	0	0	0	0	0	1
Isospin (I)	1/2	1/2	0	0	0	0
Isospin z-component (I_Z)	+1/2	-1/2	0	0	0	0

anti-quark are associated with anti-red, anti-blue, and anti-green charges. A quark possesses green color quantum number, implying it has one unit of greenness and zero units of blueness and redness. Similarly, anti-quark having an anti-red quantum number implies it has one unit of anti-redness and zero units of others. Color charge symmetry also forms $SU(3)$ group as follows by flavors of quarks. Hadrons exist as color singlets or colorless under $SU(3)_{color}$ group. "Colorless hadron" specifies either constituent within the hadron have zero color charge or all quark takes an equal unit of three colors. The possible bound states of quarks which are colorless are mesons ($q\bar{q}$), baryons (qqq), tetraquarks ($qq\bar{q}\bar{q}$), pentaquarks ($qqqq\bar{q}$), antibaryons ($\bar{q}\bar{q}\bar{q}$), etc. In group theory language, the possible combination of two quarks/ antiquarks or with a combination of quark and antiquark can be represented as:

$$q\bar{q} : 3 \otimes \bar{3} = 1 \oplus 8$$

$$qq : 3 \otimes 3 = \bar{3} \oplus 6$$

$$\bar{q}\bar{q} : \bar{3} \otimes \bar{3} = 3 \oplus \bar{6}$$

Out of these three combinations, $q\bar{q}$ pair is observable since it has color singlet states. In the same manner, baryons in color space can be expressed as

$$3 \otimes 3 \otimes 3 = 1 \oplus 8 \oplus 8 \oplus 10$$

The tensor decomposer of the baryon also consists of color singlets, so baryons are also observable. Also, gluons appear in colors like quarks and form $SU(3)$ group. This $SU(3)$ group of gluons forms singlet and octet states. The octet of gluons are $r\bar{b}, b\bar{r}, r\bar{g}, g\bar{r}, g\bar{b}, b\bar{g}$, $\frac{(r\bar{r}-g\bar{g})}{\sqrt{2}}$ and $\frac{1}{\sqrt{2}}(r\bar{r}+g\bar{g}-2b\bar{b})$. The octet of gluons intermediates QCD force between color charges.

1.3 Bound States of Quarks

No experiment gives any evidence for the existence of free quarks. Quarks reside within hadrons. This is called quark confinement or color confinement [19]. Bound states of three quarks are known as baryons, while the bound state of quark-antiquark pair is known as mesons. As quarks having spin 1/2 are fermions and mesons consist of pair of quarks and anti-quarks, therefore mesons are bosonic systems. And baryons form a fermionic system. Some other bound states that are colorless - are tetraquarks and pentaquarks. These are also supported by the theory of quantum chromodynamics and referred to as exotic hadrons.

1.3.1 Baryons

The combination of three quarks forms baryons. The familiar baryons are protons and neutrons, basic nuclei constituents. They are the most stable and lightest baryons. Baryon and its antiparticle (antibaryon) have baryon number of 1 and -1 respectively. The conservation of the baryon number is very important in studying baryon interactions. In the non-relativistic quark model, the wavefunction of the baryon is

$$\Psi(\rho, \xi, \phi, \eta) = \rho_{\text{color}} \times \xi_{\text{flavor}} \times \phi_{\text{spin}} \times \eta_{\text{space}} \tag{1.4}$$

According to Fermi statistics, the total wave function of the baryon should be antisymmetric. Since all observed baryons are color singlets, the wave function associated with the color component (ρ_{color}) is antisymmetric. For ground state spatial component wavefunction is symmetric, so $\xi_{\text{flavor}} \times \phi_{\text{spin}}$ have to be symmetric to get total wavefunction antisymmetric. In group theory representation, the baryonic system formed multiplets and is given as:

$$3 \otimes 3 \otimes 3 = 1_A \oplus 8_{MS} \oplus 8_{MA} \oplus 10_S$$

Here notations are as follows: A - antisymmetric, MS -mixed symmetric, MA - mixed antisymmetric, and S - symmetric states. It represents the decomposition of the tensor product of three triplets (3) in flavor space. The decomposition indicates that the resulting baryonic system can be expressed as a direct sum of three irreducible representations or multiplets in flavor space: a singlet (1), two octets (8), and a decuplet (10). The octet (8) consists of eight members, which are baryons with a total angular momentum and parity of $J^P = 1/2^+$. The decuplets (10) of baryons consist of 10 members with $J^P = 3/2^+$. The present thesis mainly focuses on studies of heavy mesons, so we will discuss mesons in detail in the next subsection.

1.3.2 Mesons

It can be observed from Table 1.2 that there is a good range of mass differences between quarks. Thus, quarks are classified by some fundamental scale Λ_{QCD}, which is the order of 200 MeV [20]. This scale divides quarks into two groups - heavy quarks and light quarks. Heavy quarks are then defined as having mass $m_Q \gg \Lambda_{QCD}$ and light quarks having mass $m_q \ll \Lambda_{QCD}$. Thus heavy quarks are charm (c), bottom (b), and top (t), and light quarks are up (u), down (d), and strange (s). Bound states of quarks can also be further categorized based on the mass group of quarks. Three categories are light-light mesons, heavy-light mesons, and heavy-heavy mesons. In group theory language, the product decomposition of quark-antiquark is given as:

$$\text{Color Space} \qquad 3 \otimes \overline{3} = 8 \oplus 1,$$

$$\text{Flavor Space} \qquad 3 \otimes \overline{3} = 8 \oplus 1,$$

$$\text{Spin Space} \qquad 2 \otimes \overline{2} = 1 \oplus 3.$$

Here quarks belong to SU(3) fundamental representation, whereas anti-quarks belong to $SU(\overline{3})$ representation. In color space, $SU(3)$ symmetry is exact, and in flavor space, this $SU(3)$ symmetry is approximate. In spin space, quarks belong to $SU(2)$ symmetry. Decompositions of $2 \otimes \overline{2} = 1 \oplus 3$ result in singlet and triplet spin states.

1.3.2.1 Light-Light Mesons

Light-light mesons consist of one of the three light quarks, namely, up (u), down (d), or strange (s), paired with one of their corresponding light antiquarks, which are denoted as $\overline{u}$, $\overline{d}$, or $\overline{s}$. For a quark (q) and an antiquark ($\overline{q}$) to be in the bound system, spin combinations of quark ($s_1 = 1/2$) and anti-quark ($s_2 = 1/2$) will give total spin $S = s_1 - s_2 = 1/2$ - $1/2 = 0$ to $s_1 - s_2 = 1/2 + 1/2 = 1$, thus $S = 0$ and 1. The simplest case is to have orbital angular momentum $L = 0$. The total angular momentum is $J = L + S$. Hence, we get a doublet in $L = 0$ state with $J = 0$ and 1. The parity of quark and anti-quark is opposite, so the intrinsic parity of meson is $(-1)^{L+1}$. From this, the ground state of the meson has negative parity ($L = 0$). Thus, we get $J^P = 0$ called pseudoscalar mesons and $J^P = 1$ called vector mesons. Pseudoscalar mesons are the lightest in all mesons spectroscopy. Vector mesons exhibit more mass than their pseudoscalar meson counterparts. They both form a nonet due to the isospin symmetry of light quarks. Excited states of these mesons have been discovered and very well studied theoretically. As for $L = 0$, parity is negative, and parity varies with L; we generally have parity (P) of mesons given by $(-1)^{L+1}$. Octet of pseudoscalar mesons reflected due to breaking of chiral symmetry [21, 22]. This will be discussed later in this chapter. Pseudoscalar mesons and vector mesons with their quark configurations are tabulated in Table 1.3 and Table 1.4. For studying light mesons, we have to look for some basic properties of quarks. As light quarks have very low mass, they are treated relativistically. This poses a problem, as the Schrodinger equation cannot be used. But we get interesting results if we apply isospin and color symmetry with spin interactions of quark and antiquark. We get masses and dipole moments of mesons theoretically without applying any other interactions. Thus, spin interactions of quarks and symmetries have a huge significance in hadron spectroscopy.

Table 1.3: Pseudoscalar mesons ($J^P = 0^-$) with associated quark compositions and quantum numbers.

Mesons	Quark compositions	Quantum numbers				
		I	I_Z	Y	Masses (MeV)[16]	
π^+	$u\overline{d}$	1	1	0	139.57	octet
π^0	$\frac{1}{\sqrt{2}}(d\overline{d} - u\overline{u})$	1	0	0	134.97	octet
π^-	$d\overline{u}$	1	-1	0	139.57	octet
K^+	$u\overline{s}$	$\frac{1}{2}$	$+\frac{1}{2}$	1	493.67	octet
K^0	$d\overline{s}$	$\frac{1}{2}$	$-\frac{1}{2}$	1	497.61	octet
K^-	$\overline{u}s$	$\frac{1}{2}$	$-\frac{1}{2}$	-1	493.67	octet
$\overline{K}^0$	$\overline{d}s$	$\frac{1}{2}$	$+\frac{1}{2}$	-1	497.61	octet
η_8	$\frac{1}{\sqrt{6}}(d\overline{d} + u\overline{u} - 2s\overline{s})$	0	0	0	547.86	octet
η_0	$\frac{1}{\sqrt{3}}(d\overline{d} + u\overline{u} + s\overline{s})$	0	0	0	957.78	singlet

Light quarks (u, d, s) lie in the fundamental representation $SU(3)$, and antiquarks lie in the complex conjugate representation $SU(\overline{3})$. Under flavor space for mesons, we have $3 \otimes \bar{3} = 1(singlet) \oplus 8(octet)$. Similarly, for color space, we have $3 \otimes \bar{3} = 1(singlet) \oplus 8(octet)$. But as color must be confined, only singlet is allowed. Furthermore, both quark and anti-quark have spins-1/2, and each can take two orientations. We have a representation for spin as $2 \otimes \bar{2} = 1(singlet) \oplus 3(triplets)$. Here $\bar{2}$ represents spin space for anti-quark. Singlet state gives pseudoscalar mesons, while triplet gives vector mesons. Color and spin symmetries are perfect symmetries. But flavor symmetry is an approximate one due to the fact that different quarks have different masses.

Table 1.4: Vector mesons ($J^P = 1^-$) with associated quark compositions and quantum numbers.

Mesons	Quark compositions	Quantum numbers				
		I	I_Z	Y	Masses (MeV)[16]	
ρ^+	$u\overline{d}$	1	1	0	775.26	*octet*
ρ^0	$\frac{1}{\sqrt{2}}(u\overline{u} - d\overline{d})$	1	0	0	775.26	
ρ^-	$d\overline{u}$	1	-1	0	775.26	
K^{*+}	$u\overline{s}$	$\frac{1}{2}$	$+\frac{1}{2}$	1	891.76	
K^{*0}	$d\overline{s}$	$\frac{1}{2}$	$-\frac{1}{2}$	1	895.55	
K^{*-}	$s\overline{u}$	$\frac{1}{2}$	$-\frac{1}{2}$	-1	891.76	
$\overline{K}^{*0}$	$s\overline{d}$	$\frac{1}{2}$	$+\frac{1}{2}$	-1	895.55	
ω	$\frac{1}{\sqrt{2}}(d\overline{d} + u\overline{u})$	0	0	0	782.65	
ϕ	$s\overline{s}$	0	0	0	1019.46	*singlet*

1.3.2.2 Heavy-Heavy Mesons

As the name suggests, Heavy-Heavy mesons are composite systems of heavy quarks (c, b) with anti-heavy quarks $(\overline{c}, \overline{b})$. Composite states of t (top) quark are not yet found due to its heavy mass and short decay lifetime [16]. As both c and b quarks are heavy, these quarks are treated non-relativistically. So, we can solve a Schrodinger equation for this system. To study such a system, we need interaction potential (V) between quarks and gluons [23–25]. In general, this potential has two parts. First is for short distances where quarks are nearly free by asymptotic freedom (a property of strong interaction), so only coulombic potential is present $V \sim 1/r$. The second part is for large distances where strong interaction confines quarks, so potential increases with distance, $V \sim r$. So, the total potential is given by $V \sim a/r + br$ where a and b are treated as constant parameters for convenience but can vary with distances. The linear potential is not the only possibility for large distances, but other potentials like $V \sim r^2$ and logarithmic potential $V \sim ln(r)$ [26–29] are also a good form for studying hadrons at large distances. But the results can be matched with any of the above potentials as they do not differ much over the narrow range of distances for which we can probe. Schrodinger equation can't be solved exactly with these potentials, but numerical solutions can be obtained by Runge -Kutta method using the Mathematica notebook [30].

Charmonium ($c\bar{c}$) and Bottomonium ($b\bar{b}$) are two major heavy-heavy mesons. The first charmonium state J/ψ was detected by two independent experimental facilities simultaneously in November 1974 [31, 32]. This discovery is called the "November revolution" in the history of particle physics. It has a lifetime of 7.2×10^{-21} and a narrow decay width of order 93.2 KeV. The first presence of bottonium state γ was noticed by Fermilab in 1977 [33, 34]. Quarkoniums are not the only candidates for heavy mesons; there are hybrid mesons also (quark-antiquark-gluons). Recently observed particles by experimental facilities are being considered as hybrid heavy mesons ($c\bar{b}g$ or $c\bar{c}g$). As excited heavy meson masses fall in the range of exotic particles, they need to be studied and placed properly. Several potential models have investigated charmonium and bottomonium spectroscopy[23–25, 35], but very few experimentally flourished [16]. In the realm of heavy-flavor hadrons, numerous experimental facilities—including LHCb, COMPASS, BESIII, STAR, CMS, ATLAS, BABAR, Belle, and others—are persistently striving to produce a plethora of data. Charmonium states like $X(3872)$, $\psi_2(3823)$, $\psi(3842)$, $X(3930)$, $\psi(4040)$, $X(4050)^{\pm}$, $X(4055)$, $X(4100)$, $X(4140)$, $\psi(4160)$, $X(4160)$, $Z_c(4200)$, $\psi(4230)$, $R_{co}(4240)$, $X(4250)$, $\chi_{ci}(4274)$, $\chi(4350)$, $\psi(4415)$, $Z_c(4430)$, $\chi_{co}(4500)$, $X(4630)$, $\psi(4660)$, $\chi_{c1}(4680)$, $\chi_{co}(4700)$ and bottomonium states like $\Upsilon(1S)$, $\Upsilon(2S)$, $\Upsilon(3S)$, $\chi_{bJ}(2P)$, $Z_b(10610)$, $Z_b(10650)$, $\Upsilon(10860)$, $\Upsilon(11020)$ have explored spectra of heavy mesons [11, 33, 34, 36–46].

1.3.2.3 Heavy-Light Mesons

Heavy-light mesons are bound systems containing a heavy quark and a light antiquark or vice versa. Two kinds of heavy-light mesons are D-meson ($c\bar{q}$) and B-meson($b\bar{q}$). D-meson has a charm (c) quark with a light anti-quark or vice-versa. Similarly, B-meson has a bottom (b) quark. We have no bound state with the top

(t) quark. It decays through electroweak interaction before forming a bound state. Its mean lifetime is about $10^{-25}s$, which is too short for the top quark to form a bound state [16]. The D and B mesons can be further classified with their quantum numbers or J^P values.

It can be assumed that a heavy quark is stationary with respect to the light quark, just as a proton is assumed to be stationary with respect to electrons in hydrogen. By this assumption, we can neglect the orbital motion of the heavy quark. This implies ($l_Q = 0$) and therefore, heavy quark is left only with spin $S_Q = 1/2$. Light quark has spin $S_q = 1/2$, which will couple with the orbital angular momentum (L) of the light quark. The simplest case is when $L = 0$ and $S_q = 1/2$ of light quark, we get $S_l = 1/2$. This $S_l = 1/2$ couples with $S_Q = 1/2$ of heavy quark to give total angular momentum $J = 0$ and 1. As discussed above, the parity of mesons is decided by $(-1)^{(L+1)}$. Thus for $L = 0$, $P = -1$. This gives two $J^P = 0^-$ and 1^- states. These are called doublet for $L = 0$. For $L = 1$ and $S_q = 1/2$ of the light quark, $S_l = 1/2$ and $3/2$. $S_l = 1/2$ couples with $S_Q = 1/2$ to give doublet $J^P = 0^+$ and 1^+. Also $S_l = 3/2$ couples with $S_Q = 1/2$ to give $J^P = 1^+$ and 2^+ doublet. In this way, we can get the spectrum of both D and B mesons for higher states. Similarly, we can also define another quantum number n like in a hydrogen atom, which depends on the radial part of the total wavefunction of the meson.

The First D-meson was found experimentally in the year 1976 by the experimental group "SLAC"[47, 48]. It is the neutral state having mass 1865 ± 15 MeV and decay width of order 40 MeV. Experimental observation of B-meson was first made in 1983 by CLEO collaborations [49]. In the last 50 years, several new states were announced by different facilities like LHCb, Belle, BESIII, etc., which stimulated heavy-light mesons. Recently discovered new charm meson states are $D_0(2560)$, $D_1^*(2680)$, $D_2(2740)$, $D_3^*(2760)$, $D_J(3000)$, $D_J^*(3000)$, $D_{s1}(2860)$, $D_s(3040)$, $D_{s0}(2590)$ and bottom meson states are $B_{sJ}(6064)$, $B_{sJ}(6114)$, $B_J(5840)$, $B_J(5960)$, $B_{s1}(5830)$, $B_{s2}^*(5840)$, $B_s^0(6063)$, $B_s^0(6108)$ [16, 50–58].

Heavy-light meson systems are an active area of research because of the recent discoveries of new heavy-light mesonic states at LHCb and other accelerator facilities like DO, Belle, BESIII, CDF, etc. As the masses predicted by some potential models, HQET and other models lie in the region of discovered particles. It is necessary to assign them quantum numbers according to their masses, decay modes, decay widths, and branching ratios.

1.3.3 Exotic Hadrons

Within the framework of Quantum Chromodynamics (QCD), gluons, characterized by their color charges, serve as intermediaries mediating interactions between quarks and also engage in self-interactions. States belong to $J^{PC} = 0^{--}, 0^{-+}, 1^{+-}, 2^{+-}$ with parity $P = (-1)^{l+1}$ and C-parity $C = (-1)^{l+s}$, are not accommadated in quark model. That is why these states are known as exotic states. Although Gell Mann and Zweing suggested the existence of such multiquark configurations, due to a lack of evidence, they did not get placed in the quark model. These multiquarks were tetraquarks ($qq\bar{q}\bar{q}$), pentaquarks ($qqqq\bar{q}$), hexaquarks ($qqqqqq$), gluballs, hybrid hadrons etc [13, 14, 59, 60]. Over decades, various new exotic states have been observed by different experimental facilities, which flourished a spectrum of exotic hadrons [61–71]. Recently in 2022, LHCb announced observations of two tetraquarks $T^{0,++}_{c\bar{s}0}(2900)$ with quark content $c\bar{s}\bar{u}d$, $c\bar{s}u\bar{d}$ respectively. The first confirmed tetraquark $X(3872)$ having quark contents $c\bar{c}d\bar{u}$ was found by Belle in 2003 [72]. Till now, many states like $Z_{cs}(3985)$, $Z_{cs}(4003)$, $Z(4430)$, $Y(3940)$, $X(3872)$ are observed which made hardon's world more affluent [16]. Theoretically, spectra of quarkonium can be achieved by the different potential models available in the literature [73–76]. The first disclosure of pentaquark entities occurred in 2003 at Laser Electron-Photon Experiment at Spring (LEPS). However, it was only in 2015 that these findings were definitively validated by the LHCb detector at CERN [77]. They reported two pentaquarks $P_c(4380)^+$ and $P_c(4450)^+$ with quark configuration $c\bar{c}uud$ and assigned as molecular state of $\Sigma(2455)\bar{D}^*$ and $\Sigma^*(2520)\bar{D}^*$ respectively [78]. Recently pentaquarks states $P_c(4459)$, $P_c(4337)$, $P_cs(4338)$ are detected by LHCb group [79, 80]. Such discoveries began a new era of exotic hadron matters.

1.4 Quantum Chromodynamics

Quantum chromodynamics (QCD) is a quark-gluon color theory that describes strong interactions. The field quanta gluons are neutral and massless particles having spin 1, associated with strong interactions. The QCD Lagrangian is expressed in a generalized form as follows:

$$\mathcal{L} = L_{bosons} + L_{fermions}$$

The first term represents gauge Lagrangian and the expression for it:

$$L_{bosons} = -\frac{1}{4}G_a^{\alpha\beta}G_{a\alpha\beta}$$

with

$$G_a^{\alpha\beta} = \partial^\alpha A_a^\beta - \partial^\beta A_a^\alpha - gf_{abc}A_b^\alpha A_c^\beta \quad (a = 1, 2......8)$$

Here $G_a^{\alpha\beta}$ is the second-order tensor field of gluons, which represents gluons propagation and their interactions. The symbol f_{abc} denotes structure constants of $SU(3)_c$ symmetry group (c stands for color). Indices a, b, and c are color flavors that have values 1 to $n_c^2 - 1$ where n_c represents the number of distinct quark color states. Generally, we take $n_c = 3$. g is a strong coupling constant that describes the strength of strong interactions ($g = \frac{\alpha_s^2}{4\pi}$). The second part labels fermionic Lagrangian and is given by:

$$L_{fermions} = \sum_i \overline{\Psi}_i(i\not{D}_i - m_i)\Psi_i \tag{1.5}$$

Here $\overline{\Psi}_i$ describes the dirac spinors of i^{th} quark (u, d, s, c, b, t) with mass m_i. The covariant derivative D_μ is endowed as $D_\mu = \partial_\mu + igA_{a\mu}t_a$ This part explains the dynamics of quark propagation as well as their interactions coupled with gluon fields $A_\alpha = A_{a\alpha}t_a$. α, β labels the spatial and temporal parts of vector gauge fields. t_a are matrices belong to non- abelian gauge group $SU_c(3)$ and follows commutation relations $[t_a, t_b] = if_{abc}t_c$ [81–85].

QCD looks like QED except for the fact that QCD possesses a non-Abelian nature, which arises from gluons self-interactions. This renders the coupling constant into a dynamic, or "running," form. In QCD, coupling constant $\alpha_S(\mu)$ addressed hadronic interactions for the entire range in terms of momentum transfer (μ) [86]:

$$\alpha_s(\mu) = \frac{12\pi}{(33 - 2N_q)ln(\frac{\mu^2}{\Lambda_{QCD}^2})} \tag{1.6}$$

Here N_q = number of flavors. Λ_{QCD} is QCD fundamental scale which dictates the behavior of running coupling constant. To understand hadronic interactions, knowing the dynamics of QCD coupling over the entire range of momentum scale is crucial. The graphical representation of the coupling constant's dependence on the momentum parameter is illustrated in the fig 1.1.

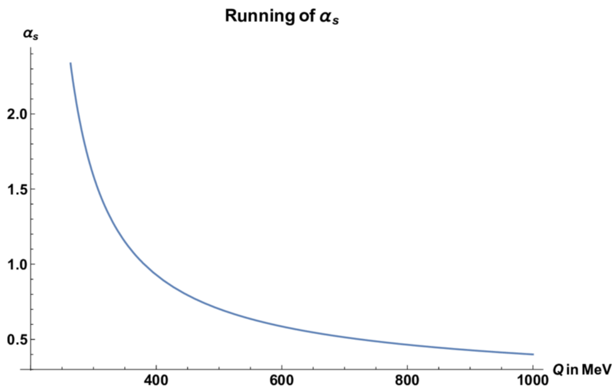

Figure 1.1: The variation in the strong coupling constant, denoted as α_s, with respect to the momentum transfer parameter Q.

By examining the figure, we can understand two important aspects of QCD: color confinement and asymptotic freedom.

- At high momentum transfer (high energies), the value of α_s ceased logarithmically. This means at high energies, the coupling constant becomes weak, and quarks reside hadrons act as free particles. This leads to a peculiar property of QCD known as **asymptotic freedom**. In this domain, one can perform calculations of processes using perturbative techniques. High-energy electron-proton scattering processes support this feature.

- At low momentum transfer, the coupling constant increases linearly, which implies the coupling constant becomes large with the decrease in μ. This results in quark-gluons confinement within hadrons. This feature of QCD is known as **quark or color confinement**. Experimentally, isolated quarks and gluons have not been detected up to now, which supports the existence of the color-confinement hypothesis. In this regime, perturbative methods are not further applicable because of the large value of the QCD scale parameter (α_s). However, several non-perturbative techniques can be used to perform the calculations for processes at low energy regimes.

So, to study the dynamics of hadrons at different energy scales, we have two kinds of approaches: Perturbative methods and Non-perturbative methods. In the thesis, we will adopt phenomenological field theories to calculate the various properties of the charm and bottom mesons. Also, we will study quarkonia spectra and their decay properties by potential model.

1.5 Phenomenological Approaches

As we know, for describing systems of quarks - mesons, baryons, or other bound states of quarks, there are two different techniques: perturbative and non-perturbative techniques. At low energies, the coupling constant diverges, which shows that perturbation methods will not be compatible in this domain. The perturbation methods become complicated above the scale of 0.1 fm or momentum transfer of 2 GeV. Even some essential phenomena that lie in the infrared region cannot be investigated by perturbation theory. This shows that only perturbative approaches are not enough to get the complete picture of QCD. At low energy transfer ~ 500 MeV, the running coupling constant reaches 1, which switches QCD into a non-perturbative region. There are several non-perturbative approaches to studying processes or systems in low energy scales: potential models, lattice QCD, effective theories, sum rules, etc. A brief discussion of some approaches is mentioned below:

1.5.1 QCD Sum Rules

QCD sum rules is a formidable tool for examining the complicated dynamics and behaviours of hadrons. It was formulated in 1979 by Shifman, Vainshtein, and Zakharov (SVZ) and has become a popular method in hadron spectroscopy [87]. This approach is successful for studying S, P, D, F-wave mesons [88] and S, P, D-wave heavy baryons [89]. This method also appears to be suitable for computing the hadronic parameters of the exotic hadron [90]. Within this method, hadrons are characterized by their interpolating quark currents, which are considered under high virtuality conditions. The correlation function of these quark currents is then introduced and scrutinized using the operator product expansion (OPE). This application of OPE allows for the calculation of short-range interactions through QCD perturbation theory, while long-range interactions are expressed in terms of universal vacuum condensation or light cone distributions. Both calculations are then matched to sum over hadronic states with dispersion relations. This sum rule can then be used to get observable properties of hadronic ground states. Conversely, one can extract the parameters of Quantum Chromodynamics (QCD), such as the quark masses and vacuum condensate densities, from sum rules that incorporate experimentally determined hadronic components. This is a model-independent method, as it doesn't use constituent masses of quarks as a parameter. Also, this method gives an insight into how hadrons of different quantum numbers are different as hadronic currents depend on it. This method is extensively used to extract hadronic parameters [91, 92]. In heavy hadron sectors, QCD sum rules are employed in HQET limit [93].

1.5.2 Potential Model

One of crucial challenges in theoretical frameworks of particle physics lies in the concept of quark confinement, where a solitary, color-charged quark is not found in isolation; rather, quarks and gluons remain perpetually bound within hadrons. The assumption of quark confinement within hadrons underpins various phenomenological models. In this phenomenological method, both relativistic and non-relativistic treatments of quarks within hadrons are employed for a comprehensive analysis. One of the important phenomenological approaches is the Potential Model. The most commonly used potentials are Cornell potential [24, 25], Harmonic potential, Logarithmic potential [27], Martin potential [26], Richardson potential [28], Mixed power-law potentials, etc. With these potentials, the study of heavy mesons like charmonium, bottomonium, D mesons, B mesons, etc can be explored. This approach involves constituent masses of quarks and incorporates quark-antiquark interactions. The potential model exhibits both non-relativistic and relativistic methods. In the non-relativistic model, quarks are treated as non-relativistic particles, and changes in hadronic parameters arise by a gluonic field endowed by effective potential. The simplest form of a potential model for the study hadron containing a heavy quark and their hadronic properties is given as:

$$V = -C_F \frac{\alpha(r)}{r} + br \tag{1.7}$$

This potential emerges as a consequence of Quantum Chromodynamics (QCD), which exhibits asymptotic freedom when dealing with close-range interactions and, conversely, confinement phenomena when considering interactions at substantial distances. The first term represents short-distance interactions, and for large r, there is a linear increase in potential given by the second term. Later, this model was modified by including some interactions like spin-spin, spin-orbit interactions, etc [24, 25]. These potential models are very helpful in examining the properties of hadrons. However, these models are associated with unknown parameters, which demand experimental data for further calculations. We will provide a thorough exploration of the potential model in Chapter 5, where we will calculate the masses and how bottomonia particles decay.

1.5.3 Lattice QCD

Lattice QCD is a remarkable non-perturbative computational technique for describing the hadronic spectrum and matrix elements of any operators or process. It is formulated on a discrete Euclidean space-time grid. This grid has lattice spacing between points, with L being the total length of the lattice. The quark fields appear at these lattice points, and gluons link neighboring sites, which are expressed by color fields [94, 95]. These color fields transform under $SU(3)$ group transformations. Some technical issues are associated with QCD calculations, which even generate unknown systematic errors. Calculations for systems having large numbers of lattice points are costly and time-consuming. The Monte Carlo technique to perform lattice QCD calculations needs supercomputers. By employing quenched approximations and Dyson- Schwinger equation formalism, the computational expense associated with this method can be reduced.

1.6 Effective Field Theory

Another phenomenological approach for probing non-perturbative aspects of QCD is provided by effective field theory. These effective theories have some approximations that help in extracting information on the physical quantities of the system at a particular scale. This approach describes QCD dynamics below some scale Λ_{QCD}, rather than fundamental field theory, which is applicable at any scale. An effective field theory, if valid to a particular scale Λ_{QCD}, only finite numbers of parameters can unravel physical process. Thus, effective field theory simplifies complex hard processes into a consistent yet limited framework. There are various effective theories available in the literature, like bag model, chiral perturbation theory, heavy quark effective theory, heavy hadron chiral perturbation, etc.

1.6.1 Bag Model

Bag Models are famous for investigating light hadrons. In MIT bag model, quarks and gluons are assumed as massless objects moving freely inside the hadronic bag of radius R. These quarks and gluons create inward bag pressure P which describes large distance behaviors of QCD. The balance of bag pressure leads to confinement aspects of QCD. Wavefunctions of these quarks are developed to compute hadronic properties like masses, lifetimes, branching ratio, nuclear charge radii, etc [96, 97]. The radius R of the hadronic bag is estimated by the fact that external pressure is generated to compensate for the pressure exerted by freely moving quarks and gluons. This can be achieved by matching the model parameters to the experimental data, such as masses, magnetic moments, etc.

1.6.2 Heavy Quark Effective Theory

A system containing heavy quarks and light quarks can be seen as a hydrogen atom system. In a hydrogen atom, heavy protons sit at the center, and around it, light electron interacts with the proton's field with the exchange of photons. In a similar manner, here, heavy quarks are present with light quarks and gluons. Although much more complexities are involved in these systems than in hydrogen atoms, as already stated in the introduction, gluons can interact with quarks and other gluons also. For a brief illustration, let us look into heavy-light mesonic systems($Q\bar{q}$). In heavy-light mesonic systems, a heavy quark (Q) is present with a light quark(q) and gluons (g). The heavy quark of mass $m_Q \gg \Lambda_{QCD}$ can be assumed to be at rest with respect to light quarks and gluons present in the mesonic system. It can be assumed that the velocity of hadron can be approximated as the velocity of heavy quark because momentum exchanged between heavy quark with light particles will be negligible in respect to m_Q in the limit $m_Q \to \infty$ [86, 98–100]. In this condition, the transferred momentum is called on shell momentum transfer, where heavy quarks are unaffected by transferred momentum. Also, heavy quarks can only acquire zero orbital angular quantum numbers. Thus the total angular momentum of a heavy quark is the same as its spin quantum number $S_Q = 1/2$. Also, light quarks and gluons interact with heavy quarks with low momentum in comparison to the mass of heavy quarks, the heavy quarks spin is almost invisible to light quark. This is called Heavy Quark Spin Symmetry. In limit $m_Q \to \infty$ light quarks are also unaffected by the flavor of heavy-quark. This is called a Heavy Quark flavor symmetry. Combining both symmetries, we simply called spin-flavor heavy quark symmetry.

The spin and orbital angular momentum of light quark couples to form a resultant angular momentum of light degree of freedom (S_l). Now, this S_l couples with the spin of heavy quark (S_Q) to give total angular momentum (J). As S_Q is conserved separately due to heavy quark spin symmetry, S_l is also conserved. For any L we get a doublet of J. They are called spin partners. For baryons containing heavy quarks, we can apply the heavy quark symmetries and decouple the spin of heavy quarks from light degrees of freedom. Then we can take care of the spin and orbital angular momentum of light quarks separately and then couple the resultant angular momentum with heavy quark spin to again give total angular momentum (J) like in mesons. Here, we get some isospin singlets, doublets, and triplets depending on quark contents.

Now, QCD Lagrangian can be modified for these approximations and symmetries. The QCD Lagrangian for the quark field is expanded in orders of $(1/m_Q)$. The leading order is free of m_Q, which relates to $m_Q \to \infty$, but is not free of light degrees of freedom like the mass of light quark and spins, etc. Also, many of the parameters of the heavy quark are not included here, which makes the theory easy to handle. Resultant effective HQET Lagrangian can be solved for these systems under consideration by defining the fields of particles and their interaction fields. Then, the effective Lagrangian of these systems is written and solved for masses and decay widths of particles.

In the present thesis, our focus is employing heavy quark effective theory to examine several aspects of the heavy-light meson system. This theory is extensively discussed in Chapter 2. In our present study, we explored charm and bottom mesons only, as the top quark, significantly heavier and associated with weak decays, hasn't been independently predicted at this scale.

1.6.3 Heavy Hadron Chiral Perturbation Theory

Heavy hadron chiral perturbation theory is one of the effective approaches for describing interactions and dynamics of heavy hadrons. This theory combines the chiral symmetry of light quarks (q) and the spin-flavor symmetry of heavy quarks(Q) [101–103]. Heavy quark symmetry appears by approximations $m_Q \to \infty$. The behaviour of light quarks become unaffected by the flavor and spin of heavy quarks in this limit. Chiral symmetry manifests in the limit as $m_Q \to 0$, wherein left-handed quarks persist as left-handed and right-handed quarks persist as right-handed under a change of frame of references. Thus light quarks possess $SU(3)_L \times SU(3)_R$ symmetry. Due to the significant mass difference between strange and up/down quarks, this symmetry spontaneously breaks, resulting in eight pseudoscalar mesons: $\pi^{\pm}, \pi^0, K^{\pm}, K^0, \overline{K}^0$, and η. They are considered approximate goldstone bosons. The effective Lagrangian is made by defining some chiral operators and goldstone boson fields with scalar and vector matter fields. Using this effective Lagrangian, properties of heavy-light hadrons can be extracted.

1.6.4 Regge Phenomenology

Regge phenomenology is widely used method to study hadron physics. The theory associated with this method i.e Regge theory is based on Lorentz invariance, unitary and analyticity of scattering matrix and quite successful theory at high energy region. In two to two-particle scattering phenomenon, poles are estimated by equation $\alpha(t) = l$, where t is Mandelstan time. In Regge theory, $\alpha(t)$ labels Regge trajectories and expressed in function of time t as $\alpha(t) = \alpha^{'} t + \alpha(0)$. $\alpha^{'}, \alpha(0)$ are slope and intercept of Regge lines respectively [104–106]. On Regge line, the square masses of the hadron are proportional to the total angular momentum of that hadron. Each resonance on Regge line is called Reggeon. Chew and Frautshi employed Regge theory to investigate strong interactions and predicted that missing excited states of hadrons appear on Regge trajectories in the (J, M^2) plane. Hadrons lie on particular Regge lines and carry the same internal quantum numbers. Thus Regge trajectories are very helpful in identifying hadrons with masses and their J^P values. Most general formula is

$$M^2 = \alpha J + \beta n + C \tag{1.8}$$

where α, β are slopes of lines, C is constant, and M is mass of hadron. Thus Regge trajectories are one of the leading techniques to study QCD at high energies. In Chapter 3, we constructed Regge trajectories for predicted masses for heavy -light meson $3S, 3P, 1F$ states in planes (M^2, n_r), (M^2, J^P) and also calculated their slopes and intercepts.

1.7 Symmetries

Symmetries play a pivotal role, especially in low-energy QCD, and act as a powerful tool to probe the dynamics of strongly interacting systems. Symmetries put constraints on possible interactions for a given physical process, and its Lagrangian gets simplified. There are two types of symmetries: global symmetry and gauge symmetry [107]. In global symmetry, associated parameters are space-time independent, whereas in gauge symmetries, parameters are space-time independent. Generally, local symmetries are governed by gauge theories, and the existence of massless particles is often associated with global symmetries. Quantum Chromodynamics (QCD) is a gauge theory tied to the $SU(N_c)$ local symmetry group, specifically concerning the color degree of freedom. The Lagrangian of QCD remains unchanged under gauge transformation group $SU(3)$, in which all quarks feel the same interactions. The mass parameter is the parameter based on which one can distinguish different quarks. This term of the Lagrangian can be expressed in the following manner:

$$\mathcal{L}^m_{QCD} = \overline{q}(i\gamma^\mu D_\mu - m_q)q + \overline{Q}(i\gamma^\mu D_\mu - m_Q)Q \tag{1.9}$$

where the first part expresses light quarks u, d, s, with $m_q \ll \Lambda_{QCD}$ and second part denoting heavy quarks c and b with $m_q \gg \Lambda_{QCD}$. This effective Lagrangian brings some symmetries that arise due to some approximations of quark masses. At a low energy scale, QCD has some global symmetries like chiral symmetry, heavy quark symmetry, and isospin symmetry.

Chiral symmetry is the internal symmetry of massless Dirac spinors. It remains invariant under rotation transformation i.e, and left-handed quark remain left-handed and right-handed quarks remain right-handed under chiral rotations. Mathematically, dirac spinors can be separated with the help of projection operators $P_L = \frac{1}{2}(1 - \gamma_5)$ and $P_R = \frac{1}{2}(1 + \gamma_5)$ [85, 108, 109]. Modified Lagrangian in terms of left-handed and right-handed quark can be expressed as:

$$\mathcal{L}_{QCD} = i\overline{q}_L \not{D} q_L + i\overline{q}_R \not{D} q_R - \overline{q}_R m q_L - \overline{q}_L m q_R \tag{1.10}$$

Since masses of u, d, s are small in comparison to Λ_{QCD}, and we can consider approximation $m_Q \to 0$ and Lagrangian become:

$$\mathcal{L}_{QCD} = i\overline{q}_L \not{D} q_L + i\overline{q}_R \not{D} q_R \tag{1.11}$$

Terms in Eq.(1.11) lead symmetry, known as chiral symmetry. This symmetry helps to investigate the properties of hadrons and makes QCD Lagrangian simpler.

Heavy Quark Symmetry- It is an approximate symmetry that arises when we set the mass of a heavy quark approaches infinity. Due to this symmetry, the dynamics of light quarks remain independent of the spin and flavor of heavy quarks. In this limit, the higher order Lagrangian terms in form of $\frac{1}{m_Q}$ factor vanish, thus making it heavy quark flavor free. This symmetry contrasts with chiral symmetry, emerging under different quark mass conditions.

Isospin Symmetry: The masses of up and down quarks are nearly identical. This degeneracy results in the existence of isospin symmetry. This symmetry is followed by the $SU(2)$ group under isospin space. Isospin is exact symmetry in strong interactions but violated in electromagnetic and weak interactions.

1.8 Spontaneous Symmetry Breaking

In nature, quarks come with masses. Thus chiral symmetry cannot remain the exact symmetry of QCD and is explicitly broken by mass terms of quarks [107]. Moreover, the dynamical breaking of chiral symmetry can also be represented by the QCD vacuum state. This vacuum state is associated with quark-antiquark creation. The amount of energy needed to generate such a quark-antiquark pair is small if quarks are massless. Due to strong interactions of flavors, one can expect $q\bar{q}$ pair condensation. The mechanism of spontaneous breaking of chiral symmetry is given by the Nambu-goldstone model [47, 109]. This model states that continuous symmetry-breaking couples with the generation of massless particles, which are known as goldstone bosons. Each symmetry breaking is associated with the generation of one massless particle and is equal to a number of broken generators. N_F^2-1 is a number of generated Nambu goldstone bosons where N_F denotes number of flavors. For $N_F = 2$, we get 3 massless boson, identified as pions and for $N_F = 3$, we get octet of pseudoscalar bosons.

1.9 Experimental Status

Due to large advancements in accelerator facilities to provide high-energy outputs and collaborations, high-energy physics is flourishing. A large amount of data comes from experimental groups like LHCb, BABAR, BESIII, CDF, CMS, Belle at KEKB, J-PARC, SLAC, CLEO, SELEX, FOCUS, etc [10, 11, 42, 49, 57]. Many new candidates are being observed by these collaborations, which developed the interest of theoreticians to check the validity of available models and formulate new methods to explain newly announced resonances. Each experimental facility is constructed to perform specific tasks and investigate specific kinds of particles. The recent discovery of Higgs bosons [10, 11], pentaquarks [110–112], neutrino oscillations [113–115], etc., by the different experimental groups, has ignited curiosity in high-energy physics and motivated experiments to go beyond the standard model [116, 117].

Exploring physics beyond standard models enables us to unravel mysteries such as the composition of dark matter, the surprisingly light nature of Higgs particles, the early stages of the universe, the potential unification of all forces, and more. The emerging data from different experiment facilities like LHCb, BESIII, CDF, etc., for new hadrons made hadron spectroscopy an active area of research [58, 61, 62, 80, 118, 119]. Despite many riddles, these experiments give crucial information that helps in a better understanding of hadronic structures.

1.10 Experimental Facilities

1.10.1 LHCb Experiment

LHCb experiment is specially designed single-arm forward spectroscopy at CERN for bottom physics. The prime feature of this experiment is the search for new physics via CP violation in heavy mesons. The LHCb experiment also measured decay-time resolution for B mesons, high production cross section for quarkonium, and particle identification performance. It also extended its scope for studying exotic hadrons, charm physics, and electroweak processes. LHCb started taking data in 2010. It operated initially at the center of mass 7 TeV and then increased to 8 TeV until 2012. After two years of shutdown, LHCb restarted and operated between 2015 to 2018 with a center of mass energy of 13 TeV and again restarted in 2022. During the running period, many new states are observed and push physics to the edges. In 2013, the LHCb detector made noteworthy discoveries, identifying two resonances with natural parity, namely $D_J^*(2650)^0$ and $D_0^*(2760)$, as well as two resonances with unnatural parity, labeled $D_J(2580)^0$ and $D_J(2740)^0$ by analyzing the invariant mass spectrum of $D^+\pi^-$, $D^0\pi^+$, $D^{*+}\pi^-$ [55]. Furthermore, a state with unnatural parity, $D_J(3000)^0$, and a state with natural parity, $D_J^*(3000)^0$, were identified in the mass spectra of $D^{*+}\pi^-$ and $D^+\pi^-$, respectively [55]. In 2015, the LHCb group investigated $B^0 \longrightarrow \bar{D}^0\pi^-\pi^+$ decays, determining the charm meson states $D_0^*(2300)$ and $D_0^*(2460)$. They also assigned the state $D_3^*(2760)$, with $J^P = 3^-$, for the first time [57]. More recently, the LHCb collaboration studied $B^- \longrightarrow D^+\pi^-\pi^+$ decays using the Dalitz plot analysis technique. Their findings indicated the presence of charm resonances with spins 1, 2, and 3 in the $D^+\pi^-$ mass spectrum. Notably, these charm resonances predominantly arise from the contributions of $D_3^*(2760)$, $D_1^*(2680)$, $D_2^*(2460)$, and $D_2^*(3000)$ charmed meson decays into S-wave $D^+\pi^-$ [55]. In the charm strange meson family, ground states $(1S)$ and low-lying states $(1P)$ are well established [16]. In 2015, the LHCb group analyzed decay $B_s^0 \to \bar{D}^0K^-\pi^+$ and observed $D_{s1}^*(2860)$, $D_{s1}^*(2860)$ states. They also determined their masses and decay widths.

In B meson family, Analysis of mass spectra of $B^+\pi^-$ and $B^0\pi^-$ investigated by LHCb at the center of mass energies of 7 and 8 TeV on data sample corresponding to $3.0fb^{-1}$ and have observed $B_1(5721)$, $B_2^*(5747)$, $B_J(5840)^{0,+}$, $B_J(5960)^{0,+}$ which is consistent with previous observation of CDF and DO experiments [16]. In strange bottom mesons family, only some states $B_s(5366)$, $B_s^*(5415)$, $B_{s1}(5830)$, $B_{s2}^*(5840)$ are well established and collected in PDG[16]. Among them, states $B_s(5366)$, $B_s^*(5415)$ are classified as $1S$ states and states $B_{s1}(5830)$, $B_{s2}^*(5840)$ are assigned as $1P$ $(1^+, 2^+)$ states. In a recent breakthrough, the LHCb collaboration identified two resonance states, $B_{sJ}(6063)$ and $B_{sJ}(6114)$, within the mass spectrum of B^+K^-. Furthermore, they determined the masses and decay widths of these newly discovered meson states. [118].

1.10.2 BABAR Experiment

BABAR experiment is an important particle experiment situated at SLAC National Acceleration Laboratory in Menlo Park, California, and specially designed to probe charge parity violation. In 2010, BABAR experiment conducted a thorough analysis of e^+e^- inclusive collision at center of mass energy 10.58 GeV and resulted in observation of non-strange excited charm mesons $D_J(2550)^0$, $D_J^*(2600)^0$, $D_J^*(2600)^+$, $D_3^*(2750)^0$, $D_J^*(2760)^+$ and $D_J(2760)^0$ for the first time [42]. The BABAR experiment investigates decays of states $D_{s1}^*(2700)$ and $D_{sJ}^*(2860)$ into D^*K [120]and computed their respective branching ratios relative to DK decay mode as:

$$\frac{\mathcal{B}(D_{s1}^*(2700) \to D^*K)}{\mathcal{B}(D_{s1}^*(2700) \to DK)} = 0.91 \pm 0.13 \pm 0.12 \tag{1.12}$$

$$\frac{\mathcal{B}(D_{sJ}^*(2860)^+ \to D^*K)}{\mathcal{B}(D_{sJ}^*(2860) \to DK)} = 1.10 \pm 0.15 \pm 0.19 \tag{1.13}$$

In addition, by analyzing $e^+e^- \to \bar{c}c$ decay processes, BABAR also reconstructed first orbital excited states of charmed strange mesons $D_{s0}^*(2317)^\pm$ and $D_{s1}(2460)^\pm$, using the data 232 fb^{-1} [121]. Recently BABAR measures absolute branching fractions of decay $B^+ \to X(3872)K^+ = [2.1 \pm 0.6 \pm 0.3] \times 10^{-4}$ [122].

1.10.3 BESIII Experiment

The BESIII experiment is one of the famous experimental facilities located at the Beijing Electron Positron Collider in Beijing, China. It is motivated to examine charmonium particles and other particles having charm quarks. $Z_c(4020)$ was first announced by BESIII in 2013 in decay process $e^+e^- \to \pi^+\pi^- h_c$ and other observed charmonium states are reconfirmed by BESIII experiment [123]. This experiment reobserved states $D_{s1}(2560)$ and $D^*_{s2}(2573)^-$ in decay channels $e^+e^- \to D^+_s \bar{D}^{*0} K^-$ and $D^+_s \bar{D}^0 K^-$ and measured their messes and decay widths which are consistent with other experimental results [16].

1.10.4 CDF Experiment

The Collider Detector at Fermilab was a particle physics experiment conducted at Fermilab's Tevatron particle accelerator in Batavia, Illinois. In 2007, CDF collaboration announced two strange bottom meson states $B_{s1}(5830)$, $B^*_{s2}(5840)$ [52] and in 2009, CDF II detector at Fermilab Tevatron also observed states $B_1(5721)$, $B^*_2(5747)$ [53]. In 2013, CDF collaboration observed new resonances - $B(5970)^+$ and $B(5970)^0$ by analyzing invariant mass distribution of $B^0\pi^+$ and $B^-\pi^+$. In 2013, CDF collaboration observed new resonances - $B(5970)^+$ and $B(5970)^0$ by analyzing the invariant mass distribution of $B^0\pi^+$ and $B^-\pi^+$ and measured their masses and decay widths [124]. The first candidate of the beauty-charmed meson family was observed in $p\bar{p}$ collision at Fermilab Tevatron by CDF collaboration in 1998 and measured mass and lifetime of B^+_c [125].

1.10.5 CMS Experiment

The CMS (Compact Muon Solenoid) experiment is one of the major particle physics experiments conducted at the Large Hadron Collider (LHC), the world's largest and most powerful particle accelerator. In the year 2018, the CMS experiment conducted an investigation on the mesons $B^*_{s2}(5840)$ and $B_{s1}(5830)$ using a data sample obtained from proton-proton collisions. The data sample had an integrated luminosity of 19.6 fb^{-1} and was collected at a center of mass energy of 8 TeV. The measured values of the branching fractions of $B^*_{s2}(5840)$ in the final states $B^*{+}K^-$ and B^+K^- are reported in the reference [16]:

$$\frac{\mathcal{B}(B^*_{s2}(5840)^0 \to B^{+*}K^-)}{\mathcal{B}(B^*_{s2}(5840)^0 \to B^{+*}K^-)} = 0.081 \pm 0.021 \pm 0.015 \tag{1.14}$$

At the latest, the CMS experiment observed two beauty-charmed states $B^+_c(2S)$ and $B^{*+}_c(2S)$ using an integrated luminosity of 143 fb^{-1} with the center of mass energy

13 TeV and measured their masses also [126].

1.10.6 Belle Experiment

Belle experiment was one of the two main experiments at the KEKB (b-factory) accelerator, the other being the BELLE II experiment, which is an upgraded version of Belle located at Tsukuba, Japan. It was designed and optimized for the observation of CP violations in the B-meson system. The state $X(3872)$ was first observed by Belle in 2003 in decay process $B^{\pm} \rightarrow K^{\pm}\pi^{+}\pi^{-}$ [127]. and the state $X(3823)$ in 2013 also observed by belle collaboration in decay process $B \rightarrow \chi_{c1}\gamma K$ [16]. Many charmonium-like states are observed and reconfirmed by this experiment.

Bibliography

[1] J.J. Thomson, Phil. Mag. Ser. 5 **44**, 293 (1897)

[2] E. Rutherford, Phil. Mag. Ser. 6 **21**, 669 (1911)

[3] C.L. Cowan, F. Reines, F.B. Harrison, H.W. Kruse, A.D. McGuire, Science **124**, 103 (1956)

[4] E.D. Bloom et al., Phys. Rev. Lett. **23**, 930 (1969)

[5] R.E. Taylor, Reviews of Modern Physics **63**, 573 (1991)

[6] H.W. Kendall, in *A Distant Light: Scientists and Public Policy* (Springer, 2000), pp. 94–126

[7] S. Weinberg, Phys. Rev. Lett. **19**, 1264 (1967)

[8] A. Salam, Conf. Proc. C **680519**, 367 (1968)

[9] S.L. Glashow, Nucl. Phys. **22**, 579 (1961)

[10] S. Chatrchyan et al. (CMS), Phys. Lett. B **716**, 30 (2012), 1207.7235

[11] G. Aad, B. Abbott, J. Abdallah, A.A. Abdelalim, A. Abdesselam, O. Abdinov, B. Abi, M. Abolins, O.S. AbouZeid, H. Abramowicz et al. (ATLAS Collaboration), Phys. Rev. Lett. **108**, 152001 (2012)

[12] J.D. Lykken, *Beyond the Standard Model* (2010), `1005.1676`

[13] M. Gell-Mann, Phys. Lett. **8**, 214 (1964)

[14] G. Zweig, *An SU(3) model for strong interaction symmetry and its breaking. Version 2* (1964), pp. 22–101

[15] S. Abachi et al. (D0), Phys. Rev. Lett. **74**, 2632 (1995), `hep-ex/9503003`

[16] R.L. Workman, Others (Particle Data Group), PTEP **2022**, 083C01 (2022)

[17] K. Nishijima, Prog. Theor. Phys. **13**, 285 (1955)

[18] O.W. Greenberg, Phys. Rev. Lett. **13**, 598 (1964)

[19] K.G. Wilson, Phys. Rev. D **10**, 2445 (1974)

[20] M. Neubert, *Heavy quark effective theory*, in *20th Johns Hopkins Workshop on Current Problems in Particle Theory: Non-Perturbative Particle Theory and Experimental Tests* (1996), pp. 39–78, `hep-ph/9610385`

[21] Y. Nambu, G. Jona-Lasinio, Phys. Rev. **122**, 345 (1961)

[22] J. Goldstone, A. Salam, S. Weinberg, Phys. Rev. **127**, 965 (1962)

[23] E. Eichten, K. Gottfried, T. Kinoshita, K.D. Lane, T.M. Yan, Phys. Rev. D **21**, 203 (1980)

[24] N.R. Soni, B.R. Joshi, R.P. Shah, H.R. Chauhan, J.N. Pandya, Eur. Phys. J. C **78**, 592 (2018), `1707.07144`

[25] V. Kher, R. Chaturvedi, N. Devlani, A.K. Rai, Eur. Phys. J. Plus **137**, 357 (2022), `2201.08317`

[26] A. Martin, Phys. Lett. B **93**, 338 (1980)

[27] C. Quigg, J.L. Rosner, Phys. Lett. B **71**, 153 (1977)

[28] J.L. Richardson, Phys. Lett. B **82**, 272 (1979)

[29] X.t. Song, H.f. Lin, Z. Phys. C **34**, 223 (1987)

[30] W. Lucha, F.F. Schoberl, Int. J. Mod. Phys. C **10**, 607 (1999), `hep-ph/9811453`

[31] J.E. Augustin et al. (SLAC-SP-017), Phys. Rev. Lett. **33**, 1406 (1974)

[32] J.J. Aubert et al. (E598), Phys. Rev. Lett. **33**, 1404 (1974)

[33] S.W. Herb et al. (E288), Phys. Rev. Lett. **39**, 252 (1977)

[34] W.R. Innes et al. (E288), Phys. Rev. Lett. **39**, 1240 (1977), [Erratum: Phys.Rev.Lett. 39, 1640 (1977)]

[35] B. Chen, A. Zhang, J. He, Phys. Rev. D **101**, 014020 (2020), `1910.06065`

[36] K. Han, T. Böhringer, P. Franzini, G. Mageras, D. Peterson, E. Rice, J.K. Yoh, J.E. Horstkotte, C. Klopfenstein, J. Lee-Franzini et al., Phys. Rev. Lett. **49**, 1612 (1982)

[37] G. Eigen, G. Blanar, H. Dietl, E. Lorenz, F. Pauss, H. Vogel, T. Böhringer, P. Franzini, K. Han, G. Mageras et al., Phys. Rev. Lett. **49**, 1616 (1982)

[38] C. Klopfenstein, J.E. Horstkotte, J. Lee-Franzini, R.D. Schamberger, M. Sivertz, L.J. Spencer, P.M. Tuts, P. Franzini, K. Han, E. Rice et al., Phys. Rev. Lett. **51**, 160 (1983)

[39] F. Pauss, H. Dietl, G. Eigen, E. Lorenz, G. Mageras, H. Vogel, P. Franzini, K. Han, D. Peterson, E. Rice et al., Physics Letters B **130**, 439 (1983)

[40] D. Besson, J. Green, R. Namjoshi, F. Sannes, P. Skubic, A. Snyder, R. Stone, A. Chen, M. Goldberg, N. Horwitz et al., Phys. Rev. Lett. **54**, 381 (1985)

[41] D.M.J. Lovelock, J.E. Horstkotte, C. Klopfenstein, J. Lee-Franzini, L. Romero, R.D. Schamberger, S. Youssef, P. Franzini, D. Son, P.M. Tuts et al., Phys. Rev. Lett. **54**, 377 (1985)

[42] P. del Amo Sanchez, J.P. Lees, V. Poireau, E. Prencipe, V. Tisserand, J. Garra Tico, E. Grauges, M. Martinelli, A. Palano, M. Pappagallo et al. (BABAR Collaboration), Phys. Rev. D **82**, 111102 (2010)

[43] J.P. Lees, V. Poireau, E. Prencipe, V. Tisserand, J. Garra Tico, E. Grauges, M. Martinelli, D.A. Milanes, A. Palano, M. Pappagallo et al. (The BABAR Collaboration), Phys. Rev. D **84**, 091101 (2011)

[44] I. Adachi, H. Aihara, K. Arinstein, D.M. Asner, T. Aushev, T. Aziz, A.M. Bakich, E. Barberio, K. Belous, V. Bhardwaj et al. (Belle Collaboration), Phys. Rev. Lett. **108**, 032001 (2012)

[45] V.M. Abazov, B. Abbott, B.S. Acharya, M. Adams, T. Adams, G.D. Alexeev, G. Alkhazov, A. Alton, G. Alverson, M. Aoki et al. (D0 Collaboration), Phys. Rev. D **86**, 031103 (2012)

[46] R. Aaij, , B. Adeva, M. Adinolfi, A. Affolder, Z. Ajaltouni, S. Akar, J. Albrecht, F. Alessio, M. Alexander et al., Journal of High Energy Physics **2014**, 088 (2014)

[47] G. Goldhaber et al., Phys. Rev. Lett. **37**, 255 (1976)

[48] I. Peruzzi et al., Phys. Rev. Lett. **37**, 569 (1976)

[49] S. Behrends et al. (CLEO), Phys. Rev. Lett. **50**, 881 (1983)

[50] J.C. Anjos et al. (Tagged Photon Spectrometer), Phys. Rev. Lett. **62**, 1717 (1989)

[51] V.M. Abazov et al. (D0), Phys. Rev. Lett. **99**, 172001 (2007), 0705.3229

[52] T. Aaltonen et al. (CDF), Phys. Rev. Lett. **100**, 082001 (2008), 0710.4199

[53] T. Aaltonen et al. (CDF), Phys. Rev. Lett. **102**, 102003 (2009), 0809.5007

[54] V.M. Abazov et al. (D0), Phys. Rev. Lett. **100**, 082002 (2008), 0711.0319

[55] R. Aaij et al. (LHCb), Phys. Rev. Lett. **110**, 151803 (2013), 1211.5994

[56] R. Aaij et al. (LHCb), Phys. Rev. D **94**, 072001 (2016), 1608.01289

[57] R. Aaij et al. (LHCb), Phys. Rev. D **92**, 032002 (2015), 1505.01710

[58] R. Aaij et al. (LHCb), Phys. Rev. Lett. **126**, 122002 (2021), 2011.09112

[59] H.J. Lipkin, Physics Letters B **195**, 484 (1987)

[60] R.L. Jaffe, Phys. Rev. D **15**, 267 (1977)

[61] R. Aaij et al. (LHCb), Phys. Rev. Lett. **125**, 242001 (2020), 2009.00025

[62] R. Aaij et al. (LHCb), Phys. Rev. D **102**, 112003 (2020), 2009.00026

[63] Z.Q. Liu et al. (Belle), Phys. Rev. Lett. **110**, 252002 (2013), [Erratum: Phys.Rev.Lett. 111, 019901 (2013)], 1304.0121

[64] T. Xiao, S. Dobbs, A. Tomaradze, K.K. Seth, Phys. Lett. B **727**, 366 (2013), 1304.3036

[65] X.L. Wang et al. (Belle), Phys. Rev. D **91**, 112007 (2015), 1410.7641

[66] R. Aaij et al. (LHCb), Eur. Phys. J. C **78**, 1019 (2018), 1809.07416

[67] T. Aaltonen et al. (CDF), Mod. Phys. Lett. A **32**, 1750139 (2017), 1101.6058

[68] V.M. Abazov et al. (D0), Phys. Rev. D **89**, 012004 (2014), 1309.6580

[69] J.P. Lees et al. (BaBar), Phys. Rev. D **86**, 051102 (2012), 1204.2158

[70] A. Bondar et al. (Belle), Phys. Rev. Lett. **108**, 122001 (2012), 1110.2251

[71] M. Ablikim et al. (BESIII), Phys. Rev. Lett. **106**, 072002 (2011), 1012.3510

[72] S.K. Choi et al. (Belle), Phys. Rev. Lett. **91**, 262001 (2003), hep-ex/0309032

[73] A. Esposito, A. Pilloni, A.D. Polosa, Phys. Rept. **668**, 1 (2017), 1611.07920

[74] X. Chen, X. Lü, Eur. Phys. J. C **75**, 98 (2015), 1411.3424

[75] X. Chen, X. Lü, Phys. Rev. D **97**, 114005 (2018)

[76] D. Ebert, R.N. Faustov, V.O. Galkin, Eur. Phys. J. C **58**, 399 (2008), 0808.3912

[77] R. Aaij et al. (LHCb), Phys. Rev. Lett. **115**, 072001 (2015), 1507.03414

[78] M.I. Eides, V.Y. Petrov, M.V. Polyakov, Eur. Phys. J. C **78**, 36 (2018), 1709.09523

[79] R. Aaij et al. (LHCb), Sci. Bull. **66**, 1278 (2021), 2012.10380

[80] R. Aaij et al. (LHCb), Phys. Rev. Lett. **128**, 062001 (2022), 2108.04720

[81] S. Scherer, M.R. Schindler (2005), hep-ph/0505265

[82] G. Ecker, *Quantum chromodynamics*, in *2005 European School of High-Energy Physics* (2006), hep-ph/0604165

[83] A.V. Smilga, *Lectures on quantum chromodynamics* (WSP, Singapore, 2001)

[84] D. Bailin, A. Love, *Introduction to Gauge Field Theory Revised Edition* (Taylor & Francis, 1993), ISBN 978-1-351-43700-4, 978-0-203-75010-0, 978-1-138-40639-1, 978-0-7503-0281-4

[85] M.E. Peskin, *An Introduction To Quantum Field Theory*, 1st edn. (CRC Press, 1995)

[86] M. Neubert, Phys. Rept. **245**, 259 (1994), hep-ph/9306320

[87] M. Shifman, A. Vainshtein, V. Zakharov, Nuclear Physics B **147**, 385 (1979)

[88] D. Zhou, H.X. Chen, L.S. Geng, X. Liu, S.L. Zhu, Phys. Rev. D **92**, 114015 (2015), 1506.00766

[89] H.X. Chen, Q. Mao, A. Hosaka, X. Liu, S.L. Zhu, Phys. Rev. D **94**, 114016 (2016), 1611.02677

[90] H.X. Chen, D. Zhou, W. Chen, X. Liu, S.L. Zhu, Eur. Phys. J. C **76**, 602 (2016), 1605.07453

[91] Z.G. Wang, Z.B. Wang, Chin. Phys. Lett. **25**, 444 (2008), 0710.5274

[92] P. Colangelo, A. Khodjamirian, pp. 1495–1576 (2000), hep-ph/0010175

[93] A.F. Falk, H. Georgi, B. Grinstein, M.B. Wise, Nucl. Phys. B **343**, 1 (1990)

[94] T. Kawanai, S. Sasaki, Phys. Rev. D **92**, 094503 (2015), 1508.02178

[95] K.D. Born, E. Laermann, N. Pirch, T.F. Walsh, P.M. Zerwas, Phys. Rev. D **40**, 1653 (1989)

[96] M. Sadzikowski, Phys. Lett. B **579**, 39 (2004), hep-ph/0307084

[97] A. Chodos, R.L. Jaffe, K. Johnson, C.B. Thorn, V.F. Weisskopf, Phys. Rev. D **9**, 3471 (1974)

[98] R. Casalbuoni, A. Deandrea, N. Di Bartolomeo, R. Gatto, F. Feruglio, G. Nardulli, Phys. Rept. **281**, 145 (1997), hep-ph/9605342

[99] A.V. Manohar, M.B. Wise, *Heavy quark physics*, Vol. 10 (2000), ISBN 978-0-521-03757-0

[100] M.B. Wise, *Heavy quark physics: Course*, in *Les Houches Summer School in Theoretical Physics, Session 68: Probing the Standard Model of Particle Interactions* (1997), pp. 1051–1089, hep-ph/9805468

[101] E.E. Jenkins, Nucl. Phys. B **412**, 181 (1994), hep-ph/9212295

[102] T. Mehen, R.P. Springer, Phys. Rev. D **72**, 034006 (2005), hep-ph/0503134

[103] D.B. Kaplan, M.J. Savage, M.B. Wise, Nucl. Phys. B **534**, 329 (1998), nucl-th/9802075

[104] G.F. Chew, S.C. Frautschi, Phys. Rev. Lett. **7**, 394 (1961)

[105] Y. Nambu, Phys. Rev. D **10**, 4262 (1974)

[106] Y. Nambu, Phys. Lett. B **80**, 372 (1979)

[107] H. Sazdjian, EPJ Web Conf. **137**, 02001 (2017), 1612.04078

[108] S. Scherer, Adv. Nucl. Phys. **27**, 277 (2003), hep-ph/0210398

[109] V. Koch, Int. J. Mod. Phys. E **6**, 203 (1997), nucl-th/9706075

[110] E. Santopinto, A. Giachino, Phys. Rev. D **96**, 014014 (2017), 1604.03769

[111] R. Aaij et al. (LHCb), Phys. Rev. Lett. **117**, 082003 (2016), [Addendum: Phys.Rev.Lett. 117, 109902 (2016), Addendum: Phys.Rev.Lett. 118, 119901 (2017)], 1606.06999

[112] A. Ali, J.S. Lange, S. Stone, Prog. Part. Nucl. Phys. **97**, 123 (2017), 1706.00610

[113] Z. Maki, M. Nakagawa, S. Sakata, Prog. Theor. Phys. **28**, 870 (1962)

[114] B. Pontecorvo, Zh. Eksp. Teor. Fiz. **53**, 1717 (1967)

[115] M. Kobayashi, T. Maskawa, Prog. Theor. Phys. **49**, 652 (1973)

[116] F. Abe et al. (CDF), Phys. Rev. Lett. **74**, 2626 (1995), `hep-ex/9503002`

[117] S. Abachi et al. (D0), Phys. Rev. Lett. **74**, 2632 (1995), `hep-ex/9503003`

[118] R. Aaij et al. (LHCb), Eur. Phys. J. C **81**, 601 (2021), `2010.15931`

[119] A.M. Sirunyan et al. (CMS), Phys. Rev. Lett. **126**, 252003 (2021), `2102.04524`

[120] B. Aubert, M. Bona, Y. Karyotakis, J.P. Lees, V. Poireau, E. Prencipe, X. Prudent, V. Tisserand, J. Garra Tico, E. Grauges et al. (BABAR Collaboration), Phys. Rev. Lett. **101**, 071801 (2008)

[121] B. Aubert et al. (BABAR), Phys. Rev. D **74**, 032007 (2006), `hep-ex/0604030`

[122] J.P. Lees et al. (BABAR), Phys. Rev. Lett. **124**, 152001 (2020), `1911.11740`

[123] M. Ablikim et al. (BESIII), Phys. Rev. Lett. **111**, 242001 (2013), `1309.1896`

[124] T.A. Aaltonen et al. (CDF), Phys. Rev. D **90**, 012013 (2014), `1309.5961`

[125] F. Abe et al. (CDF), Phys. Rev. Lett. **81**, 2432 (1998), `hep-ex/9805034`

[126] A.M. Sirunyan et al. (CMS), Phys. Rev. Lett. **122**, 132001 (2019), `1902.00571`

[127] S.K. Choi et al. (Belle), Phys. Rev. Lett. **91**, 262001 (2003), `hep-ex/0309032`

Chapter 2

Heavy Quark Effective Theory

2.1 Introduction

The recent experimental developments in the meson sector significantly challenge the basic quark model. The major challenge is that mesons consist of heavy quarks, i.e., heavy-light and heavy-heavy mesons. The spectra of light-light mesons are confirmed both through experimental observations and theoretical approaches. At the latest, heavy quark physics is an active area of high-energy physics. Several experimental facilities, LHCb, BESIII, BABAR, CDF, Belle, DO etc., are involved for analyzing mesons, and measurement provides information on their structures and properties [1–4, 4–19]. It is better to use theoretical methods to get complete details of mesons from experimental data. Heavy quark within meson helps us in exploring different QCD parameters. This heavy quark also helps describe heavy hadrons by formulating effective field theories at different energy scales. Each effective theory works well at a particular energy parameter and only gives precise results for that scale. Some examples of effective field theories are chiral perturbation theory, heavy quark effective theory, QCD sum rules, etc. The Lagrangian of these effective theories is formulated by QCD symmetries and adding interaction terms in the form of some expansion parameters. Experimental findings of heavy-heavy mesons are limited. Only a few states are experimentally observed. So, we are motivated to explore the heavy-light mesons, i.e., charm and bottom mesons. Analyzing heavy-light mesons provides a better understanding of the role of strong interactions in calculating hadronic properties. For analysis, we have two QCD symmetries: one is heavy quark symmetry, and another one is chiral symmetry inherent in light quarks. These two symmetries are used to construct a theoretical framework known as the Heavy Quark Effective Theory (HQET). In the present chapter, we will explore HQET as a quantum field theory employed to calculate the spectra of the charm and bottom mesons. HQET is a phenomenological theory formulated to extract properties of hadrons having a heavy quark (c, b) bonded by gluon dynamics [20–23].

Heavy-light mesons consist of a heavy quark (Q) coupled with an antiquark ($\bar{q}$), as well as gluons and quark-antiquark pairs. The other components, excluding the heavy quark, are collectively referred to as the light degree of freedom (l). As we know, Λ_{QCD} is the energy scale that arises from QCD dynamics, and its value is approximately 200 MeV. The interaction between the heavy quark Q and the light degree of freedom occurs through momentum exchange, and the momentum of the heavy quark [23–26] is determined by:

$$p_Q = m_Q v + K \tag{2.1}$$

where v denotes the velocity of a heavy quark, while K represents the small residual momentum that arises from the off-shell interaction between a heavy quark and light degrees of freedom. K is order of Λ_{QCD}. This K basically depicts the momentum of light constituents. Thus, in strong interaction processes, momentum exchanged between heavy quark and light degree of freedom is the order of Λ_{QCD}. This leads to a change in the velocity of heavy quark expressed as $\Delta v = \frac{p}{m_Q}$. This Δv is very small, which shows the velocity of heavy quarks remains constant during interaction processes. Any variation in the velocity of heavy quarks is the consequence of non-QCD effects such as weak and electromagnetic interactions.

The system of a heavy-light meson is similar to the hydrogen atom in the first approximation, where the proton is the static source of the electromagnetic field and can only emit or absorb photons, whereas other recoil effects can be ignored. In a similar manner, the heavy quark assumes the role analogous to that of the proton, while the light constituents act as electron clouds. The heavy quark is viewed as a stationary external source for the light degree of freedom, transferring as a color triplet. The dynamics of the light degree of freedom involve non-perturbative interactions among its constituents, yet the interaction with the heavy quark Q has been simplified for clarity.

Thus, in the limit, $m_Q \to \infty$, light constituents cannot feel the mass of heavy quark, which leads to the emergence of $U(N_H)$ flavor heavy quark symmetry. This symmetry implies dynamics remain unaffected under the exchange of heavy quark (b or c). Also, in the limit $m_Q \to \infty$, heavy quark interacts with gluons via chromoelectric charge, making a system of heavy-light meson independent of the spin orientation of heavy quark. This arises $SU(2)$ heavy quark symmetry. Embedding both symmetries, i.e., $U(N_H)$ flavor heavy quark symmetry and $SU(2)$ heavy quark symmetry, results in large $SU(2N_H)$ spin-flavor symmetry [27–29]. However, the $1/m_Q$ corrections lead to the breaking of $SU(2N_H)$ symmetry, which will be discussed later in this chapter.

2.2 Quantum Numbers

To study heavy-light mesons ($Q\bar{q}$), it is crucial to know about their spectroscopy. Several quantum numbers are involved in specifying $Q\bar{q}$ mesons. The heavy-light mesons are labeled as $nL_{s_l}J^P$, where "n" represents the radial quantum number, "J" represents the system's total angular momentum, and "P" signifies the parity of the system. In the infinity mass limit ($m_Q \to \infty$), the spin of light quarks becomes independent of the spin of heavy quark (S_Q). Consequently, the total angular momentum of the light degree of freedom persists as a conserved quantity [25, 30]. The total angular momentum of the light degree of freedom is given by:

$$\overrightarrow{S}_l = \overrightarrow{S}_q + \overrightarrow{L} \tag{2.2}$$

, where $\overrightarrow{S}_q$ signifies spin of light quark (1/2) and $\overrightarrow{L}$ denotes total orbital momentum of light quarks. The total angular momentum of heavy-light mesons is given by

$$\overrightarrow{J} = \overrightarrow{S}_l + \overrightarrow{S}_Q \tag{2.3}$$

The quantum values j, s_Q and s_l serves as eigenvalues of the operators $\mathbf{J}^2, \mathbf{S_Q^2}, \mathbf{S}_l^2$ as $\mathbf{J}^2 = j(j+1)$, $\mathbf{S_Q^2} = s_Q(s_Q+1)$ and $\mathbf{S}_l^2 = s_l(s_l+1)$ for the $Q\overline{q}$ system. Eq.(2.3) reveals that heavy light meson manifest in doublets exhibiting total angular momentum $j_\pm = s_l \pm 1/2$. For ground state, $L = 0$, total angular momentum of light constituents is $\overrightarrow{S}_l = 1/2$ ($\overrightarrow{S}_l = 1/2 + 0 = 1/2$) and spin of heavy quark $\overrightarrow{S}_Q = 1/2$.

Thus J^P for ground state comes as $\frac{1}{2} \otimes \frac{1}{2} = 0^- \oplus 1^-$, with P $= (-1)^{L+1}$, representing parity of system. Ground states of heavy-light meson are notated as D and

D^* when heavy quark (Q) is charm quark. Similarly, ground states are notated by B and B^* if the heavy quark is the bottom quark. The field operators responsible for annihilating the ground states of heavy-light mesons are denoted as $P^{(Q)}$ for spin 0 pseudoscalars and $P_\mu^{*(Q)}$ for spin 1 vector mesons. In the same manner, for P-wave mesons having $L = 0$, the total angular momentum of light constituents is given as:

$$S_l = \frac{1}{2} \otimes 1 = \begin{cases} \frac{1}{2} \\ \frac{3}{2} \end{cases}$$

Value of $S_l = 1/2$ corresponds two degenerate states $(0^+, 1^+)$ and represented by $(P_0^*, P_1^{'})$ and $S_l = 3/2$ give two degenerate states $(1^+, 2^+)$ and notated by (P_1, P_2^*). In $m_Q \to \infty$, 1^+ states corresponds to $S_l = 1/2$ and $S_l = 3/2$ mix with angle $35.3°$ [31]. Although they can be identified by their different angular momentum of light constituents and different decay angular distribution. The natural parity is defined as $P = (-1)^J$ corresponds to cases where J^P takes values like $0^+, 1^-, 2^+$ etc., and unnatural parity is defined as $P = (-1)^{J+1}$ associated with J^P states $0^-, 1^+, 2^-$ etc.

2.2.1 Representation of Fields

In the above section, we come to know that each value of S_l forms two degenerate states under heavy quark symmetry. It is convenient to develop a formalism in which degenerate multiplets can be treated as a single entity in the form of fields that transform linearly under heavy quark symmetry.

So, we will delineate each S_l corresponding to $L = 0, 1, 2, 3$ in terms of fields. The ground state of meson comprises two degenerate states $(0^-, 1^-)$, in which 0^- state (pseudoscalar meson) is denoted by P and 1^- state (vector meson) is denoted by P_i^* [25, 32]. The expressions are :

$$P_i = \bar{q}\gamma_5 h_v^i \sqrt{M_P} \tag{2.4}$$

$$P_i^* = \bar{q}\not{\epsilon} h_v^i \sqrt{M_{P^*}} \tag{2.5}$$

where h_v^i is a heavy quark field, and v is the four-vector velocity of meson. ϵ is the polarization vector of vector particle and follows $\epsilon \cdot \epsilon = -1$, $v \cdot \epsilon = 0$. These two fields are combined in a single field H in such a way:

$$H = \frac{i\not{D} + m_P}{2m_P}[\gamma^\mu P_\mu^* + iP\gamma^5] \tag{2.6}$$

Where m_P represents the mass of the heavy-light meson. In infinity mass limit, the term $\frac{i\not{D}+m_P}{2m_P}$ convert to projection operator $\frac{1+\not{v}}{2}$. So the expression for field H is given as:

$$H = \frac{1+\not{v}}{2}[\gamma^\mu P^*_\mu + iP\gamma^5] \tag{2.7}$$

This ground state field H is constructed by the combination of P and P^*_μ fields. It annihilates $S_l = 1/2$ meson doublets and transforms as a bispinor under the Lorentz transformation:

$$H'(x') = D(\Lambda)H(x)D(\Lambda)^{-1}, \qquad x' = \Lambda x \tag{2.8}$$

here $D(\Lambda)$ is the 4×4 Lorentz transformation matrix for spinors so that

$$H(x) \to H'(x) = D(\Lambda)H(\Lambda^{-1}x)D(\Lambda)^{-1} \tag{2.9}$$

The expression $\frac{1+\not{v}}{2}$ provides the particle aspect of the heavy quark Q and the relative phase between the P and P^*_μ states depends on choice of phase between the pseudoscalar and vector meson states [32–34].

The field as denoted in Eq.(2.7) retains its invariance under Lorentz transformation, where γ^5 and γ^μ transform the pseudoscalar field P and the vector field P^*_μ into bispinors respectively.

By the relations $\not{v}(1+\not{v}) = (1+\not{v})$ and $v.P^* = 0$, this field also follow the relations

$$\not{v}H = H \qquad \text{and} \qquad H\not{v} = -H$$

The conjugate field Of H is given by $\overline{H}$ and expression for it is given as:

$$\overline{H} = \gamma^0 H^\dagger \gamma^0 = [P^{*\dagger}_\mu \gamma^\mu + iP^\dagger \gamma^5]\frac{1+\not{v}}{2} \tag{2.10}$$

Because of $\gamma^0 D(\Lambda)^\dagger \gamma^0 = D(\Lambda)^{-1}$, conjugate field $\overline{H}$ also transforms as a bispinor

$$\overline{H}'(x) = D(\Lambda)\overline{H}((\Lambda)^{-1}x)D(\Lambda)^{-1} \tag{2.11}$$

and satisfies the relations

$$\overline{H}\not{v} = \overline{H} \qquad \text{and} \qquad \not{v}\overline{H} = -\overline{H}$$

In same manner, the P-wave doublets $(0^+, 1^+)_{1/2}$ and $(1^+, 2^+)_{3/2}$ are denoted by fields "S" and "T" respectively [35–37] and expressions are:

$$S = \frac{1+\not{v}}{2}\{P_1'^{\mu}\gamma_\mu\gamma_5 - P_0^*\} \tag{2.12}$$

$$T^\mu = \frac{1+\not{v}}{2}\{P_2^{*\mu\nu}\gamma_\nu - P_{1\nu}\sqrt{\frac{3}{2}}\gamma_5[g^{\mu\nu} - \frac{\gamma^\nu(\gamma^\mu - v^\mu)}{3}]\}. \tag{2.13}$$

obeying

$$\not{v}S = S\not{v} = S, \quad \not{v}T^\mu = -T^\mu\not{v} = T^\mu, \quad \not{v}\overline{S} = \overline{S}\not{v} = \overline{S} \quad -\not{v}\overline{T}^\mu = \overline{T}^\mu\not{v} = \overline{T}^\mu$$

Field S consists of scalar P_0^* and axial vector state $P_1^{'\mu}$, while T field is constructed by axial vector $P_{1\nu}$ and tensor $P_2^{*\mu\nu}$ states.

The doublets corresponding to the excited D-wave ($l = 2$) states are designated as (P_1^*, P_2) and $(P_2^{'}, P_3^*)$ associated with $J_{s_l}^P = (1^-, 2^-)_{\frac{3}{2}}$ and $(2^-, 3^-)_{\frac{5}{2}}$ respectively. Additionally, the doublets of F-wave ($l = 3$) are expressed by (P_2^*, P_3) and $(P_3^{'}, P_4^*)$ associated with $J_{s_l}^P = (2^+, 3^+)_{\frac{5}{2}}$ and $(3^+, 4^+)_{\frac{7}{2}}$ respectively. In correspondence to the Eqs.(2.7), 2.12, 2.13, these doublets are expressed by the effective field X_a, Y_a, Z_a and R_a [36, 37] as:

$$X_a^\mu = \frac{1+\not{v}}{2}\{P_{2a}^{\mu\nu}\gamma_5\gamma_\nu - P_{1a\nu}^*\sqrt{\frac{3}{2}}[g^{\mu\nu} - \frac{\gamma^\nu(\gamma^\mu + \gamma^\mu)}{3}]\} \tag{2.14}$$

$$Y_a^{\mu\nu} = \frac{1+\not{v}}{2}\{P_{3a}^{*\mu\nu\sigma}\gamma_\sigma - P_{2a}^{'\alpha\beta}\sqrt{\frac{5}{3}}\gamma_5[g_\alpha^\mu g_\beta^\nu - \frac{g_\beta^\nu\gamma_\alpha(\gamma^\mu - v^\mu)}{5} - \frac{g_\alpha^\mu\gamma_\beta(\gamma^\nu - v^\nu)}{5}]\} \tag{2.15}$$

$$Z_a^{\mu\nu} = \frac{1+\not{v}}{2}\{P_{3a}^{\mu\nu\sigma}\gamma_5\gamma_\sigma - P_{2a}^{*\alpha\beta}\sqrt{\frac{5}{3}}[g_\alpha^\mu g_\beta^\nu - \frac{g_\beta^\nu\gamma_\alpha(\gamma^\mu + v^\mu)}{5} - \frac{g_\alpha^\mu\gamma_\beta(\gamma^\nu + v^\nu)}{5}]\} \tag{2.16}$$

$$R_a^{\mu\nu\rho} = \frac{1+\not{v}}{2}\{P_{4a}^{*\mu\nu\rho\sigma}\gamma_5\gamma_\sigma - P_{3a}^{'\alpha\beta\tau}\sqrt{\frac{7}{4}}[g_\alpha^\mu g_\beta^\nu g_\tau^\rho - \frac{g_\beta^\nu g_\tau^\rho\gamma_\alpha(\gamma^\mu - v^\mu)}{7} - \frac{g_\alpha^\mu g_\tau^\rho\gamma_\beta(\gamma^\nu - v^\nu)}{7} - \frac{g_\alpha^\mu g_\beta^\nu\gamma_\tau(\gamma^\rho - v^\rho)}{7}]\} \tag{2.17}$$

The specified indices a or b in the fields expressions are $SU(3)$ flavor index (u, d or s). For the radially excited states ($n = 2$), the mesonic state is replaced by a tilde "$\sim$" sign on their head i.e. $\widetilde{P}, \widetilde{P}^*$ and so on. The equation governing the effective fields for radially excited doublets retains its form with replacement by $\widetilde{H}$, $\widetilde{S}$, $\widetilde{T}$, $\widetilde{X}$, etc. Similarly, for radially excited states $n = 3$, the mesonic state is replaced by a tilde "$\approx$" sign on their head i.e.$\tilde{\tilde{P}}$, $\tilde{\tilde{P}}^*$ and so on. These effective fields (H, S, T, X, Y, R) introduced for each doublet of heavy-light meson interact with themselves and with light pseudoscalar or vector or both mesons. The interaction between heavy-light mesons and light pseudoscalar mesons is described with $\xi = \exp\left[\frac{2i\mathcal{M}}{f}\right]$; $\Sigma = \xi^2$ with the hermitian matrix $\mathcal{M}$ incorporates π, η, K fields [32, 37]. Similarly, the interaction of light vector mesons with heavy-light mesons is defined with $\rho_\mu = \frac{ig_v}{\sqrt{2}}\hat{\rho}_\mu$, $\hat{\rho}_\mu$ is hermitian matrix incorporates fields of ρ, ϕ, K^* vector meson [38, 39]. In this thesis, spectroscopy of heavy-light mesons with emission light pseudoscalar mesons has been studied. The chiral perturbation theory subsection explains light pseudoscalar mesons' details, interactions, and fields.

2.3 Effective Feynman Rules in $m_Q \to \infty$

To describe Feynman's rules for heavy quark, HQS (heavy quark symmetry) can be incorporated in the theory of strong interactions (QCD). A system consisting of heavy quark with mass m_Q and moving with velocity v_μ, momentum of system can be defined as $p_\mu = m_Q v_\mu$. As we know, the momentum of the heavy quark is approximately equal to the bound state of a heavy-light meson ($Q\bar{q}$) as in Eq.(2.1) [22, 40]. The velocity of the heavy quark is given by:

$$v_Q^\mu = \frac{p^\mu}{m_Q} = v^\mu + \frac{k^\mu}{m_Q} \tag{2.18}$$

The momentum of an on-shell heavy quark carries almost all the momentum of the meson state. During QCD interactions, the velocity of a heavy quark almost remains the same. And QCD fermion propagator $\frac{i}{\not{p}-m_Q}$ is simplified using on shell condition as follows: by

$$\frac{i}{\not{p}-m_Q} = \frac{i(\not{p}+m_Q)}{p^2-m_Q^2} = \frac{i(m_Q\not{v}+\not{k}+m_Q)}{2m_Q v.k+k^2} \simeq \frac{i}{v.k}\frac{1+\not{v}}{2} \tag{2.19}$$

The propagator consists of a velocity-dependent projection operator $P_+ = \frac{1+\not{v}}{2}$ which depicts particle component of Dirac spinor. The projection operator P_- is defined for the antiquark particle as: $P_- = \frac{1-\not{v}}{2}$. These operators P_+ and P_- obeys following relations:

$$P_\pm P_\mp = 0, \qquad P_\pm^2 = P_\pm \qquad \text{and}$$
$$P_+\gamma_\mu P_+ = P_+ v_\mu P_+.$$

The last relation shows that it is possible to estimate the coupling between the heavy quark and gluons. The quark-gluon vertex of QCD denoted as $igT_a\gamma^\mu$ can be convert as follows at the leading order in $\frac{1}{m_Q}$:

$$igT_a\gamma^\mu = igT_a v^\mu \tag{2.20}$$

where g is the QCD strong coupling constant and T_a are $SU(3)$ color generators. The depicted Fig 2.1 shows effective Feynman rules [41, 42] governing the heavy quark propagator and heavy quark-gluon vertex. The heavy quark propagator illustrated in the aforementioned figure is delineated by a double line, serving to distinguish it

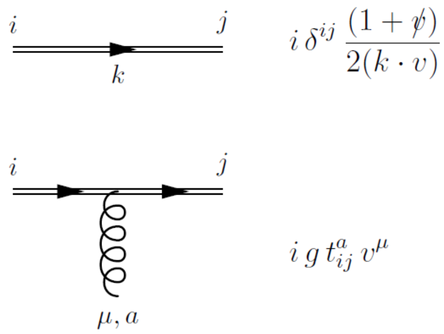

Figure 2.1: Modified Feynman rules for the heavy quark effective theory (i, j, a are color indices.).

from the QCD propagator.

In modified Feynman rules, the disappearance of the heavy quark mass term, reflects the incorporation of the heavy quark flavor symmetry into the picture. Also, the absence of gamma matrices in the modified rules signifies the manifestation of heavy quark spin symmetry. This projection operator changes to $\frac{1+\gamma^0}{2}$ in the static frame of heavy quark, projecting the quark component of four vector Dirac spinor. In this rest frame, the phenomenon becomes non-relativistic, and hence the propagator and charge density can be approximated as [42],

$$\frac{i}{v.k} \to \frac{i}{k^0} = \frac{i}{E - m_Q} \tag{2.21}$$

$$-igv^\mu T_a = -ig\delta^{\mu 0} T_a. \tag{2.22}$$

The next section will use these modified Feymann rules to construct the general Lagrangian for the heavy quark effective theory.

2.4 General Lagrangian of HQET

The symmetries associated with heavy quarks can be incorporated in the Lagrangian by expanding the effective Lagrangian in powers of $1/m_Q$. In the limit $m_Q \to \infty$, the heavy quark field Q with four velocity v^μ in terms of velocity-dependent components (h_v^Q and H_v^Q) [40–42] can be expressed as

$$Q = e^{-im_Q v.x}(h_v^Q + H_v^Q) \tag{2.23}$$

with

$$h_v(x) = e^{im_Q v.x}\frac{1+\not{v}}{2}Q(x) \tag{2.24}$$

$$H_v(x) = e^{im_Q v.x}\frac{1-\not{v}}{2}Q(x) \tag{2.25}$$

where $h_v(x)$ and $H_v(x)$ are smaller and larger components of quark field Q, respectively. From phase factor $\exp(im_Q v.x)$ of equations 2.244, 2.25 the derivative over H_v^Q and $h_v(x)$ give momentum k, called as residual momentum. The relation $v.v = 1$ is convenient to impose to obey on shell condition on Q. On applying this constraint, fields H_v^Q and $h_v(x)$ obeys following projection properties:

$$\not{v}h_v^Q = h_v^Q \tag{2.26}$$

$$\not{v}H_v^Q = -H_v^Q \tag{2.27}$$

The field h_v^Q provides large two components of the heavy quark field Q whereas H_v^Q provides smaller two components in the rest frame of heavy hadron. h_v^Q annihilates a heavy quark with velocity v while H_v^Q creates a heavy anti-quark with velocity v.

By exploiting definitions of h_v^Q and H_v^Q in QCD Lagrangian [40, 43, 44], we can construct HQET Lagrangian in term of $\frac{1}{m_Q}$:

$$L_{QCD} = \overline{h}_v i\not{D}h_v + \overline{H}_v(i\not{D} - 2m_Q)H_v + \overline{h}_v(i\not{D} - 2m_Q)H_v + \overline{H}_v i\not{D}h_v \tag{2.28}$$

On applying Feymann rules and using projection relations Eqs.(2.26),2.27), the first term for the above Lagrangian becomes as:

$$\overline{h}(\frac{1+\not{v}}{2})(i\gamma^\mu D_\mu)(\frac{1+\not{v}}{2})h = \overline{h}(iv.D)(\frac{1+\not{v}}{2})h = \overline{h}(iv.D)h \tag{2.29}$$

and the $\mathscr{L}_{eff}$ changes

$$\mathscr{L}_{eff} = \overline{h}_v iv.Dh_v - \overline{H}_v(iv.D + 2m_Q)H_v + \overline{h}_v i\not{D}_\perp H_v + \overline{H}_v i\not{D}_\perp h_v \tag{2.30}$$

We proposed perpendicular component $D_\perp^\mu = D^\mu - v^\mu v.D$ in the above Lagrangian and it presents the spatial part of the covariant derivative in the limit $m_Q \to \infty$. It also follows $v.D_\perp = 0$. This Lagrangian consists of fields h_v and H_v in which h_v illustrate the massless degree of freedom, while H_v field represents fluctuations with mass $2m_Q$. The third and fourth terms in the lagrāngian refer to pair creation and annihilation of heavy quarks and heavy anti-quarks. These virtual processes describing pair creation of heavy quark are shown in Figure 2.2

For the formation of effective theory, it is necessary to remove mass dependence of

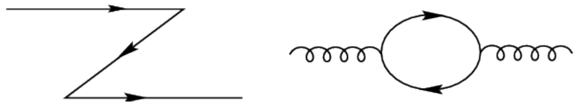

Figure 2.2: Virtual processes for pair creation of heavy quark.

heavy quark (H_v) [23, 45]. To get rid of the heavy degree of freedom, we use the equation of motion, which results in the following:

$$\frac{\partial \mathscr{L}}{\partial \overline{H}} = -(iv.D + 2m_Q)H + (i\not{D}_\perp)h = 0 \tag{2.31}$$

On solving eq.2.31

$$H_v = \frac{1}{2m_Q + iv.D} i\not{D}_\perp h_v \tag{2.32}$$

By inserting value of eq.2.32 in eq.2.30 effective Lagrangian in terms of h_v is given as:

$$\mathscr{L}_{eff} = \overline{h}_v iv.Dh_v + \overline{h}_v i\not{D}_\perp \frac{1}{2m_Q + iv.D} i\not{D}_\perp h_v \tag{2.33}$$

The second term in eq. 2.33 specifies the virtual fluctuations due to heavy quark degree of freedom as illustrated in Figure 2.2. Taylor series expansion in powers of $\frac{i\not{D}_\perp}{m_Q}$ of the above Lagrangian is given by:

$$\mathscr{L}_{eff} = \overline{h}_v iv.Dh_v + \frac{1}{2m_Q}\sum_{m=0}^{\infty} \overline{h}_v i\not{D}_\perp \left(-\frac{iv.D}{2m_Q}\right)^m i\not{D}_\perp h_v \tag{2.34}$$

Further, this expression can be more simplified for $m = 0$ with the standard gamma matrix identities:

$$\not{D}_\perp \not{D}_\perp = D_\perp^2 + \frac{1}{2}[\gamma_\mu, \gamma_\nu] D_\perp^\mu D_\perp^\nu = D_\perp^2 + \frac{1}{4}[\gamma_\mu, \gamma_\nu][D_\perp^\mu, D_\perp^\nu] \tag{2.35}$$

with the identities $[D_\perp^\mu, D_\perp^\nu] = igG^{\mu\nu}$, $[\gamma_\mu, \gamma_\nu] = -\frac{i}{2}\sigma_{\mu\nu}$ and $\overline{h}\sigma_{\mu\nu}v^\mu h = 0$, HQET Lagrangian in $\frac{1}{m_Q}$ order is derived as follow:

$$\mathscr{L}_{eff} = \overline{h}_v iv.Dh_v + \frac{1}{2m_Q}\overline{h}_v (iD_\perp)^2 h_v + \frac{g}{4m_Q}\overline{h}_v \sigma_{\mu\nu} G^{\mu\nu} h_v + \mathcal{O}\left(\frac{1}{m_Q^2}\right) \tag{2.36}$$

By including power corrections, it is expressed as:

$$\mathscr{L}_{HQET} = \mathscr{L}_0 + \frac{1}{m_Q}\mathscr{L}_1 + \frac{1}{m_Q^2}\mathscr{L}_2 + ... \tag{2.37}$$

Retaining only the quark component h_v^Q, effective Lagrangian at the leading order in limit $m_Q \to 0$ is

$$\mathscr{L}_{eff} = \overline{h}_v iv.Dh_v = \overline{h}_v (iv^\mu \partial_\mu + gT_a v^\mu A_\mu^a) h_v \tag{2.38}$$

where $D_\mu = \partial_\mu - igT_a v^\mu A_\mu^a$ is the gauge covariant derivative [40, 45]. Now the

Lagrangian no longer depends on heavy quark mass ultimately exhibits the heavy quark flavor symmetry. Also, leading order Lagrangian does not contain Dirac gamma matrices since they are being replaced by the velocity v of the heavy quark. Thus, the Lagrangian under the $SU(2)$ spin symmetry group is invariant.

The flavor and spin symmetry of the heavy quark is preserved by the leading order term of the Lagrangian, which is the first term in Eq.(2.36). The second term in equation 2.36 arises from the off-shell residual momentum of the heavy quark and describes the heavy quark kinetic energy in the non-relativistic model. This term is of order $(\frac{1}{m_Q})^1$ breaks the heavy quark flavor symmetry. The third term in this Lagrangian breaks both the heavy quark spin and flavor symmetry as it describes the chromo-magnetic moment interaction of the heavy quark spin with gluon field [46, 47].

2.4.1 Chiral Perturbation Theory

In this section, we discuss the chiral Lagrangian describing low momentum interactions of pions (π, η, K) with hadron having a heavy quark. When masses of light quarks are approaching zero, QCD Lagrangian exhibits $SU(3)_L \otimes SU(3)_R \otimes U(1)_V$ chiral symmetry. But, due to finite masses of these light quarks (u, d, s), the symmetry $SU(3)_L \otimes SU(3)_R$ breaks into $SU(3)_V$ subgroup. The spontaneous breaking of chiral symmetry gives eight Goldstone bosons $\pi^{\pm,0}, K^{\pm,0}, \bar{K}^0$ and η [32, 33]. These bosons are treated as Goldstone bosons and identified as octets of pseudoscalar mesons with $J^P = 0^-$. This octet consists of π, η as non-strange mesons and K as strange mesons. Interaction among these Goldstone bosons is described by chiral perturbation theory [35, 44, 48, 49]. These observed bosons are represented by unitary matrices of order 3× 3, described by $\Sigma = \xi^2$, $\Sigma \in \mathrm{SU(3)}$ and ξ is defined as:

$$\xi = \exp\left[\frac{2i\mathcal{M}}{f}\right] \tag{2.39}$$

where $\mathcal{M}$ is a 3×3 hermitian traceless matrix

$$\mathcal{M} = \begin{pmatrix} \frac{1}{\sqrt{2}}\pi^0 + \frac{1}{\sqrt{6}}\eta & \pi^+ & K^+ \\ \pi^- & -\frac{1}{\sqrt{2}}\pi^0 + \frac{1}{\sqrt{6}}\eta & K^0 \\ K^- & \overline{K}^0 & -\sqrt{\frac{2}{3}}\eta \end{pmatrix} \tag{2.40}$$

and $f = 130\ MeV$ is the pion decay constant. Under chiral symmetry $SU(3)_L \otimes SU(3)_R$, the octet field transforms as

$$\Sigma \rightarrow L\Sigma R^\dagger$$

with L and R represents the global elements of $SU(3)_L$ and $SU(3)_R$. This ξ field under the chiral limit $SU(3)_L \otimes SU(3)_R$ transforms as

$$\xi \rightarrow L\xi U^\dagger = U\xi R^\dagger$$

with U being the special unitary matrix depending on L, R, and the mesonic field $\mathcal{M}$.

By including matter fields in ξ, chiral theory becomes more useful and more information can be extracted [50–53]. At the leading order, interactions of π, η, K with heavy-light meson field can be described by Lagrangian and the form of this Lagrangian is given by

$$\begin{aligned}\mathcal{L} = iTr[\overline{H}_b v^\mu D_{\mu ba} H_a] + \frac{f_\pi^2}{8} Tr[\partial^\mu \Sigma \partial_\mu \Sigma^+] + Tr[\overline{S_b}(iv^\mu D_{\mu ba} - \delta_{ba}\Delta_S)S_a] \\ + Tr[\overline{T_b^\alpha}(iv^\mu D_{\mu ba} - \delta_{ba}\Delta_T)T_{a\alpha} + Tr[\overline{X_b^\alpha}(iv^\mu D_{\mu ba} - \delta_{ba}\Delta_X)X_{a\alpha} \\ + Tr[\overline{Y_b^{\alpha\beta}}(iv^\mu D_{\mu ba} - \delta_{ba}\Delta_Y)Y_{a\alpha\beta} + Tr[\overline{R_b^{\alpha\beta\rho}}(iv^\mu D_{\mu ba} - \delta_{ba}\Delta_R)R_{a\alpha\beta\rho}]\end{aligned} \quad (2.41)$$

The indices a, and b are light quark flavor indices (u, d, s). This is general Lagrangian for heavy-light mesons and remains invariant under chiral symmetry and heavy quark symmetry. The covariant derivative $D_{\mu ab} = -\delta_{ab}\partial_\mu + \mathcal{V}_{\mu ab} = -\delta_{ab}\partial_\mu + \frac{1}{2}(\xi^+\partial_\mu\xi + \xi\partial_\mu\xi^+)_{ab}$ and axial vector field $A_{\mu ab} = \frac{i}{2}(\xi\partial_\mu\xi^\dagger - \xi^\dagger\partial_\mu\xi)_{ab}$. This covariant derivative and axial vector field describe the coupling of Goldstone bosons with mesons. Explicit breaking of chiral symmetry can modify this Lagrangian. The details of the modified Lagrangian and incorporated corrections are discussed in Chapter 3.

2.5 Leading Order Chiral Lagrangian

Different states of heavy-light mesons interact via the exchange of goldstone bosons (π, η, K). These interactions arise by interactions among ground states, excited states, or between ground states and excited states. When the same field doublets, e.g., ground states doublets P, P^* interact within themselves via goldstone bosons in the following way:$P^* \rightarrow P + G$, that emitted goldstone boson (G) is virtual because such processes are kinematically forbidden. But when different field doublets (P, P_0^*) interact via exchanging goldstone bosons, emitted bosons may be observed because it is a kinematically allowed process. The thesis aims to analyze the strong interactions of heavy-light mesons and determine their properties like strong coupling constants, decay widths, and branching ratios.

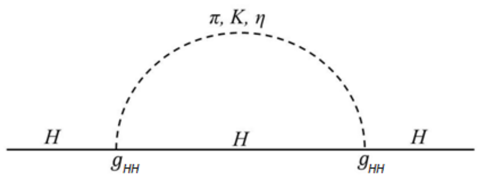

(a) Interaction of ground state fields via pseudoscalar mesons.

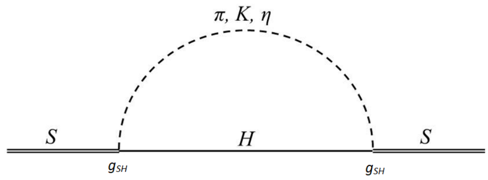

(b) Interaction of excited states with ground state via pseudoscalar mesons.

Two body strong interactions via π, η, K (light pseudoscalar meson) can be deduced from heavy meson chiral Lagrangian L_{HH}, L_{SH}, L_{TH}, L_{XH}, L_{YH}, L_{ZH} and these interaction terms [54] are expressed as:

$$L_{HH} = g_{HH} Tr\{\overline{H}_a H_b \gamma_\mu \gamma_5 A^\mu_{ba}\} \tag{2.42}$$

$$L_{SH} = g_{SH} Tr\{\overline{H}_a S_b \gamma_\mu \gamma_5 A^\mu_{ba}\} + h.c. \tag{2.43}$$

$$L_{TH} = \frac{g_{TH}}{\Lambda} Tr\{\overline{H}_a T^\mu_b (iD_\mu \not{A} + i\not{D} A_\mu)_{ba} \gamma_5\} + h.c. \tag{2.44}$$

$$L_{XH} = \frac{g_{XH}}{\Lambda} Tr\{\overline{H}_a X^\mu_b (iD_\mu \not{A} + i\not{D} A_\mu)_{ba} \gamma_5\} + h.c. \tag{2.45}$$

$$L_{YH} = \frac{1}{\Lambda^2} Tr\{\overline{H}_a Y^{\mu\nu}_b [k^Y_1 \{D_\mu, D_\nu\} A_\lambda + k^Y_2 (D_\mu D_\lambda A_\nu + D_\nu D_\lambda A_\mu)]_{ba} \gamma^\lambda \gamma_5\} + h.c. \tag{2.46}$$

$$L_{ZH} = \frac{1}{\Lambda^2} Tr\{\overline{H}_a Z^{\mu\nu}_b [k^Z_1 \{D_\mu, D_\nu\} A_\lambda + k^Z_2 (D_\mu D_\lambda A_\nu + D_\nu D_\lambda A_\mu)]_{ba} \gamma^\lambda \gamma_5\} + h.c. \tag{2.47}$$

$$L_{RH} = \frac{1}{\Lambda^3} Tr\{\overline{H}_a R^{\mu\nu\rho}_b [k^R_1 \{D_\mu, D_\nu D_\rho\} A_\lambda + k^R_2 (\{D_\mu, D_\rho\} D_\lambda A_\nu + \{D_\nu, D_\rho\} D_\lambda A_\mu + \{D_\mu, D_\nu\} D_\lambda A_\rho)]_{ba} \gamma^\lambda \gamma_5\} + h.c. \tag{2.48}$$

In these equations $D_\mu = \partial_\mu + V_\mu$, $\{D_\mu, D_\nu\} = D_\mu D_\nu + D_\nu D_\mu$ and $\{D_\mu, D_\nu D_\rho\} = D_\mu D_\nu D_\rho + D_\mu D_\rho D_\nu + D_\nu D_\mu D_\rho + D_\nu D_\rho D_\mu + D_\rho D_\mu D_\nu + D_\rho D_\nu D_\mu$. $\Lambda = 1\ GeV$ is the chiral symmetry breaking parameter. Here g_{HH}, g_{SH}, g_{TH}, $g_{YH} = k^Y_1 + k^Y_2$ and $g_{ZH} = k^Z_1 + k^Z_2$ are strong coupling constants. For radially excited states, these chiral Lagrangians are notated by $L_{\widetilde{H}H}$, $L_{\widetilde{S}H}$, $L_{\widetilde{T}H}$ etc.

2.6 Decays of Heavy-Light Mesons

Different experimental facilities like DASP, CLEO, ITEP, SERP, BABAR, LHCb, SELEX, CDF, and BESIII have observed many elementary particles. These experimental facilities detect stable particles like electrons, protons, neutrons, etc. These detected stable particles are products of long-chain decays of massive unstable particles, which are needed to be observed. These observed particles cannot be seen directly on the quark level, so we experimentally measure the modes via which particles decay. Particle decay is a spontaneous process in which particles reach lower stable possible energy states. Each particle has a characteristic lifetime which is inverse of its decay width Γ. The decay rates of the particle are measured by its half-life, decay constants, or average lifetime.

Decay of heavy-light mesons can occur via three interaction modes, i.e., strong interaction, electromagnetic, and weak interactions. There is some set of rules which decides whether decay is allowed or forbidden. For allowed decays, all conservation laws like charge, baryon number, lepton number, energy, linear momentum, strangeness, charge conjunction, parity, isospin, angular momentum are obeyed, and such decays are allowed under strong interactions. All conservation laws except isospin should be satisfied for decay to be allowed via electromagnetic interactions. For decays allowed via weak interactions, all conservation laws except parity, isospin, and charge conjunction should be obeyed by the decay process. The total decay width of the heavy-light system can be given by

$$\Gamma_{Total}(Q\overline{q}) = \Gamma_{EM} + \Gamma_{Weak} + \Gamma_{Strong}$$

Decays through strong interactions contribute to total decay width much more than electromagnetic and weak decays. This is because the coupling constant parameter for strong interactions is much larger than for electromagnetic and weak interactions. Even strong decays via light pseudoscalar mesons (π, η, K) give maximum contribution to the total decay width of mesons.

In this thesis, we will study strong decays of heavy-light mesons through emissions of light pseudoscalar mesons (π, η, K). The study of the decay behavior of heavy-light mesons is an active area of experimental and theoretical research. Several experimental facilities, like LHCb, BABAR, Belle, BESIII, CDF, etc., predicted decay widths of various B and D mesons. Along with decay widths, branching ratios, branching fractions, partial decay widths are also estimated by these experimental facilities. Measured parameters like masses, decay widths, branching ratios, branching fractions by experimental facilities are analyzed by available theoretical models. The strong decay of an excited heavy light meson to lower state heavy-light meson via the exchange of light pseudo-scalar mesons: $P_1 \to P_2 + G(\pi, \eta, K)$ [36, 37] is expressed as:

$$\Gamma = \frac{1}{2J+1} \sum \frac{p_G}{8\pi M_1^2} |\mathscr{A}|^2 \tag{2.49}$$

where $\mathscr{A}$ is the scattering amplitude, 1 and 2 notate the initial and final state of the heavy-light meson. The summation $\sum$ is over all the polarization vectors. And the term p_G gives the momentum of the light pseudo-scalar meson by this formula:

$$p_G = \frac{\sqrt{(M_1^2 - (M_2 + M_G)^2)(M_1^2 - (M_2 - M_G)^2)}}{2M_1} \tag{2.50}$$

The formulae provided in Eq.(2.49) will be applied to examine and analyze various properties of the excited heavy-light charm and bottom mesons [37, 55, 56]. Here, we need to emphasize that decays of heavy-light mesons only not with the emission of light pseudo scalar meson occurs but with emissions of vector mesons also take place $(\omega, \rho, K^*, \phi)$ [38, 39]. But in this thesis, we will explore the decay of B and D mesons with the emission of light pseudoscalar mesons.

2.7 Strong Decays of Heavy-Light Mesons with Light Pseudoscalar Mesons

Excited heavy-light mesons decay to ground states along with the emission of light pseudoscalar mesons (π, η, K). The heavy meson chiral Lagrangians L_{HH}, L_{SH}, L_{TH}, L_{XH}, L_{YH}, L_{ZH} which we discussed in the previous section are used to compute scattering amplitude $\mathscr{A}$ for corresponding fields H, S, T, X, Y. The obtained scattering amplitude $\mathscr{A}$ is substituted in eq.2.49 and we yield the following expressions of decay widths for different decay channels [57, 58]:

$(0^-, 1^-) \to (0^-, 1^-) + G$

$$\Gamma(1^- \to 1^-) = C_G \frac{g_{HH}^2 M_2 p_G^3}{3\pi f_\pi^2 M_1} \tag{2.51}$$

$$\Gamma(1^- \to 0^-) = C_G \frac{g_{HH}^2 M_2 p_G^3}{6\pi f_\pi^2 M_1}$$

$$\Gamma(0^- \to 1^-) = C_G \frac{g_{HH}^2 M_2 p_G^3}{2\pi f_\pi^2 M_1}$$

$(0^+, 1^+) \to (0^-, 1^-) + G$

$$\Gamma(1^+ \to 1^-) = C_G \frac{g_{SH}^2 M_2 (p_G^2 + m_G^2) p_G}{2\pi f_\pi^2 M_1} \tag{2.52}$$

$$\Gamma(0^+ \to 0^-) = C_G \frac{g_{SH}^2 M_2 (p_G^2 + m_G^2) p_G}{2\pi f_\pi^2 M_1}$$

$(1^+, 2^+) \to (0^-, 1^-) + G$

$$\Gamma(2^+ \to 1^-) = C_G \frac{2 g_{TH}^2 M_2 p_G^5}{5\pi f_\pi^2 \Lambda^2 M_1} \tag{2.53}$$

$$\Gamma(2^+ \to 0^-) = C_G \frac{4 g_{TH}^2 M_2 p_G^5}{15\pi f_\pi^2 \Lambda^2 M_1}$$

$$\Gamma(1^+ \to 1^-) = C_G \frac{2 g_{TH}^2 M_2 p_G^5}{3\pi f_\pi^2 \Lambda^2 M_1}$$

$(1^-, 2^-) \to (0^-, 1^-) + G$

$$\Gamma(1^- \to 0^-) = C_G \frac{4 g_{XH}^2}{9\pi f_\pi^2 \Lambda^2} \frac{M_2}{M_1} [p_G^3 (m_G^2 + p_G^2)] \tag{2.54}$$

$$\Gamma(1^- \to 1^-) = C_G \frac{2 g_{XH}^2}{9\pi f_\pi^2 \Lambda^2} \frac{M_2}{M_1} [p_G^3 (m_G^2 + p_G^2)]$$

$$\Gamma(2^- \to 1^-) = C_G \frac{2 g_{XH}^2}{3\pi f_\pi^2 \Lambda^2} \frac{M_2}{M_1} [p_G^3 (m_G^2 + p_G^2)]$$

$(2^-, 3^-) \to (0^-, 1^-) + G$

$$\Gamma(2^- \to 1^-) = C_G \frac{4 g_{YH}^2}{15\pi f_\pi^2 \Lambda^4} \frac{M_2}{M_1} [p_G^7] \tag{2.55}$$

$$\Gamma(3^- \to 0^-) = C_G \frac{4 g_{YH}^2}{35\pi f_\pi^2 \Lambda^4} \frac{M_2}{M_1} [p_G^7]$$

$$\Gamma(3^- \to 1^-) = C_G \frac{16 g_{YH}^2}{105\pi f_\pi^2 \Lambda^4} \frac{M_2}{M_1} [p_G^7]$$

$(2^+, 3^+) \to (0^-, 1^-) + G$

$$\Gamma(2^+ \to 1^-) = C_G \frac{8 g_{ZH}^2}{75\pi f_\pi^2 \Lambda^4} \frac{M_2}{M_1} [p_G^5 (m_G^2 + p_G^2)] \tag{2.56}$$

$$\Gamma(2^+ \to 0^-) = C_G \frac{4 g_{ZH}^2}{25\pi f_\pi^2 \Lambda^4} \frac{M_2}{M_1} [p_G^5 (m_G^2 + p_G^2)]$$

$$\Gamma(3^+ \to 1^-) = C_G \frac{4 g_{ZH}^2}{25\pi f_\pi^2 \Lambda^4} \frac{M_2}{M_1} [p_G^5 (m_G^2 + p_G^2)]$$

$(3^+, 4^+) \to (0^-, 1^-) + M$

$$\Gamma(3^+ \to 1^-) = C_G \frac{36 g_{RH}^2}{35\pi f_\pi^2 \Lambda^6} \frac{M_2}{M_1} [p_G^9] \tag{2.57}$$
$$\Gamma(4^+ \to 1^-) = C_G \frac{4 g_{RH}^2}{7\pi f_\pi^2 \Lambda^6} \frac{M_2}{M_1} [p_G^9]$$
$$\Gamma(4^+ \to 0^-) = C_G \frac{16 g_{RH}^2}{35\pi f_\pi^2 \Lambda^6} \frac{M_2}{M_1} [p_G^9]$$

In the above expressions, M_1, M_2 represents initial and final meson masses, $\Lambda = 1\ GeV$ is chiral symmetry breaking scale. p_G, m_G denotes to final momentum and mass of light pseudoscalar meson. The coupling constant plays a key role in the phenomenology study of heavy-light mesons. These dimensionless coupling constants g_{HH}, g_{SH}, g_{TH}, etc describe the strength of transition between $H - H$ field (negative-negative parity), $S - H$ field (positive-negative parity), $T - H$ field (positive-negative parity). For transition from $n = 3$ to $n = 1$ coupling constants are given by $\tilde{\tilde{g}}_{HH}$, $\tilde{\tilde{g}}_{SH}$, $\tilde{\tilde{g}}_{TH}$ etc. and transition from $n = 2$ to $n = 1$ is denoted by $\tilde{g}_{HH}$, $\tilde{g}_{SH}$, $\tilde{g}_{TH}$. The coefficient C_G for different pseudoscalar particles are: $C_{\pi^\pm}$, $C_{K^\pm}$, C_{K^0}, $C_{\overline{K}^0} = 1$, $C_{\pi^0} = \frac{1}{2}$ and $C_\eta = \frac{2}{3}(c\bar{u}, c\bar{d})$ or $\frac{1}{6}(c\bar{s})$. Higher order corrections of $\frac{1}{m_Q}$ for spin and flavor violations are not included in bringing new couplings. In comparison to leading-order contributions, we anticipate that higher-order corrections have small contributions. When applied to charm and bottom meson decays, there are distinct advantages and drawbacks. Specifically, for bottom meson decays, the expansion in $\Delta k/m_B$ converges rapidly.

2.8 Masses of Heavy-Light Mesons

The effective Lagrangian formulated for heavy-light mesons in the previous section can be used to determine and analyze their spectroscopy. To analyze spectroscopy of heavy-light mesons, masses are the prime property that determines many other properties of the mesons [25, 40]. From the effective Lagrangian 2.36 at first order of $1/m_Q$, the mass of the $Q\bar{q}$ state can be obtained, and its expression is :

$$M_X = m_Q + \overline{\Lambda} - \frac{\lambda_1}{2m_Q} + 4(S_Q.S_l)\frac{\lambda_2}{2m_Q} \tag{2.58}$$

In this equation, m_Q = heavy quark mass, $4(S_Q.S_l)$ = Clebsch factor, $\overline{\Lambda}$, λ_1 and λ_2 are HQET parameters. These parameters are the order of Λ_{QCD}^2 and give the same value for states within the same spin-flavor multiplet. The parameter $\overline{\Lambda}$ remains invariant with respect to light quark flavor. λ_1 term describes mass shift due to kinetic operators, and λ_2 describes the chromomagnetic interaction energy. Also, λ_1 is unaffected by heavy quark while λ_2 parameter depends on m_Q through the dependence of $a(\mu)$ on m_Q. Detailed information on these parameters will be discussed in the next chapter.

2.9 Splittings

Degeneracy in hyperfine splittings or mass splitting between different doublets of D and B mesons results from heavy quark spin flavor symmetry. Since mass splitting between different doublets is independent of heavy quark flavor in the frame of heavy quark spin flavor symmetry. The following are the predicted values of mass splitting in D and B mesons:

$$D^{*+} - D^{+} = 141.01\ MeV$$
$$B^{*+} - B^{+} = 45.37\ MeV$$

These hyperfine splitting should give the same values, corresponding to heavy quark spin flavor symmetry. But due to finite masses of charm and bottom quarks, degeneracy in hyperfine splitting is not exact but approximate [34, 40, 59]. Also, the bottom quark is much heavier than the charm quark, so the bottom mesons give better approximations than charm mesons in hyperfine splittings. It is natural to expect that hyperfine splittings are smaller for excited states than ground states. Since as energy increases, energy levels get closer, i.e., higher excited states are much closer, that makes hyperfine splitting values smaller for higher excited states. For e.g., predicted values for P-waves $(1^+, 2^+)$ D mesons and B mesons are from PDG:

$$D_2^* - D_1 = 39.77\ MeV$$
$$B_2^* - B_1 = 11.30\ MeV$$

These computed values for P-wave are much smaller than ground state values, which are natural to be expected. The hyperfine splittings can also be defined as such $m_V^2 - m_P^2$, where m_P = mass of vector meson and m_v = mass of pseudoscalar meson. The predicted values $m_{D^*}^2 - m_D^2 = 0.54\ GeV^2$, $m_{B^*}^2 - m_B^2 = 0.48\ GeV^2$

for charm and bottom mesons respectively, have approximately same values. The values of hyperfine splitting for strange mesons are:

$$D_s^* - D_s = 143.85\ MeV$$
$$B_s^* - B_s = 48.48\ MeV$$

The behavior of these splitting is similar to non-strange mesons. However, this splitting is not quite the same for non-strange and strange mesons, because of the large mass difference between u, d, and s quarks.

The difference between the strange and non-strange states for a given J^P is independent of the heavy quark within the framework of heavy quark flavor symmetry. It implies $D_s - D \simeq B_s - B \simeq 100\ MeV$. Experimentally, $D_s - D = 103.51\ MeV$ for the charm ground state and $B_s - B = 87.26\ MeV$ for the bottom ground state mesons.

2.10 Couplings

As we discussed, strong decay width formulas depend upon strong coupling constants. These coupling constants are an important key in describing the nature of hadronic processes. Measurements of the strong coupling constant determine the nature of participating mesons and the strong interaction between them. These coupling constants can be computed from experimental decay widths or with available theoretical decay widths of mesons. Theoretical models like QCD sum rules [60–63], Lattice QCD [64], Heavy hadron chiral perturbation theory [53], etc., can estimate heavy-light mesons' decay widths. Accuracy in estimating coupling is crucial, as they are directly related to decay rates. Implications of heavy quark spin flavor symmetry reduce the number of independent coupling parameters to a great extent. The strong coupling constants can be constrained between 0 and 1 with the implication of heavy quark symmetry [65]. The value of coupling constants for states of the same doublets of D and B mesons is assumed to be equal. With the help of this symmetry, we can estimate decay widths of unknown excited states of mesons. In the next chapter, we will apply heavy quark effective theory and discuss spectra of charm and bottom mesons.

Bibliography

[1] R.L. Workman et al. (Particle Data Group), PTEP **2022**, 083C01 (2022)

[2] P. del Amo Sanchez, J.P. Lees, V. Poireau, E. Prencipe, V. Tisserand, J. Garra Tico, E. Grauges, M. Martinelli, A. Palano, M. Pappagallo et al. (BABAR Collaboration), Phys. Rev. D **82**, 111101 (2010)

[3] R. Aaij et al. (LHCb), JHEP **09**, 145 (2013), `1307.4556`

[4] R. Aaij et al. (LHCb), Phys. Rev. D **91**, 092002 (2015), [Erratum: Phys.Rev.D 93, 119901 (2016)], `1503.02995`

[5] B. Aubert et al. (BABAR), Phys. Rev. Lett. **97**, 222001 (2006), `hep-ex/0607082`

[6] J. Brodzicka et al. (Belle), Phys. Rev. Lett. **100**, 092001 (2008), `0707.3491`

[7] R. Aaij et al. (LHCb), JHEP **02**, 133 (2016), `1601.01495`

[8] R. Aaij et al. (LHCb), Phys. Rev. Lett. **126**, 122002 (2021), `2011.09112`

[9] D. Besson et al. (CLEO), Phys. Rev. D **68**, 032002 (2003), [Erratum: Phys.Rev.D 75, 119908 (2007)], `hep-ex/0305100`

[10] Y. Mikami et al. (Belle), Phys. Rev. Lett. **92**, 012002 (2004), `hep-ex/0307052`

[11] B. Aubert et al. (BABAR), Phys. Rev. D **74**, 032007 (2006), `hep-ex/0604030`

[12] B. Aubert et al. (BABAR), Phys. Rev. D **69**, 031101 (2004), `hep-ex/0310050`

[13] R. Aaij et al. (LHCb), Phys. Rev. D **94**, 072001 (2016), `1608.01289`

[14] S. Behrends et al. (CLEO), Phys. Rev. Lett. **50**, 881 (1983)

[15] T. Aaltonen et al. (CDF), Phys. Rev. Lett. **100**, 082001 (2008), `0710.4199`

[16] T.A. Aaltonen et al. (CDF), Phys. Rev. D **90**, 012013 (2014), `1309.5961`

[17] V.M. Abazov et al. (D0), Phys. Rev. Lett. **100**, 082002 (2008), `0711.0319`

[18] M. Ablikim et al. (BESIII), Phys. Rev. Lett. **106**, 072002 (2011), `1012.3510`

[19] M. Ablikim et al. (BESII), Chin. Phys. C **36**, 1031 (2012)

[20] B. Grinstein, Nucl. Phys. B **339**, 253 (1990)

[21] E. Eichten, B.R. Hill, Phys. Lett. B **234**, 511 (1990)

[22] H. Georgi, Phys. Lett. B **240**, 447 (1990)

[23] M. Neubert, *Heavy quark effective theory*, in *20th Johns Hopkins Workshop on Current Problems in Particle Theory: Non-Perturbative Particle Theory and Experimental Tests* (1996), pp. 39–78, `hep-ph/9610385`

[24] H. Georgi, *Heavy quark effective field theory*, in *Theoretical Advanced Study Institute in Elementary Particle Physics (TASI 91): Perspectives in the Standard Model* (1991)

[25] A.V. Manohar, M.B. Wise, *Heavy quark physics*, Vol. 10 (2000), ISBN 978-0-521-03757-0

[26] M.B. Wise, *Heavy quark physics: Course*, in *Les Houches Summer School in Theoretical Physics, Session 68: Probing the Standard Model of Particle Interactions* (1997), pp. 1051–1089, `hep-ph/9805468`

[27] R. Casalbuoni, A. Deandrea, N. Di Bartolomeo, R. Gatto, F. Feruglio, G. Nardulli, Phys. Rept. **281**, 145 (1997), `hep-ph/9605342`

[28] E.E. Jenkins, Nucl. Phys. B **412**, 181 (1994), `hep-ph/9212295`

[29] F. Hussain, G. Thompson, *An Introduction to the heavy quark effective theory*, in *ICTP Summer School in High-energy Physics and Cosmology* (1994), pp. 0045–115, `hep-ph/9502241`

[30] N. Isgur, M.B. Wise, Phys. Rev. Lett. **66**, 1130 (1991)

[31] T. Matsuki, T. Morii, K. Seo, Prog. Theor. Phys. **124**, 285 (2010), `1001.4248`

[32] T.M. Yan, H.Y. Cheng, C.Y. Cheung, G.L. Lin, Y.C. Lin, H.L. Yu, Phys. Rev. D **46**, 1148 (1992), [Erratum: Phys.Rev.D 55, 5851 (1997)]

[33] M.A. Nowak, M. Rho, I. Zahed, Phys. Rev. D **48**, 4370 (1993), `hep-ph/9209272`

[34] A.F. Falk, Nucl. Phys. B **378**, 79 (1992)

[35] U. Kilian, J.G. Korner, D. Pirjol, Phys. Lett. B **288**, 360 (1992)

[36] Z.G. Wang, Eur. Phys. J. Plus **129**, 186 (2014), 1401.7580

[37] P. Colangelo, F. De Fazio, F. Giannuzzi, S. Nicotri, Phys. Rev. D **86**, 054024 (2012), 1207.6940

[38] S. Campanella, P. Colangelo, F. De Fazio, Phys. Rev. D **98**, 114028 (2018), 1810.04492

[39] J. Schechter, A. Subbaraman, Phys. Rev. D **48**, 332 (1993), hep-ph/9209256

[40] M. Neubert, Phys. Rept. **245**, 259 (1994), hep-ph/9306320

[41] M.J. Dugan, M. Golden, B. Grinstein, Phys. Lett. B **282**, 142 (1992)

[42] J.M. Flynn, N. Isgur, J. Phys. G **18**, 1627 (1992), hep-ph/9207223

[43] T.W. Yeh, C.e. Lee (1995), hep-ph/9510241

[44] P.L. Cho, Nucl. Phys. B **396**, 183 (1993), [Erratum: Nucl.Phys.B 421, 683–686 (1994)], hep-ph/9208244

[45] T. Mannel, W. Roberts, Z. Ryzak, Nucl. Phys. B **368**, 204 (1992)

[46] H.Y. Cheng, F.S. Yu, Phys. Rev. D **89**, 114017 (2014), 1404.3771

[47] G. Amoros, M. Beneke, M. Neubert, Phys. Lett. B **401**, 81 (1997), hep-ph/9701375

[48] A.F. Falk, M.E. Luke, Phys. Lett. B **292**, 119 (1992), hep-ph/9206241

[49] R. Casalbuoni, A. Deandrea, N. Di Bartolomeo, R. Gatto, F. Feruglio, G. Nardulli, Phys. Lett. B **299**, 139 (1993), hep-ph/9211248

[50] J. Gasser, H. Leutwyler, Nucl. Phys. B **250**, 465 (1985)

[51] S. Scherer, Adv. Nucl. Phys. **27**, 277 (2003), hep-ph/0210398

[52] H. Davoudiasl, Phys. Rev. D **54**, 6830 (1996), hep-ph/9604418

[53] M.B. Wise, Phys. Rev. D **45**, R2188 (1992)

[54] R. Casalbuoni, A. Deandrea, N. Di Bartolomeo, R. Gatto, F. Feruglio, G. Nardulli, Phys. Lett. B **294**, 106 (1992), hep-ph/9209247

[55] K. Gandhi, A.K. Rai, Eur. Phys. J. C **82**, 777 (2022), 2208.08791

[56] P. Gupta, A. Upadhyay, Phys. Rev. D **99**, 094043 (2019), 1803.03136

[57] Z.G. Wang, Phys. Rev. D **88**, 114003 (2013), 1308.0533

[58] Z.G. Wang, Commun. Theor. Phys. **66**, 671 (2016), 1608.02176

[59] T. Matsuki, T. Morii, K. Sudoh, Phys. Lett. B **659**, 593 (2008), 0710.0325

[60] P. Colangelo, F. De Fazio, Eur. Phys. J. C **4**, 503 (1998), hep-ph/9706271

[61] M.E. Bracco, M. Chiapparini, F.S. Navarra, M. Nielsen, Prog. Part. Nucl. Phys. **67**, 1019 (2012), 1104.2864

[62] P. Colangelo, G. Nardulli, A. Deandrea, N. Di Bartolomeo, R. Gatto, F. Feruglio, Phys. Lett. B **339**, 151 (1994), hep-ph/9406295

[63] F.S. Navarra, M. Nielsen, M.E. Bracco, M. Chiapparini, C.L. Schat, Phys. Lett. B **489**, 319 (2000), hep-ph/0005026

[64] T. Kawanai, S. Sasaki, Phys. Rev. D **85**, 091503 (2012), 1110.0888

[65] I.W. Stewart, Nucl. Phys. B **529**, 62 (1998), hep-ph/9803227

Chapter 3

Analysis of Excited Charm and Bottom Mesons

3.1 Introduction

The systematic study of the mesonic system, which consists of a heavy quark (Q) and a light antiquark ($\bar{q}$), can be conducted within the framework of heavy quark effective theory. [1]. It is an effective QCD theory describing the dynamics of heavy-light mesons systems, where the mass of heavy quark m_Q defined as $m_Q \gg \Lambda_{QCD}$, where Λ_{QCD} is the non-perturbative scale of 0.2 GeV. This theory provides us a unique opportunity to explore the understanding of low energy QCD physics and the associated properties like color confinement, chiral symmetry breaking, etc. This theory is based upon approximate symmetry - Heavy quark symmetry where the mass of heavy quark $\Lambda_{QCD} \ll m_Q$, so by taking limit $m_Q \to \infty$, manifests heavy quark symmetry into the picture. In this limit, the dynamics of light quarks remain invariant if the spin and flavor of heavy quarks (c or b) change, i.e., light quarks become blind to the flavor of heavy quarks (c or b). This is known as the spin-flavor symmetry of heavy quark. This symmetry is a key tool in the comprehensive investigation of mesons.

Meson spectroscopy has received remarkable progress experimentally as well as theoretically. Different experimental facilities like LHCb, CDF, BABAR, DO, BESIII, Belle, etc., provide data for masses, spins, parity, decay widths, branching ratios in this sector. [2–9]. In D meson family, addition of numerous new candidates like $D_2^*(3000)$, $D_J^*(3000)$, $D_J(3000)$, $D_1^*(2760)$, $D_1^*(2680)$, $D_2^*(2460)$, $D_J^*(2760)$, $D_{sJ}(3040)^{\pm}$, $D_{s1}(2860)^{\pm}$, $D_{s3}^*(2860)^{\pm}$, $D_{s0}(2590)^+$ [7–9] have flourished charm meson spectrum. The masses and decay widths of charm mesons for the ground state ($1S$) and first excited state ($1P$) are well established experimentally and mentioned in PDG [10] for both non-strange and strange sectors. Recently, LHCb collaboration analyzed $B^0 \longrightarrow D^-D^+K^+\pi^-$ decays at centre of mass energy 13 TeV in pp collision and observed $D_{s0}(2590)^+$ state. The measured mass and decay width are $M = 2591 \pm 13$ MeV, $\Gamma = 89 \pm 28$ MeV respectively. This new resonance is suggested to be a strong candidate for radially excited $D_s(2S)$ state, i.e., $n = 2$, $l = 0$. Also, LHCb collaboration studied $B^- \longrightarrow D^+\pi^-\pi^+$ decays with Dalitz plot analysis technique and reported the existence of charm resonances with spin 1, 2, 3 at $D^+\pi^-$ mass spectrum [8]. Their investigation found that these charm resonances are mainly coming from contribution of $D_3^*(2760)$, $D_1^*(2680)$, $D_2^*(2460)$ and $D_2^*(3000)$ charmed meson decays into S-wave $D^+\pi^-$. The obtained masses and decay widths for these resonances are:

$$M(D_2^*(2460)) = 2463.7 \pm 0.4(stat) \pm 0.4(syst)MeV \tag{3.1}$$

$$\Gamma(D_2^*(2460)) = 47 \pm 0.8 \pm 0.9MeV \tag{3.2}$$

$$M(D_1^*(2680)) = 2681.1 \pm 5.6(stat) \pm 4.9(syst)MeV \tag{3.3}$$

$$\Gamma(D_1^*(2680)) = 186.7 \pm 8.5 \pm 8.6MeV \tag{3.4}$$

$$M(D_3^*(2760)) = 2775.5 \pm 4.5(stat) \pm 4.5(syst)MeV \tag{3.5}$$

$$\Gamma(D_3^*(2760)) = 95.3 \pm 9.6 \pm 7.9MeV \tag{3.6}$$

$$M(D_2^*(3000)) = 3214 \pm 29(stat) \pm 33(syst)MeV \tag{3.7}$$

$$\Gamma(D_2^*(3000)) = 186 \pm 38 \pm 34MeV \tag{3.8}$$

In 2015, LHCb group examined $B^0 \longrightarrow \bar{D}^0\pi^-\pi^+$ decays and measured $D_0^*(2300)$ and $D_0^*(2460)$ charm meson state. They assigned state $D_3^*(2760)$ with $J^P = 3^-$ for the first time [7]. In the years 2013 and 2010, a remarkable achievement was received by BABAR and LHCb groups [6, 11]. LHCb (2013) detector discovered two resonances $D_J^*(2650)^0$, $D_0^*(2760)$ with natural parity and two resonances $D_J(2580)^0$ and $D_J(2740)^0$ with unnatural parity by analysing invariant mass spectrum of $D^+\pi^-$, $D^0\pi^+$, $D^{*+}\pi^-$. In addition, state $D_J(3000)^0$ with unnatural parity and state $D_J^*(3000)^0$ with natural parity were found in $D^{*+}\pi^-$, $D^+\pi^-$ mass spectrum respectively. In 2010, BABAR experiment analyzed e^+e^- inclusive collision at center of mass energy 10.58 GeV and observed $D_J(2560)^0$, $D_J(2600)^0$, $D_J(2600)^+$, $D_J(2750)^0$, $D_J^*(2760)^+$ and $D_J(2760)^0$. Masses and decay widths of states confirmed by LHCb and BABAR are listed in Table 3.1.

In D_s meson family, $1S$ and $1P$ ($D_{s0}^*(2317), D_{s1}(2460), D_{s1}(2536), D_{s2}^*(2573)$) states are well established and mentioned in PDG [10]. In 2006, BABAR observed two new states $D_{sJ}(2700)^+$ and $D_{sJ}(2860)^+$ in DK decay mode [22]. The state $D_{sJ}(2700)^+$ is reconfirmed by Belle and also gives assignment $J^P = 1^-$ [23]. In 2009, BABAR announced new state $D_{sJ}(3040)^+$ [24]. Also LHCb collaboration analysed $B_s^0 \longrightarrow \overline{D^0}K^-\pi^+$ decays and observed two new resonances $D_{s1}^*(2860)$, $D_{s3}^*(2860)$ with $J^P = 1^-, 2^-$ respectively [25]. Recently, LHCb collaboration analyzed $B^0 \longrightarrow D^-D^+K^+\pi^-$ decays at centre of mass energy 13 TeV in pp collision and observed $D_{s0}(2590)^+$ state [9].

Different theoretical approaches like $^3P_0$ model [35, 36], HQET [37, 38], QCD sum rule [39, 40], and relativized quark model [41, 42] have examined all above-mentioned states, computed their masses and suggested their J^P values. The states $D_0^*(2300)$, $D_1(2420)$, $D_1(2430)$ and $D_2^*(2460)$ were reported by PDG [10] and their assigned J^Ps are 1^3P_0, 1^1P_1, 1^3P_1, 1^3P_2 respectively. The results for $D_0(2550)^0$ state observed by BABAR [11] are similar to those of the $D_J(2580)^0$ state reported by LHCb [8] and are considered as a candidate for 2^1S_0 state. The data given by LHCb detector in 2016 for the state $D_1^*(2680)$ [8] and $D_J^*(2650)$ in 2013 [6] matches closely with results of the state $D_1^*(2600)$ reported by BABAR collaborations [11]. It is plausible that states $D_1^*(2680)$, $D_1^*(2600)$, $D_J^*(2650)$ reflects same particle and theoretical investigation interpreted them as 2^3S_1 state [43–52]. The findings of state $D_3^*(2760)$ in 2015 [7] and $D_1^*(2760)^0$ in 2013 [6] announced by LHCb detector are closely resembled with data of state $D_2(2750)^0$ provided by BABAR group [11]. Thus, it is conceivable that states $D_3^*(2760)$, $D_1^*(2760)^0$, $D_2(2750)^0$ represents same resonance and classified as $1D$ 3^- candidate by theoretical studies [42, 53] . Observations of the state $D_J(3000)$ with unnatural parity, $D_J^*(3000)$ with natural parity by LHCb group[6] gives possible J^P values for state $D_J^*(3000)$ are 3^3S_1, 2^3P_2, 1^3F_2 and 1^3F_4 and for state $D_J(3000)$ are 3^3S_0, 2^3P_1 respectively. LHCb detector observed the state

Table 3.1: List of observed non-strange charm mesons by different experimental facilities.

Resonance	J^P	Mass (MeV)	Width (MeV)	Experiment
D^0	0^-	1864.83 ± 0.05	$(410.1 \pm 1.5) \times 10^{-15}$	MARK I [12]
$D^\pm$	0^-	1869.58 ± 0.09	$(1040 \pm 7) \times 10^{-15}$	MARK I [13]
D^{*0}	1^-	2006.85 ± 0.05	< 2.1	MARK I [14]
$D^{*\pm}$	1^-	2010.26 ± 0.05	$(83.4 \pm 1.8) \times 10^{-3}$	MARK I [14]
$D_0^*(2400)^0$	0^+	2318 ± 29	267 ± 40	Belle [15]
$D_0^*(2400)^\pm$	0^+	2351 ± 7	230 ± 17	FOCUS [16]
$D_1(2420)^0$	1^+	2420.8 ± 0.5	31.7 ± 2.5	ARGUS [17]
$D_1(2420)^\pm$	1^+	2423.2 ± 2.4	25 ± 6	TPS [18]
$D_1(2430)^0$	1^+	$2427 \pm 26 \pm 25$	$384^{+107}_{-75} \pm 75$	Belle [15]
$D_2^*(2460)^0$	2^+	2460.57 ± 0.15	47.7 ± 1.3	TPS [18]
$D_2^*(2460)^\pm$	2^+	2465.40 ± 1.3	46.7 ± 1.2	ARGUS [19]
$D(2550)^0$	0^-	$2539.4 \pm 4.5 \pm 6.8$	$130 \pm 12 \pm 13$	BABAR [11]
$D_J^*(2580)^0$	0^-	$2579.5 \pm 3.4 \pm 5.5$	$177.5 \pm 17.8 \pm 46.0$	LHCb [20]
$D_1^*(2600)^0$	1^-	$2608.7 \pm 2.4 \pm 2.5$	$93 \pm 6 \pm 13$	BABAR [11]
		$2649.2 \pm 3.5 \pm 3.5$	$140.2 \pm 17.1 \pm 18.6$	LHCb [20]
		$2681.1 \pm 5.6 \pm 4.9$	$186.7 \pm 8.5 \pm 8.6$	LHCb [8]
$D(2750)^0$	–	$2752.4 \pm 1.7 \pm 2.7$	$71 \pm 6 \pm 11$	BABAR [11]
$D(2740)^0$	2^-	$2737.0 \pm 3.5 \pm 11.2$	$73.2 \pm 13.4 \pm 25$	LHCb [20]
$D^*(2760)^0$	–	$2763.3 \pm 2.3 \pm 2.3$	$60.9 \pm 13.4 \pm 5.1 \pm 3.6$	BABAR [11]
$D_J^*(2760)^0$	–	$2760.1 \pm 1.1 \pm 3.7$	$74.4 \pm 3.4 \pm 19.1$	LHCb [20]
$D_1^*(2760)^0$	1^-	$2781 \pm 18 \pm 11 \pm 6$	$177 \pm 32 \pm 20 \pm 7$	LHCb [21]
$D_3^*(2760)^-$	3^-	$2798 \pm 7 \pm 1 \pm 7$	$105 \pm 18 \pm 6 \pm 23$	LHCb [7]
$D_3^*(2760)^0$	3^-	$2775.5 \pm 4.5 \pm 4.5 \pm 4.7$	$95.3 \pm 9.6 \pm 7.9 \pm 33.1$	LHCb [8]
$D_J(3000)^0$	-	2971.8 ± 8.7	$188.1 \pm 44.8 \pm 20 \pm 7$	LHCb [20]
$D_J^*(3000)^0$	-	3008.1 ± 4.0	110.5 ± 11.5	LHCb [20]
$D_2^*(3000)^0$	2^+	$3214 \pm 29 \pm 33 \pm 36$	$186 \pm 38 \pm 34 \pm 63$	LHCb [8]

Table 3.2: List of observed strange charm mesons by different experimental facilities.

Resonance	J^P	Mass (MeV)	Width (MeV)	Experiment
D_s	0^-	1968.27 ± 0.10	$(500 \pm 7) \times 10^{-15}$	DASP [26]
D_s^*	1^-	2112.1 ± 0.4	< 1.9	DASP [26]
$D_{s0}(2317)^*$	0^+	2317.7 ± 0.6	< 3.8	BABAR [27]
$D_{s1}(2460)$	1^+	2459.5 ± 0.6	< 3.5	CLEO [28]
$D_{s1}(2536)$	1^+	2535.10 ± 0.06	$0.92 \pm 0.03 \pm 0.04$	ITEP, SERP [29]
$D_{s2}^*(2573)$	2^+	2569.1 ± 0.8	16.9 ± 0.8	CLEO[30]
$D_{sJ}^*(2632)$	-	$2632.5 \pm 1.7 \pm 5.0$	< 17	SELEX [31]
$D_{s1}^*(2700)$	1^-	$2688 \pm 4.0 \pm 3.0$	$112 \pm 7 \pm 36$	BABAR [22]
		$2708 \pm 9^{+11}_{-10}$	$108 \pm 23^{+36}_{-31}$	Belle [23]
		$2710 \pm 2^{+12}_{-10}$	$149 \pm 7^{+39}_{-52}$	BABAR [24]
		$2709.2 \pm 1.9 \pm 4.5$	$115.8 \pm 7.3 \pm 12.1$	LHCb [32]
		2699^{+14}_{-7}	127^{+24}_{-19}	BABAR [33]
$D_{sJ}^*(2860)$	-	$2856.6 \pm 1.5 \pm 5.0$	$47 \pm 7 \pm 10$	BABAR [22]
		$2862 \pm 2^{+5}_{-2}$	$48 \pm 3 \pm 6$	BABAR [24]
		$2866.1 \pm 1.0 \pm 6.3$	$69.9 \pm 3.2 \pm 6.6$	LHCb [32]
$D_{s3}(2860)$	3^-	$2860.5 \pm 2.6 \pm 2.5$	$69.9 \pm 3.2 \pm 6.6$	LHCb [25, 34]
$D_{s1}^*(2860)$	1^-	$2859 \pm 12 \pm 6$	$159 \pm 23 \pm 27$	LHCb [25, 34]
$D_{sJ}(3040)$	-	$3044 \pm 8^{+30}_{-5}$	$239 \pm 35^{+46}_{-42}$	BABAR [24]

$D_2^*(3000)^0$ with $J^P = 2^+$ [8] and suggested it to be a candidate of 3^3P_2, 1^3F_2 state. Theoretical approaches also examined $D_2^*(3000)^0$, $D_J^*(3000)$, $D_J(3000)$ states and tried to assign their proper J^P state. In Ref.[54] Zhi-Gang Wang et.al analyzed the state $D_2^*(3000)^0$ and assigned it 1F 2^+. They also examined state $D_2^*(3000)^0$ with QPC (quark pair creation) model by studying decays of 3^3P_2 and 2^3F_2 charmed mesons. They suggested it to be 3^3P_2 state, but the possibility of 2^3F_2 state was also not excluded. The states $D_J^*(3000)$ and $D_J(3000)$ also studied by S.Godfrey and K.Moats, identified them as 3^3P_2, 1^3F_2 respectively [42]. Authors in Ref.[55] studied the state $D_J^*(3000)$, $D_J(3000)$ and suggested most favourable assignment for them to be $2P(0^+, 1^+)$ respectively. In Ref. [48], the state $D_2^*(3000)$ is studied with the instantaneous Bethe-Salpeter method and gives 2^3P_2, 2^3F_2 assignments.

Several theoretical models also investigate observed charmed-strange mesons and try to place them in spectra of charmed-strange mesons. The state $D_{sJ}(2700)^+$ is studied by QPC model [56], constituent quark model [57], effective Lagrangian [58] and give its J^P value. Authors in Ref. [59] adopted phenomenological potential model to analyze state $D_{sJ}(2700)^+$ and suggested mixture of 2^3S_1 and 1^3D_1 state. Two states $D_{s1}^*(2860)$ and $D_{s3}^*(2860)$ observed by LHCb is investigated by QPC model [53], QCD sum rules [39, 40] and other models [37, 44] and interpret them as $1D$ candidates. The state $D_{sJ}(3040)$ announced by BABAR with unnatural parity is investigated theoretically by flux tube method [60], effective Lagrangian approach [61] and constitute quark model [62]. All these models interpret this state as $1P(1^+)$. Recently observed state $D_{s0}(2590)^+$ studies through decays in Ref. [63] and measured its decay widths, which is lower than the experimental value. Thus, authors in Ref. [63] disagree with assignment $D_s(2^1S_0)$ given by LHCb [9]. This state is also analyzed with semi-relativistic potential model [47] and unquenched quark model [64]. They concluded that more experimental observations are needed to reveal the nature of $D_{s0}(2590)^+$ state. Also, state $D_{s0}(2590)^+$ examined in coupled-channel framework [65] and relativistic quark model with a screening effect [66]. They support experimental results of LHCb [9].

In B-meson spectroscopy, only ground states $B^0(5279)$, $B^{\pm}(5279)$, $B^*(5324)$, $B_s(5366)$, $B_s^*(5415)$ and few orbitally excited states $B_1(5721)$, $B_2^*(5747)$ are available in PDG [10]. But higher radially and orbitally excited bottom states demand further experimental investigation. In 2007, DO collaboration discovered $B_1(5721)$, $B_2^*(5747)$ states for the first time and obtained masses are $M_{B_1(5721)} = 5720.6 \pm 2.2 \pm 1.4\ MeV$ and $M_{B_2(5747)} = 5746.8 \pm 2.4 \pm 1.7\ MeV$ respectively [2]. Consequently, in 2009, CDFII detector at Fermilab Tevatron also observed the same states $B_1(5721)$, $B_2^*(5747)$ [5]. The measured masses and decay widths are mentioned in Table 3.3. Also, in 2007, CDF collaboration observed two strange bottom meson states $B_{s1}(5830)$, $B_{s2}^*(5840)$ [3]. The obtained masses are $M_{B_{s1}(5830)} = 5829.4 \pm 0.7\ MeV$ and $M_{B_{s2}(5840)} = 5839.6 \pm 0.7\ MeV$. Later DO collaboration and LHCb reconfirmed these bottom states and identified them as $1P_{\frac{3}{2}}1^+$, $1P_{\frac{3}{2}}2^+$ respectively [4, 6]. In 2013, CDF collaboration announced new resonances - $B(5970)^+$ and $B(5970)^0$ by analyzing invariant mass distribution of $B^0\pi^+$ and $B^-\pi^+$ [67]. Masses and decay widths of these resonances are listed in Table 3.3. In 2015, analysis of mass spectra of $B^+\pi^-$ and $B^0\pi^-$ investigated by LHCb at center of mass energies 7, 8 TeV on data sample corresponding to 3.0 fb^{-1} have observed $B_1(5721)$, $B_2^*(5747)$, $B_J(5840)^{0,+}$, $B_J(5960)^{0,+}$ [68]. Recently, LHCb collaborations discovered two new states $B_{sJ}(6063)$ and $B_{sJ}(6114)$ in B^+K^- mass spectrum [9] and enriched bottom meson spectra. Masses and decay widths for these resonances are reported in Table 3.3.

Various theoretical approaches like lattice QCD [69, 70], potential models [41, 71–73], heavy quark effective theory [37, 58], coupled channel model [74], screened potential model [75] have analyzed above mentioned bottom meson states to calculate their masses and assign them J^P values. For states $B_1(5721)$ and $B_2^*(5747)$, some theoretical models have assigned J^P values - $1P_{\frac{3}{2}}1^+$, $1P_{\frac{3}{2}}2^+$ respectively [76–79]. Beside this, some theoretical work suggests that $B_1(5721)$ state is mixture of $1P_{\frac{1}{2}}$, $1P_{\frac{3}{2}}$ states [76, 77]. Recently authors in Ref. [80] studied $B_2^*(5747)$ with relativistic Bethe-Salpeter method and identified it as $1P\ 2^+$ wave state. For strange bottom meson states $B_{s1}(5830)$, $B_{s2}^*(5840)$, various theoretical models identified them as strange partners of $B_1(5721)$, $B_2^*(5747)$ respectively and assigned quantum number 1^3P_1, 1^3P_2 respectively [76, 79, 81]. Further state $B_J(5960)$ studied through QPC (quark pair creation) model [79] and HQET [81, 82] suggested it to be $2S\ 1^-$ state. But in Ref.[77], authors analyzed state $B_J(5960)$ through different spin-parity hypotheses and assumed it to be $1D\ 3^-$ state. State $B_J(5840)$ examined by authors in

Ref.[83] based upon relativistic model favours it to be $1P_{\frac{1}{2}}1^{+}$ state, also authors in Ref.[77] suggested it to be $2S\ 0^{-}$. However, experimental information and theoretical work for this state is limited and also excluded from PDG [10], which indicates it needs more experimental and theoretical exploration.

On review of the literature, we find that experimental observations of higher orbitally and radially excited states, along with their strange partners, are not available till now. So, the theoretical study of experimentally missing charm D and bottom meson B with their strange partners is the motivation for this chapter. We analyzed some properties like decay widths, branching ratios, and coupling constants for these states in the framework of HQET. Using the same framework, in Ref. [87], masses and decay widths for $n = 2$ bottom mesons are predicted using mass symmetry parameters and heavy quark symmetry. We are extending this work for $n = 3$ with some new results.

In the next Section 3.2, we briefly discuss HQET parameters, their importance, and how, using them, we can predict masses of heavy-light mesons. In Section 3.3, We predicted mass spectra for the radially excited charm and bottom mesons by exploring HQET. We also examined OZI-allowed strong decays in the form of couplings with calculated masses. OZI (Okubo, Zweig, and Iizuka) allowed decays result from QCD. This rule states, "The decays which correspond to disconnected quark diagrams are forbidden" [88, 89]. Basically, this rule determines which strong processes are preferred and which are allowed but strongly suppressed. We also determine the upper bounds of couplings by comparing these decays with available total decay widths. We construct Regge trajectories in planes (J, M^2) and (n_r, M^2) for our estimated data. and computed masses for $n = 4$ using Regge slopes and intercepts. These Regge trajectories and study of branching ratio are used to assign $D_2^*(3000)$ state as 1^3F_2 state. In addition to this, we also analyzed missing F-wave bottom mesons with the same procedure and found out masses, decay widths, and upper bounds. In Section 3.4, the conclusions derived from our investigation are presented.

Table 3.3: List of observed bottom and bottom strange mesons by different experimental facilities.

State	J^P	Mass (MeV)	Width (MeV)	Experiment
$B(5279)^0$	0^-	5279.61 ± 0.16	-	CLEO [84]
$B(5279)^\pm$	0^-	5279.61 ± 0.15	-	CLEO [84]
$B(5324)^*$	1^-	5324.83 ± 0.32	-	CUSB [85]
$B_s(5366)$	0^-	5366.79 ± 0.23	-	CUSB-II [86]
$B_s^*(5415)$	1^-	5415.40 ± 0.15	-	CUSB-II [86]
$B_J(5721)$	1^+	5727.7 ± 0.7	30.1 ± 1.5	LHCb [68]
		5720.6 ± 0.24		DO [2]
		5725.3 ± 1.6		CDF [67]
$B_2^*(5747)$	2^+	5739.44 ± 0.37	24.5 ± 1.0	LHCb [68]
		5746.8 ± 0.24		DO [2]
		5740.2 ± 1.7	22.7 ± 32	CDF [5]
$B_{s1}(5830)$	1^+	5828.40 ± 0.04	-	LHCb [6]
		5828.3 ± 0.1	0.5 ± 0.3	CDF [67]
		5829.4 ± 0.7		CDF [3]
$B_{s2}(5840)$	2^+	5839.60 ± 1.1	-	DO [4]
		5839.70 ± 0.7	-	CDF [3]
		5839.70 ± 0.1	1.40 ± 0.4	CDF [67]
		5839.99 ± 0.05	1.56 ± 0.13	LHCb [6]
$B_J(5840)$	-	5862.9 ± 5.0	127.4 ± 16.7	LHCb[68]
$B_J(5960)$	-	5978.9 ± 5.0	-	CDF [5]
	-	5969.2 ± 2.9	82.3 ± 7.7	LHCb [68]
$B_J(5970)^0$	-	5961 ± 5.0	60 ± 40	CDF [67]
$B_{sJ}(6064)$	-	6063.5 ± 1.4	26 ± 6	LHCb [9]
$B_{sJ}(6114)$		6114 ± 6	66 ± 6	LHCb [9]

3.2 Masses of Mesons in HQET

Mass is a fundamental property for studying hadron spectroscopy. As we discussed in Chapter 2, mesons are classified in doublets, and these doublets are defined in the form of fields (H, S, T, X, Y, Z, R). These fields interact with themselves and with goldstone bosons and gluons. All these interactions are combined and expressed in terms of Lagrangian, which is known as effective Lagrangian. On expanding this Lagrangian in terms of $1/m_Q$, and expression is given by [1]:

$$\mathcal{L}_{eff} = \overline{H}_v(iv.D)H_v - \overline{H}_v\frac{D_\perp^2}{2m_Q}H_v + \overline{H}_v\frac{g\sigma_{\mu\nu}G^{\mu\nu}}{4m_Q}H_v + \mathrm{O}(\frac{1}{m_Q^2}) \tag{3.9}$$

where, $D_\perp^\mu \equiv D^\mu - v^\mu v.D$ and $D^\mu \equiv \partial^\mu - igA^\mu$ which describes spatial part of the covariant derivative in the rest frame. v is the heavy quark velocity, which becomes the velocity of hadron in the limit $m_Q \to \infty$. $G^{\mu\nu}$ gives the gluon field strength tensor. Only the first term survives in the limit $m_Q \to \infty$. We obtained HQET Hamiltonian H_0 from the first term, which gives degenerate mass states. All other terms having $\frac{1}{m_Q}$ factor break the heavy quark symmetry. H_v is the effective heavy field. The term $D_\perp^2$ comes in equation 3.9 due to the off-shell momentum of heavy quark and describes the kinetic energy of heavy quark. This second term in eq 3.9 breaks flavor symmetry but holds spin symmetry. The third term in this Lagrangian breaks both the heavy quark spin and flavor symmetry as it describes the chromo-magnetic moment interaction of the heavy quark spin with the gluon field. From this HQET Lagrangian, the mass of hadron can be written as:

$$M_{Q\bar{q}} = m_Q + \overline{\Lambda} - \frac{\lambda_1}{2m_Q} - d_N\frac{\lambda_2}{2m_Q} \tag{3.10}$$

where, $d_N = -4(S_Q.S_l)$ is the Clebsch factor. For $S_l = 1/2$, J have value 0 or 1 and d_N obtained -3 or 1 values respectively. Similarly for $S_l = 3/2$, J have value 1 or 2 and d_N obtained -5 or 3 values. The expressions for terms mentioned in eq 3.10 are given below:

$$\overline{\Lambda} \equiv \frac{1}{2}\left\langle H^{(Q)}\middle|H_0\middle|H^{(Q)}\right\rangle \tag{3.11}$$

$$2\lambda_1 = -\left\langle H^{(Q)}\middle|\overline{Q}_v D_\perp^2 Q_v\middle|H^{(Q)}\right\rangle \tag{3.12}$$

$$16(S_Q.s_l)\lambda_2^Q = a(\mu)\left\langle H^{(Q)}\middle|\overline{Q}_v g\sigma_{\alpha\beta}G^{\alpha\beta}Q_v\middle|H^{(Q)}\right\rangle \tag{3.13}$$

Here H_0 is HQET hamiltonian of order $(1/m_Q)^0$ order (leading order), comes from the first term of Lagrangian ($H_0 = \overline{H}_v(iv.D)H_v$), which is only term exists in limit $m_Q \to \infty$. $H^{(Q)}$ represents hadron states with velocity $v = (1, \mathbf{0})$ in effective field theory. $\overline{\Lambda}$ is the mass parameter of HQET of order Λ_{QCD}, which has the same value for all members of the spin-flavor multiple. This HQET parameter $\overline{\Lambda}$ is independent of light quark flavor, but if we incorporate the breaking of $SU(3)$ symmetry, then it will have different values. λ_1 in eq 3.12 and λ_2 in eq 3.13 are independent of heavy quark mass and order of Λ^2_{QCD}. λ_1 describes mass shift due to kinetic energy operator, and λ_2 describes chromomagnetic interactions of gluons with heavy quark field. These low energy parameters (λ_1, λ_2) also have the same values for given spin-flavor multiples. As we discussed in Chapter 2, different meson fields interact with goldstone bosons, so by including all these interaction fields, effective Lagrangian is given by :

$$\begin{aligned}\mathcal{L} = iTr[\overline{H}_b v^\mu D_{\mu ba} H_a] + \frac{f_\pi^2}{8} Tr[\partial^\mu U \partial_\mu U^+] + Tr[\overline{S_b}(iv^\mu D_{\mu ba} - \delta_{ba}\Delta_S)S_a] \\ + Tr[\overline{T_b^\alpha}(iv^\mu D_{\mu ba} - \delta_{ba}\Delta_T)T_{a\alpha} + Tr[\overline{X_b^\alpha}(iv^\mu D_{\mu ba} - \delta_{ba}\Delta_X)X_{a\alpha} \\ + Tr[\overline{Y_b^{\alpha\beta}}(iv^\mu D_{\mu ba} - \delta_{ba}\Delta_Y)Y_{a\alpha\beta} + Tr[\overline{R_b^{\alpha\beta\rho}}(iv^\mu D_{\mu ba} - \delta_{ba}\Delta_R)T_{a\alpha\beta\rho}]\end{aligned} \tag{3.14}$$

The mass parameter Δ_F (Here $F = S, T, X, Y, R$) in eq 3.14 defined as the mass difference between F state doublets ($F = S, T, X, Y, Z, R$) and ground state doublet (H) in terms of spin average masses with same principle quantum number (n). The expressions for mass parameters are given below:

$$\Delta_F = \overline{M_F} - \overline{M_H}, \quad F = S, T, X, Y, Z, R \tag{3.15a}$$

$$\text{where,} \quad \overline{M_H} = (3m^Q_{P_1^*} + m^Q_{P_0})/4 \tag{3.15b}$$

$$\overline{M_S} = (3m^Q_{P_1'} + m^Q_{P_0^*})/4 \tag{3.15c}$$

$$\overline{M_T} = (5m^Q_{P_2^*} + 3m^Q_{P_1})/8 \tag{3.15d}$$

$$\overline{M_X} = (5m^Q_{P_2} + 3m^Q_{P_1^*})/8 \tag{3.15e}$$

$$\overline{M_Y} = (5m^Q_{P_3^*} + 3m^Q_{P_2'})/8 \tag{3.15f}$$

$$\overline{M_Z} = (7m^Q_{P_3} + 5m^Q_{P_2^*})/12 \tag{3.15g}$$

$$\overline{M_R} = (9m^Q_{P_4^*} + 7m^Q_{P_3'})/12 \tag{3.15h}$$

The $1/m_Q$ corrections to the heavy quark limit are given by symmetry-breaking terms. The effective Lagrangian by including corrections :

$$\mathcal{L}_{1/m_Q} = \frac{1}{2m_Q}[\lambda_H Tr(\overline{H}_a\sigma^{\mu\nu}H_a\sigma_{\mu\nu}) + \lambda_S Tr(\overline{S}_a\sigma^{\mu\nu}S_a\sigma_{\mu\nu}) + \lambda_T Tr(\overline{T}^{\alpha}_a\sigma^{\mu\nu}T^{\alpha}_a\sigma_{\mu\nu})$$
$$+ \lambda_X Tr(\overline{X}^{\alpha}_a\sigma^{\mu\nu}X^{\alpha}_a\sigma_{\mu\nu}) + \lambda_Y Tr(\overline{Y}^{\alpha\beta}_a\sigma^{\mu\nu}Y^{\alpha\beta}_a\sigma_{\mu\nu})$$
$$+ \lambda_Z Tr(\overline{Z}^{\alpha\beta}_a\sigma^{\mu\nu}Z^{\alpha\beta}_a\sigma_{\mu\nu}) + \lambda_R Tr(\overline{R}^{\alpha\beta\rho}_a\sigma^{\mu\nu}R^{\alpha\beta\rho}_a\sigma_{\mu\nu})] \quad (3.16)$$

Here parameters λ_H, λ_S, λ_T, λ_X, λ_Y, λ_Z, λ_R appears in Lagrangian are analogous with hyperfine splittings and expressed in Eq.3.17. These mass terms in Lagrangian are first order in $1/m_Q$, but higher order terms may also be present otherwise. We are restricting to the first order corrections in $(1/m_Q)$.

$$\lambda_H = \frac{1}{8}(M^2_{P^*} - M^2_P) \quad (3.17a)$$
$$\lambda_S = \frac{1}{8}(M^2_{P'_1} - M^2_{P^*_0}) \quad (3.17b)$$
$$\lambda_T = \frac{3}{8}(M^2_{P^*_2} - M^2_{P_1}) \quad (3.17c)$$
$$\lambda_X = \frac{3}{8}(M^2_{P_2} - M^2_{P^*_1}) \quad (3.17d)$$
$$\lambda_Y = \frac{3}{8}(M^2_{P_3} - M^2_{P'^*_2}) \quad (3.17e)$$
$$\lambda_Z = \frac{5}{8}(M^2_{P^*_3} - M^2_{P'_2}) \quad (3.17f)$$
$$\lambda_R = \frac{5}{8}(M^2_{P^*_4} - M^2_{P'^*_3}) \quad (3.17g)$$

In HQET, at the scale of 1 GeV, flavor symmetry spontaneously arises for b (bottom quark) and c (charm quark), and hence elegance of flavor symmetry implies to:

$$\Delta^{(c)}_F = \Delta^{(b)}_F \quad (3.18a)$$
$$\lambda^{(c)}_F = \lambda^{(b)}_F \quad (3.18b)$$

By taking higher order terms of factor $1/m_Q$ in HQET Lagrangian, heavy quark symmetry breaks. This makes parameters Δ_F, λ_F flavor dependent and relations in eq 3.18 are modified by $\delta\Delta_F$, $\delta\lambda_F$ respectively. The hyperfine splitting of the ground state vector and pseudoscalar meson doublets for flavor-dependent parameter λ^Q_F is given as:

$$\frac{\lambda^{(b)}_H}{\lambda^{(c)}_H} = \frac{m^2_{B^*} - m^2_B}{m^2_{D^*} - m^2_D} = \left(\frac{\alpha_s(m_b)}{\alpha_s(m_c)}\right)^{9/25}\left[1 - \mathcal{O}(\frac{\alpha_s}{\pi})\right] + \Lambda_R\left(\frac{1}{2m_c} - \frac{1}{2m_b}\right) \quad (3.19)$$

Where Λ_R is a non-perturbative parameter that accounts for higher order corrections in heavy quark expansion. QCD corrections change the λ_F relation to

$$\lambda_F^{(b)} = \lambda_F^{(c)} \left(\frac{\alpha_s(m_b)}{\alpha_s(m_c)}\right)^{9/25} \tag{3.20}$$

where $\delta\lambda_F = \frac{\alpha_s(m_b)}{\alpha_s(m_c)})^{9/25}$. Also, we are taking $m_c = 1180MeV$ and $m_b = 4390MeV$ in our calculations. The parameter Δ_F modified by $\delta\Delta_F$ is given by:

$$\Delta_F^{(b)} = \Delta_F^{(c)} + \delta\Delta_F \tag{3.21}$$

and

$$\delta\Delta_F = \left(\lambda_1^F - \lambda_1^H\right)\left(\frac{1}{2m_c} - \frac{1}{2m_b}\right) \tag{3.22}$$

where

$$\lambda_1^F - \lambda_1^H = 2m_b m_c \left[\left(\frac{(\overline{M}_F^{b\bar{q}} - \overline{M}_H^{b\bar{q}}) - (\overline{M}_F^{c\bar{q}} - \overline{M}_H^{c\bar{q}})}{m_b - m_c}\right) - 1\right] \tag{3.23}$$

Strange states in HQET have the property that a strange quark in a particular state shifts the mass by the same amount for $n = 1$, $n = 2$, $n = 3$ i.e.

$$M_{P_s} - M_P = \tilde{M}_{P_s} - \tilde{M}_P = \tilde{\tilde{M}}_{P_s} - \tilde{\tilde{M}}_P \tag{3.24}$$

Masses are further used to investigate other properties of mesons, like decay widths, branching ratios, branching fractions, coupling constants, magnetic moments, etc. In the next section, we predicted masses for $n = 3$ for both charm and bottom mesons. We investigated their decay widths and associated upper bounds using predicted masses of charm and bottom mesons. We also included isospin-violating factor in strange bottom meson decay modes. We further construct Regge trajectories, which will check the reliability of HQET.

3.3 Numerical Analysis

Recently observed states like $D_0(2560)$, $D_1^*(2680)$, $D_2(2740)$, $D_3^*(2760)$, $D_J(3000)$, $D_J^*(3000)$ and strange states $D_{s1}^*(2860)$, $D_{s3}(2860)$, $D_{sJ}(3040)$ have stimulated charm sector [10]. Similarly, new observations in the bottom sector like $B_J(5840)^{0,\pm}$, $B_J(5960)$, $B_J(5970)$ and strange states $B_{s2}^*(5840)$, $B_{sJ}(6064)$, $B_{sJ}(6114)$ have enriched bottom sector [10]. Despite these new states, the spectrum of higher charm and bottom mesons is not much explored experimentally. So, in this section, we explored the higher charm and bottom sector and calculated masses, decay widths, and associated coupling constants for $n = 3$ in the HQET framework. Firstly, we calculated masses and then predicted decay widths using calculated masses to check the authenticity of the HQET model. We divided our calculations into two parts - the first one in which we predicted masses of charm and bottom mesons for $n = 3$ with their strange partners and the other one in which we determined strong decay widths in terms of coupling constants using these predicted masses.

3.3.1 Mass Spectroscopy

Mass is a fundamental property to describe spectroscopy of heavy-light mesons. Input values used to calculate masses of charm and charm strange mesons are mentioned in Table 3.4.

To compute the masses of $n = 3$ charm meson states, we first calculated values of average masses $\overline{M_{\approx \atop H}}$, $\overline{M_{\approx \atop S}}$, $\overline{M_{\approx \atop T}}$ ($\approx$ labels for $n = 3$) introduced in Eqs. 3.15 for bottom meson states from Table 3.4, then HQS parameters (heavy quark symmetry) $\Delta_{\approx \atop H}$, $\Delta_{\approx \atop S}$, $\Delta_{\approx \atop T}$, $\lambda_{\approx \atop H}$, $\lambda_{\approx \atop S}$, and $\lambda_{\approx \atop T}$ described in Eqs.3.17 are calculated for same bottom meson states. Since Δ_F, λ_F are flavor independent in HQET, which implies $\Delta_F^{(c)} = \Delta_F^{(b)}$, $\lambda_F^{(c)} = \lambda_F^{(b)}$. With the calculated symmetry parameters Δ_F, λ_F for bottom meson states and then applying heavy quark symmetry, we predicted the masses for $n = 3$ charm mesons listed in Table 3.5. For the details, we elaborate on the calculation part of the mass $D(3^1S_0)$. From Table 3.4, using bottom states, we calculated $\overline{M^b_{\approx \atop H}} = 6338.61\ MeV$, $\overline{M^b_{\tilde{H}}} = 5902\ MeV$. Then, using these two values, we have $\Delta^b_{\approx \atop H} = \overline{M^b_{\approx \atop H}} - \overline{M^b_{\tilde{H}}} = 436.61\ MeV$. Using Eq. 3.17, we get $\lambda^b_{\approx \atop H} = 26161.40$ MeV^2. The symmetry of these parameters given by Eq. 3.18 and implies that $\Delta^c_{\approx \atop H} = 436.61\ MeV$, $\lambda^c_{\approx \atop H} = 26161.40\ MeV^2$. Using the values of $\Delta^c_{\approx \atop H} = 436.61$ MeV and $\lambda^c_{\approx \atop H} = 26161.40\ MeV^2$, we obtained the mass of $D(3^1S_0) = 3030\ MeV$. Similarly, by following the same procedure, we obtained other masses for $n = 3$ charm mesons listed in Table 3.5. Now, using these calculated masses for $n = 3$ charm states, we predicted masses for $n = 3$ bottom meson states by using the same procedure and symmetries. We have taken input for S-wave from Ref. [73], and for P-waves, we take inputs from Table 3.5 for both non-strange and strange states. Results for $n = 3$ bottom meson states are listed in Table 3.7. As we know, experimental observations for higher excited states concerning B-mesons are less as compared to D-mesons. It motivates us to explore more bottom spectra and check validity of our theoretical model (HQET). In this concern, we have predicted masses of experimental missing $1F$-states. It also needs to be mentioned that the study of F-wave charm mesons was done by our team using the same framework [90]. So, we are not calculating or mentioning it in the thesis. Input values used to calculate $1F$ bottom and bottom-strange are shown in Table 3.8. Using the same procedure, we also calculated $1F$ states in the HQET framework and the results are mentioned in Table 3.9

Table 3.4: Input values $3S$ taken from Ref. [91] and remaining are taken from Ref. [73] (MeV).

State	J^P	$b\bar{q}$	$b\bar{s}$	$c\bar{q}$	$c\bar{s}$
3^1S_0	0^-	6326 [91]	6463 [91]	-	-
3^3S_1	1^-	6342 [91]	6474 [91]	-	-
3^3P_0	0^+	6629	6731	-	-
3^1P_1	1^+	6685	6768	-	-
3^3P_1	1^+	6650	6761	-	-
3^3P_2	2^+	6678	6780	-	-
2^1S_0	0^-	5890	5976	2581	2688
2^3S_1	1^-	5906	5992	2632	2731
2^3P_0	0^+	6221	6318	2919	3054
2^1P_1	1^+	6281	6345	3021	3154
2^3P_1	1^+	6209	6321	2932	3067
2^3P_2	2^+	6260	6359	3012	3142

On comparison, our calculated masses for $n = 3$ charm and bottom mesons and also for $1F$-wave bottom mesons nicely agree with other theoretical models. On observing Table 3.5, we found that our estimated masses lie below the predictions of the relativistic quark model in Ref. [73] with the difference of 25-50 MeV. On comparing with Ref. [71], our results lie above their values with few MeV. However, our computed masses for $n = 3$ charm meson without and with strangeness are in overall good agreement with other theoretical estimates. Similarly, on observing Table 3.7, it is also noticed our mass results are in good agreement with other theoretical predictions [73, 92] for both strange and non-strange states. The masses obtained using the heavy quark symmetry for experimentally missing $1F$ states

Table 3.5: Predicted masses for $n = 3$ charm mesons.

$J^P(n^{2S+1}L_J)$	Masses of $n = 3$ charm Mesons (MeV)					
	Non-Strange			Strange		
	Present Results	[73]	[71]	Present Results	[73]	[71]
$0^-(3^1S_0)$	3030	3062	2904	3186.5	3219	3044
$1^-(3^3S_1)$	3064	3096	2947	3209	3242	3087
$0^+(3^3P_0)$	3243	3346	3050	3496	3541	3214
$1^+(3^1P_1)$	3356	3461	3082	3567	3618	3234
$1^+(3^3P_1)$	3281	3365	3085	3508	3519	3244
$2^+(3^3P_2)$	3337	3407	3142	3563	3580	3283

mentioned in Table 3.9 are in agreement with the masses obtained by the relativistic quark model in Ref.[73] with a deviation of $\pm 1.2\%$ for non-strange states while strange states are deviated by $\pm 0.6\%$. On comparing with Ref.[92], our results are deviated by $\pm 3\%$. So, our results are in overall good agreement with other theoretical models.

3.3.2 Decay Widths and Upper Bounds of Associated Couplings

Using our calculated masses, we analyzed strong decay widths and predicted the upper bounds of associated couplings. The strong decays of excited mesons involve the emission of π, K, η, which are treated as goldstone bosons; hence, it is convenient to analyze these interactions. We have studied decays of excited heavy-light mesons (charm and bottom mesons) with emission of pseudoscalar meson only. The decays with emissions of vector mesons (ω, ρ, K^*, ϕ) are also possible and studied in Ref.[93–95]. The contribution of decays with the emission of vector mesons into total decay widths is substantial for these mesonic states. The formulation for decay widths is discussed in Chapter 2. We apply the effective Lagrangian approach discussed in Chapter 2 to calculate OZI-allowed two body strong decay widths in terms of associated couplings.

Numerical values used for calculating decay width are $M_{\pi^0} = 134.97\ MeV$, M_{π^+}

Table 3.6: Input values $3S$ taken from Ref. [73] and remaining are our calculated masses from Table 3.5 (MeV).

State	J^P	$c\bar{q}$	$c\bar{s}$	$b\bar{q}$	$b\bar{s}$
3^1S_0	0^-	3062 [73]	3219 [73]	-	-
3^3S_1	1^-	3096 [73]	3242 [73]	-	-
3^3P_0	0^+	3243	3496	-	-
3^1P_1	1^+	3356	3367	-	-
3^3P_1	1^+	3281	3508	-	-
3^3P_2	2^+	3337	3563	-	-
2^1S_0	0^-	2581	2688	5890	5976
2^3S_1	1^-	2632	2731	5906	5992

Table 3.7: Predicted masses for radially excited bottom mesons.

$J^P(n^{2S+1}L_J)$	Masses of $n=3$ bottom Mesons (MeV)					
	Non-Strange			Strange		
	Present Results	[73]	[92]	Present Results	[73]	[92]
$0^-(3^1S_0)$	6326	6379	6335	6463	6467	6301
$1^-(3^3S_1)$	6342	6387	6355	6474	6475	6319
$0^+(3^3P_0)$	6568	6629	6576	6789	6731	6504
$1^+(3^1P_1)$	6624	6685	6585	6826	6768	6519
$1^+(3^3P_1)$	6581	6650	6557	6792	6761	6516
$2^+(3^3P_2)$	6610	6678	6570	6821	6780	6527

$= 139.57\ MeV$, $M_{K^+} = 493.67\ MeV$, $M_{\eta^0} = 547.85\ MeV$, $M_{K^0} = 497.61\ MeV$, $M_{B^0} = 5279.63\ MeV$, $M_{B^*} = 5324.65\ MeV$, $M_{B_s^0} = 5366.89\ MeV$, $M_{B_s^*} = 5415.40\ MeV$,$M_{D^0} = 1864.83\ MeV$, $M_{D^\mp} = 1869.65\ MeV$, $M_{D_s^\pm} = 1968.34\ MeV$ $M_{D^{*0}} = 2006.85\ MeV$, $M_{D^{*\pm}}= 2010.26\ MeV$, $M_{D_s^{*\pm}}= 2112.20\ MeV$, $M_{D_0^{*0}}= 2318\ MeV$, $M_{D_{s0}^{*\pm}} = 2317.70\ MeV$, $M_{D_1^{\prime 0}} = 2420.80\ MeV$, $M_{D_{s1}^{\prime\pm}} = 2459.50\ MeV$ and estimated masses for $n=3$ charm and bottom mesons and also $1F$-wave bottom meson states.

The computed strong decay widths in terms of $\tilde{\tilde{g}}_{HH}, \tilde{\tilde{g}}_{SH}, \tilde{\tilde{g}}_{TH}$ for radially excited $n=3$ charm and bottom mesons and in terms of g_{ZH}, g_{RH} for $1F$ bottom meson states are presented in Table 3.10, 3.11, 3.12, 3.13, 3.14, 3.15 respectively. We

Table 3.8: Input values used to calculate $1F$ bottom states (MeV).

State	J^P	$c\bar{q}$	$c\bar{s}$	$b\bar{q}$	$b\bar{s}$
1^1S_0	0^-	1869.5 [10]	1969.0[10]	5279.5[10]	5366.91[10]
1^3S_1	1^-	2010.26[10]	2106.6[10]	5324.71[10]	5415.8[10]
1^3F_2	2^+	3132[42]	3208[42]	-	-
$1F_3$	3^+	3143[42]	3218[42]	-	-
$1F_3'$	3^+	3108[42]	3186[42]	-	-
1^3F_4	2^+	3113[42]	3190 [42]	-	-

Table 3.9: Obtained masses for $1F$ bottom mesons.

$J^P(n^{2S+1}L_J)$	Masses of $1F$ Bottom Mesons (MeV)					
	Non-Strange			Strange		
	Calculated	[73]	[92]	Calculated	[73]	[92]
$2^+(1^3F_2)$	6473	6412	6387	6518	6501	6358
$3^+(1F_3)$	6478	6420	6396	6523	6515	6369
$3^+(1F_3')$	6447	6391	6358	6506	6468	6318
$4^+(1^3F_4)$	6450	6380	6364	6508	6475	6328

also include suppression factors in decays, which arise due to violation of isospin symmetry in decays. When the mass difference between the parent heavy-light meson with strangeness and the daughter non-strange heavy-light meson is less than the mass of kaons, then the breaking of isospin symmetry takes place, and suppression factor ϵ incorporated in associated decay mode [96]. To account for isospin violation, suppression factor is given by :

$$\epsilon^2 = \frac{3}{16}\left(\frac{m_d - m_u}{m_s - (\frac{m_u+m_d}{2})}\right) \approx 10^{-4} \tag{3.25}$$

Here m_u, m_d, and m_s are current quark masses. This suppression factor ϵ is multiplied with decay modes, which occur with isospin violation.

Table 3.10: Decay widths of predicted masses for $n = 3$ charm mesons.

States	J^P	Decay modes	Partial Decay widths (MeV)	Total decay width (MeV) [42]	Upper bounds
$D(3030)$	0^-	$D^{*\pm}\pi^-$	$3703.68\tilde{\tilde{g}}^2_{HH}$		
		$D^{*0}\pi^0$	$1867.45\tilde{\tilde{g}}^2_{HH}$		
		$D^{*0}\eta^0$	$378.62\tilde{\tilde{g}}^2_{HH}$		
		$D_s^{*+}K^-$	$1833.79\tilde{\tilde{g}}^2_{HH}$		
		Total	$7783.54\tilde{\tilde{g}}^2_{HH}$	106	
			$\tilde{\tilde{g}}_{HH}$		0.12
$D(3064)$	1^-	$D^+\pi^-$	$1668.5\tilde{\tilde{g}}^2_{HH}$		
		$D^0\pi^0$	$841.07\tilde{\tilde{g}}^2_{HH}$		
		$D^{*+}\pi^-$	$2665.54\tilde{\tilde{g}}^2_{HH}$		
		$D^{*0}\pi^0$	$1343.38\tilde{\tilde{g}}^2_{HH}$		
		$D^0\eta^0$	$208.05\tilde{\tilde{g}}^2_{HH}$		
		$D^{*0}\eta^0$	$282.52\tilde{\tilde{g}}^2_{HH}$		
		$D_s^+K^-$	$1031.87\tilde{\tilde{g}}^2_{HH}$		
		D_sK^0	$1233.43\tilde{\tilde{g}}^2_{HH}$		
		$D_s^+K^-$	$1031.87\tilde{\tilde{g}}^2_{HH}$		
		$D_s^{*+}K^-$	$1389.41\tilde{\tilde{g}}^2_{HH}$		
		Total	$9430.27\tilde{\tilde{g}}^2_{HH}$	103	
			$\tilde{\tilde{g}}_{HH}$		0.11
$D(3243)$	0^+	$D^+\pi^-$	$6893.15\tilde{\tilde{g}}^2_{SH}$		
		$D^0\pi^0$	$3464.3\tilde{\tilde{g}}^2_{SH}$		
		$D^0\eta^0$	$1145.25\tilde{\tilde{g}}^2_{SH}$		
		$D_s^+K^-$	$6061.58\tilde{\tilde{g}}^2_{SH}$		
		Total	$17564.28\tilde{\tilde{g}}^2_{SH}$	163.8	
			$\tilde{\tilde{g}}_{SH}$		0.09
$D(3356)$	1^+	$D^{*0}\pi^0$	$3528.38\tilde{\tilde{g}}^2_{SH}$		
		$D^{*+}\pi^-$	$7028.54\tilde{\tilde{g}}^2_{SH}$		
		$D^{*0}\eta^0$	$1160.11\tilde{\tilde{g}}^2_{SH}$		
		$D_s^{*+}K^-$	$6053.09\tilde{\tilde{g}}^2_{SH}$		

Table 3.10: Decay widths of predicted masses for $n = 3$ charm mesons.

States	J^P	Decay modes	Partial Decay widths (MeV)	Total decay width (MeV) [42]	Upper bounds
		Total	$17770.12\widetilde{\widetilde{g}}^2_{SH}$	120.2	
			$\widetilde{\widetilde{g}}_{SH}$		0.08
$D(3281)$	1^+	$D^{*0}\pi^0$	$4258.74\widetilde{\widetilde{g}}^2_{TH}$		
		$D^{*+}\pi^-$	$8426.74\widetilde{\widetilde{g}}^2_{TH}$		
		$D^{*0}\eta^0$	$854.16\widetilde{\widetilde{g}}^2_{TH}$		
$D(3281)$		$D^{*+}_s K^-$	$3968.1\widetilde{\widetilde{g}}^2_{TH}$		
		Total	$17507.75\widetilde{\widetilde{g}}^2_{TH}$	187.6	
			$\widetilde{\widetilde{g}}_{TH}$		0.10
$D(3337)$	2^+	$D^+\pi^-$	$2705.93\widetilde{\widetilde{g}}^2_{TH}$		
		$D^0\pi^0$	$1367.81\widetilde{\widetilde{g}}^2_{TH}$		
		$D^{*+}\pi^-$	$5977.98\widetilde{\widetilde{g}}^2_{TH}$		
		$D^{*0}\pi^0$	$3029.18\widetilde{\widetilde{g}}^2_{TH}$		
		$D^0\eta^0$	$312.75\widetilde{\widetilde{g}}^2_{TH}$		
		$D^{*0}\eta^0$	$635.44\widetilde{\widetilde{g}}^2_{TH}$		
		$D^+_s K^-$	$1564.54\widetilde{\widetilde{g}}^2_{TH}$		
		$D^{*+}_s K^-$	$3010.47\ \widetilde{\widetilde{g}}^2_{TH}$		
		Total	$18604.10\widetilde{\widetilde{g}}^2_{TH}$	116.3	
			$\widetilde{\widetilde{g}}_{TH}$		0.08

Table 3.11: Decay widths of obtained masses for $n = 3$ strange charm mesons.

States	J^P	Decay modes	Partial Decay widths (MeV)	Total decay width (MeV)[42]	Upper bounds
$D^+_s(3186)$	0^-	D^*K^+	$3869.08\widetilde{\widetilde{g}}^2_{HH}$		
		$D^{*+}K^0$	$3848.36\widetilde{\widetilde{g}}^2_{HH}$		
		$D^{*+}_s\eta^0$	$1858.32\widetilde{\widetilde{g}}^2_{HH}$		
		Total	$9575.76\widetilde{\widetilde{g}}^2_{HH}$	106	

Table 3.11: Decay widths of obtained masses for $n = 3$ strange charm mesons.

States	J^P	Decay modes	Partial Decay widths (MeV)	Total decay width (MeV)[42]	Upper bounds
			$\widetilde{\widetilde{g}}_{HH}$		0.09
$D_s^+(3209)$	1^-	D^+K^0	$1720.77\widetilde{\widetilde{g}}^2_{HH}$		
		D^0K^+	$1739.82\widetilde{\widetilde{g}}^2_{HH}$		
		$D^{*+}K^0$	$2712.35\widetilde{\widetilde{g}}^2_{HH}$		
		$D^{*0}K^+$	$2744.24\widetilde{\widetilde{g}}^2_{HH}$		
$D_s^+(3209)$		$D_s^+\eta^0$	$915.91\widetilde{\widetilde{g}}^2_{HH}$		
		$D_s^{*+}\eta^0$	$1329.13\widetilde{\widetilde{g}}^2_{HH}$		
		$D_s^{*+}\pi^0$	$948.81\widetilde{\widetilde{g}}^2_{HH}$		
		Total	$82111.03\widetilde{\widetilde{g}}^2_{HH}$	103	
			$\widetilde{\widetilde{g}}_{HH}$		0.29
$D_s^+(3496)$	0^+	$D_S^+\pi^0$	$4517.26\widetilde{\widetilde{g}}^2_{SH}$		
		$D_s^+\eta$	$6002.88\widetilde{\widetilde{g}}^2_{SH}$		
		D^0K^+	$9826.27\widetilde{\widetilde{g}}^2_{SH}$		
		D^+K^0	$9863.43\widetilde{\widetilde{g}}^2_{SH}$		
		Total	$30209.84\widetilde{\widetilde{g}}^2_{SH}$	163.8	
			$\widetilde{\widetilde{g}}_{SH}$		0.06
$D_s^+(3567)$	1^+	D^*K^+	$8194.67\widetilde{\widetilde{g}}^2_{SH}$		
		$D^{*+}K^0$	$8179.21\widetilde{\widetilde{g}}^2_{SH}$		
		$D_s^{*+}\eta^0$	$5723.21\widetilde{\widetilde{g}}^2_{HH}$		
		$D_s^{+*}\pi^0$	$4333.65\widetilde{\widetilde{g}}^2_{SH}$		
		Total	$26430.74\widetilde{\widetilde{g}}^2_{SH}$	120.2	
			$\widetilde{\widetilde{g}}_{SH}$		0.07
$D_s^+(3508)$	1^+	D^*K^+	$9302.31\widetilde{\widetilde{g}}^2_{TH}$		
		$D^{*+}K^0$	$9246.22\widetilde{\widetilde{g}}^2_{TH}$		
		$D_s^{*+}\eta^0$	$5675.62\widetilde{\widetilde{g}}^2_{TH}$		
		$D_s^{+*}\pi^0$	$7613.48\widetilde{\widetilde{g}}^2_{TH}$		
		Total	$31837.63\widetilde{\widetilde{g}}^2_{TH}$	187.6	

Table 3.11: Decay widths of obtained masses for $n = 3$ strange charm mesons.

States	J^P	Decay modes	Partial Decay widths (MeV)	Total decay width (MeV)[42]	Upper bounds
			$\tilde{\tilde{g}}_{TH}$		0.06
$D_s^+(3563)$	2^+	$D^* K^+$	$16804.3\tilde{\tilde{g}}_{TH}^2$		
		$D^{*+} K^0$	$16885.1\tilde{\tilde{g}}_{TH}^2$		
		$D_s^{*+} \eta^0$	$5675.62\tilde{\tilde{g}}_{TH}^2$		
		$D_s^{*+} \pi^0$	$1150.23\tilde{\tilde{g}}_{TH}^2$		
$D_s^+(3563)$		$D_s^+ \eta$	$11505.4\tilde{\tilde{g}}_{SH}^2$		
		$D^+ K^0$	$22261.8\tilde{\tilde{g}}_{SH}^2$		
		$D^0 K^+$	$22204.4\tilde{\tilde{g}}_{SH}^2$		
		$D_s^+ \pi^0$	$11872.7\tilde{\tilde{g}}_{TH}^2$		
		Total	$108359.38\tilde{\tilde{g}}_{TH}^2$	116.3	
			$\tilde{\tilde{g}}_{TH}$		0.035

Table 3.12: Decay widths of obtained masses for $n = 3$ bottom mesons.

States	J^P	Decay modes	Partial Decay widths (MeV)	Total decay width (MeV) [92]	Upper bounds
$B(6326)$	0^-	$B^* \pi^+$	$6036.89\tilde{\tilde{g}}_{HH}^2$		
		$B^* \pi^0$	$3024.30\tilde{\tilde{g}}_{HH}^2$		
		$B^* \eta^0$	$2423.70\tilde{\tilde{g}}_{HH}^2$		
		$B_s^* K^0$	$2883.13\ \tilde{\tilde{g}}_{HH}^2$		
		Total	$17222.24\tilde{\tilde{g}}_{HH}^2$	150.6	
			$\tilde{\tilde{g}}_{HH}$		0.09
$B(6342)$	1^-	$B^+ \pi^-$	$2351.72\tilde{\tilde{g}}_{HH}^2$		
		$B^0 \pi^0$	$1178.60\tilde{\tilde{g}}_{HH}^2$		
		$B^{*+} \pi^-$	$2102.57\tilde{\tilde{g}}_{HH}^2$		
		$B^{*0} \pi^0$	$1053.26\tilde{\tilde{g}}_{HH}^2$		

Table 3.12: Decay widths of obtained masses for $n = 3$ bottom mesons.

States	J^P	Decay modes	Partial Decay widths (MeV)	Total decay width (MeV) [92]	Upper bounds
		$B^0\eta^0$	$1010.34\tilde{\tilde{g}}^2_{HH}$		
		B_sK^0	$1233.43\tilde{\tilde{g}}^2_{HH}$		
		$B_s^{*0}K^0$	$1020.49\tilde{\tilde{g}}^2_{HH}$		
		Total	$9950.41\tilde{\tilde{g}}^2_{HH}$	140.6	
			$\tilde{\tilde{g}}_{HH}$		0.12
$B(6568)$	0^+	$B^+\pi^-$	$11857.7\tilde{\tilde{g}}^2_{SH}$		
$B(6568)$		$B^0\pi^0$	$5925.86\tilde{\tilde{g}}^2_{SH}$		
		$B^0\eta^0$	$6280.66\tilde{\tilde{g}}^2_{SH}$		
		$B_s^0K^0$	$9420.99\tilde{\tilde{g}}^2_{SH}$		
		Total	$33485.21\tilde{\tilde{g}}^2_{SH}$	166.8	
			$\tilde{\tilde{g}}_{SH}$		0.07
$B(6624)$	1^+	$B^{*0}\pi^0$	$6084.5\tilde{\tilde{g}}^2_{SH}$		
		$B^{*+}\pi^-$	$12166.2\tilde{\tilde{g}}^2_{SH}$		
		$B^{*0}\eta^0$	$8445.9\tilde{\tilde{g}}^2_{SH}$		
		$B_s^{*0}K^0$	$9620.58\tilde{\tilde{g}}^2_{SH}$		
		Total	$36317.18\tilde{\tilde{g}}^2_{SH}$	93.4	
			$\tilde{\tilde{g}}_{SH}$		0.05
$B(6581)$	1^+	$B^*\pi^+$	$18708.7\tilde{\tilde{g}}^2_{TH}$		
		$B^*\pi^0$	$9373.41\tilde{\tilde{g}}^2_{TH}$		
		$B^{*0}\eta^0$	$9218.74\tilde{\tilde{g}}^2_{TH}$		
		$B_s^{*0}K^0$	$8432.98\tilde{\tilde{g}}^2_{TH}$		
		Total	$45733.83\tilde{\tilde{g}}^2_{TH}$	174.8	
			$\tilde{\tilde{g}}_{TH}$		0.06
$B(6610)$	2^+	$B^+\pi^-$	$9587.29\tilde{\tilde{g}}^2_{TH}$		
		$B^0\pi^0$	$4793.99\tilde{\tilde{g}}^2_{TH}$		
		$B^{*+}\pi^-$	$12394.20\tilde{\tilde{g}}^2_{TH}$		
		$B^{*0}\pi^0$	$6209.21\tilde{\tilde{g}}^2_{TH}$		
		$B^{*0}\eta^0$	$5130.64\tilde{\tilde{g}}^2_{TH}$		

Table 3.12: Decay widths of obtained masses for $n = 3$ bottom mesons.

States	J^P	Decay modes	Partial Decay widths (MeV)	Total decay width (MeV) [92]	Upper bounds
		$B_s^0 K^0$	$4756.24\tilde{\tilde{g}}_{TH}^2$		
		$B_s^{*0} K^0$	$3850.11\ \tilde{\tilde{g}}_{TH}^2$		
		Total	$46721.68\tilde{\tilde{g}}_{TH}^2$	87.7	
			$\tilde{\tilde{g}}_{TH}$		0.043

Table 3.13: Decay widths of obtained masses for $n = 3$ strange bottom mesons.

States	J^P	Decay modes	Partial Decay widths (MeV)	Total decay width (MeV) [92]	Upper bounds
$B_s(6463)$	0^-	$B^{*+}K^-$	$6334.56\tilde{\tilde{g}}_{HH}^2$		
		$B^{*0}K^0$	$6299.04\tilde{\tilde{g}}_{HH}^2$		
		$B_s^*\eta^0$	$4349\tilde{\tilde{g}}_{HH}^2$		
		$B_s^*\pi^0$	$3434.59\tilde{\tilde{g}}_{HH}^2 \times 10^{-4}$		
		Total	$33965.54\tilde{\tilde{g}}_{HH}^2$	120.80	
			$\tilde{\tilde{g}}_{HH}$		0.06
$B_s(6474)$	1^-	B^+K^-	$2461.5\tilde{\tilde{g}}_{HH}^2$		
		B^0K^0	$2449.5\tilde{\tilde{g}}_{HH}^2$		
		$B^{*+}K^-$	$4363.97\tilde{\tilde{g}}_{HH}^2$		
		$B^{*0}K^0$	$4340.19\tilde{\tilde{g}}_{HH}^2$		
		$B_s^0\eta^0$	$295.15\tilde{\tilde{g}}_{HH}^2$		
		$B_s^*\pi^0$	$2357.22\ \tilde{\tilde{g}}_{HH}^2 \times 10^{-4}$		
		$B_s^*\eta^0$	$503.26\tilde{\tilde{g}}_{HH}^2$		
		Total	$38777.78\tilde{\tilde{g}}_{HH}^2$	129.8	
			$\tilde{\tilde{g}}_{HH}$		0.06
$B_s(6789)$	0^+	B^+K^-	$17188.00\tilde{\tilde{g}}_{SH}^2$		
		B^0K^0	$17168.00\tilde{\tilde{g}}_{SH}^2$		

Table 3.13: Decay widths of obtained masses for $n = 3$ strange bottom mesons.

States	J^P	Decay modes	Partial Decay widths (MeV)	Total decay width (MeV) [92]	Upper bounds
		$B_s^0\eta^0$	$2447.79\tilde{\tilde{g}}_{SH}^2$		
		$B_s^0\pi^0$	$7676.52\tilde{\tilde{g}}_{SH}^2 \times 10^{-4}$		
		Total	$70286.76\tilde{\tilde{g}}_{SH}^2$	51	
			$\tilde{\tilde{g}}_{SH}$		0.03
$B_s(6826)$	1^+	$B_s^{*0}\pi^0$	$7544.37\tilde{\tilde{g}}_{SH}^2 \times 10^{-4}$		
		$B_s^{*0}\eta^0$	$2402.4\tilde{\tilde{g}}_{SH}^2$		
		$B^{*0}K^0$	$16993.60\ \tilde{\tilde{g}}_{SH}^2$		
		$B^{*+}K^-$	$17003.21\ \tilde{\tilde{g}}_{SH}^2$		
		Total	$36399.96\tilde{\tilde{g}}_{SH}^2$	108.2	
			$\tilde{\tilde{g}}_{SH}$		0.05
$B_s(6792)$	1^+	$B^{*+}K^-$	$27966.7\tilde{\tilde{g}}_{TH}^2$		
		$B^{*0}K^0$	$27822.9\tilde{\tilde{g}}_{TH}^2$		
		$B_s^{*0}\pi^0$	$14178.2\tilde{\tilde{g}}_{TH}^2 \times 10^{-4}$		
		$B_s^{*0}\eta^0$	$3132.08\tilde{\tilde{g}}_{TH}^2$		
		Total	$58923.09\tilde{\tilde{g}}_{TH}^2$	47.7	
			$\tilde{\tilde{g}}_{TH}$		0.03
$B_s(6821)$	2^+	$B^{*+}K^-$	$18439.00\tilde{\tilde{g}}_{TH}^2$		
		$B^{*0}K^0$	$18348.20\tilde{\tilde{g}}_{TH}^2$		
		$B_s^{*0}\pi^0$	$9303.23\tilde{\tilde{g}}_{TH}^2 \times 10^{-4}$		
		$B_s^{*0}\eta^0$	$2091.96\tilde{\tilde{g}}_{TH}^2$		
		B^+K^-	$14139.4\tilde{\tilde{g}}_{TH}^2$		
		B^0K^0	$14058.10\tilde{\tilde{g}}_{TH}^2$		
		$B_s^0\pi^0$	$7158.8\ \tilde{\tilde{g}}_{TH}^2 \times 10^{-4}$		
		$B_s^0\eta^0$	$1655.24\ \tilde{\tilde{g}}_{TH}^2$		
		Total	$68733.35\tilde{\tilde{g}}_{TH}^2$	106.8	
			$\tilde{\tilde{g}}_{TH}$		0.04

Table 3.14: Decay widths of obtained masses for $1F$ non strange bottom mesons.

States	J^P	Decay modes	Partial Decay widths (MeV)	Total decay width (MeV)[92]	Upper bounds
$B(6473)$	2^+	$B^{*+}\pi^-$	$3347.69g^2_{ZH}$		
		$B^{*0}\pi^0$	$1672.14g^2_{ZH}$		
		$B^{*0}\eta^0$	$1367.92g^2_{ZH}$		
		$B^*_sK^0$	$1328.31g^2_{ZH}$		
		$B^+\pi^-$	$6262.1g^2_{ZH}$		
$B(6473)$		$B^0\eta^0$	$2657.76g^2_{ZH}$		
		$B^0_sK^0$	$2774.61g^2_{ZH}$		
		$B^0\pi^0$	$3128.25g^2_{ZH}$		
		Total	$22538.78g^2_{ZH}$	202.4	
			g_{ZH}		0.09
$B(6478)$	3^+	$B^{*0}\pi^0$	$4609.40g^2_{ZH}$		
		$B^{*+}\pi^-$	$9201.01g^2_{ZH}$		
		$B^{*0}\eta^0$	$3823.83g^2_{ZH}$		
		$B^{*0}_sK^0$	$3700.1g^2_{ZH}$		
		Total	$21334.34g^2_{ZH}$	105.2	
			g_{ZH}		0.07
$B(6447)$	3^+	$B^{*0}\pi^0$	$29675g^2_{RH}$		
		$B^{*+}\pi^-$	$14898.6g^2_{RH}$		
		$B^{*0}\eta^0$	$7117.82g^2_{RH}$		
		$B^{*0}_sK^0$	$5933.87g^2_{RH}$		
		Total	$57625.29g^2_{RH}$	221.8	
			g_{RH}		0.06
$B(6450)$	4^+	$B^{*+}\pi^-$	$16168g^2_{RH}$		
		$B^{*0}\pi^0$	$8117.39g^2_{RH}$		
		$B^{*0}\eta^0$	$3856.74g^2_{RH}$		
		$B^*_sK^0$	$3208.9g^2_{RH}$		
		$B^+\pi^-$	$21811.5g^2_{RH}$		
		$B^0\eta^0$	$5638.37g^2_{RH}$		

Table 3.14: Decay widths of obtained masses for $1F$ non strange bottom mesons.

States	J^P	Decay modes	Partial Decay widths (MeV)	Total decay width (MeV)[92]	Upper bounds
		$B_s^0 K^0$	$5731.86g_{RH}^2$		
		$B^0\pi^0$	$10925.9g_{ZH}^2$		
		Total	$22538.78g_{ZH}^2$	110.0	
			g_{RH}		0.07

Table 3.15: Decay widths of obtained masses for $1F$ strange bottom mesons.

States	J^P	Decay modes	Partial Decay widths (MeV)	Total decay width (MeV) [92]	Upper bounds
$B_s(6518)$	2^+	$B^{*0}K^0$	$1850.44g_{ZH}^2$		
		$B^{*-}K^+$	$1864.99g_{ZH}^2$		
		$B_s^{*0}\eta^0$	$152.47g_{ZH}^2$		
		$B_s^*\pi^0$	$861.63g_{ZH}^2\ \times10^{-4}$		
		B^0K^0	$3601.08g_{ZH}^2$		
		B^-K^+	$3632.92g_{ZH}^2$		
		$B_s^0\eta^0$	$317.73g_{ZH}^2$		
		$B_s^0\pi^0$	$1687.81g_{ZH}^2\ \times10^{-4}$		
		Total	$11419.88g_{ZH}^2$	256.3	
			g_{ZH}		0.15
$B_s(6523)$	3^+	$B^{*-}K^+$	$4762.7g_{ZH}^2$		
		$B^{*0}K^0$	$4727.53g_{ZH}^2$		
		$B_s^{*0}\eta^0$	$394.77g_{ZH}^2$		
		$B_s^{*0}\pi^0$	$2216.24g_{ZH}^2\ \times10^{-4}$		
		Total	$9885.22g_{ZH}^2$	138.4	
			g_{ZH}		0.12
$B_s(6506)$	3^+	$B^{*-}K^+$	$12627.5g_{RH}^2$		

Table 3.15: Decay widths of obtained masses for $1F$ strange bottom mesons.

States	J^P	Decay modes	Partial Decay widths (MeV)	Total decay width (MeV) [92]	Upper bounds
		$B^{*0}K^0$	$12434.2g_{RH}^2$		
		$B_s^{*0}\eta^0$	$714.78g_{RH}^2$		
		$B_s^{*0}\pi^0$	$7469.58g_{RH}^2 \times10^{-4}$		
		Total	$25777.23g_{RH}^2$	274	
			g_{RH}		0.10
$B_s(6508)$	4^+	$B^{*0}K^0$	$7023.53g_{RH}^2$		
		$B^{*-}K^+$	$7131.87g_{RH}^2$		
		$B_s^{*0}\eta^0$	$405.17g_{RH}^2$		
		$B_s^{*}\pi^0$	$4211.83g_{RH}^2 \times10^{-4}$		
		B^0K^0	$8073.71g_{RH}^2$		
$B_s(6508)$		B^-K^+	$8207.52g_{RH}^2$		
		$B_s^0\eta^0$	$518.27\ g_{RH}^2$		
		$B_s^0\pi^0$	$4787.05g_{RH}^2 \times10^{-4}$		
		Total	$31360.97g_{RH}^2$	138.6	
			g_{RH}		0.07

The computed strong decay widths in terms of coupling constants $\tilde{\tilde{g}}_{HH}$, $\tilde{\tilde{g}}_{SH}$, $\tilde{\tilde{g}}_{TH}$ for $n = 3$ charm mesons and bottom mesons and $1F$ states are presented in Table 3.10, 3.11, 3.12, 3.13, 3.14, 3.15 respectively. Without enough experimental data, it is not possible to determine values of coupling constants from heavy quark symmetry solely, but the upper bounds to these coupling are mentioned in Table 3.10,3.11, 3.12, 3.13, 3.14, 3.15. In our study, we are taking limited modes of decay and that also only to ground state. We believe that a particular state like $D(3030)$ give $7783.54\tilde{\tilde{g}}^2_{HH}$ total decay width; when compared with total decay widths mentioned by other theoretical paper [42, 92], we provided an upper bound on $\tilde{\tilde{g}}_{HH}$ value. Now if we take additional modes, then value of $\tilde{\tilde{g}}_{HH}$ will be lesser than 0.12 ($\tilde{\tilde{g}}_{HH} < 0.12$). So, these upper bounds may give important information to other associated charm states. Large fractions of the decay width of any excited state are dominated by modes that include the ground state. This work also provides a lower limit to total decay width, giving important clues to forthcoming experimental studies. The weak and radiative decays are not included in the computed decay widths of charm and bottom mesons. We also exclude decays via emissions of vector mesons (ω, ρ, K^*, ϕ). They give the contribution of ± 50 MeV [42, 92] to total decay widths for states analyzed above.

The coupling constant plays an important role in hadron spectroscopy. They are coupled with decays and give information about the strength of strong transitions of excited heavy meson doublets into the highest heavy meson doublets. Here, dimensionless coupling constants g_{HH}, g_{SH}, g_{TH}, g_{ZH}, g_{RH} give the strength of transitions between $H-H, S-H, T-H, Z-H$, and $R-H$ fields, respectively. Values of coupling constants are more for ground state transitions ($H-H$ fields) than excited states ($S-H, T-H, X-H, Z-H, R-H$ fields) transition shown by value of $g_{HH} = 0.64 \pm 0.075$ [44] while $g_{SH} = 0.56 \pm 0.04$, $g_{TH} = 0.43 \pm 0.01$ [44], $g_{XH} = 0.24$ [78]. Also, values of coupling constants are low at higher orders ($n = 2$, $n = 3$) in comparison to lower order ($n = 1$) interactions [44, 97] like $\tilde{g}_{HH} = 0.28 \pm 0.015$, $\tilde{g}_{SH} = 0.18 \pm 0.01$ so on. This progression also supports the values of coupling constants computed here.

3.3.3 Regge Trajectories

Regge trajectory is an effective phenomenological approach to describe hadrons spectroscopy. The plot between total angular momentum(J) and radial quantum number(n_r) of hadrons against the square of their masses(M^2) provides information about the quantum number of the particular state and also helps to identify recently observed states. We use the following definitions:

(a). The (J,M^2) Regge trajectories:

$$J = \alpha M^2 + \alpha_0 \tag{3.26}$$

(b). The (n_r, M^2) Regge trajectories:

$$n_r = \beta M^2 + \beta_0 \tag{3.27}$$

Here α, β are slopes and α_0, β_0 are intercepts. We plot Regge trajectories in plane (J, M^2) with natural parity $P = (-1)^J$ and unnatural parity $P = (-1)^{J-1}$ for heavy-light mesons using predicted spectroscopic data. The plots of Regge trajectories in the (J, M^2) plane are also known as Chew-Frautschi plots [98–100]. For charm mesons $n = 3$, we construct Regge trajectories in the plane (J, M^2) with natural parity $P = (-1)^J$ and unnatural parity $P = (-1)^{J-1}$ depicted in fig. 3.1 – 3.4. Regge trajectories in plane (n_r, M^2) are constructed in Fig. 3.5 – 3.6 using spin averaged masses for S and P-waves where spin averaged masses for S-wave is given by $S = (3m^Q_{H^*} + m^Q_H)/8$ and for P-wave is $P = (5m^Q_{S^*} + 3m^Q_S)/8$. In fig 3.1 – 3.6, masses for $n = 1$ are taken from PDG [10]; for $n = 2$ masses are taken from Ref. [73] and for $n = 3$, we are taking our calculated masses (Table 3.5). Our calculated data fit on Regge lines with good accuracy. By fixing slopes and intercepts of these Regge trajectories (Table 3.16), we calculate higher masses listed in Tables 3.17 and 3.18. Using Regge trajectories, we also assign a quantum number to state $D^*_2(3000)$. The state $D^*_2(3000)$ is reported by LHCb collaboration in 2016 by studying $B^- \to D^+\pi^-\pi^-$ decay . This state is analyzed by different theoretical models and suggested different assignments. Using relativistic quark model, Zhi-Gang Wang studied $D^*_2(3000)$ state and assign it to be $1F^+_{\frac{5}{2}}$ state [54]. They also analyzed this state by help of $^3P_0$ model and suggested it to be 3^3P_2. There is an ambiguity in J^P of the state $D^*_2(3000)$. So, here we assigned J^P for $D^*_2(3000)$ using Regge trajectories with plane (J, M^2) and suggested it to be 1^3F_2 and 2^3P_2 state respectively. In fig.3.7, mass for 1^3P_0 is taken from PDG [10]; mass for 1^3D_1 is from Ref.[73] and we take $D^*_2(3000)$ as 1^3F_2. To clearify its assignment out of these two states (2^3P_2, 1^3F_2), we studied branching ratio $BR = \frac{\Gamma(D^*_2(3000)\to D^*\pi)}{\Gamma(D^*_2(3000)\to D\pi)}$. The value of the branching ratio for 2^3P_2 is 1.06, suggesting $D^*\pi$ to be the dominant mode over $D\pi$. But the value of the branching ratio for 1^3F_2 is 0.40, suggesting $D\pi$ to be the dominant mode. Experimentally $D^*\pi$ decay mode for $D^*_2(3000)$ is suppressed. Hence 1^3F_2 is most favourable assignment for $D^*_2(3000)$ Ref.[90].

For $n = 3$ bottom mesons, we construct Regge trajectories in plane (J, M^2) with natural parity $P = (-1)^J$ and unnatural parity $P = (-1)^{J-1}$ depicted in fig. 3.8 – 3.11. Regge trajectories in the plane (n_r, M^2) are constructed in Fig. 3.12 – 3.13 using spin averaged masses for S and P-waves bottom mesons similar to charm mesons. In fig 3.8 – 3.13, masses for $n = 1$ are taken from PDG [10]; for $n = 2$ masses are taken from Ref. [73] and for $n = 3$, we are taking our calculated masses (Table 3.7). Using calculated slopes and intercepts (Table 3.19), we predicted masses for $n = 4$ bottom mesons for both non-strange and strange states listed in Tables 3.20 and 3.21.

For $1F$ states, the plots are shown in fig. 3.14 – 3.17. In fig 3.14 – 3.17, masses for S-wave and P-wave $(1^+, 2^+)$ are taken from PDG; remaining masses are taken from Ref.[73] and for $1F$, we are taking our calculated masses. Regge trajectories are known to be linear for mesons; it supports our obtained results and helps to define spin parity state to higher resonance. Since Regge lines are almost linear, parallel and equidistant in fig 3.14 – 3.17. Regge slopes (α) and Regge intercepts α_0 are listed in Table 3.22. Our results are nicely fit on Regge lines, which justifies the authenticity of HQET formulation also.

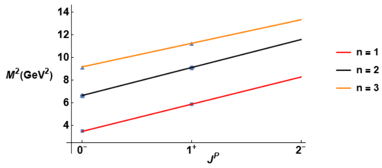

Figure 3.1: Regge trajectories with unnatural parity for non-strange charm mesons.

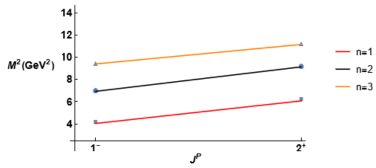

Figure 3.2: Regge trajectories with natural parity for non-strange charm mesons.

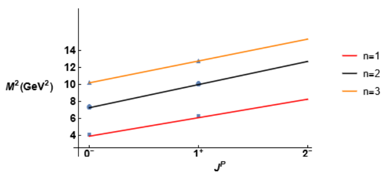

Figure 3.3: Regge trajectories with unnatural parity for strange charm mesons.

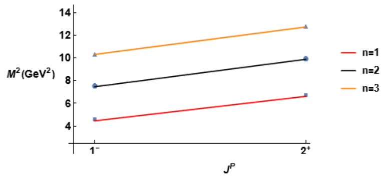

Figure 3.4: Regge trajectories with natural parity for strange charm meson.

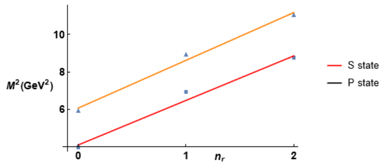

Figure 3.5: Regge trajectories for spin average masses for non-strange charm meson in plane($M^2 \to n_r$).

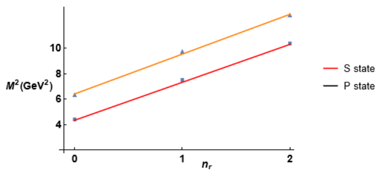

Figure 3.6: Regge trajectories for spin average masses for strange charm meson in plane($M^2 \to n_r$).

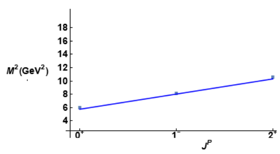

Figure 3.7: Regge lines in plane($M^2 \to J^P$) to identify $D_2(3000)$.

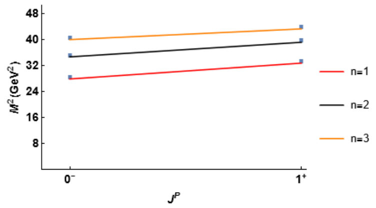

Figure 3.8: Regge trajectories with unnatural parity for non-strange bottom mesons.

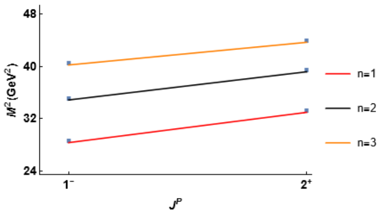

Figure 3.9: Regge trajectories with natural parity for non-strange bottom mesons.

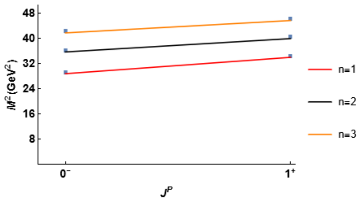

Figure 3.10: Regge trajectories with unnatural parity for strange bottom mesons.

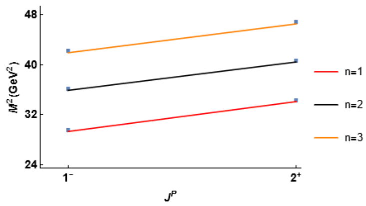

Figure 3.11: Regge trajectories with natural parity for strange bottom meson.

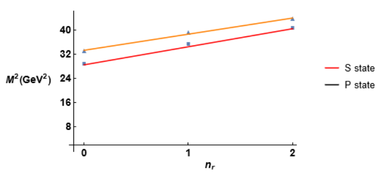

Figure 3.12: Regge trajectories for spin average masses for non strange bottom meson in plane($M^2 \rightarrow n_r$).

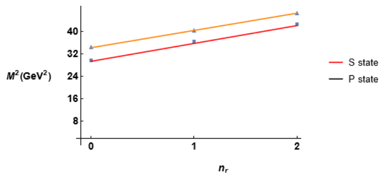

Figure 3.13: Regge trajectories for spin average masses for strange bottom meson in plane($M^2 \rightarrow n_r$).

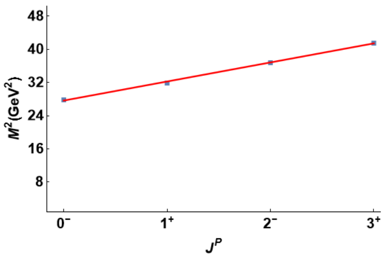

Figure 3.14: Regge trajectories with unnatural parity for non-strange $1F$ bottom meson in the plane($M^2 \rightarrow J^P$).

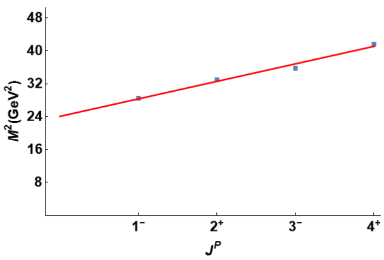

Figure 3.15: Regge trajectories with natural parity for non-strange $1F$ bottom meson in the plane($M^2 \rightarrow J^P$).

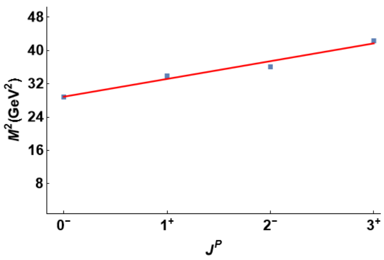

Figure 3.16: Regge trajectories with unnatural parity for strange $1F$ bottom meson in the plane($M^2 \rightarrow J^P$).

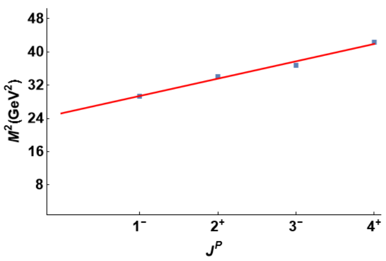

Figure 3.17: Regge trajectories with natural parity for strange 1F bottom meson in the plane $(M^2 \to J^P)$.

Table 3.16: Regge slopes and Regge intercepts for charm mesons.

Mesons	State	Slope (β)	Intercepts (β_0)
D	0^-	0.350	-1.258
	1^-	0.372	-1.536
	0^+	0.417	-2.460
	1^+	0.372	-2.189
	1^+	0.404	-2.423
	2^+	0.926	-2.394
D_s	0^-	0.317	-1.188
	1^-	0.339	-1.456
	0^+	0.291	-1.535
	1^+	0.299	-1.780
	1^+	0.332	-2.028
	2^+	0.325	-2.075

Table 3.17: Non strange charm masses lying in Regge lines in plane (n_r, M^2).

State	J^P	Masses (MeV)	Ref.[42]
4^1S_0	0^-	3484	3468
4^3S_1	1^-	3489	3497
4^3P_0	0^+	3618	3697
4^1P_1	1^+	3733	3709
4^3P_1	1^+	3662	3681
4^3P_2	1^+	3716	3701

Table 3.18: Strange charm masses lying in Regge lines in (n_r, M^2).

State	J^P	Masses (MeV)	Ref.[42]
4^1S_0	0^-	3633	3547
4^3S_1	1^-	3621	3575
4^3P_0	0^+	3946	3764
4^1P_1	1^+	3998	3778
4^3P_1	1^+	3889	3764
4^3P_2	1^+	3951	3783

Table 3.19: Regge slopes and Regge intercepts for $1F$ bottom mesons.

Mesons	State	Slope (β)	Intercepts (β_0)
B	0^-	0.164	-4.602
	1^-	0.168	-4.790
	0^+	0.197	-6.554
	1^+	0.188	-6.312
	1^+	0.189	-6.213
	2^+	0.185	-6.151
B_s	0^-	0.154	-4.453
	1^-	0.159	-4.669
	0^+	0.165	-5.625
	1^+	0.164	-5.622
	1^+	0.164	-5.583
	2^+	0.161	-5.495

Table 3.20: Non strange bottom masses lying in Regge lines in plane (n_r, M^2).

State	J^P	Masses (MeV)	Ref.[92]
4^1S_0	0^-	6812	6689
4^3S_1	1^-	6811	6703
4^3P_0	0^+	6959	6890
4^1P_1	1^+	7037	6872
4^3P_1	1^+	6985	6897
4^3P_2	1^+	7029	6883

Table 3.21: Strange bottom masses Lying in Regge lines in (n_r, M^2).

State	J^P	Masses (MeV)	Ref.[92]
4^1S_0	0^-	6958	6759
4^3S_1	1^-	6951	6773
4^3P_0	0^+	7217	6950
4^1P_1	1^+	7254	6946
4^3P_1	1^+	7224	6959
4^3P_2	1^+	7265	6956

Table 3.22: Regge slopes and Regge intercepts.

Figure No.	Slope (α) $[MeV^{-2}]$	Intercepts (α_0)
3.14	0.195	-5.304
3.15	0.217	-5.078
3.16	0.222	-6.521
3.17	0.236	-5.905

3.3.4 Determination of Coupling Constants from Heavy Quark Symmetry

In this section, we studied and analyzed decay widths of $n = 3$ S-wave bottom mesons by using predicted masses listed in Table 3.7. In the previous section, we studied the upper bounds of associated couplings, and only ground state decays are taken into account. But in this Section, we studied all strong decays of S-wave bottom meson via emission of light pseudoscalar mesons and calculated the value of coupling constants by heavy quark symmetry. Calculated strong decay widths in terms of coupling constants $\tilde{g}_{HH}$, $\tilde{\tilde{g}}_{HH}$, $\tilde{\tilde{g}}_{SH}$, $\tilde{\tilde{g}}_{TH}$, branching ratios and fractions for radially excited bottom mesons with and without strangeness are presented in Table 3.23.

Table 3.23: Decay widths of obtained masses for $n = 3$ bottom mesons. 5^{th} column gives the branching ratios. 6^{th} column gives branching fractions.

States	J^P	Strong decay modes	Decay widths (MeV)	Ratios	Fractions
$B(6326)$	0^-	$B^*\pi^+$	$6036.89\tilde{\tilde{g}}^2_{HH}$	1	26.62
		$B^*\pi^0$	$3024.30\tilde{\tilde{g}}^2_{HH}$	0.50	13.34
		$B^0(1^3P_0)\pi^0$	$699.49\tilde{\tilde{g}}^2_{SH}$	0.04	2.36
		$B^+(1^3P_0)\pi^-$	$1396.66\tilde{\tilde{g}}^2_{SH}$	0.09	4.71
		$B^0(1^3P_2)\pi^0$	$538.33\tilde{\tilde{g}}^2_{TH}$	0.02	0.59
		$B^+(1^3P_2)\pi^-$	$1066.60\tilde{\tilde{g}}^2_{TH}$	0.04	1.18
		$B^*\eta^0$	$2423.70\tilde{\tilde{g}}^2_{HH}$	0.40	10.68
		$B^0(1^3P_0)\eta^0$	$326.56\tilde{\tilde{g}}^2_{TH}$	0.01	0.36
		$B^*_sK^-$	$2854.22\tilde{\tilde{g}}^2_{HH}$	0.47	12.58
		$B^*_sK^0$	$2883.13\tilde{\tilde{g}}^2_{HH}$	0.47	12.71
		$B^-(2^3S_1)\pi^+$	$494.85\tilde{g}^2_{HH}$	0.46	9.85
		$B^0(2^3S_1)\pi^0$	$250.42\tilde{g}^2_{HH}$	0.01	4.99
		Total	145.15		
$B(6342)$	1^-	$B^+\pi^-$	$2351.72\tilde{\tilde{g}}^2_{HH}$	1	15.62
		$B^0\pi^0$	$1178.60\tilde{\tilde{g}}^2_{HH}$	0.50	7.83

Table 3.23: Decay widths of obtained masses for $n = 3$ bottom mesons. 5^{th} column gives the branching ratios. 6^{th} column gives branching fractions.

States	J^P	Strong decay modes	Decay widths (MeV)	Ratios	Fractions
		$B^{*+}\pi^-$	$2102.57\tilde{\tilde{g}}^2_{HH}$	0.89	13.96
		$B^0\eta^0$	$1010.34\tilde{\tilde{g}}^2_{HH}$	0.42	6.72
		$B(1P(1^+))\pi^-$	$802.42\tilde{\tilde{g}}^2_{SH}$	0.13	4.08
		$B(1P(1^+))\pi^0$	$402.25\tilde{\tilde{g}}^2_{SH}$	0.06	2.04
		$B(1P^{'}(1^+))\pi^0$	$357.08\ \tilde{\tilde{g}}^2_{SH}$	0.07	1.82
		B_sK^+	$1243.74\tilde{\tilde{g}}^2_{HH}$	0.52	8.26
		$B^0_sK^0$	$1233.43\tilde{\tilde{g}}^2_{HH}$	0.52	8.19
		$B^*_sK^-$	$1030.28\tilde{\tilde{g}}^2_{HH}$	0.43	6.85
		$B^*_sK^0$	$1020.49\tilde{\tilde{g}}^2_{HH}$	0.43	6.78
		$B^0(2^1S_0)\pi^0$	$105.51\tilde{g}^2_{HH}$	0.25	3.16
		$B^+(2^1S_0)\pi^-$	$208.89\tilde{g}^2_{HH}$	0.50	6.26
		$B^0(2^3S_1)\pi^0$	$94.30\tilde{g}^2_{HH}$	0.22	2.82
		$B^-(2^3S_1)\pi^+$	$186.55\tilde{g}^2_{HH}$	0.44	5.59
		Total	96.34		
$B_s(6463)$	0^-	$B^{*+}K^-$	$6334.56\tilde{\tilde{g}}^2_{HH}$	1	30.76
		$B^{*0}K^0$	$6299.04\tilde{\tilde{g}}^2_{HH}$	0.99	30.59
		$B(1^3P_0)K^-$	$1963.02\tilde{\tilde{g}}^2_{SH}$	0.12	7.29
		$B(1^3P_0)K^0$	$1950.26\tilde{\tilde{g}}^2_{SH}$	0.12	7.25
		$B(1^3P_2)K^-$	$677.47\tilde{\tilde{g}}^2_{TH}$	0.02	0.82
		$B(1^3P_2)K^0$	$653.88\tilde{\tilde{g}}^2_{TH}$	0.02	0.80
		$B^*_s\eta^0$	$4349\tilde{\tilde{g}}^2_{HH}$	0.68	21.11
		$B_s(1^3P_0)\eta^0$	$162.45\tilde{\tilde{g}}^2_{SH}$	0.009	0.60
		$B_s(1^3P_2)\eta^0$	$630\tilde{\tilde{g}}^2_{TH}$	0.02	0.78
		Total	131.79		
$B_s(6474)$	1^-	B^+K^-	$2461.75\tilde{\tilde{g}}^2_{HH}$	0.56	13.60
		B^0K^0	$2449.5\tilde{\tilde{g}}^2_{HH}$	0.56	13.51
		$B^{*+}K^-$	$4363.97\tilde{\tilde{g}}^2_{HH}$	1	24.09

Table 3.23: Decay widths of obtained masses for $n = 3$ bottom mesons. 5^{th} column gives the branching ratios. 6^{th} column gives branching fractions.

States	J^P	Strong decay modes	Decay widths (MeV)	Ratios	Fractions
		$B^{*0}K^0$	$4340.19\tilde{\tilde{g}}_{HH}^2$	0.99	23.96
		$B^+(1P(1^+))K^-$	$1833.13\tilde{\tilde{g}}_{SH}^2$	0.16	7.75
		$B^0(1P(1^+))K^0$	$1820.2\tilde{\tilde{g}}_{SH}^2$	0.16	7.70
		$B^+(1P'(1^+))K^-$	$479.21\tilde{\tilde{g}}_{TH}^2$	0.02	0.66
		$B^0(1P'(1^+))K^0$	$464.74\tilde{\tilde{g}}_{TH}^2$	0.02	0.64
		$B_s\eta^0$	$295.15\tilde{\tilde{g}}_{HH}^2$	0.06	1.63
		$B_s^*\eta$	$503.26\tilde{\tilde{g}}_{HH}^2$	0.11	2.78
		$B(2^1S_0)K^+$	$76.11\tilde{g}_{HH}^2$	0.09	1.90
		$B(2^1S_0)K^0$	$71.60\tilde{g}_{HH}^2$	0.09	1.78
		Total	115.94		

Column 4 of Table 3.23 present decay widths in terms of coupling constants $\tilde{g}_{HH}$, $\tilde{\tilde{g}}_{HH}$, $\tilde{\tilde{g}}_{SH}$, $\tilde{\tilde{g}}_{TH}$ and total decay widths of these states can be obtained by determining values of unknown couplings.

Coupling constants have an essential role in the study of heavy quark phenomenology. They are coupled with decays and give information about the strength of the strong transition of excited heavy meson doublets into the lightest heavy meson doublets. Values of these effective coupling constants can be estimated theoretically. In literature, we can see values of coupling constants to be matching for B-mesons and D-mesons; this is the beauty of heavy quark symmetry. The ground state mesons coupling like $g_{HH} = 0.40$ for D meson and 0.39 for B mesons respectively as in Ref.[97]. Similar observations are seen for the higher charm and bottom meson couplings as Ref. [78, 101]. Also $\tilde{g}_{HH} = 0.28 \pm 0.015$ for D meson is consistent with $\tilde{g}_{HH} = 0.27 \pm 0.01$ of B meson in Ref.[44, 102]. It seems more usual for excited states too for these heavy-light mesons. Because of this symmetry, we extracted values of coupling constants from recently observed radially excited charmed meson $D_J(3000)$ and $D_J^*(3000)$ [6]. These states are analyzed with different theoretical models and suggested their J^P value. The state $D_J(3000)$ favored as 3^1S_0 state [42, 45, 49, 103], $2P$ with $J^P = 1^+$ [55, 104] or $1F$ with $J^P = 3^+$ [83]. The state $D_J^*(3000)$ assigned with $D(3^3S_1)$ [42, 45, 49, 103], $D(1^3F_2)$ [55], $D(2^3P_2)$ [83] or $D(2^3P_2)$ [62]. The state $D_sJ(3040)$ lies in same mass domain and analyzed theoretically in Ref.[61] and give four tentative assignments (1^1D_2, 1^3D_2, 2^1P_1, 2^3P_1). In our work, the states $D_J(3000)$ and $D_J^*(3000)$ are considered as 3^1S_0, 3^1S_1 respectively. By using theoretical decay widths [42] of these states ($D_J(3000)$, $D_J^*(3000)$) as 3^1S_0, 3^1S_1, we have analyzed strong decay behavior of the states $D_J(3000)$ and $D_J^*(3000)$ with all possible strong decay modes and we get two equations:

$$8356.65\tilde{\tilde{g}}^2_{HH} + 2842.15\tilde{\tilde{g}}^2_{SH} + 1535.92\tilde{\tilde{g}}^2_{TH} + 970.06\tilde{g}^2_{HH} = 106 \tag{3.28}$$

$$10259.08\tilde{\tilde{g}}^2_{HH} + 1372.71\tilde{\tilde{g}}^2_{SH} + 942.51\tilde{\tilde{g}}^2_{TH} + 637.62\tilde{g}^2_{HH} = 102 \tag{3.29}$$

Then, we applied constraints on the associated couplings from 0 to 0.5 [105]. We have fixed couplings in such a way that it follows order $g_{HH} > g_{SH} > g_{TH}$. The strength of transitions from H to H field is greater than the strength of transition from S to H field and T to H field. With the above conditions, we get many sets of solutions for solving Eqn.3.28 and Eqn.3.29. By these set of solutions, we performed Pearson chi-square test with multivariate normal distribution to get mean set as $\tilde{g}_{HH} = 0.17$, $\tilde{\tilde{g}}_{HH} = 0.08$, $\tilde{\tilde{g}}_{SH} = 0.07$, $\tilde{\tilde{g}}_{TH} = 0.04$. The condition $g_{HH} > g_{SH} > g_{TH}$ was imposed while performing the test. From these values of coupling constants, we calculated total decay widths $\Gamma(B(3^1S_0)) = 145.15 MeV$, $\Gamma(B(3^3S_1)) = 96.34$ MeV, $\Gamma(B_s(3^1S_0)) = 131.79$ MeV, $\Gamma(B_s(3^3S_1)) = 115.94$ MeV. Branching ratio of $B(6326) \to B_s^*K^-$ and $B(6326) \to B^*\pi^+$ is given by $BR = \frac{\Gamma(B(6326)\to B_s^*K^-)}{\Gamma(B(6326)\to B^*\pi^+)}$ for $B(6326)$ state. The branching ratio can be helpful in identifying J^P values for the associated states in the future. The Branching fraction tells about the contribution of a particular decay mode to the total decay width of the state. Column 6 of Table 3.23 gives branching fractions. The leading decay channel for bottom meson state $B(3^1S_0)$ is $B^*\pi$ with fraction of 26.62%. For state $B(3^3S_1)$, $B^+\pi^-$ is leading decay mode with fraction of 15.62%. For their strange partners $B_s(3^1S_0)$ and $B_s^*(3^3S_1)$, $B^{*+}K^-$ mode is leading decay channel with branching fraction of 30.76% and 24.09% respectively. Apart from modes mentioned in Table 3.23, there are also some kinematically allowed modes that are not considered because of their small contribution. The total decay width for $B(3^1S_0)$ state is 145.15 MeV lying below the prediction by Godfrey-Isgur model [92]. But for strange partner $B_s(3^1S_0)$, our results are in good agreement with Ref.[92]. Also total decay widths for states $B(3^3S_1)$, $B_s(3^3S_1)$ matches with available theoretical estimates [92]. By observing values of decay widths, we conclude that states $B(3^1S_0)$, $B(3^3S_1)$ are broader than their strange partners $B_s(3^1S_0)$, $B_s(3^3S_1)$. There are states other than $3S$ states like $2P$ and $1F$ which lie in similar mass regions. The states $2P$ and $1F$ bottom meson states are already discussed in Ref.[87] and in the above section respectively using the same framework. So, we have extended previous work for $n = 3$ bottom mesons here. Studying these decay channels and widths may help in the future experimental exploration of bottom mesons for $n = 3$.

3.4 Summary

Heavy quark symmetry is one of the important tools to describe the spectroscopy of hadrons containing a single heavy quark. Using available experimental as well as theoretical data on bottom mesons and applying heavy quark symmetry, we predicted masses for $n = 3$ charm mesons spectra. Taking these predicted masses for $n = 3$ charm meson as input, we calculated masses for $n = 3$ bottom mesons. We also explore HQET for $1F$-wave bottom mesons. With computed masses for $n = 3$ charm mesons, bottom mesons and $1F$ bottom mesons, we analyzed decay widths from an excited state to a ground state with emission of pseudoscalar mesons and expressed decay widths in terms of coupling constants. These coupling constants are computed by comparing our decay widths with the theoretically available total decay widths. The total decay widths may give an upper bound on these coupling constants, hence providing an important clue to other associated states of excited mesons. Using our calculated for $n = 3$, $1F$ states, we construct Regge trajectories in (J,M^2) and (n_r, M^2) planes. These Regge lines are almost linear, parallel, and equidistant. Most of our predicted data nicely fit them. We also computed masses for $n = 4$ charm and bottom spectra by fixing Regge slopes and intercepts in the plane (n_r, M^2). Our calculated masses and upper bounds findings may help experimentalists look into higher excited states. Further we calculated decay widths and hadronic coupling constants $\tilde{g}_{HH}$, $\tilde{\tilde{g}}_{HH}$, $\tilde{\tilde{g}}_{SH}$, $\tilde{\tilde{g}}_{TH}$ etc using heavy quark symmetry. We also computed branching ratios and branching fractions of $n = 3$ S-wave states to have a better understanding. It may help in upcoming experiments at LHCb, PANDA, BESIII, etc., to look into these predictions.

Bibliography

[1] M. Neubert, Phys. Rept. **245**, 259 (1994), hep-ph/9306320

[2] V.M. Abazov et al. (D0), Phys. Rev. Lett. **99**, 172001 (2007), 0705.3229

[3] T. Aaltonen et al. (CDF), Phys. Rev. Lett. **100**, 082001 (2008), 0710.4199

[4] V.M. Abazov et al. (D0), Phys. Rev. Lett. **100**, 082002 (2008), 0711.0319

[5] T. Aaltonen et al. (CDF), Phys. Rev. Lett. **102**, 102003 (2009), 0809.5007

[6] R. Aaij et al. (LHCb), Phys. Rev. Lett. **110**, 151803 (2013), 1211.5994

[7] R. Aaij et al. (LHCb), Phys. Rev. D **92**, 032002 (2015), 1505.01710

[8] R. Aaij et al. (LHCb), Phys. Rev. D **94**, 072001 (2016), 1608.01289

[9] R. Aaij et al. (LHCb), Phys. Rev. Lett. **126**, 122002 (2021), 2011.09112

[10] R.L. Workman, Others (Particle Data Group), PTEP **2022**, 083C01 (2022)

[11] P. del Amo Sanchez et al. (BABAR), Phys. Rev. D **82**, 111101 (2010), 1009.2076

[12] G. Goldhaber et al., Phys. Rev. Lett. **37**, 255 (1976)

[13] I. Peruzzi et al., Phys. Rev. Lett. **37**, 569 (1976)

[14] G. Goldhaber et al., Phys. Lett. B **69**, 503 (1977)

[15] K. Abe et al. (Belle), Phys. Rev. D **69**, 112002 (2004), hep-ex/0307021

[16] J.M. Link et al. (FOCUS), Phys. Lett. B **586**, 11 (2004), hep-ex/0312060

[17] H. Albrecht et al. (ARGUS), Phys. Rev. Lett. **56**, 549 (1986)

[18] J.C. Anjos et al. (Tagged Photon Spectrometer), Phys. Rev. Lett. **62**, 1717 (1989)

[19] H. Albrecht et al. (ARGUS), Phys. Lett. B **231**, 208 (1989)

[20] R. Aaij et al. (LHCb), JHEP **09**, 145 (2013), 1307.4556

[21] R. Aaij et al. (LHCb), Phys. Rev. D **91**, 092002 (2015), [Erratum: Phys.Rev.D 93, 119901 (2016)], 1503.02995

[22] B. Aubert et al. (BABAR), Phys. Rev. Lett. **97**, 222001 (2006), hep-ex/0607082

[23] J. Brodzicka et al. (Belle), Phys. Rev. Lett. **100**, 092001 (2008), 0707.3491

[24] B. Aubert et al. (BABAR), Phys. Rev. D **80**, 092003 (2009), 0908.0806

[25] R. Aaij et al. (LHCb), Phys. Rev. Lett. **113**, 162001 (2014), 1407.7574

[26] R. Brandelik et al. (DASP), Phys. Lett. B **70**, 132 (1977)

[27] B. Aubert et al. (BABAR), Phys. Rev. Lett. **90**, 242001 (2003), hep-ex/0304021

[28] D. Besson et al. (CLEO), Phys. Rev. D **68**, 032002 (2003), [Erratum: Phys.Rev.D 75, 119908 (2007)], hep-ex/0305100

[29] A.E. Asratian et al., Z. Phys. C **40**, 483 (1988)

[30] Y. Kubota et al. (CLEO), Phys. Rev. Lett. **72**, 1972 (1994), hep-ph/9403325

[31] A.V. Evdokimov et al. (SELEX), Phys. Rev. Lett. **93**, 242001 (2004), hep-ex/0406045

[32] R. Aaij et al. (LHCb), JHEP **10**, 151 (2012), 1207.6016

[33] J.P. Lees et al. (BABAR), Phys. Rev. D **91**, 052002 (2015), 1412.6751

[34] R. Aaij et al. (LHCb), Phys. Rev. D **90**, 072003 (2014), 1407.7712

[35] L. Micu, Nucl. Phys. B **10**, 521 (1969)

[36] A. Le Yaouanc, L. Oliver, O. Pene, J.C. Raynal, Phys. Rev. D **8**, 2223 (1973)

[37] H. Georgi, Phys. Lett. B **240**, 447 (1990)

[38] E. Eichten, B.R. Hill, Phys. Lett. B **234**, 511 (1990)

[39] M.A. Shifman, A.I. Vainshtein, V.I. Zakharov, Nucl. Phys. B **147**, 385 (1979)

[40] L.J. Reinders, H. Rubinstein, S. Yazaki, Phys. Rept. **127**, 1 (1985)

[41] S. Godfrey, N. Isgur, Phys. Rev. D **32**, 189 (1985)

[42] S. Godfrey, K. Moats, Phys. Rev. D **93**, 034035 (2016), 1510.08305

[43] Z.G. Wang, Phys. Rev. D **83**, 014009 (2011), 1009.3605

[44] P. Colangelo, F. De Fazio, F. Giannuzzi, S. Nicotri, Phys. Rev. D **86**, 054024 (2012), 1207.6940

[45] Q.F. Lü, D.M. Li, Phys. Rev. D **90**, 054024 (2014), 1407.3092

[46] M. Allosh, Y. Mustafa, N. Khalifa Ahmed, A. Sayed Mustafa, Few Body Syst. **62**, 26 (2021)

[47] R.H. Ni, Q. Li, X.H. Zhong, Phys. Rev. D **105**, 056006 (2022), 2110.05024

[48] X.Z. Tan, T. Wang, Y. Jiang, Q. Li, L. Huo, G.L. Wang, Phys. Rev. D **105**, 094019 (2022), 2203.04171

[49] V. Patel, R. Chaturvedi, A.K. Rai, Eur. Phys. J. Plus **136**, 42 (2021)

[50] H.X. Chen, W. Chen, X. Liu, Y.R. Liu, S.L. Zhu, Rept. Prog. Phys. **86**, 026201 (2023), 2204.02649

[51] F. Gil-Domínguez, R. Molina, Phys. Lett. B **843**, 137997 (2023), 2302.12861

[52] K. Gandhi, A.K. Rai, Eur. Phys. J. A **57**, 23 (2021), 1911.06063

[53] Q.T. Song, D.Y. Chen, X. Liu, T. Matsuki, Phys. Rev. D **91**, 054031 (2015), 1501.03575

[54] G.L. Yu, Z.G. Wang, Z.Y. Li, Phys. Rev. D **94**, 074024 (2016), 1609.00613

[55] Y. Sun, X. Liu, T. Matsuki, Phys. Rev. D **88**, 094020 (2013), `1309.2203`

[56] B. Zhang, X. Liu, W.Z. Deng, S.L. Zhu, Eur. Phys. J. C **50**, 617 (2007), `hep-ph/0609013`

[57] J. Segovia, D.R. Entem, F. Fernandez, Phys. Rev. D **91**, 094020 (2015), `1502.03827`

[58] P. Colangelo, F. De Fazio, S. Nicotri, M. Rizzi, Phys. Rev. D **77**, 014012 (2008), `0710.3068`

[59] F.E. Close, C.E. Thomas, O. Lakhina, E.S. Swanson, Phys. Lett. B **647**, 159 (2007), `hep-ph/0608139`

[60] B. Chen, D.X. Wang, A. Zhang, Phys. Rev. D **80**, 071502 (2009), `0908.3261`

[61] P. Colangelo, F. De Fazio, Phys. Rev. D **81**, 094001 (2010), `1001.1089`

[62] G.L. Yu, Z.G. Wang, Z.Y. Li, Chin. Phys. C **39**, 063101 (2015), `1402.5955`

[63] G.L. Wang, W. Li, T.F. Feng, Y.L. Wang, Y.B. Liu, Eur. Phys. J. C **82**, 267 (2022), `2107.01751`

[64] J.M. Xie, M.Z. Liu, L.S. Geng, Phys. Rev. D **104**, 094051 (2021), `2108.12993`

[65] P.G. Ortega, J. Segovia, D.R. Entem, F. Fernandez, Phys. Lett. B **827**, 136998 (2022), `2111.00023`

[66] Z. Gao, G.Y. Wang, Q.F. Lü, J. Zhu, G.F. Zhao, Phys. Rev. D **105**, 074037 (2022), `2201.00552`

[67] T.A. Aaltonen et al. (CDF), Phys. Rev. D **90**, 012013 (2014), `1309.5961`

[68] R. Aaij et al. (LHCb), JHEP **04**, 024 (2015), `1502.02638`

[69] R. Lewis, R.M. Woloshyn, Phys. Rev. D **62**, 114507 (2000), `hep-lat/0003011`

[70] A.M. Green, J. Koponen, C. McNeile, C. Michael, G. Thompson (UKQCD), Phys. Rev. D **69**, 094505 (2004), `hep-lat/0312007`

[71] T.A. Lahde, C.J. Nyfalt, D.O. Riska, Nucl. Phys. A **674**, 141 (2000), `hep-ph/9908485`

[72] M. Di Pierro, E. Eichten, Phys. Rev. D **64**, 114004 (2001), hep-ph/0104208

[73] D. Ebert, R.N. Faustov, V.O. Galkin, Eur. Phys. J. C **66**, 197 (2010), 0910.5612

[74] J. Ferretti, E. Santopinto, Phys. Rev. D **90**, 094022 (2014), 1306.2874

[75] W. Hao, Y. Lu, E. Wang, Eur. Phys. J. C **83**, 520 (2023), 2212.10068

[76] X.h. Zhong, Q. Zhao, Phys. Rev. D **78**, 014029 (2008), 0803.2102

[77] Q.F. Lü, T.T. Pan, Y.Y. Wang, E. Wang, D.M. Li, Phys. Rev. D **94**, 074012 (2016), 1607.02812

[78] Z.G. Wang, Eur. Phys. J. Plus **129**, 186 (2014), 1401.7580

[79] Y. Sun, Q.T. Song, D.Y. Chen, X. Liu, S.L. Zhu, Phys. Rev. D **89**, 054026 (2014), 1401.1595

[80] T.T. Liu, S.Y. Pei, W. Li, M. Han, G.L. Wang, Eur. Phys. J. C **82**, 737 (2022), 2207.12069

[81] P. Gupta, A. Upadhyay, Phys. Rev. D **99**, 094043 (2019), 1803.03136

[82] K. Gandhi, A.K. Rai, Eur. Phys. J. C **82**, 777 (2022), 2208.08791

[83] J.B. Liu, C.D. Lu, Eur. Phys. J. C **77**, 312 (2017), 1605.05550

[84] S. Behrends et al. (CLEO), Phys. Rev. Lett. **50**, 881 (1983)

[85] K. Han et al., Phys. Rev. Lett. **55**, 36 (1985)

[86] J. Lee-Franzini, U. Heintz, D.M.J. Lovelock, M. Narain, R.D. Schamberger, J. Willins, C. Yanagisawa, P. Franzini, P.M. Tuts, Phys. Rev. Lett. **65**, 2947 (1990)

[87] P. Gupta, A. Upadhyay, Eur. Phys. J. A **54**, 160 (2018), 1806.05366

[88] S. Okubo, Physics Letters **5**, 165 (1963)

[89] J. Iizuka, Prog. Theor. Phys. Suppl. **37**, 21 (1966)

[90] P. Gupta, A. Upadhyay, Phys. Rev. D **97**, 014015 (2018), 1801.00404

[91] R. Garg, A. Upadhyay, Eur. Phys. J. Plus **137**, 828 (2022)

[92] S. Godfrey, K. Moats, E.S. Swanson, Phys. Rev. D **94**, 054025 (2016), 1607.02169

[93] R. Casalbuoni, A. Deandrea, N. Di Bartolomeo, R. Gatto, F. Feruglio, G. Nardulli, Phys. Lett. B **292**, 371 (1992), hep-ph/9209248

[94] J. Schechter, A. Subbaraman, Phys. Rev. D **48**, 332 (1993), hep-ph/9209256

[95] S. Campanella, P. Colangelo, F. De Fazio, Phys. Rev. D **98**, 114028 (2018), 1810.04492

[96] D.J. Gross, S.B. Treiman, F. Wilczek, Phys. Rev. D **19**, 2188 (1979)

[97] R. Casalbuoni, A. Deandrea, N. Di Bartolomeo, R. Gatto, F. Feruglio, G. Nardulli, Phys. Rept. **281**, 145 (1997), hep-ph/9605342

[98] G.F. Chew, S.C. Frautschi, Phys. Rev. Lett. **7**, 394 (1961)

[99] Y. Nambu, Phys. Rev. D **10**, 4262 (1974)

[100] Y. Nambu, Phys. Lett. B **80**, 372 (1979)

[101] Z.G. Wang, Phys. Rev. D **88**, 114003 (2013), 1308.0533

[102] P. Gupta, Ph.D. thesis, Thapar University (2019), http://hdl.handle.net/10266/5906

[103] J.K. Chen, Eur. Phys. J. C **78**, 648 (2018)

[104] L.Y. Xiao, X.H. Zhong, Phys. Rev. D **90**, 074029 (2014), 1407.7408

[105] P. Colangelo, F. De Fazio, R. Ferrandes, Mod. Phys. Lett. A **19**, 2083 (2004), hep-ph/0407137

Chapter 4

Analysis of Bottom Strange States $B_{sJ}(6063)$ and $B_{sJ}(6114)$

4.1 Introduction

In recent decades, various experimental groups like LHCb, FOCUS BABAR, CDF, BESIII, SLAC, Belle, etc., have actively pursued discoveries and enriched the spectrum of heavy-light mesons. The flavor of the heavy quark classifies heavy-light mesons as charm and bottom mesons. Experimental growth for charm and bottom mesons had a similar scenario up to the year 2003. But, in the past few years, experimental observations for charm mesons have rapidly increased and are noteworthy compared to the bottom meson sector. In the charm meson sector, confirmation of ground and various excited states like $D_0(2550)$, $D_1^*(2600)$, $D_2(2740)$, $D_3^*(2750)$, $D^0(3000)$, $D_J^*(3000)$ with strange states $D_{s1}(2860)$, $D_{sJ}(3040)$, $D_{s0}(2590)$ [1–7] have not only enriched the spectra but also facilitated the exploration of their properties through detailed decay studies. However, there is still a dearth of experimental progress in firmly establishing the bottom sector. Only ground states $B^{0,\pm}(5279)$, $B^*(5324)$, $B_s(5366)$, $B_s^*(5415)$ and some low lying states $B_1(5721)$, $B_J^*(5732)$, $B_2^*(5747)$, $B_{s1}(5830)$, $B_{s2}^*(5840)$, $B_{sJ}^*(5850)$, $B_J(5840)$, $B_J(5970)$ are announced experimentally and mentioned in PDG [8]. However, beyond these identified states, the complete spectra of the bottom meson remain unrevealed. For the establishment of bottom spectra, experimentalists, and theoreticians are trying to investigate new states that could fill voids in spectra. In this journey, recently, LHCb collaborations announced new states $B_{sJ}(6063)$ and $B_{sJ}(6114)$ in B^+K^- mass spectrum [9]. They also precisely measured masses and decay widths for these states. The discovery of these bottom meson states by LHCb has provided an opportunity to explore further and improve our comprehension of higher excited states.

The successes of the observations of these radially excited states by LHCb have demonstrated that more excited bottom meson states will be discovered in future LHC experiments. Exploring higher excited B mesons is not continuing. The ground state of bottom mesons, i.e., $B^0, B^{\pm}$, were reported by the CLEO group in the year 1983 [10]. They precisely measured masses and lifetime of the lowest lying meson states $B^0, B^{\pm}$. They also observed a large number of their decay modes. Consequently, in 1985, vector bottom meson, i.e. $J^P = 1^-$, was identified [11], and its existence was reconfirmed by different experimental facilities. In 2012, the LHCb collaboration measured its mass precisely and dominating decay mode [12]. In 1994, the first orbitally excited member of the bottom meson $B_{sJ}(5732)$ was announced by LEP and also reconfirmed by other experimental facilities [13]. In 2000, this state was analyzed again by LEP and measured its branching ratio [14]:

$$\mathcal{B}(B_J \to B^*\pi) = 0.74^{+0.12}_{-0.10} \tag{4.1}$$

But, still, its J^P is not confirmed, which shows it needs experimental attention. Also, LEP (Large electron-positron collider) 1999 reported an orbitally excited bottom meson state in the hadronic Z decays process [15]. This bottom meson's measured mass and decay width are $5937 \pm 21 \pm 4MeV$ and $50 \pm 22 \pm 5MeV$, respectively. However, this state was never reconfirmed by other experimental facilities. In 2007, DO collaboration announced two orbitally excited states $B_1(5721)^0$ and $B_2^*(5747)_0$ in $B^*\pi^-$ invariant mass distribution [16, 17]. They measured their masses and dominated decay channels. Further, LHCb reconfirmed these states and also measured the branching ratio of the state $B_2^*(5747)^{0,+}$ [18]:

$$\frac{\mathcal{B}(B_2^*(5747)^0 \to B^{+*}\pi^-)}{\mathcal{B}(B_2^*(5747)^0 \to B^0\pi^-)} = 0.71 \pm 0.14 \pm 0.30 \tag{4.2}$$

$$\frac{\mathcal{B}(B_2^*(5747)^+ \to B^{0*}\pi^+)}{\mathcal{B}(B_2^*(5747)^+ \to B^0\pi^+)} = 1.0 \pm 0.5 \pm 0.8 \tag{4.3}$$

The CDF collaboration in 2013 announced new excited resonance $B(5970)$ in decay modes $B^0\pi^+$ and $B^+\pi^-$ simultaneously [19] and measured their masses. Two years after LHCb collaboration in 2015, four resonances $B_J(5840)^{0,+}$ and $B_J(5960)^{0,+}$ were reported in $B\pi$ mass distribution [18]. They precisely measured their masses and decay widths. Despite these observations of mesons, the spectrum of excited bottom mesons is not much explored.

In strange bottom mesons family, only some states $B_s(5366)$, $B_s^*(5415)$, $B_{s1}(5830)$, $B_{s2}^*(5840)$ are well established and collected in PDG [8]. Among them, states $B_s(5366)$, $B_s^*(5415)$ are classified as $1S$ states and states $B_{s1}(5830)$, $B_{s2}^*(5840)$ are assigned as $1P$ $(1^+, 2^+)$ states. The ground state bottom meson was first observed in CUSB-II collaboration in $\Upsilon(5S)$ decays [20]. The spin partner B_s^* having $J^P = 1^-$ was also reported in same experiment. CUSB-II collaboration precisely measured their masses and mean life and also observed many decay modes during the experiment [20]. All associated data are listed in PDG [8]. First excited strange bottom meson $B_{sJ}^*(5850)$ of mass $5853 \pm 15 MeV$ and decay width $47 \pm 22 MeV$ announced by LEP in year 1994 [21]. In 2008, CDF collaboration announced two orbitally excited $(L = 1)$ bottom strange mesons; $B_{s1}(5830)^0$ with $J^P = 1^+$ and $B_{s2}^*(5840)^0$ with $J^P = 2^+$ [22]. These two states are also confirmed by DO [17] and LHCb collaborations [12]. LHCb collaborations also measured branching fraction of $B_{s2}^*(5840)^0$ relative to BK mode i.e.

$$\frac{\mathcal{B}(B_{s2}^*(5840)^0 \to B^{+*}K^-)}{\mathcal{B}(B_{s2}^*(5840)^0 \to B^+K^-)} = 0.081 \pm 0.021 \pm 0.015 \tag{4.4}$$

This shows experimentalists continue trying to establish the bottom strange meson spectrum. In this process, recently, LHCb announced two strange bottom meson states, which are mentioned as $B_{sJ}(6063)$ and $B_{sJ}(6114)$ [23]. The measured masses and decay widths are given below:

$M(B_{sJ}(6063)) = 6063.5 \pm 1.2(stat) \pm 0.8(syst) MeV$

$\Gamma(B_{sJ}(6063)) = 26 \pm 4 \pm 4\ MeV$

$M(B_{sJ}(6114)) = 6114 \pm 3(stat) \pm 5(syst) MeV$

$\Gamma(B_{sJ}(6114)) = 66 \pm 18 \pm 21\ MeV$

These observations are obtained under the assumption of direct decay through $B^{\pm}K^{\pm}$. LHCb perform experiment with decays through $B^{*\pm}K^{\pm}$, then shift in masses and decay widths are:

$M(B_{sJ}(6109)) = 6108.8 \pm 1.1(stat) \pm 0.7(Syst) MeV$

$\Gamma(B_{sJ}(6109)) = 22 \pm 5 \pm 4\ MeV$

$M(B_{sJ}(6158)) = 6158 \pm 4(stat) \pm 5(syst)MeV$
$\Gamma(B_{sJ}(6158)) = 72 \pm 18 \pm 25\ MeV$

These newly announced states $B_{sJ}(6063)$ and $B_{sJ}(6114)$ are suggested as D-wave states by LHCb collaborations [23]. The success of observations of these radially excited states by various experiment facilities has demonstrated that more excited bottom meson states will be discovered in future experiments.

In theory, various theoretical studies have performed different analyses for higher excited bottom non-strange and bottom strange meson states [24–44]. With the help of theoretical models, states $B^{0,\pm}(5279)$, $B^*(5324)$, $B_s(5366)$, $B_s^*(5415)$ are assigned as $1S$ state which very well matches with experimental data. Further the states $B_1(5721)$, $B_2^*(5747)$ are also well established experiemntally and classified as $1P(1^+, 2^+)$ respectively. But theoretically, state $B_1(5721)$ is still a disputed candidate because some of the theoretical work with heavy meson effective theory favors it as $1P(1^+)$ state [43, 45], while other work using relativistic quark model and non-relativistic quark model explained this state as a mixture of $^3P_1$ and $^1P_1$ states [25, 27, 44]. The J^P of state $B_J(5840)$ is still ambiguous as different models suggest different J^P's state for it. Authors in [27, 28] explained $B_J(5840)$ with the quark model and suggested the assignment as 2^1S_0 while G. L. Yu and Z. G. Wang with $^3P_0$ decay model analysis favors the assignments of state $B_J(5840)$ as 2^3S_1 [31]. But Heavy quark effective theory explained resonances $B_J(5840)$ as 1^3D_1 state [39]. The state $B_J(5960)^{0,+}$ is assigned as 2^3S_1 or 1^3D_3 state or 1^3D_1 state with different theoretical models [25–27, 29, 35, 45, 46]. But its J^P value is still a question mark in PDG, which only mentions its mass and decay width. We have discussed here a brief literature on these non-strange bottom states. The assignments of these states ($B_1(5721)$, $B_2^*(5747)$, $B_J(5970)$) are also suggested in our previous work [39]. In the case of the strange bottom sector, only a few states have been observed, out of which $B_{s1}(5830)$, $B_{s2}(5840)$ states are well observed by CDF [19, 22], DO [17], and LHCb [12] collaborations and are identified as $1P(1^+, 2^+)$ respectively. But, there is ambiguity for recently observed strange bottom meson states $B_{sJ}(6063)$ and

$B_{sJ}(6114)$. The states $B_{sJ}(6063)$ and $B_{sJ}(6114)$ in non-relativistic quark potential model identified as 1^3D_1 and 1^3D_3 states respectively [32, 47]. While authors in Ref. [33] assign these states as 1^3D_1 and 2^3S_1 states, respectively. Qi Li et al. [32] studied mass spectrum and decay properties of B and B_s states with constituent quark model and analyzed state $B_{sJ}(6114)$ as $2^3S_1 - 1^3D_1$ mixed state with mixing angle $\theta \sim -45° \pm 16°$. This interpretation for state $B_{sJ}(6114)$ was supported by Ref.[48]. The state $B_{sJ}(6063)$ is also analyzed and interpreted as pure $B_s(1^3D_3)$ state or $1^1D_2 - 1^3D_2$ mixed state [32]. In Ref [49], Chen et al. systematically investigated two body $b\bar{s}$ and four body $b\bar{s}q\bar{q}$ systems by taking each color configuration into account in the chiral quark model. They suggested state $B_{sJ}(6063)$ as $B_s(2S)$ and state $B_{sJ}(6114)$ as $B_s(1D)$. They also give the possibility of these newly observed states as exotic $b\bar{s}q\bar{q}$ tetraquark states. In Ref. [50], authors studied heavy-strange mesons using the quasipotential Bethe- Salpeter equation approach. They interpreted state $B_{sJ}(6114)$ as best candidate for $\bar{B}K^*$ molecular state with $J^P = 1^+$. Theoretical analysis for these newly observed states is thus limited in the literature, indicating it needs more attention. As a continuation of previous work [39], we analyzed observed strange bottom mesons states $B_{sJ}(6063)$ and $B_{sJ}(6114)$ and give their J^P values within this framework. From the experimental and theoretical literature survey, we concluded the following points:

- The lowest lying states i.e B, B^* and their strange partners B_s, B_s^* are well established.
- The state $B_1(5721)$, $B_2^*(5747)$ and their strange partner $B_{s1}(5730)$, $B_{s2}^*(5840)$ are identified as lowest orbitally excited states i.e $1P(1^+, 2^+)$ states.
- The state $B_J(5840)$ and $B_J(5970)$ are good candidate of 2^1S_0, 2^3S_1, 1^3D_1, 1^3D_3 states according to their observed masses. Since state $B_J(5840)$ and $B_J(5970)$ are observed in $B\pi$ decay mode, so 2^1S_0 assignment can be excluded. This is concluded because of the fact that only a natural parity state can decay to two pseudoscalar mesons.

The organization of this chapter is as follows: Section 4.2 represents the numerical analysis of $B_{sJ}(6063)$ and $B_{sJ}(6114)$ based on predicted masses and decay widths. By exploring flavor independent parameters $\Delta_F^{(c)} = \Delta_F^{(b)}$ and $\lambda_F^{(c)} = \lambda_F^{(b)}$, we predicted masses of unobserved bottom strange meson states $2S, 1P$, and $1D$. We have also examined these bottom strange states by incorporating $1/m_Q$ corrections which results in modifications of parameters $\Delta_F^{(b)} = \Delta_F^{(c)} + \delta\Delta_F$ and $\lambda_F^{(b)} = \lambda_F^{(c)}\delta\lambda_F$. Further, we have explored strong decays and associated properties with the emission of light pseudoscalar mesons. We assigned the states $B_{sJ}(6063)$ and $B_{sJ}(6114)$ on the basis of predicted masses and decay widths. Section 4.3 presents our final conclusion.

4.2 Numerical Analysis

Assigning a particular J^P (spin-parity quantum number) to the experimentally predicted excited states is crucial. A specific position of the state in its mass spectra can help redeem many other important strong interaction parameters such as hadronic coupling constants, branching ratios, spins and mass splittings, decay widths and many more. Therefore, in this analysis, we aim to suggest a particular J^P state to the recently strange bottom states observed by LHCb. Moreover, we also completed the empty spaces of these strange mass spectra by predicting the masses and other parameters of the missing bottom spectra in the framework of HQET.

In the bottom strange sector, only ground states 1S $(0^-, 1^-)$ states are confirmed both experimentally and theoretically. The rest of the spectra is still unknown. Although many other theoretical models, such as the chiral perturbation theory, the chiral unitary approach, the Regge trajectory, the $^3P_0$ model, the relativistic flux tube model, QCD sum rules, and the lattice QCD, etc tried to fill the gaps but yet they are not verified experimentally [24–44]. In addition to this, such theoretically calculated masses are unreliable because all these theoretical models depend on certain unknown parameters. The HQET framework chosen by us is free from such parameters and uses the most important relations of spin and flavor symmetry present in heavy-light mesons.

4.2.1 Mass Spectroscopy:

Mass is the key property that determines many other properties of mesons, which are important for understanding the behavior of heavy-light mesons. Therefore, we begin our calculations by estimating the masses of unavailable strange bottom states using the flavor and spin symmetry property $\Delta_F^{(c)} = \Delta_F^{(b)}$ and $\lambda_F^{(c)} = \lambda_F^{(b)}$. As discussed in Chapter 2 in Section 2.9 and in Chapter 3 in eq 3.14, eq 3.15, eq 3.17 the parameter Δ_F is the spin averaged mass splittings between F state doublets $(F = S, T, X, Y, R)$ and H state doublet (ground state), whereas the other parameter λ_F is the hyperfine splittings of the F state doublets.

The main aim of our calculation is to incorporate the J^P to recently observed strange states of the bottom flavor $B_{sJ}(6063)$ and $B_{sJ}(6114)$ and to fill the gaps near these states so that our calculations can provide motivation and reference to the yet to be predicted experimental information. The details of the numerical analysis on the mass spectrum are as follows:

Using the masses of charm and bottom states tabulated in Table 4.1, the spin

Table 4.1: Input values used in this work (MeV).

State	J^P	$c\bar{s}$	$b\bar{s}$
1^1S_0	0^-	1968.35 [8]	5366.92 [8]
1^3S_1	1^-	2112.20 [8]	5415.40 [8]
1^3P_0	0^+	2317.80	-
1^1P_1	1^+	2459.50	-
1^3P_1	1^+	2535.11	-
1^3P_2	2^+	2569.10	-
1^3D_1	1^-	2859.00	-
1^1D_2	2^-	2902.40	-
1^3D_2	2^-	2895.40	-
1^3D_3	3^-	2860.50	-
2^1S_0	0^-	2676.20	-
2^3S_1	1^-	2714.00	-

averaged mass splittings $\Delta_F^{(c)}$ and the hyperfine splittings $\lambda_F^{(c)}$ for $1S, 1P, 1D$ and $2S$ comes out to be

$$\Delta_{\tilde{H}}^{(c)} = 628.313\ MeV$$

$$\Delta_S^{(c)} = 347.838\ MeV$$
$$\Delta_T^{(c)} = 480.116\ MeV$$
$$\Delta_X^{(c)} = 763.513\ MeV$$
$$\Delta_Y^{(c)} = 798.804\ MeV$$
$$\lambda_{\tilde{H}}^{(c)} = (159.589)^2 MeV^2$$
$$\lambda_S^{(c)} = (290.892)^2 MeV^2$$
$$\lambda_T^{(c)} = (180.360)^2 MeV^2$$
$$\lambda_X^{(c)} = (181.228)^2 MeV^2$$
$$\lambda_Y^{(c)} = (204.573)^2 MeV^2$$

Table 4.2: Computed masses of the excited strange $2S, 1P$ and $1D$ bottom meson states (MeV).

	Without corrections	Corrections in λ_F	Corrections in Δ_F	Correction in both parameters λ_F and Δ_F
$0^-(2^1S_0)$	6019	6021	6018	6020
$1^-(2^3S_1)$	6036	6035	6035	6034
$0^+(1^3P_0)$	5707	5714	5705	5713
$1^+(1^1P_1)$	5766	5763	5764	5762
$1^+(1^3P_1)$	5874	5876	5867	5869
$2^+(1^3P_2)$	5889	5888	5882	5881
$1^-(1^3D_1)$	6176	6174	6180	6179
$2^-(1^1D_2)$	6161	6162	6166	6167
$2^-(1^3D_2)$	6211	6205	6211	6209
$3^-(1^3D_3)$	6195	6194	6194	6196

The charm mesons with $J^P = 2^-$ of D-wave with $j = 3/2$ and $j = 5/2$ for 1^1D_2 and 1^3D_2 are experimentally unavailable, so we have taken the average of the theoretical masses [24, 51, 52] for them.

Masses obtained for B_s mesons with the help of the symmetries are listed in the 2^{nd}

column of Table 4.2. Masses predicted for P-wave j = 3/2 strange bottom states 1^3P_1 and 1^3P_2 are in very good agreement with the experimental masses predicted for these states by LHCb [12], CDF [19, 22] and D0 [17]. Our calculated masses for 1^3P_1 and 1^3P_2 are only 0.78% , 0.84% deviating from their experimental values respectively. In comparison with predictions of other theoretical models shown in Table 4.3, our calculated masses are in good agreement. Note that predictions of Ref.[24, 26] are smaller by 100 MeV than our results. While data in [33] is larger than our masses by order of 100 MeV. Also, the calculated mass for $J^P = (1^-, 2^-), 3^-$ belonging to D-wave with $j = 3/2$, $j = 5/2$ and $J^P = 1^-$ of radially excited S-wave have also beautifully matched with the LHCb states $B_{sJ}(6114)$ and $B_{sJ}(6063)$ respectively. Since masses of these two states $B_{sJ}(6114)$ and $B_{sJ}(6063)$ deviates only by 61, 47, 81 MeV and 28 MeV from our predicted values, so one easily conclude that $B_{sJ}(6063)$ state belong to J^P $2S1^-$ while the other state $B_{sJ}(6114)$ belong to one of the J^P of 1 D-wave. Authors in Ref.[33] predicted the J^P for $B_{sJ}(6114)$ as $1D1^-$ for $j = 3/2$. But, to prove convincingly, we computed the masses by taking higher order corrections as splitting parameters (Δ_F and λ_F) can drastically change in the presence of QCD and higher order ($1/m_Q$) corrections in the HQET Lagrangian. Also, the calculated masses should be able to predict other parameters, such as decay width, which should match with experimental data. Therefore, in the next part, we present the analysis of such corrections to these splittings and calculate the two-body strong decay widths of these bottom states.

QCD and higher order ($1/m_Q$) corrections are applied to a scale of Λ_{QCD}/m_Q, where they can significantly decide the level of symmetry breaking. The corrections to Δ_F and λ_F parameters change heavy quark symmetry relations to $\Delta_F^{(b)} = \Delta_F^{(c)} + \delta\Delta_F$ and $\lambda_F^{(b)} = \lambda_F^{(c)}\delta\lambda_F$. We apply such corrections to these splittings one by one and check the effect of these corrections on the bottom masses, followed by a step in which both corrections would be applied simultaneously. In the case of λ_F parameter, QCD corrections are dominant over $1/m_Q$ corrections because these mass splitting parameters λ_F originate from the chromomagnetic interactions. The leading QCD corrections to the λ_F are in the form of $\lambda_F^{(b)} = \lambda_F^{(c)}(\frac{\alpha_s(m_b)}{\alpha_s(m_c)})^{9/25}$. The parameters $\alpha_s(m_b)$ and $\alpha_s(m_c)$ for applying the QCD corrections to this splitting parameters are taken as 0.22 and 0.36 [53]. The corrections in λ_F parameters modify the value to:

$$\lambda_{\tilde{H}}^{(c)} = (133.662)^2 MeV^2$$
$$\lambda_{S}^{(c)} = (243.632)^2 MeV^2$$
$$\lambda_{T}^{(c)} = (151.058)^2 MeV^2$$
$$\lambda_{X}^{(c)} = (151.785)^2 MeV^2$$
$$\lambda_{Y}^{(c)} = (171.33)^2 MeV^2$$

The B_s masses inherited using these corrections are mentioned in the 3^{rd} column of Table 4.2. The resulting masses are deflected upto 7.5 MeV from their initial masses and have resulted in reducing the gap between our and LHCb masses. Now we analyze the effect of $1/m_Q$ and QCD corrections to our other parameter Δ_F, which depicts the mass splittings between F state doublet (higher mass states) and the ground state H field states. The corrections to these parameters are in the form of $\delta\Delta_F$, where $F = S, T, X, Y, \tilde{H}$. The best-fitted values of these corrections come to be $\mathcal{O}$ (0.63) GeV, $\mathcal{O}(0.35)$ GeV, $\mathcal{O}(0.49)$ GeV, $\mathcal{O}(0.77)$ GeV and $\mathcal{O}(0.80)$ GeV for doublets $2S(0^-, 1^-)$, $1P(0^+, 1^+)$, $1P(1^+, 2^+)$, $1D(1^-, 2^-)$ and $1D(2^-, 3^-)$ respectively. To calaculate corrections in Δ_F parameter i.e $\delta\Delta_F$, we followed similar prodecure as in Ref.[54]. Masses calculated using these corrections are mentioned in 4^{th} column of Table 4.2. A comparison of masses concluded that the deviation lies in the range of 0.83 - 6.90 MeV, which again shows that masses are not affected much by corrections, too, but again resulted in narrowing the gap between our and experimental masses. Lastly, applying both corrections simultaneously the masses obtained are mentioned in the last column of Table 4.2. It can be summarized that the effect of such corrections is very small in the higher excited states. Because of the higher angular momentum, such states do not remain in their stable state for much time and thus do not explicitly show chromomagnetic effects. However, such corrections have resulted in narrowing the gap between the predicted and experimentally predicted mass values but have not adversely affected the masses. To suggest a particular J^P value for LHCb observed strange bottom states $B_{sJ}(6063)$ and $B_{sJ}(6114)$, we explore the second utmost important property of heavy-light mesons i.e. decay widths.

Table 4.3: Comparison of our findings with predictions of other models (MeV).

$J^P(n^{2S+1}L_j)$	Present results	Ref.[55]	Ref.[24]	Ref.[33]
$0^-(2^1S_0)$	6019	6003	5985	6025
$1^-(2^3S_1)$	6036	6029	6019	6033
$0^+(1^3P_0)$	5707	5812	5804	5709
$1^+(1^1P_1)$	5766	5828	5805	5768
$1^+(1^3P_1)$	5874	5842	5842	5875
$2^+(1^3P_2)$	5889	5840	5820	5890
$1^-(1^3D_1)$	6176	6119	6127	6247
$2^-(1^1D_2)$	6161	6128	6095	6256
$2^-(1^3D_2)$	6211	6157	6140	6292
$3^-(1^3D_3)$	6195	6172	6103	6297

4.2.2 Strong Decays

Using an effective Lagrangian approach, we investigated OZI allowed strong decays and associated properties strong decay widths, branching ratios, branching fractions for $B_s(2S)$, $B_s(1P)$ and $B_s(1D)$ states. The computed values for these states are given in Table 4.5 and 4.4. Here, it is noticed that the computed total decay widths do not incorporate the contribution from decays involving the emission of vector mesons (ω, ρ, K^*, ϕ). Since the contribution of vector mesons to total decay widths is small compared to pseudoscalar mesons. They contribute $\pm 10MeV$ [26] to total decay widths for the above-analyzed states.

To choose the possible J^P for the LHCb bottom state $B_{sJ}(6114)$, we calculated the total decay width for all the possible J^P's 1^3D_1, 1^1D_2 and 1^3D_3 in terms of strong coupling constants. Values come out to be

$$\Gamma(1^3D_1) = 6052.34 g_{XH}^2$$
$$\Gamma(1^1D_2) = 4416.36 g_{XH}^2$$
$$\Gamma(1^3D_3) = 933.75 g_{YH}^2$$

On comparing these calculated decay widths with the experimental decay width of 66 MeV, the coupling constant values come out to be

$$g_{XH} = 0.104$$

$$g_{XH} = 0.12$$
$$g_{YH} = 0.26$$

The available theoretical values of g_{YH} are 0.61 [56], 0.53 [45], 0.42 [57]. Our computed value of g_{YH} is much smaller, ruling out 1^3D_3 state from possible J^P's for state $B_{sJ}(6114)$. Now, we are left with two available J^P (1^3D_1 and 1^1D_2). In literature, the available theoretical values of g_{XH} are 0.41 [39], 0.45 [43], 0.53 [58], 0.19 [45]. In Ref.[45], the coupling constant g_{XH} is calculated for state $B(5970)^0$ is 0.19 ± 0.049. They assigned 1^3D_1 for this state and computed coupling constant by comparing their theoretical decay width with the experimental value. We are also following the same procedure, and the obtained value of g_{XH} enables us to assign the J^P state of $B_{sJ}(6114)$. The coupling values for 1^3D_1 and 1^1D_2 obtained are consistent with $g_{XH} = 0.19$. We suggest these two J^P 1^3D_1 and 1^1D_2 as most favorable for state $B_{sJ}(6114)$. But $B_{sJ}(6114)$ were observed in BKm modes, so it cannot have $J^P = 2^-$. Since it does not satisfy the conservation of parity and angular momentum simultaneously for $J^P = 2^-$. So, we are assigning a particular $J^P = 2^-(1^3D_1)$ to state $B_{sJ}(6114)$. Further experimental investigations like branching ratios may provide the necessary conclusions.

4.2.2.1 $1D$

The natural parity D states 1^3D_1 and 1^3D_3 both are dominant in BK decay mode with branching fractions of 56.73% and 36.67% respectively, while the unnatural parity states 1^1D_2 and 1^3D_2 shows dominance in B^*K decay channel with branching fractions of 77.51% and 67.02% respectively. The ratio of the partial decay widths for $1D$ bottom states to its partial decay width $B^{*+}K^-$ is mentioned in Column 4 of Table 4.5. In addition to the decay modes mentioned in Table 4.5, these bottom states also decay to P-wave bottom mesons via D-waves. But, such decays are suppressed because of small phase space. Thus these decays are not shown in Table 4.5. The calculated value of $g_{XH} = 0.12$ is useful to find the total and partial decay width of experimentally missing bottom state 1^3D_1. Thus, the calculated total decay width for this state is 87.15 MeV, which deviates by 34.47% from the result of Ref.[32] (Total decay width = 133 MeV)

4.2.2.2 $1P$

We studied the strong decay widths $1P$ bottom states and estimated the different branching ratios involved. The calculated value of the partial decay widths for the bottom states 1^3P_0, 1^1P_1, 1^3P_1 and 1^3P_2 are listed in Table 4.4. The state 1^3P_0 decaying to BK decay channel is kinematically suppressed as the predicted mass for this state is lower than the BK threshold value. This is a similar situation as seen in the charm sector for the same J^P state $D^*_{s0}(2317)$, thus reflecting the flavor symmetry in heavy hadrons. The only kinematically allowed decay channel for this state is $B_s\pi$. Its spin partner 1^1P_1 is also decaying to $B^*_s\pi^0$ decay mode only while all other modes are suppressed. Using the available value of coupling constant $g_{SH} = 0.56$ [43], predicted decay widths for $(0^+, 1^+)$ doublet are calculated as

$$\Gamma(1^3P_0) = 46.25\ MeV$$
$$\Gamma(1^1P_1) = 50.51\ MeV$$

Our estimated values are highly overestimated with the results of Ref.[33] and underestimated with the data of QPC model, and chiral quark model [25, 27, 44].
The study of the doublet $(1^+, 2^+)$ shows that $B^*_s\pi^0$ and $B_s\pi^0$ are the dominant decay modes for 1^3P_1 and 1^3P_2 states with branching ratio of 85.33% and 32.30% respectively. Total decay width calculated by taking a sum of its partial decay widths listed in Table 4.4

$$\Gamma(1^3P_1) = 14.33\ MeV$$
$$\Gamma(1^3P_2) = 26.74\ MeV$$

These decay values depict these states to be narrower but are still overestimated with their experimental values measured by LHCb and CDF collaborations [12, 19] but are in good agreement with the theoretical data [33] where authors used mixing angle to calculate the width of 1^3P_1 state.

4.2.2.3 $2S$

Table 4.4 shows that B^*K^+ mode is the dominating decay mode for the radially ground state S-wave bottom states, $\widetilde{B}^*_{1s}$ and $\widetilde{B}_{0s}$ bottom states with branching fraction of 22.53% and 33.46%, respectively. Thus, the decay channel B^*K^+ is an appropriate mode for the experimental investigation of missing strange $2S$ bottom meson state. Using the strong coupling value $\widetilde{g}_{HH} = 0.31$ [56], total decay widths for bottom state $\widetilde{B}^{*}_{1s}$ and its spin partner $\widetilde{B}_{0s}$ are predicted as 207.44 MeV and 231.11 MeV respectively. These speculated values indicate these radial bottom states to have broad resonance, which is in good agreement with the results of Ref.[25, 27]. In addition to the decay modes mentioned in Table 4.4, $2S$ bottom states also decay to D-wave bottom mesons. However, these decays are suppressed because of their small phase space and are not shown in Table 4.4.

Table 4.4: Predicted strong decay widths of $B_s(2S0^-)$, $B_s(2S1^-)$, $B_s(1P0^+)$, $B_s(1P1^+)$, $B_s(1P1^+)$, $B_s(1P2^+)$ states. 4^{th} column gives the $\widehat{\mathbf{\Gamma}} = \frac{\Gamma}{\Gamma(B^{*}_{sJ} \to B^{*0}K^{+})}$. Fraction provides the contribution of individual decay mode to the total decay width.

nLs_lJ^P	Decay channel	Decay widths(MeV)	Ratio	Fraction
$2S_{s1/2}0^-$	$B^{*0}K^0$	$785.160\widetilde{g}^2_{HH}$	1	32.64
	$B^{*+}K^-$	$804.921\widetilde{g}^2_{HH}$	1.02	33.46
	$B^{*}_s\pi^0$	$737.438\widetilde{g}^2_{HH}$	0.93	30.66
	$B^{*}_s\eta$	$77.419\widetilde{g}^2_{HH}$	0.09	3.21
	Total	$2404.940\widetilde{g}^2_{HH}$		
$2S_{s1/2}1^-$	B^0K^0	$342.716\widetilde{g}^2_{HH}$	0.72	15.87
	B^+K^-	$350.669\widetilde{g}^2_{HH}$	0.73	16.24
	$B_s\pi^0$	$292.676\widetilde{g}^2_{HH}$	0.61	13.55
	$B_s\eta$	$58.29\widetilde{g}^2_{HH}$	0.12	2.70
	$B^{*0}K^0$	$474.96\widetilde{g}^2_{HH}$	1	22.00
	$B^{*+}K^-$	$486.477\widetilde{g}^2_{HH}$	1.2	22.53
	$B^{*}_s\pi^0$	$466.530\widetilde{g}^2_{HH}$	0.98	21.61
	$B^{*}_s\eta$	$36.988\widetilde{g}^2_{HH}$	0.07	1.71
	Total	$2158.650\widetilde{g}^2_{HH}$		
$1P_{s1/2}0^+$	$B_s\pi^0$	$147.500g^2_{SH}$	-	100
	$B_s\eta$	-		-
	B^+K^0	-	-	-

Table 4.4: Predicted strong decay widths of $B_s(2S0^-)$, $B_s(2S1^-)$, $B_s(1P0^+)$, $B_s(1P1^+)$, $B_s(1P1^+)$, $B_s(1P2^+)$ states. 4^{th} column gives the $\widehat{\mathbf{\Gamma}} = \frac{\Gamma}{\Gamma(B^*_{sJ} \to B^{*0}K^+)}$. Fraction provides the contribution of individual decay mode to the total decay width.

nLs_lJ^P	Decay channel	Decay widths(MeV)	Ratio	Fraction
	B^-K^+	-	-	-
	Total	$147.500g^2_{SH}$		
$1P_{s1/2}1^+$	$B^*_s\pi^0$	$161.080g^2_{SH}$	-	-
	$B^*_s\eta$	-	-	-
	$B^{*+}K^0$	-	-	-
	$B^{*-}K^+$	-	-	-
	Total	$1161.080g^2_{SH}$		
$1P_{s13/2}1^+$	$B^{*0}K^0$	$5.970g^2_{TH}$	1	6.66
	$B^{*+}K^-$	$7.12g^2_{TH}$	1.19	7.93
	$B^*_s\pi^0$	$76.49g^2_{TH}$	12.81	85.37
	$B^*_s\eta$	-	-	-
	Total	$89.59g^2_{TH}$		
$1P_{s13/2}2^+$	B^0K^0	$18.48g^2_{TH}$	22.67	11.05
	B^+K^-	$20.13g^2_{TH}$	2.91	12.04
	$B_s\pi^0$	$59.590g^2_{TH}$	8.62	35.65
	$B_s\eta$	-	-	-
	$B^{*0}K^0$	$6.92g^2_{TH}$	1	4.13
	$B^{*+}K^-$	$7.92g^2_{TH}$	1.14	4.73
	$B^*_s\pi^0$	$54.09g^2_{TH}$	7.82	32.36
	$B^*_s\eta$	-	-	-
	Total	$167.15g^2_{TH}$		

Table 4.5: Computed strong decay widths of $B_s(1D1^-)$, $B_s(1D2^-)$, $B_s(1D2^-)$ and $B_s(1D3^-)$ states. 4^{th} column gives the $\widehat{\mathbf{\Gamma}} = \frac{\Gamma}{\Gamma(B^*_{sJ} \to B^{*0}K^+)}$. Fraction gives the contribution of individual decay mode to the total decay width.

nLs_lJ^P	Decay channel	Decay widths(MeV)	Ratio	Fraction
$1D_{s3/2}1^-$	B^0K^0	$1706.81g^2_{XH}$	2.71	28.20
	B^+K^-	$1727.24g^2_{XH}$	2.74	28.53
	$B_s\pi^0$	$863.737g^2_{XH}$	1.37	14.27
	$B_s\eta$	$126.531g^2_{XH}$	0.20	2.09
	$B^{*0}K^0$	$628.449g^2_{XH}$	0.51	5.35
	$B^{*+}K^-$	$635.727g^2_{XH}$	0.06	0.66
	$B^*_s\pi^0$	$323.847g^2_{XH}$	1	10.38
	$B^*_s\eta$	$40.0077g^2_{XH}$	1.01	10.50
	Total	$6052.34g^2_{XH}$		
$1D_{s3/2}2^-$	$B^{*0}K^0$	$1701.43g^2_{XH}$	1	38.52
	$B^{*+}K^-$	$1722.22g^2_{XH}$	1.01	38.99
	$B^*_s\pi^0$	$889.31g^2_{XH}$	0.52	20.13
	$B^*_s\eta$	$103.31g^2_{XH}$	0.06	2.34
	Total	$4416.36g^2_{XH}$		
$1D_{s5/2}2^-$	$B^{*0}K^0$	$290.97g^2_{YH}$	1	33.08
	$B^{*+}K^-$	$298.45g^2_{YH}$	1.02	33.93
	$B^*_s\pi^0$	$251.13g^2_{YH}$	0.868	28.55
	$B^*_s\eta$	$38.85g^2_{YH}$	0.13	4.41
	Total	$879.41g^2_{XH}$		
$1D_{s5/2}3^-$	B^0K^0	$168.95g^2_{YH}$	1.21	18.09
	B^+K^-	$173.47g^2_{YH}$	1.24	18.57
	$B_s\pi^0$	$140.16g^2_{YH}$	18	15.01
	$B_s\eta$	$27.27g^2_{YH}$	0.19	2.92
	$B^{*0}K^0$	$139.01g^2_{YH}$	1	14.88
	$B^{*+}K^-$	$142.78g^2_{YH}$	1.02	15.29

Table 4.5: Computed strong decay widths of $B_s(1D1^-)$, $B_s(1D2^-)$, $B_s(1D2^-)$ and $B_s(1D3^-)$ states. 4^{th} column gives the $\widehat{\mathbf{\Gamma}} = \frac{\Gamma}{\Gamma(B^*_{sJ} \to B^{*0}K^+)}$. Fraction gives the contribution of individual decay mode to the total decay width.

nLs_lJ^P	Decay channel	Decay widths(MeV)	Ratio	Fraction
	$B_s^*\pi^0$	$125.11g^2_{YH}$	0.90	13.39
	$B_s^*\eta$	$16.98g^2_{YH}$	0.12	1.81
	Total	$933.75g^2_{YH}$		

4.3 Conclusion

In this chapter, we have applied the Heavy Quark Effective Theory to examine the recently observed strange bottom mesons, $B_{sJ}(6063)$ and $B_{sJ}(6114)$ by LHCb collaborations. In this framework, we have calculated masses of strange bottom meson $2S, 1P, 1D$ with the use of available experimental and theoretical data on charm mesons and including non-perturbative parameters (Δ_F and λ_F). These predicted masses for the above-said states have beautifully matched with other models predictions. Also, by taking $1/m_Q$ corrections in terms of $\delta\Delta_F$ and $\delta\lambda_F$, we estimated masses of strange bottom mesons $2S, 1P, 1D$, which narrow the gap between our results and experimental data. On the basis of computed masses, we have identified strange bottom states $B_{sJ}(6063)$ as 2^3S_1 and give three possible J^P's ($1^-, 2^-, 3^-$) belonging D-wave to $B_{sJ}(6114)$ state. We have analyzed strong decay widths for possible J^P's state for $B_{sJ}(6114)$ and concluded that most favourable states for $B_{sJ}(6114)$ are 1^3D_1. In addition to this, we have predicted the branching ratios and the coupling constants for the above states, which can provide crucial information for future experimental searches.

Bibliography

[1] P. del Amo Sanchez et al. (BABAR), Phys. Rev. D **82**, 111101 (2010), 1009.2076

[2] R. Aaij et al. (LHCb), JHEP **09**, 145 (2013), 1307.4556

[3] R. Aaij et al. (LHCb), Phys. Rev. D **91**, 092002 (2015), [Erratum: Phys.Rev.D 93, 119901 (2016)], 1503.02995

[4] B. Aubert et al. (BABAR), Phys. Rev. Lett. **97**, 222001 (2006), hep-ex/0607082

[5] J. Brodzicka et al. (Belle), Phys. Rev. Lett. **100**, 092001 (2008), 0707.3491

[6] R. Aaij et al. (LHCb), JHEP **02**, 133 (2016), 1601.01495

[7] R. Aaij et al. (LHCb), Phys. Rev. Lett. **126**, 122002 (2021), 2011.09112

[8] R.L. Workman, Others (Particle Data Group), PTEP **2022**, 083C01 (2022)

[9] R. Aaij et al. (LHCb), Eur. Phys. J. C **81**, 601 (2021), 2010.15931

[10] S. Behrends et al. (CLEO), Phys. Rev. Lett. **50**, 881 (1983)

[11] K. Han et al., Phys. Rev. Lett. **55**, 36 (1985)

[12] R. Aaij et al. (LHCb), Phys. Rev. Lett. **110**, 151803 (2013), 1211.5994

[13] R. Akers et al. (OPAL), Z. Phys. C **66**, 19 (1995)

[14] G. Abbiendi et al. (OPAL), Eur. Phys. J. C **23**, 437 (2002), hep-ex/0010031

[15] M. Acciarri et al. (L3), Phys. Lett. B **465**, 323 (1999), hep-ex/9909018

[16] V.M. Abazov et al. (D0), Phys. Rev. Lett. **99**, 172001 (2007), 0705.3229

[17] V.M. Abazov et al. (D0), Phys. Rev. Lett. **100**, 082002 (2008), 0711.0319

[18] R. Aaij et al. (LHCb), JHEP **04**, 024 (2015), 1502.02638

[19] T.A. Aaltonen et al. (CDF), Phys. Rev. D **90**, 012013 (2014), 1309.5961

[20] J. Lee-Franzini, U. Heintz, D.M.J. Lovelock, M. Narain, R.D. Schamberger, J. Willins, C. Yanagisawa, P. Franzini, P.M. Tuts, Phys. Rev. Lett. **65**, 2947 (1990)

[21] R. Akers et al. (OPAL), Z. Phys. C **66**, 19 (1995)

[22] T. Aaltonen et al. (CDF), Phys. Rev. Lett. **100**, 082001 (2008), 0710.4199

[23] R. Aaij et al. (LHCb), Eur. Phys. J. C **81**, 601 (2021), 2010.15931

[24] M. Di Pierro, E. Eichten, Phys. Rev. D **64**, 114004 (2001), hep-ph/0104208

[25] Y. Sun, Q.T. Song, D.Y. Chen, X. Liu, S.L. Zhu, Phys. Rev. D **89**, 054026 (2014), 1401.1595

[26] S. Godfrey, K. Moats, E.S. Swanson, Phys. Rev. D **94**, 054025 (2016), 1607.02169

[27] Q.F. Lü, T.T. Pan, Y.Y. Wang, E. Wang, D.M. Li, Phys. Rev. D **94**, 074012 (2016), 1607.02812

[28] I. Asghar, B. Masud, E.S. Swanson, F. Akram, M. Atif Sultan, Eur. Phys. J. A **54**, 127 (2018), 1804.08802

[29] S. Godfrey, K. Moats, Eur. Phys. J. A **55**, 84 (2019), 1903.03886

[30] Z.H. Wang, Y. Zhang, T.h. Wang, Y. Jiang, Q. Li, G.L. Wang, Chin. Phys. C **42**, 123101 (2018), 1803.06822

[31] G.L. Yu, Z.G. Wang, Chin. Phys. C **44**, 033103 (2020), 1907.08760

[32] Q. li, R.H. Ni, X.H. Zhong, Phys. Rev. D **103**, 116010 (2021), 2102.03694

[33] K. Gandhi, A.K. Rai, Eur. Phys. J. C **82**, 777 (2022), 2208.08791

[34] K.R. Purohit, A.K. Rai, R.H. Parmar (2023), 2307.10656

[35] J. Ferretti, E. Santopinto, Phys. Rev. D **97**, 114020 (2018), 1506.04415

[36] Z.G. Wang, Eur. Phys. J. C **75**, 427 (2015), 1506.01993

[37] J.M. Zhang, G.L. Wang, Phys. Lett. B **684**, 221 (2010), 1001.1773

[38] Z.G. Luo, X.L. Chen, X. Liu, Phys. Rev. D **79**, 074020 (2009), 0901.0505

[39] P. Gupta, A. Upadhyay, Phys. Rev. D **99**, 094043 (2019), 1803.03136

[40] S.L. Zhu, Y.B. Dai, Mod. Phys. Lett. A **14**, 2367 (1999), hep-ph/9811449

[41] A.H. Orsland, H. Hogaasen, Eur. Phys. J. C **9**, 503 (1999), hep-ph/9812347

[42] G.L. Yu, Z.G. Wang, Z.Y. Li, Eur. Phys. J. C **79**, 798 (2019), 1905.11236

[43] P. Colangelo, F. De Fazio, F. Giannuzzi, S. Nicotri, Phys. Rev. D **86**, 054024 (2012), 1207.6940

[44] X.h. Zhong, Q. Zhao, Phys. Rev. D **78**, 014029 (2008), 0803.2102

[45] Z.G. Wang, Eur. Phys. J. Plus **129**, 186 (2014), 1401.7580

[46] H. Xu, X. Liu, T. Matsuki, Phys. Rev. D **89**, 097502 (2014), 1402.0384

[47] B. Chen, S.Q. Luo, K.W. Wei, X. Liu, Phys. Rev. D **105**, 074014 (2022), 2201.05728

[48] V. Patel, R. Chaturvedi, A.K. Rai (2022), 2201.01120

[49] X. Chen, Y. Tan, Y. Chen, Phys. Rev. D **104**, 014017 (2021)

[50] S.Y. Kong, J.T. Zhu, D. Song, J. He, Phys. Rev. D **104**, 094012 (2021)

[51] V. Kher, N. Devlani, A.K. Rai, Chin. Phys. C **41**, 073101 (2017), 1704.00439

[52] S. Godfrey, K. Moats, Phys. Rev. D **93**, 034035 (2016), 1510.08305

[53] G. Amoros, M. Beneke, M. Neubert, Phys. Lett. B **401**, 81 (1997), hep-ph/9701375

[54] P. Gupta, A. Upadhyay, Eur. Phys. J. A **54**, 160 (2018), 1806.05366

[55] V. Kher, N. Devlani, A.K. Rai, Chin. Phys. C **41**, 093101 (2017), 1705.08248

[56] P. Gupta, A. Upadhyay, Phys. Rev. D **97**, 014015 (2018), 1801.00404

[57] A.F. Falk, T. Mehen, Phys. Rev. D **53**, 231 (1996), hep-ph/9507311

[58] A. Upadhyay, M. Batra, P. Gupta, PTEP **2016**, 053B02 (2016), 1210.6141

Chapter 5

Bottomonia in Quark-Antiquark Confining Potential

5.1 Introduction

Various experimental facilities, such as LHCb, BABAR, BESIII, STAR, ATLAS, Belle, and others, are persistently engaged in generating vast amounts of data pertaining to heavy mesons. The theoretical studies are also heavily invested in the field to interpret the experimental data and predict the properties of hadrons. The heavy quark hadrons like charmonium and bottomonium have also indeed received remarkable experimental growth. First observation of charmonium particle ($c\bar{c}$) by Brookhaven National Laboratory in reaction $p + Be \rightarrow e^+ + e^- + X$ [1]. SLAC observed the same particle at the same time by studying $e^+ + e^- \rightarrow hadron$ decays [2]. So, this charmonium state was denoted by $J\ /\psi$. Upto 1980, experimental facilities announce ten charmonium states - some states $\eta_c(1S)$, J/ψ, $\chi_{c0}(1P)$, $\chi_{c1}(1P)$, $\chi_{c2}(1P)$, $\psi(2S)$ are below the threshold and some states $\psi(3770), \psi(4040), \psi(4160), \psi(4415)$ are above the threshold of open charm $(D\bar{D})$ meson. After this, experimental collaborations continuously searched new states of charmonium, and in 2003, with the groundbreaking discovery of $X(3872)$ [3], heavy quarkonium physics entered a new era. The state $X(3872)$ was initially detected by the Belle experiment in 2003 and later reconfirmed by BABAR [4], CDF [5], DO [6], LHCb [7], CMS [8]. Despite several experimental investigations, its nature is still enigmatic. This state is also examined by numerous theoretical models and explained as an exotic state by [9, 10], as a pure charmonium state by [11–13]. This state is also suggested as a tetra-quark state, as meson-meson molecular structure, and as charmonium core plus higher Fock components by different theoretical approaches [14–17]. Now the state $X(3872)$ is updated in PDG [18] as $\chi_{c1}(3872)$ and considered as a charmonium candidate. The state $\psi_2(3823)$ was first time observed by Belle collaborations [19] in 2013 and later confirmed by BESIII [20] in 2015 and considered as $\psi(1^3D_2)$. In 2020 LHCb [21], also observed $\psi_2(3823)$ state in the decay of $\pi^+\pi^- J/\psi$ and reconfirmed the same state in 2021 [22] with higher significance. Theoretical attempts also strongly supported experimental assignment ($\psi(1^3D_2)$) of $\psi_2(3823)$ [23, 24]. $\psi(3770)$ state is candiadte of $\psi(1D)$ with small admixtures of $\psi(2S)$. This assignment favors experimental as well as theoretical [15, 25, 26]. LHCb announced $\psi(3842)$ state [27] in 2019, and theoretical models like lattice QCD and QCD sum rules assign this state with $\psi(1^3D_3)$ [28, 29]. To expose its nature, more experimental and theoretical attention is needed. The charged charmonium like state $Z_c(3900)$ was reported by BESIII in 2013 by studing decay $e^+e^- \to \pi^-\pi^+ J/\psi$ and reconfirmed by Belle and CLEO [30–32]. Many theoretical models interpret this state as $\bar{D}D^*$ molecular state, S-wave tetraquark states, and kinematical effects [33–35]. Belle observed the state $X(3915)$ [36] in 2004 in decay process $B \to K\omega J/\psi$ and later reconfirmed by BABAR [37] in 2007 and again by Belle [38] in 2010 in photon-photon collisions. Experimental investigations suggested its $J^{PC} = 1^{--}$. State X(3915) was assigned a good candidate for P-wave charmonium by studying its decay behavior [39]. Later BABAR reconfirmed this state and gave its $J^{PC} = 0^{++}$ [40]. However, theoretical results for conventional P-wave charmonium have disagreed with BABAR's assignments [41, 42]. The nature of this state is still mysterious and needs more experimental attempts to uncover its nature. The state $X(3930)$ was announced by Belle [43] collaboration in 2006 in process $\gamma\gamma \to Z$ with $Z \to D\bar{D}$ and confirmed by BABAR [44] in 2010 by studying the same process. Also, LHCb [45] observed state $X(3930)$ in 2020 in process $B \to D^+D^-K^+$ and results are consistent with previous experimental findings. Theoretical studies suggested it as tetraquarks, $\chi_{co}(2P)$, $\chi_{co}(3P)$ [41, 46]. Recent lattice QCD results indicate that this state is dominated by the $c\bar{c}c\bar{c}$ constituents [47]. $X(3940)$ was discovered in 2007 in e^-e^+ collisions and reconfirmed the same state with high significance in 2010 by Belle [48, 49]. At the same time, Belle observed state $X(4160)$ in the process $e^+e^- \to J/\psi D^*\bar{D}^*$ [49]. The state $X(4160)$ was also announced by LHCb in 2021 [50]. Theoretical models also studied these states with different approaches and tried to uncover their nature. The authors in Ref.[51, 52] explained $X(3940)$ as $\eta_c(3S)$ and $X(4160)$ as $\xi_{c0}(3P)$ respectively. Ref.[53] studied their decay nature and assigned $X(3940)$ as $\eta_c(3S)$ and $X(4160)$ as $\eta_c(4S)$ respectively. Ref.[54] investigated $X(4160)$ by $^3P_0$ model and give possible assignment of state $X(4160)$ as $\xi_{c0}(3P)$, $\xi_{c1}(3P)$, $\eta_{c2}(2D)$ and $\eta_c(4S)$. $Z_c(4020)$ was announced by BESIII [55] in 2013 in decay process $e^+e^- \to \pi^+\pi^-h_c$ and reconfirmed by various time by same collaboration [56]. Moreover, Several candidates like $\psi(4040)$, $X(4050)^{\pm}$, $X(4055)$, $X(4100)$, $X(4140)$, $\psi(4160)$, $X(4160)$, $Z_c(4200)$, $\psi(4230)$, $R_{co}(4240)$, $X(4250)$, $\chi_{ci}(4274)$, $\chi(4350)$, $\psi(4415)$, $Z_c(4430)$, $\chi_{co}(4500)$, $X(4630)$, $\psi(4660)$, $\chi_{c1}(4680)$, $\chi_{co}(4700)$ have not only explored charmonium like states but also stimulated renewed quests for theoretical understanding. These studies are leading to intensified efforts to unravel their properties and delve deeper into the underlying mechanisms of QCD. Through the efforts of various experimental collaborations and facilities, significant progress has been made in establishing bottomonium spectra. In this chapter, we are focussing on the spectra and properties of bottomonium. The states $\Upsilon(1S)$, $\Upsilon(2S)$ and $\Upsilon(3S)$ were observed in 1977 by the E288 collaboration at the Fermi National Accelerator Laboratory (FNAL) [57, 58] and notated as $\Upsilon, \Upsilon', \Upsilon''$ states respectively. After the early detection of systems composing of $b\bar{b}$, many of the properties and new states were discovered as given in PDG[18]. During the year 1982, the first excited state $\chi_{bJ}(2P)$ were identified in E1 transition from Υ'' state [59, 60]. Subsequently, in 1983, an exciting breakthrough came with the discovery of $\chi_{bJ}(2P)$ with $J = 0,\ 1,\ 2$ in the E1 transition from Υ' state [61, 62]. In the following year, 1984, $\Upsilon(4S), \Upsilon(5S), \Upsilon(6S)$ are announced in e^+e^- cross section above $B\bar{B}$ threshold [63, 64]. These findings opened the search window to investigate higher excited states of bottomonia spectra. After several experimental attempts, in 2008, the BABAR collaboration [65] announced the observation of $\eta_b(1S)$, spin partner of $\Upsilon(1S)$. In 2010, BABAR collaboration observed $\Upsilon(1^3D_J)$ with $J = 2$ in decay chain $\Upsilon(3S) \to \gamma\gamma\Upsilon(1^3D_J) \to \gamma\gamma\Upsilon(1S)$ [66]. In 2011, the BABAR collaboration announced $h_b(1P)$ observed via decay process $\Upsilon(3S) \rightarrow \pi^0 h_b(1P)$ [67]. In 2011, Belle Collaboration reported observation of states $h_b(1P)$ and $h_b(2P)$ in $e^+e^- \rightarrow h_b(nP)\pi^+\pi^-$ process [68]. In the same year, the ATLAS group reconstructed $\chi_b(nP)$ via radiative decay $\chi_b(nP) \rightarrow \Upsilon(1S)\gamma$ and $\chi_b(nP) \rightarrow \Upsilon(2S)\gamma$. A new state $\chi_b(3P)$ is identified in these decay modes [69]. This state $\chi_b(3P)$ was also reconfirmed by D0 collaborations [70] and the LHCb group [71]. The latest CMS experiment shows resolved peaks of $\chi_{b1}(3P)$ and $\chi_{b2}(3P)$ with mass difference of $10.60 \pm 0.64(stat) \pm 0.17(syst)$ MeV using 80 fb^{-1} in pp collisions at a center-of-mass energy of 13 TeV [72]. In 2012, Belle announced the first evidence of the existence of state $\eta_b(2S)$, pseudoscalar partner of $\Upsilon(2S)$ [73]. Some charged candidates like $Z_b(10610)$ and $Z_b(10650)$ are also announced in $\pi^\pm\Upsilon(nS)$(n = 1,2,3) and $\pi^\pm h_b(mP)$ $(m = 1, 2)$ mass spectra by Belle experiment [18]. But, their nature is still enigmatic. These states have been thoroughly investigated and analyzed in theoretical frameworks and interpreted these states as molecular states, exotic states, and tetraquarks states [74–76]. Recently, there has been a resurgence of interest in the exploration and investigation of states $\Upsilon(10860)$ and $\Upsilon(11020)$, which was first announced in 1985 by CUSB experiment [64]. A recent study in 2019 by Belle investigated $\Upsilon(10860)$ state in process $e^+e^- \rightarrow \Upsilon(nS)$ $(n = 1, 2, 3)$ with high significance and measured masses are 10752.7$\pm$5.9 MeV,and decay widths are $35.5^{+17.6}_{-17.6}$ MeV respectively [77]. Now this vector state is mentioned as $\Upsilon(10753)$ state in PDG. Authors in Ref.[78], investigated $\Upsilon(10753)$ using relativistic flux tube and give assignment of 3^3D_1 $b\bar{b}$ state. In Ref.[79], with QCD sum rules, Wang et al. interpreted this state as a hidden bottom tetraquark state. Theoretically, the prevailing consensus posits that $\Upsilon(10860)$ and $\Upsilon(11020)$ states correspond to the S-wave vector $b\bar{b}$ states denoted as $\Upsilon(5S)$ and $\Upsilon(6S)$, respectively [80, 81]. Authors in Ref.[82, 83] explicated these states ($\Upsilon(10860)$ and $\Upsilon(11020)$) with instanton-induced potential obtained from the instanton liquid model for QCD vacuum and elucidated $\Upsilon(10860)$ as an admixture of $5^3S_1 - 6^3D_1$ states and $\Upsilon(11020)$ as an admixture of $5^3S_1 - 5^3D_1$ states respectively. Also state $\Upsilon(11020)$ studied in Ref.[82, 83] and suggested as an admixture of $6^3S_1 - 5^3D_1$ states. Very recently, in March 2023, the BelleII detector examined the decay process $e^+e^- \rightarrow \omega_{\chi_{bJ}}(1P)$ $(J = 0, 1, 2)$ and concluded states $\Upsilon(10860)$ and $\Upsilon(10753)$ may have different internal structures [84], which is considered same in previous studies [77]. All these recent observations of numerous states of heavy mesons developed an interest in theoreticians to explore them in all aspects. Different QCD potential models have studied all the above-observed states. It is believed that QCD potential models are the most successful phenomenological approach in the non-perturbative region. There are various kinds of potentials in literature like Cornell potential [85–87], Martin potential [88, 89], Logarithmic potential [90], Richardson potential [91], and Song and Lin potential [92], which successfully explore quarkonium and their properties. Another potential is used to study charmonium spectroscopy [93] and its decay properties. In the same context, we explore bottomonium spectra and their decay properties using the same non-relativistic potential model from Ref. [93]. Similar potentials have been harnessed with $n = 2$ to study the dynamics of light hadrons in the framework of the Bethe- Salpeter equation under Covariant Instantaneous Ansatz (CIA) [94–96]. It can extensively explore many processes like digamma decays, radiative decays, decay constants, and the structure of hadrons. This framework can also be explored for various energy scales to have better insights. Using quark - antiquark confining potential form [93], we calculated masses and decay properties of bottomonia - leptonic decays, gamma decays, gluons decays, and decay constants, which are very useful in revealing the non-perturbative domain of QCD.

The realm of heavy mesons encompasses a diverse family of particles, including the charmonium and bottomonium systems. Within this context, a particularly intriguing subclass is the B_c meson family, which consists of mesons composed of a bottom quark (b) and a charm antiquark (c), and vice versa. The first candidate of the beauty-charmed meson family was observed in $p\bar{p}$ collision at Fermilab Tevatron by CDF collaboration in 1998 [97]. The measured mass and lifetime of B_c^+ are:

$$M(B_c^+) = 6.40 \pm 0.39(stat) \pm 0.13(syst)GeV$$

$$\tau(B_c^+) = 0.46^{0.18}_{-0.16}(stat)ps$$

This discovery was later corroborated by Abulencia et al.[98], Aaltonen et al.[99], DO collaboration [100], and LHCb [101]. After a few years, in 2014, the second member $B_c(2S)$ of B_c family was observed in pp collisions by ATLAS experiment at LHC [102]. The measured mass of this candidate is $6842 \pm 4 \pm 5 MeV$, where the first error is statistical and the second is a systematic error. At the latest, CMS and LHCb detectors reconfirmed the state $B_c(2S)$ and announced a new state $B_c^*(2S)$

[103, 104]. No other beauty-charmed meson family candidate has been observed experimentally at present. However, more states of beauty charmed mesons family explored in various theoretical approaches. The B_c family is unique in the standard model as it carries two different heavy quark flavors. This exceptional feature of B_c family ignited the interest of theoreticians and explored its various aspects, such as production, decay processes, and mass spectrum. All these recent observations of numerous states of heavy mesons developed an interest in theoreticians to explore them in all aspects.

The chapter is summarized as follows: Section 5.2 gives a brief description of phenomenological quark-antiquark confining potential and extraction of potential parameters from Chi-square fitting and gives a description of the decay rates of quarkonium. Section 5.3 presents the numerical analysis where we predict the mass spectra of bottomonia for $nS, nP, nD, nF, n = 1, 2, 3, 4, 5$ and their decay properties. Section 5.4 gives the conclusions of this Chapter.

5.2 Framework

Various theoretical approaches describe the spectrum of quarkonium states (charmonium, bottomonium, beauty charmed mesons). Still, the phenomenological potential model is one of the most popular and reliable approaches. The famous form of potential model exploited in heavy quarkonium spectroscopy is coulomb plus linear potential. The Coulomb potential component arises from the one-gluon exchange (Lorentz vector exchange) interaction between the quark and antiquark, which is analogous to the electromagnetic interaction between charged particles. On the other hand, the linear potential arises from the strong force (usually associated with Lorentz scalar exchange) that acts between the quark and the antiquark. This potential increases linearly with the separation between the quark and the antiquark. As discussed in the previous section, many other forms of confining potentials are used in literature. We have adopted the following potential form to study the spectroscopy of bottomonium-bound states [93].

$$V(r) = V_V + V_S = \frac{-4\alpha_s}{3r} + \frac{Ar^2}{(1+4Br^p)^{\frac{1}{2}}} - V_0 \tag{5.1}$$

where V_V is the vector part of the potential (Coulomb), V_S is the scalar part of the potential (confining), α_s is the running coupling constant. A and B are potential parameters estimated with chi-square fitting of low-lying bottomonium states. Since for charmonium, as mentioned in Ref.[93], the results are not consistent for $p = 2$, we have also worked for $p = 1$ and $B = 1\ GeV^p$. The value of the running coupling constant can be obtained by the expression :

$$\alpha_s(\mu^2) = \frac{4\pi}{(11 - \frac{2}{3}n_f)}\left(ln\frac{\mu^2}{\Lambda^2}\right) \tag{5.2}$$

Where Λ is the QCD scale taken as 0.12 GeV, n_f is the number of active flavors, number of flavors lighter than scale μ ($m_q \ll \mu$). μ is the renormalization scale equal to $\frac{2m_Q m_{\bar{Q}}}{m_Q + m_{\bar{Q}}}$, for bottomonium $n_f = 4$, as flavors u, d, s, and c are considered light. A similar potential is used to study the ground states of light-flavoured and heavy-light mesons [95, 96, 105–112]. The scalar part of the potential Eq. (5.1) is supposed to behave as linear confinement (r) for the heavy quark (c, b) and hadronic form of the (r^2) for the light quarks. V_0 is a state-dependent constant potential. In adopted potential in eq 5.1, we added spin-dependent terms - spin-spin, spin-orbit, and tensor to describe the spectrum's splitting structure and account for each state's different quantum numbers. The spin-dependent part V_{SD} [113, 114] is given by:

$$\begin{aligned} V_{SD} = V_{SS}\left[S(S+1) - \frac{3}{2}\right] + V_{LS}\left[\frac{1}{2}(J(J+1) - S(S+1) - L(L+1))\right] \\ + V_T\left[S(S+1) - \frac{3(S_1.r)(S_2.r)}{r^2}\right] \end{aligned} \tag{5.3}$$

Where coefficients V_{SS}, V_{LS}, and V_T depend on derivatives of vector V_V and scalar V_S contributions from the adopted potential in eq 5.1. The expressions for coefficients are the following [113, 115]:

$$V_{SS}^{ij}(r) = \frac{1}{3M_iM_j}\nabla^2 V_V = \frac{16\pi\alpha_s}{9M_iM_j}\delta^3(r) \tag{5.4}$$

$$V_{LS}^{ij}(r) = \frac{1}{2M_iM_jr}\left[3\frac{dV_V}{dr} - \frac{dV_S}{dr}\right] \tag{5.5}$$

$$V_T^{ij}(r) = \frac{1}{6M_iM_j}\left[\frac{d^2V_V}{dr^2} - \frac{1}{r}\frac{dV_V}{dr}\right] \tag{5.6}$$

Where M_i, M_j are quark masses. All these spin-dependent interactions are corrections in total mass, treated as first-order perturbation corrections in heavy quark-bound states. As V_{LS}, V_{SS}, and V_T expressions are proportional to $1/m^2$ ($M_i = M_j = m$ for bottomonium), they justify their treatment as first-order perturbative corrections. The spin-orbit term containing V_{LS} and tensor term containing V_T describe the fine structure of the state, whereas the spin-spin term containing V_{SS} describes hyperfine splittings. Mass is the prime property to study the spectroscopy of hadrons. To calculate spectra of bottomonium, we estimated the parameters V_0, bottom quark m_b, and parameter A appearing in potential in eq (5.1) with Chi-square fitting procedure. We considered these parameters as free parameters in the fitting procedure for ground-state bottomonium meson in the following range:

$$0 < A < 1\ (GeV^3);\ 0 < V_0 < 0.5\ (GeV);\ 4 < m_b < 5\ (GeV).$$

The results for parameters are: $m_b = 4.72\, GeV$, $V_0 = 0.10\, GeV$, $A = 0.20\, GeV^2$. The running coupling constant is $\alpha_s = 0.2053$. The state dependent potential strength V_0 is given by relation:

$$V_0(n+1, l) = V_0 + b(n+1) + cl \tag{5.7}$$

Where n and l are the radial and angular quantum numbers of the states. Also, b and c are unknown parameters estimated by fitting the experimental masses of $2S$, $1P$ states of bottomonium. We find b = -0.105 GeV, c = 0.0007 GeV. Using all these parameters and adopted potential form, we computed mass spectra of nS, nP, nD, and nF bottomonium states listed in Table 5.1, Table 5.2, Table 5.3, and Table 5.4.

5.3 Decay Rates of Bottomonia

Precise estimation of decay rates with mass prediction is crucial for any successful model. Recently there have been several investigations on various phenomena encompassing strong, radiative, and leptonic decays of heavy quarkonium. Such investigations directly probe the hadron structure and shed light on the quark-gluon interactions. Leptonic decay constants serve as expedient probes for the short-distance structure of hadron and act as tools for studying quark dynamics in this domain. The annihilated decay rates - dileptonic, digamma, tri gamma, and digluons are studied with extracted model parameters and associated radial wave functions. As these decay rates are directly linked to the wavefunctions, they provide a better understanding of quark-antiquark interactions within meson.

5.3.1 Leptonic Decay Constants

The study of leptonic decay constants of bottomonia is a important property for understanding weak decays. It also provides information about CKM (Cabibbo-Kabayashi-Maskawa) matrix elements. For pseudoscalar and vector mesons, following are expressions of leptonic decay constants: [116]:

$$f^2_{P/V} = \frac{3|R_{nsP/V(0)}|^2}{\pi M_{nsP/V}} \bar{C}^2(\alpha_s) \tag{5.8}$$

Here the QCD correction factor $\bar{C}^2(\alpha_s)$ [117, 118] is provided by:

$$\bar{C}^2(\alpha_s) = 1 - \frac{\alpha_s}{\pi}\left(\delta_{P,V} - \frac{m_Q - m_{\bar{Q}}}{m_Q + m_{\bar{Q}}} ln\frac{m_Q}{m_{\bar{Q}}}\right) \tag{5.9}$$

with $\delta_P = 2$ and $\delta_V = 8/3$ in case of Bottomonium mesons. The second term in equation 5.9 will disappear in the case of bottomonium. Using these expressions, we computed leptonic decay constants and listed them in Table 5.5 and Table 5.6.

5.3.2 Electromagnetic Transition Widths

The study of electromagnetic transition can be understood in terms of electric and magnetic multipole expansion, and their investigation provides a better sight into the non-perturbative regime. The selection rule for $E1$ transitions is $\Delta L = 0$ and $\Delta S = \pm 1$. For $M1$ transitions, $\Delta L = \pm 1$, and $\Delta S = 0$ are selection rules. To check the authenticity of calculated masses and chi-square fit parameters, we computed $E1$ and $M1$ transitions, and the formulas for these transitions [119–122] are given below:

$$\Gamma(n^{2S+1}L_iJ_i \to n'^{2S+1}L_fJ_f + \gamma) = \frac{4\alpha_e \langle e_Q\rangle^2 \omega^3}{3}(2J_f+1)S^{E1}_{if}|M^{E1}_{if}|^2 \tag{5.10}$$

$$\Gamma(n^3S_1 \to n'^1S_0 + \gamma) = \frac{\alpha_e \mu^2 \omega^3}{3}(2J_f+1)|M^{M1}_{if}|^2 \tag{5.11}$$

where, $\langle e_Q\rangle$ is mean charge of $Q\bar{Q}$ system, μ is magnetic dipole moment and ω is photon energy and expression for them are

$$\langle e_Q\rangle = \left|\frac{m_{\bar{Q}}e_Q - e_{\bar{Q}}m_Q}{m_Q + m_{\bar{Q}}}\right| \tag{5.12}$$

$$\mu = \frac{e_Q}{m_Q} - \frac{e_{\bar{Q}}}{m_{\bar{Q}}} \tag{5.13}$$

and

$$\omega = \frac{M_i^2 - M_f^2}{2M_i} \tag{5.14}$$

The symmetrical factor S_{if}^{E1} is also given in the following way:

$$S_{if}^{E1} = max(L_i, L_f) \begin{pmatrix} J_i & 1 & J_f \\ L_f & S & L_i \end{pmatrix}^2 \tag{5.15}$$

The matrix element $|M_{if}|$ for E1 and M1 transition is given by:

$$|M_{if}^{E1}| = \frac{3}{\omega} \left\langle f \left| \frac{\omega r}{2} j_0 \left(\frac{\omega r}{2}\right) - j_1 \left(\frac{\omega r}{2}\right) \right| i \right\rangle \tag{5.16}$$

and

$$|M_{if}^{M1}| = \left\langle f \left| j_0 \left(\frac{\omega r}{2}\right) \right| i \right\rangle \tag{5.17}$$

The computed values of $E1$ and $M1$ transitions are collected in Table 5.7 and Table 5.8, respectively.

5.3.3 Leptonic Decay Widths

Single virtual photons ($Q\bar{Q} \rightarrow l^+l^-$) are used to disintegrate quarkonium into leptons ($e^-\mu^-, \tau^-$). The quarkonium state undergoes leptonic decay when it is in the same state as the photon i.e., $J^{PC} = 1^{--}$. Using Van Royen Weisskopf formula, the leptonic decay width of n^3S_1 and n^3D_1 states of bottomonium, with first-order radiative QCD corrections [116, 123], is given below:

$$\Gamma(n^3S_1 \rightarrow e^+e^-) = \frac{4e_Q^4\alpha^2|R_{nS}(0)|^2}{M_{nS}^2}\left(1 - \frac{16\alpha_s}{3\pi}\right) \tag{5.18}$$

$$\Gamma(n^3D_1 \rightarrow e^+e^-) = \frac{25e_Q^2\alpha^2|R_{nD}^{''}(0)|^2}{2m_Q^4M_{nD}^2}\left(1 - \frac{16\alpha_s}{3\pi}\right) \tag{5.19}$$

where e_Q is charge on quark, M_{nS}, M_{nD} is masses of decaying corresponding states, $\alpha = 1/137$ is fine structure constant that describes the strength of electromagnetic force, and $R_{nS}(0)$, $R_{nD}^{''}(0)$ are normalized reduced wave-function at origin for S-waves and second order derivative of normalized reduced wave function for D-waves respectively. Bracketed terms in expressions 5.18, 5.19 are the lowest order QCD corrections. The computed values of leptonic decay widths are mentioned in Table 5.9.

5.3.4 Digamma and Trigamma Decay Widths

Yang theorem rules out a decay into two photons for $J = 1$ states [124, 125]. For digamma decays, S-wave states must be in a spin-singlet state, whereas P-wave states must be in the spin-triplet state. The formula for digamma decay widths of

$^1S_0$ and $^3P_J(J=0,2)$ is given below [116, 123]:

$$\Gamma(n^1S_0 \to \gamma\gamma) = \frac{3e_Q^2\alpha^2|R_{nS}(0)|^2}{m_Q^2}\left(1-\frac{3.4\alpha_s}{\pi}\right) \tag{5.20}$$

$$\Gamma(n^3P_0 \to \gamma\gamma) = \frac{27e_Q^4\alpha^2|R^{'}_{nP}(0)|^2M_{^3P_0}}{2m_Q^5}\left[1+\left(\frac{\pi^2}{3}-\frac{28}{9}\right)\left(\frac{\alpha_s}{\pi}\right)\right] \tag{5.21}$$

$$\Gamma(n^3P_2 \to \gamma\gamma) = \frac{4}{15}\frac{27e_Q^4\alpha^2|R^{'}_{nP}(0)|^2M_{^3P_2}}{2m_Q^5}\left[1+\left(\frac{-16}{3}\right)\left(\frac{\alpha_s}{\pi}\right)\right] \tag{5.22}$$

$$\Gamma(n^3S_1 \to \gamma\gamma\gamma) = \frac{4(\pi^2-9)e_Q^6\alpha^3|R_{nS}(0)|^2}{m_Q^2}\left(1-\frac{12.6\alpha_s}{\pi}\right) \tag{5.23}$$

$R^{'}_{nl}$ is the first derivative of the normalized reduced wave function at the origin in P-wave formulas. e_Q is charge on quark. $\alpha = 1/137$ is a fine structure constant. Terms in brackets are the next to leading-order QCD radiative corrections. The calculated digamma, tri-gamma decay widths are collected in Table 5.10 and Table 5.11.

5.3.5 Digluon Decay Widths

At short range, the decay width involving two gluons serves as a sensitive indicator for quarkonium and its derivatives in the vicinity of origin. Below the $Q\bar{Q}$ threshold, the digluon decay width provides details of the total decay width of hadronic decays. Employing VRW (Van Royen Weisskopf) method [116, 123] and including QCD radiative corrections [126–128], expressions for digluon decay widths are:

$$\Gamma(n^1S_0 \to gg) = \frac{2\alpha_s^2|R_{ns}(0)|^2}{3m_Q^2}\left(1+\frac{4.4\alpha_s}{\pi}\right) \tag{5.24}$$

$$\Gamma(n^3P_0 \to gg) = \frac{6\alpha_s^2|R^{'}_{nP}(0)|^2}{m_Q^4}\left(1+\frac{10.0\alpha_s}{\pi}\right) \tag{5.25}$$

$$\Gamma(n^3P_2 \to gg) = \frac{8\alpha_s^2|R^{'}_{nP}(0)|^2}{5m_Q^4}\left(1-\frac{0.1\alpha_s}{\pi}\right) \tag{5.26}$$

$$\Gamma(n^1D_2 \to gg) = \frac{2\alpha_s^2|R^{''}_{nD}(0)|^2}{3\pi m_Q^6} \tag{5.27}$$

Terms in brackets are the next to leading-order QCD radiative corrections. $\alpha = 1/137$ is fine structure constant. $R^{'}_{nP}$ is the first order derivative of the normalized reduced wave function at the origin in P-wave formulas. Similar $R^{"}_{nD}$ is the second order derivative of the normalized reduced wave function at the origin in D-wave formulas. The calculated values of digluons are mentioned in Table 5.12.

5.4 Results and Discussions

5.4.1 Mass Spectroscopy

The masses of bottomonium mesons for S, P, D, F-waves are calculated by employing a non-relativistic potential given in Eq. (5.1) and solving the Schrödinger wave equation numerically. Our calculated mass for S, P, D, F-waves of bottomonium mesons is listed in Table 5.1, Table 5.2, Table 5.3, Table 5.4 respectively and compared with experimental data as well as different theoretical predictions.

Table 5.1: The predicted values of nS bottomonium masses (GeV) compared with some other model predictions.

$J^{PC}(n^{2S+1}L_j)$	Present	Ref.[87]	Ref.[81]	Ref.[129]	Ref.[82]	Ref.[130]	Ref. [131]	Ref.[132]	PDG [18]
$0^{-+}(1^1S_0)$	9.43297	9.423	9.398	9.402	9.41222	9.392	9.398	9.393	9.399
$1^{--}(1^3S_1)$	9.44816	9.463	9.463	9.465	9.46075	9.460	9.460	9.460	9.460
$0^{-+}(2^1S_0)$	10.00660	9.983	9.989	9.976	9.99548	9.991	9.990	9.987	9.999
$1^{--}(2^3S_1)$	10.02020	10.001	10.017	10.003	10.02622	10.024	10.023	10.023	10.023
$0^{-+}(3^1S_0)$	10.50310	10.342	10.336	10.336	10.33900	10.323	10.329	10.345	-
$1^{--}(3^3S_1)$	10.51650	10.354	10.356	10.354	10.36465	10.346	10.355	10.364	10.355
$0^{-+}(4^1S_0)$	10.96910	10.638	10.597	10.623	10.57249	10.558	10.573	10.364	-
$1^{--}(4^3S_1)$	10.98250	10.650	10.612	10.635	10.59447	10.575	10.586	10.643	10.579
$0^{-+}(5^1S_0)$	11.41690	10.901	10.810	10.869	10.74676	10.741	10.851	-	-
$1^{--}(5^3S_1)$	11.43030	10.912	10.822	10.878	10.76614	10.755	10.869	-	10.885

Our findings for the masses concur with experimentally observed masses for respective states. Our calculated masses for 1^3S_1 state 9.44816 GeV, which is well matched with experimental value 9.460 ± 0.00026 GeV and for its spin partner 1^1S_0 state, our estimated mass is roughly 11 MeV higher than experimental mass mentioned in PDG. On observing Table 5.1, we found masses of nS-wave up to $n = 5$ agree with the experimental data and other theoretical predictions with a deviation of $\pm 5\%$. For nS states, our predicted masses are close to theoretical estimations of Ref. [87, 129, 130]. In Ref. [87], Kher et al. employed a variational method with a single Gaussian trial wave functions, Ref. [129], Godfrey et al. employed

Table 5.2: The predicted values of bottomonium nP meson masses (GeV) compared with some other model predictions.

$J^{PC}(n^{2S+1}L_j)$	Present	Ref.[81]	Ref.[133]	Ref.[82]	Ref. [86]	Ref. [129]	Ref.[131]	Ref. [134]	PDG[18]
$0^{++}(1^3P_0)$	9.75011	9.858	9.845	9.84961	9.806	9.847	9.859	9.865	9.859
$1^{+-}(1^1P_1)$	9.75938	9.894	9.881	9.87456	9.819	9.876	9.892	9.897	9.899
$1^{++}(1^3P_1)$	9.75671	9.889	9.875	9.87147	9.821	9.882	9.900	9.903	9.893
$2^{++}(1^3P_2)$	9.76608	9.910	9.896	9.88140	9.825	9.897	9.912	9.918	9.912
$0^{++}(2^3P_0)$	10.25270	10.235	10.225	10.25254	10.205	10.226	10.233	10.226	10.233
$1^{+-}(2^1P_1)$	10.26000	10.259	10.250	10.27000	10.217	10.246	10.255	10.251	10.260
$1^{++}(2^3P_1)$	10.25840	10.255	10.246	10.26786	10.220	10.250	10.260	10.256	10.255
$2^{++}(2^3P_2)$	10.26670	10.269	10.261	10.27477	10.224	10.261	10.268	10.269	10.269
$0^{++}(3^3P_0)$	10.72320	10.513	10.521	10.51288	10.540	10.552	10.521	10.502	-
$1^{+-}(3^1P_1)$	10.72930	10.530	10.540	10.52650	10.553	10.538	10.541	10.524	-
$1^{++}(3^3P_1)$	10.72840	10.527	10.537	10.52484	10.556	10.541	10.544	10.529	10.514
$2^{+-}(3^3P_2)$	10.73630	10.539	10.549	10.53021	10.560	10.550	10.550	10.540	10.524
$0^{++}(4^3P_0)$	11.17450	10.736	10.773	10.70356	10.840	10.775	10.781	10.732	-
$1^{+-}(4^1P_1)$	11.17990	10.751	10.790	10.71480	10.853	10.788	10.802	10.753	-
$1^{++}(4^3P_1)$	11.17950	10.749	10.787	10.71344	10.855	10.790	10.804	10.757	-
$2^{++}(4^3P_2)$	11.18700	10.758	10.797	10.71786	10.860	10.798	10.812	10.767	-
$0^{++}(5^3P_0)$	11.61260	10.926	10.998	10.85338	11.115	11.014	-	10.933	-
$1^{+-}(5^1P_1)$	11.61730	10.938	11.013	10.86300	11.127	11.014	-	10.951	-
$1^{++}(5^3P_1)$	11.61740	10.936	11.010	10.86183	11.130	11.016	-	10.955	-
$2^{++}(5^3P_2)$	11.62460	10.944	11.020	10.86562	11.135	11.022	-	10.965	-

relativized quark model and Ref. [130], Shah et al. employed the non-relativistic potential model to investigate bottomonia mass spectroscopy. Specifically, on comparing with Ref. [81], we observed our masses are very close to their predictions up to $n = 4$ S-wave states, but our results slightly deviate for $5S$ states from them. This may happen due to screening effects employed by Ref. [81] as screening effects contribute significantly to higher excited states and affect mass values, wave functions, and decay behaviors. Similarly, for P-waves, our results are in good agreement with experimental values and theoretical estimations. For $n = 1$ P-wave masses, our mass

Table 5.3: The predicted values of bottomonium nD meson masses (GeV) compared with some other model predictions.

$J^{PC}(n^{2S+1}L_j)$	Present	Ref.[81]	Ref.[133]	Ref. [82]	Ref.[130]	Ref. [134]	Ref. [131]	Ref.[86]	PDG [18]
$1^{--}(1^3D_1)$	9.99397	10.153	10.137	10.14499	10.147	10.145	10.154	10.074	-
$2^{-+}(1^1D_2)$	9.99238	10.163	10.148	10.15380	10.162	10.151	10.161	10.075	-
$2^{--}(1^3D_2)$	9.99423	10.162	10.147	10.15277	10.166	10.152	10.163	10.074	10.164
$3^{--}(1^3D_3)$	9.99386	10.170	10.155	10.15831	10.177	10.156	10.166	10.073	-
$1^{--}(2^3D_1)$	10.46920	10.442	10.441	10.45023	10.428	10.432	10.435	10.423	-
$2^{-+}(2^1D_2)$	10.46740	10.450	10.450	10.45660	10.437	10.438	10.443	10.424	-
$2^{--}(2^3D_2)$	10.46990	10.450	10.449	10.45586	10.440	10.439	10.445	10.424	-
$3^{--}(2^3D_3)$	10.47040	10.456	10.455	10.45985	10.447	10.442	10.449	10.423	-
$1^{--}(3^3D_1)$	10.92470	10.675	10.698	10.65968	10.637	10.670	10.704	10.731	-
$2^{-+}(3^1D_2)$	10.92210	10.681	10.706	10.66470	10.645	10.676	10.711	10.733	-
$2^{--}(3^3D_2)$	10.92550	10.681	10.705	10.66412	10.646	10.677	10.713	10.733	-
$3^{--}(3^3D_3)$	10.92640	10.686	10.711	10.66725	10.652	10.680	10.717	10.733	-
$1^{--}(4^3D_1)$	11.36630	10.871	10.927	10.81883	10.805	10.877	10.949	11.013	-
$2^{-+}(4^1D_2)$	11.36290	10.876	10.934	10.82300	10.811	10.882	10.957	11.016	-
$2^{--}(4^3D_2)$	11.36710	10.876	10.934	10.82252	10.813	10.883	10.959	11.015	-
$3^{--}(4^3D_3)$	11.36810	10.880	10.939	10.82512	10.817	10.886	10.963	11.015	-
$1^{--}(5^3D_1)$	11.79730	11.041	11.137	10.94901	10.945	11.060	-	-	-
$2^{-+}(5^1D_2)$	11.79300	11.046	11.143	10.95260	10.952	11.066	-	-	-
$2^{--}(5^3D_2)$	11.79820	11.045	11.143	10.95159	10.950	11.065	-	-	-
$3^{--}(5^3D_3)$	11.79920	11.049	11.148	10.95442	10.955	11.069	-	-	-

estimations are 1.45% below experimental values. Our computation for state 2^1P_1 is 10.2600, which is in excellent agreement with the experimental value mentioned in PDG ($10.260 \pm 1.2 \times 10^{-4}$). Also, its spin partners, i.e $2^3P_0, 2^3P_1, 2^3P_2$, our results differ from experimental values by 19 MeV, 3 MeV, 2 MeV respectively which reflects reliability of our model. One more important parameter to check the authenticity of any model is hyperfine splittings. For $1P$ state, $\Delta M_{hfs}(1P) = 4.9\ MeV$ and $2P$ state $\Delta M_{hfs}(2P) = 2.4\ MeV$, which consistent to experimental values [18].

Table 5.4: The predicted values of bottomonium nF meson masses (GeV) compared with some other model predictions.

$J^{PC}(n^{2S+1}L_j)$	Present	Ref.[81]	Ref.[133]	Ref. [129]	Ref. [86]	Ref. [131]	Ref. [132]
$2^{++}(1^3F_2)$	10.20690	10.362	10.350	10.358	10.283	10.343	10.353
$3^{+-}(1^1F_3)$	10.20130	10.366	10.354	10.355	10.288	10.347	10.356
$3^{++}(1^3F_3)$	10.20430	10.366	10.354	10.355	10.287	10.346	10.356
$4^{++}(1^3F_4)$	10.20050	10.369	10.358	10.358	10.291	10.349	10.357
$2^{++}(2^3F_2)$	10.66600	10.605	10.615	10.615	10.604	10.610	10.610
$3^{+-}(2^1F_3)$	10.66080	10.609	10.619	10.619	10.607	10.647	10.613
$3^{++}(2^3F_3)$	10.66500	10.609	10.619	10.619	10.607	10.614	10.613
$4^{++}(2^3F_4)$	10.66340	10.612	10.622	10.622	10.609	10.617	10.615
$2^{++}(3^3F_2)$	11.11170	10.809	10.849	10.850	10.894	-	-
$3^{++}(3^1F_3)$	11.10530	10.812	10.853	10.853	10.897	-	-
$3^{++}(3^3F_3)$	11.11120	10.812	10.853	10.853	10.896	-	-
$4^{++}(3^3F_4)$	11.11040	10.815	10.856	10.856	10.898	-	-
$2^{++}(4^3F_2)$	11.54670	10.985	11.063	-	-	-	-
$3^{+-}(4^1F_3)$	11.53850	10.988	11.066	-	-	-	-
$3^{++}(4^3F_3)$	11.54640	10.988	11.066	-	-	-	-
$4^{++}(4^3F_4)$	11.54590	10.990	11.066	-	-	-	-

This splitting decreases more and becomes negligible for higher excited states. This shows that spin-spin contribution is negligible for higher excited states and thus reflects the vanishing of long-range chromomagnetic interactions in quarkonium. The calculated masses of $n = 4, 5$ for P are found to be overestimated in comparison to other theoretical estimations. However, masses for $n = 5$ P-wave are closer to outcomes of Ref. [86, 129, 133] than other estimations. In Ref. [129, 133], Godfrey et al. implemented a relativistic approach, while Ref. [86] used non-relativistic approach. This shows relativistic factors have very small contributions that do not much affect the mass spectroscopy of bottomonia. In Table 5.3, we listed predicted masses for nD-wave ($n = 1, 2, 3, 4, 5$) and compared them with other model predictions and experimental masses, which are also in good accord with them. Only one state 1^1D_2

of D-waves is experimentally available and the measured value of mass is 10.164 GeV. Our predicted value for this state deviates by 1.59% from the experimental value. Our result for $2D$ masses is found to be consistent with other theoretical predictions, while masses of $1D, 3D, 4D$ states are higher than predictions of other models. However, masses for $5D$ states are closer to predictions of Ref. [133], which employed relativized quark model with chromodynamics and included the concept of one-gluon-exchange-plus-linear confinement potential. This is also notable in Ref. [133], authors have not taken spin-spin, spin-orbit interaction into account, which reflects in mass degeneracy in spin states. Also, computed masses for nF-wave ($n = 1, 2, 3, 4$) listed in Table 5.4 are very close to other models' predictions. For the $1F$ state, our results are more consistent with Ref. [86], which used Cornell's potential to study bottomonium spectra. This is a similar kind of method that we used in this paper. Such comparison enhances the validity of our framework. Other results of F states are also in reasonable agreement with theoretical estimates.

5.4.2 Decay Constants

The study of leptonic decay constants is important for investigating non - perturbative QCD dynamics. Using calculated masses for S-wave collected in Table 5.1 and applying Van Royen-Weisskopf formula, extracted in eqns 5.8, 5.9, we computed values of pseudoscalar decay constants f_P and vector decay constants f_V listed in Table 5.5 and Table 5.6 respectively.

Table 5.5: Pseudoscalar decay constants of bottomonium (MeV) without and with QCD corrections.

States	f_P	f_P^C	Ref.[87]	Ref.[82]	Ref.[86]	Ref.[135]	Ref. [136]	Ref. [137]
$1S$	632.626	549.879	529	578.21	646.025	756	744	498
$2S$	551.298	479.188	317	499.48	518.803	285	577	366
$3S$	528.840	459.668	280	450.35	474.954	333	511	304
$4S$	516.337	448.800	264	413.93	449.654	40	471	259
$5S$	507.351	440.990	255	385.68	432.072	-	443	228

Our results for pseudoscalar decay constants are in tune with Ref. [82, 86,

Table 5.6: Vector decay constants of bottomonium (MeV) without and with QCD corrections.

States	f_V	f_V^C	Ref.[87]	Ref.[82]	Ref.[86]	Ref. [137]	Ref. [138]	Ref. [136]	PDG [18]
$1S$	666.036	535.517	530	551.53	647.250	498	705.4	706	715
$2S$	564.438	466.707	317	477.05	519.436	366	554.9	547	498
$3S$	542.290	447.715	280	430.42	475.440	304	436.8	484	430
$4S$	529.483	437.141	265	395.80	450.066	259	332.4	446	336
$5S$	520.281	429.544	255	368.91	432.437	228	286.5	419	-

87], while lower from Ref. [135, 136]. It is noticed that Ref. [82, 86, 87] have employed a similar kind of framework with different potential forms, which enhance the authenticity of our work. The estimated values of vector decay constant for states $1S, 2S, 3S, 4S$ differ by 179 MeV, 31 MeV, 17 MeV, and 101 MeV from experimental values, respectively. In comparison with theoretical approaches, values for vector decay constants without QCD corrections are consistent with Ref. [86], while with QCD corrections, our values concur with Ref. [82]. Ref. [82] employed instanton-induced potential by including confining terms to study bottomonium spectroscopy.

5.4.3 Radiative Transitions

The numerical result of radiative transitions in electric diploe (E1) and magnetic dipole (M1) expansion are listed in Table 5.7 and Table 5.8, respectively. Our estimations for radiative transitions widths $\Gamma(2^3S_1 \rightarrow 1^3P_0\gamma)$, $\Gamma(2^3S_1 \rightarrow 1^3P_1\gamma)$, $\Gamma(2^3S_1 \rightarrow 1^3P_2\gamma)$ differ by 0.16 keV, 1.66 keV, 3.5 keV from experimental values, respectively, and are also compatible with theoretical models estimations. These transitions ($\Gamma(2^3S_1 \rightarrow 1^3P_0\gamma)$, $\Gamma(2^3S_1 \rightarrow 1^3P_1\gamma)$, $\Gamma(2^3S_1 \rightarrow 1^3P_2\gamma)$) are closer to results of the potential model with v^2/c^2 corrections [139], quasi potential approach [131], the potential model with screened potential [134] shown in Table 5.7. The E1 transitions $\Gamma(3^3S_1 \rightarrow 2^3P_0\gamma)$, $\Gamma(3^3S_1 \rightarrow 2^3P_1\gamma)$, $\Gamma(3^3S_1 \rightarrow 2^3P_2\gamma)$ are consistent with experimental data while $\Gamma(3^3S_1 \rightarrow 1^3P_0\gamma)$, $\Gamma(3^3S_1 \rightarrow 1^3P_1\gamma)$, $\Gamma(3^3S_1 \rightarrow 1^3P_2\gamma)$ are lower by 7 keV, 3 keV, 4 keV from experimental results respectively. It is also inferred from Table 5.7, radiative transition widths for $3P \to 1S$ are suppressed than other $E1$ transitions. This shows a general feature that $E1$ transition between two states differs by two radial numbers that are highly suppressed and have very less contribution in $E1$ transitions. The calculated electric dipole transitions for $\Gamma(1^3P_2 \to 1^3S_1\gamma)$, $\Gamma(1^3P_1 \to 1^3S_1\gamma)$, $\Gamma(1^1P_1 \to 1^1S_0\gamma)$ are very close to experimental data. Also, the $E1$ transitions for $1P \to 1S$ give higher contributions relative to $2P \to 1S$ transition, which is expected. For $E1$ transition $1D \to 1P$, there is no experimental data, but compared with theoretical predictions, it is found that our results have a high degree of similarity with Ref. [131, 134], while lower values than Ref. [86]. We also calculated $M1$ transitions and listed them in Table 5.8. Generally, $M1$ transitions are weaker than $E1$ transitions but play an important role in finding spin-singlet states, which is back-breaking in other ways. It is inferred from Table 5.8 that predicted values are very small relative to $E1$ transitions. Our results for $M1$ transitions are lower than other model's predictions.

5.4.4 Annihilation Decays

The study of annihilation decays, i.e., decays of quarkonium states into photons, leptons, and gluons, sheds light on the perturbative aspect of QCD. Investigation of these decays is also helpful in the production, identification of conventional or non-conventional mesons, multiquark structures, etc. Using predicted masses and applying formulas obtained from Van Royen-Weisskopf formula, we estimate leptonic, digamma, tri gamma, digluon decay widths. These calculated decay widths are listed in Table 5.9, Table 5.10, Table 5.11, Table 5.12.

On observing Table 5.10, we found that calculated partial decay widths for nS states agree with other models' predictions. But our results for states nP are slightly off from other models' predictions. They differ from other predictions by ± 65 eV. We also calculated tri gamma decay widths mentioned in Table 5.11, and the results are in good accord with estimations deduced by other theoretical approaches.

The calculated digluon decay widths are listed in Table 5.12 and compared with predictions of other models. On comparing, it is found that our estimations are consistent with the results of other models for nS states. However, our results for nP states are higher than the predictions of other models. A similar trend can be seen in the case of nD states, i.e., our results are slightly higher than other model estimations.

The dileptonic decay widths of quarkonium play an important role in the estimation of strong coupling constants, decay constants and in checking the validity of theoretical models as its decay amplitude carries quarkonium wave function (can be seen in eqn.5.18). We calculated leptonic decay width and mentioned it in Table 5.9. On comparing, it is found that our predictions for nS states agree with the outcomes of other models. For nD states, our results agree with Ref. [82] and are higher in comparison to Ref. [81, 138, 142]. For higher n, our decay widths for D states show a monotonically increasing trend, which agrees with some of the compared models. It is also noticed on observing tables of annihilation decays that for D-wave states, values of leptonic decays and digluon decays are highly suppressed as compared to S- waves, which is expected.

As we know, the total decay width of a particular state is the sum of strong, radiative, and weak decay widths. But strong decay gives more contribution to the total decay width of that state relative to radiative and weak decay. This is inferred from Table 5.7, 5.8, 5.9, 5.10, 5.11, 5.12, which reflects the value of digluon decays (strong decays) are much more relative to radiative transitions and leptonic decays (weak decays).

5.5 Conculsion

In this Chapter, we have presented a comprehensive analysis of the mass spectra of bottomonium states and their decay properties by employing a non-relativistic potential model. Using adopted quark-antiquark confining potential, we solved Schr$\ddot{o}$dinger wave equations numerically with Runge -Kutta method using the Mathematica notebook [143]. Our calculated mass spectrum (nS, nP, nD, nF, n = 1, 2, 3, 4, 5) of bottomonia is fairly close to available experimental data and other theoretical model predictions. The hyperfine splittings of $1P$ and $2P$ states agree with the experiment observation. We have computed annihilation decays - di-leptonic, di-gamma, tri-gamma, di-gluons decay widths. Also, the electromagnetic transition widths by Van Royen - Weisskopf formula are calculated. All these decays are also estimated with first-order QCD corrections. Our findings agree with the available experimental observations and theoretical estimations. We have also explored leptonic decay constants, which are consistent with the experimental values mentioned in PDG. The present results may be helpful in upcoming experimental information in the near future.

Bibliography

[1] J.J. Aubert et al. (E598), Phys. Rev. Lett. **33**, 1404 (1974)

[2] J.E. Augustin et al. (SLAC-SP-017), Phys. Rev. Lett. **33**, 1406 (1974)

[3] S.K. Choi et al. (Belle), Phys. Rev. Lett. **91**, 262001 (2003), `hep-ex/0309032`

[4] B. Aubert et al. (BABAR), Phys. Rev. Lett. **93**, 041801 (2004), `hep-ex/0402025`

[5] D. Acosta et al. (CDF), Phys. Rev. Lett. **93**, 072001 (2004), `hep-ex/0312021`

[6] V.M. Abazov et al. (D0), Phys. Rev. Lett. **93**, 162002 (2004), `hep-ex/0405004`

[7] R. Aaij et al. (LHCb), Eur. Phys. J. C **72**, 1972 (2012), `1112.5310`

[8] S. Chatrchyan, V. Khachatryan, A.M. Sirunyan, A. Tumasyan, W. Adam, E. Aguilo, T. Bergauer, M. Dragicevic, J. Erö, C. Fabjan et al., Journal of High Energy Physics **2013**, 1 (2013)

[9] E. Braaten, L.P. He, K. Ingles, Phys. Rev. D **100**, 094024 (2019), `1811.08876`

[10] Y.S. Kalashnikova, A.V. Nefediev, Phys. Usp. **62**, 568 (2019), `1811.01324`

[11] E.S. Swanson, Phys. Lett. B **598**, 197 (2004), `hep-ph/0406080`

[12] C. Hanhart, Y.S. Kalashnikova, A.E. Kudryavtsev, A.V. Nefediev, Phys. Rev. D **76**, 034007 (2007), `0704.0605`

[13] F. Aceti, R. Molina, E. Oset, Phys. Rev. D **86**, 113007 (2012), `1207.2832`

[14] J. Ferretti, G. Galatà, E. Santopinto, Phys. Rev. C **88**, 015207 (2013), `1302.6857`

[15] T. Barnes, S. Godfrey, E.S. Swanson, Phys. Rev. D **72**, 054026 (2005), `hep-ph/0505002`

[16] M.R. Pennington, D.J. Wilson, Phys. Rev. D **76**, 077502 (2007), `0704.3384`

[17] I.V. Danilkin, Y.A. Simonov, Phys. Rev. Lett. **105**, 102002 (2010), `1006.0211`

[18] R.L. Workman, Others (Particle Data Group), PTEP **2022**, 083C01 (2022)

[19] V. Bhardwaj et al. (Belle), Phys. Rev. Lett. **111**, 032001 (2013), `1304.3975`

[20] M. Ablikim et al. (BESIII), Phys. Rev. Lett. **115**, 011803 (2015), `1503.08203`

[21] R. Aaij, C. Abellán Beteta, T. Ackernley, B. Adeva, M. Adinolfi, H. Afsharnia, C.A. Aidala, S. Aiola, Z. Ajaltouni, S. Akar et al., Journal of High Energy Physics **2020**, 1 (2020)

[22] M. Ablikim, M. Achasov, P. Adlarson, S. Ahmed, M. Albrecht, R. Aliberti, A. Amoroso, M. An, Q. An, X. Bai et al., Physical Review D **103**, L091102 (2021)

[23] W.J. Deng, H. Liu, L.C. Gui, X.H. Zhong, Phys. Rev. D **95**, 034026 (2017), `1608.00287`

[24] B. Wang, H. Xu, X. Liu, D.Y. Chen, S. Coito, E. Eichten, Front. Phys. (Beijing) **11**, 111402 (2016), `1507.07985`

[25] Y.B. Ding, D.H. Qin, K.T. Chao, Phys. Rev. D **44**, 3562 (1991)

[26] E.J. Eichten, K. Lane, C. Quigg, Phys. Rev. D **69**, 094019 (2004), `hep-ph/0401210`

[27] R. Aaij, C. Abellán Beteta, B. Adeva, M. Adinolfi, C.A. Aidala, Z. Ajaltouni, S. Akar, P. Albicocco, J. Albrecht, F. Alessio et al., Journal of High Energy Physics **2019**, 1 (2019)

[28] S. Piemonte, S. Collins, D. Mohler, M. Padmanath, S. Prelovsek, Phys. Rev. D **100**, 074505 (2019), `1905.03506`

[29] G.L. Yu, Z.G. Wang, Int. J. Mod. Phys. A **34**, 1950151 (2019), `1907.00341`

[30] M. Ablikim et al. (BESIII), Phys. Rev. Lett. **110**, 252001 (2013), 1303.5949

[31] Z.Q. Liu et al. (Belle), Phys. Rev. Lett. **110**, 252002 (2013), [Erratum: Phys.Rev.Lett. 111, 019901 (2013)], 1304.0121

[32] T. Xiao, S. Dobbs, A. Tomaradze, K.K. Seth, Phys. Lett. B **727**, 366 (2013), 1304.3036

[33] J.R. Zhang, Phys. Rev. D **87**, 116004 (2013), 1304.5748

[34] S. Patel, M. Shah, P.C. Vinodkumar, Eur. Phys. J. A **50**, 131 (2014), 1402.3974

[35] D.Y. Chen, X. Liu, T. Matsuki, Phys. Rev. D **88**, 036008 (2013), 1304.5845

[36] K. Abe et al. (Belle), Phys. Rev. Lett. **94**, 182002 (2005), hep-ex/0408126

[37] B. Aubert et al. (BABAR), Phys. Rev. Lett. **101**, 082001 (2008), 0711.2047

[38] S. Uehara et al. (Belle), Phys. Rev. Lett. **104**, 092001 (2010), 0912.4451

[39] X. Liu, Z.G. Luo, Z.F. Sun, Phys. Rev. Lett. **104**, 122001 (2010), 0911.3694

[40] J.P. Lees et al. (BABAR), Phys. Rev. D **86**, 072002 (2012), 1207.2651

[41] F.K. Guo, U.G. Meissner, Phys. Rev. D **86**, 091501 (2012), 1208.1134

[42] S.L. Olsen, Phys. Rev. D **91**, 057501 (2015), 1410.6534

[43] S. Uehara et al. (Belle), Phys. Rev. Lett. **96**, 082003 (2006), hep-ex/0512035

[44] B. Aubert et al. (BABAR), Phys. Rev. D **81**, 092003 (2010), 1002.0281

[45] R. Aaij et al. (LHCb), Phys. Rev. D **102**, 112003 (2020), 2009.00026

[46] H. Wang, Y. Yang, J. Ping, Eur. Phys. J. A **50**, 76 (2014)

[47] S. Prelovsek, S. Collins, D. Mohler, M. Padmanath, S. Piemonte, Journal of High Energy Physics **2021**, 1 (2021)

[48] K. Abe et al. (Belle), Phys. Rev. Lett. **98**, 082001 (2007), hep-ex/0507019

[49] P. Pakhlov et al. (Belle), Phys. Rev. Lett. **100**, 202001 (2008), 0708.3812

[50] D. Marzocca, S. Trifinopoulos, Phys. Rev. Lett. **127**, 061803 (2021), 2104.05730

[51] K.T. Chao, Phys. Lett. B **661**, 348 (2008), 0707.3982

[52] B.Q. Li, K.T. Chao, Phys. Rev. D **79**, 094004 (2009), 0903.5506

[53] H. Wang, Z. Yan, J. Ping, Eur. Phys. J. C **75**, 196 (2015), 1412.7068

[54] Y.c. Yang, Z. Xia, J. Ping, Phys. Rev. D **81**, 094003 (2010), 0912.5061

[55] M. Ablikim et al. (BESIII), Phys. Rev. Lett. **111**, 242001 (2013), 1309.1896

[56] M. Ablikim et al. (BESIII), Phys. Rev. D **100**, 111102 (2019), 1906.00831

[57] S.W. Herb, D.C. Hom, L.M. Lederman, J.C. Sens, H.D. Snyder, J.K. Yoh, J.A. Appel, B.C. Brown, C.N. Brown, W.R. Innes et al., Phys. Rev. Lett. **39**, 252 (1977)

[58] W.R. Innes, J.A. Appel, B.C. Brown, C.N. Brown, K. Ueno, T. Yamanouchi, S.W. Herb, D.C. Hom, L.M. Lederman, J.C. Sens et al., Phys. Rev. Lett. **39**, 1240 (1977)

[59] K. Han, T. Böhringer, P. Franzini, G. Mageras, D. Peterson, E. Rice, J.K. Yoh, J.E. Horstkotte, C. Klopfenstein, J. Lee-Franzini et al., Phys. Rev. Lett. **49**, 1612 (1982)

[60] G. Eigen, G. Blanar, H. Dietl, E. Lorenz, F. Pauss, H. Vogel, T. Böhringer, P. Franzini, K. Han, G. Mageras et al., Phys. Rev. Lett. **49**, 1616 (1982)

[61] C. Klopfenstein, J.E. Horstkotte, J. Lee-Franzini, R.D. Schamberger, M. Sivertz, L.J. Spencer, P.M. Tuts, P. Franzini, K. Han, E. Rice et al., Phys. Rev. Lett. **51**, 160 (1983)

[62] F. Pauss and Others, Physics Letters B **130**, 439 (1983)

[63] D. Besson, J. Green, R. Namjoshi, F. Sannes, P. Skubic, A. Snyder, R. Stone, A. Chen, M. Goldberg, N. Horwitz et al., Phys. Rev. Lett. **54**, 381 (1985)

[64] D.M.J. Lovelock, J.E. Horstkotte, C. Klopfenstein, J. Lee-Franzini, L. Romero, R.D. Schamberger, S. Youssef, P. Franzini, D. Son, P.M. Tuts et al., Phys. Rev. Lett. **54**, 377 (1985)

[65] B. Aubert, M. Bona, Y. Karyotakis, J.P. Lees, V. Poireau, E. Prencipe, X. Prudent, V. Tisserand, J. Garra Tico, E. Grauges et al. (BABAR Collaboration), Phys. Rev. Lett. **101**, 071801 (2008)

[66] P. del Amo Sanchez, J.P. Lees, V. Poireau, E. Prencipe, V. Tisserand, J. Garra Tico, E. Grauges, M. Martinelli, A. Palano, M. Pappagallo et al. (BABAR Collaboration), Phys. Rev. D **82**, 111102 (2010)

[67] J.P. Lees, V. Poireau, E. Prencipe, V. Tisserand, J. Garra Tico, E. Grauges, M. Martinelli, D.A. Milanes, A. Palano, M. Pappagallo et al. (The BABAR Collaboration), Phys. Rev. D **84**, 091101 (2011)

[68] I. Adachi, H. Aihara, K. Arinstein, D.M. Asner, T. Aushev, T. Aziz, A.M. Bakich, E. Barberio, K. Belous, V. Bhardwaj et al. (Belle Collaboration), Phys. Rev. Lett. **108**, 032001 (2012)

[69] G. Aad, B. Abbott, J. Abdallah, A.A. Abdelalim, A. Abdesselam, O. Abdinov, B. Abi, M. Abolins, O.S. AbouZeid, H. Abramowicz et al. (ATLAS Collaboration), Phys. Rev. Lett. **108**, 152001 (2012)

[70] V.M. Abazov, B. Abbott, B.S. Acharya, M. Adams, T. Adams, G.D. Alexeev, G. Alkhazov, A. Alton, G. Alverson, M. Aoki et al. (D0 Collaboration), Phys. Rev. D **86**, 031103 (2012)

[71] R. Aaij, , B. Adeva, M. Adinolfi, A. Affolder, Z. Ajaltouni, S. Akar, J. Albrecht, F. Alessio, M. Alexander et al., Journal of High Energy Physics **2014**, 088 (2014)

[72] A.M. Sirunyan, A. Tumasyan, W. Adam, F. Ambrogi, E. Asilar, T. Bergauer, J. Brandstetter, M. Dragicevic, J. Erö, A. Escalante Del Valle et al. (CMS Collaboration), Phys. Rev. Lett. **120**, 231801 (2018)

[73] R. Mizuk, D.M. Asner, A. Bondar, T.K. Pedlar, I. Adachi, H. Aihara, K. Arinstein, V. Aulchenko, T. Aushev, T. Aziz et al. (Belle Collaboration), Phys. Rev. Lett. **109**, 232002 (2012)

[74] Q. Wu, D.Y. Chen, T. Matsuki, Phys. Rev. D **102**, 114037 (2020)

[75] Z.G. Wang, T. Huang, Nucl. Phys. A **930**, 63 (2014)

[76] D.Y. Chen, X. Liu, T. Matsuki, Chin. Phys. C **38**, 053102 (2014)

[77] R. Mizuk, A. Bondar, I. Adachi, H. Aihara, D. Asner, V. Aulchenko, T. Aushev, R. Ayad, I. Badhrees, S. Bahinipati et al., Journal of High Energy Physics **2019** (2019), Cited by: 33; All Open Access, Gold Open Access, Green Open Access

[78] B. Chen, A. Zhang, J. He, Phys. Rev. D **101**, 014020 (2020)

[79] Z.G. Wang, Chin. Phys. C **43**, 123102 (2019)

[80] W.J. Deng, H. Liu, L.C. Gui, X.H. Zhong, Phys. Rev. D **95**, 074002 (2017)

[81] J.Z. Wang, Z.F. Sun, X. Liu, T. Matsuki, Eur. Phys. J. C **78**, 915 (2018), 1802.04938

[82] B. Pandya, M. Shah, P.C. Vinodkumar, Eur. Phys. J. C **81**, 116 (2021)

[83] R. Chaturvedi, A.K. Rai, N.R. Soni, J.N. Pandya, Journal of Physics G: Nuclear and Particle Physics **47**, 115003 (2020)

[84] I. Adachi, L. Aggarwal, H. Ahmed, H. Aihara, N. Akopov, A. Aloisio, N. Anh Ky, D.M. Asner, T. Aushev, V. Aushev et al. (Belle II Collaboration), Phys. Rev. Lett. **130**, 091902 (2023)

[85] E. Eichten, K. Gottfried, T. Kinoshita, K.D. Lane, T.M. Yan, Phys. Rev. D **21**, 203 (1980)

[86] N.R. Soni, B.R. Joshi, R.P. Shah, H.R. Chauhan, J.N. Pandya, Eur. Phys. J. C **78**, 592 (2018)

[87] V. Kher, R. Chaturvedi, N. Devlani, A.K. Rai, Eur. Phys. J. Plus **137**, 357 (2022)

[88] A. Martin, Physics Letters B **93**, 338 (1980)

[89] S.N. Jena and T. Tripati, Physics Letters B **122**, 181 (1983)

[90] C. Quigg and Jonathan L. Rosner, Physics Letters B **71**, 153 (1977)

[91] John L. Richardson, Physics Letters B **82**, 272 (1979)

[92] X.t. Song, H.f. Lin, Z. Phys. C **34**, 223 (1987)

[93] S. Patel, P.C. Vinodkumar, S. Bhatnagar, Chin. Phys. C **40**, 053102 (2016)

[94] A. Mittal, A.N. Mitra, Phys. Rev. Lett. **57**, 290 (1986)

[95] K.K. Gupta, A.N. Mitra, N.N. Singh, **42**, 1604 (1990)

[96] A. Sharma, S.R. Choudhury, A.N. Mitra, Phys. Rev. D **50**, 454 (1994)

[97] F. Abe, H. Akimoto, A. Akopian, M.G. Albrow, A. Amadon, S.R. Amendolia, D. Amidei, J. Antos, S. Aota, G. Apollinari et al. (CDF Collaboration), Phys. Rev. Lett. **81**, 2432 (1998)

[98] A. Abulencia, D. Acosta, J. Adelman, T. Affolder, T. Akimoto, M.G. Albrow, D. Ambrose, S. Amerio, D. Amidei, A. Anastassov et al. (CDF Collaboration), Phys. Rev. Lett. **96**, 082002 (2006)

[99] T. Aaltonen, J. Adelman, T. Akimoto, M.G. Albrow, B. Álvarez González, S. Amerio, D. Amidei, A. Anastassov, A. Annovi, J. Antos et al. (CDF Collaboration), Phys. Rev. Lett. **100**, 182002 (2008)

[100] V.M. Abazov, B. Abbott, M. Abolins, B.S. Acharya, M. Adams, T. Adams, E. Aguilo, S.H. Ahn, M. Ahsan, G.D. Alexeev et al. (D0 Collaboration), Phys. Rev. Lett. **101**, 012001 (2008)

[101] R. Aaij, C. Abellan Beteta, A. Adametz, B. Adeva, M. Adinolfi, C. Adrover, A. Affolder, Z. Ajaltouni, J. Albrecht, F. Alessio et al. (LHCb Collaboration), Phys. Rev. Lett. **109**, 232001 (2012)

[102] G. Aad, B. Abbott, J. Abdallah, S. Abdel Khalek, O. Abdinov, R. Aben, B. Abi, M. Abolins, O.S. AbouZeid, H. Abramowicz et al. (ATLAS Collaboration), Phys. Rev. Lett. **113**, 212004 (2014)

[103] A.M. Sirunyan, A. Tumasyan, W. Adam, F. Ambrogi, T. Bergauer, J. Brandstetter, M. Dragicevic, J. Erö, A. Escalante Del Valle, M. Flechl et al. (CMS Collaboration), Phys. Rev. Lett. **122**, 132001 (2019)

[104] R. Aaij, C. Abellán Beteta, B. Adeva, M. Adinolfi, C.A. Aidala, Z. Ajaltouni, S. Akar, P. Albicocco, J. Albrecht, F. Alessio et al. (LHCb Collaboration), Phys. Rev. Lett. **122**, 232001 (2019)

[105] N.N. Singh, A.N. Mitra, Phys. Rev. D **38**, 1454 (1988)

[106] S. Chakrabarty, K. Gupta, N. Singh, A. Mitra, Progress in Particle and Nuclear Physics **22**, 43 (1989)

[107] A. Mittal, A.N. Mitra, Phys. Rev. Lett. **57**, 290 (1986)

[108] R. Alkofer, L. von Smekal, Physics Reports **353**, 281 (2001)

[109] R. Alkofer, P. Watson, H. Weigel, Phys. Rev. D **65**, 094026 (2002)

[110] G. Cvetič and C.S. Kim and Guo-Li Wang and Wuk Namgung, Physics Letters B **596**, 84 (2004)

[111] S. Bhatnagar, S.Y. Li, Journal of Physics G: Nuclear and Particle Physics **32**, 949 (2006)

[112] S. Bhatnagar, J. Mahecha, Y. Mengesha, Phys. Rev. D **90**, 014034 (2014)

[113] M.B. Voloshin, Progress in Particle and Nuclear Physics **61**, 455 (2008)

[114] V. Berestetskii, E. Lifshits, L. Pitaevskii, *Quantum Electrodynamics* (Pergamon, 1982)

[115] S.S. Gershtein, V.V. Kiselev, A.K. Likhoded, A.V. Tkabladze, Phys. Rev. D **51**, 3613 (1995)

[116] R. Van Royen, V.F. Weisskopf, Nuovo Cim. A **50**, 617 (1967), [Erratum: Nuovo Cim.A 51, 583 (1967)]

[117] E. Braaten, S. Fleming, Phys. Rev. D **52**, 181 (1995)

[118] A.V. Berezhnoy, V.V. Kiselev, A.K. Likhoded, Z. Phys. A **356**, 89 (1996)

[119] E. Eichten, K. Gottfried, T. Kinoshita, J. Kogut, K.D. Lane, T.M. Yan, Phys. Rev. Lett. **34**, 369 (1975)

[120] E. Eichten, K. Gottfried, T. Kinoshita, K.D. Lane, T.M. Yan, Phys. Rev. D **17**, 3090 (1978)

[121] N. Brambilla, Y. Jia, A. Vairo, Phys. Rev. D **73**, 054005 (2006)

[122] D.M. Li, P.F. Ji, B. Ma, Eur. Phys. J. C **71**, 1582 (2011)

[123] W. Kwong, P.B. Mackenzie, R. Rosenfeld, J.L. Rosner, Phys. Rev. D **37**, 3210 (1988)

[124] L.D. Landau, Dokl. Akad. Nauk SSSR **60**, 207 (1948)

[125] C.N. Yang, Phys. Rev. **77**, 242 (1950)

[126] J.P. Lansberg, T.N. Pham, Phys. Rev. D **79**, 094016 (2009)

[127] R. Barbieri, M. Caffo, R. Gatto, E. Remiddi, Nucl. Phys. B **192**, 61 (1981)

[128] M.L. Mangano, A. Petrelli, Phys. Lett. B **352**, 445 (1995)

[129] S. Godfrey, K. Moats, Phys. Rev. D **92**, 054034 (2015)

[130] M. Shah, A. Parmar, P.C. Vinodkumar, Phys. Rev. D **86**, 034015 (2012)

[131] D. Ebert, R.N. Faustov, V.O. Galkin, Eur. Phys. J. C **71**, 1825 (2011)

[132] S.F. Radford, W.W. Repko, Nucl. Phys. A **865**, 69 (2011)

[133] S. Godfrey, N. Isgur, Phys. Rev. D **32**, 189 (1985)

[134] B.Q. Li, K.T. Chao, Commun. Theor. Phys. **52**, 653 (2009)

[135] A. Krassnigg, M. Gomez-Rocha, T. Hilger, J. Phys. Conf. Ser. **742**, 012032 (2016)

[136] B. Patel, P.C. Vinodkumar, J. Phys. G **36**, 035003 (2009)

[137] G.L. Wang, Phys. Lett. B **633**, 492 (2006)

[138] T. Bhavsar, M. Shah, P.C. Vinodkumar, Eur. Phys. J. C **78**, 227 (2018)

[139] S.F. Radford, W.W. Repko, Phys. Rev. D **75**, 074031 (2007)

[140] D. Ebert, R.N. Faustov, V.O. Galkin, Phys. Rev. D **67**, 014027 (2003)

[141] Bhaghyesh, K.B.V. Kumar, A.P. Monteiro, Journal of Physics G: Nuclear and Particle Physics **38**, 085001 (2011)

[142] J. Segovia, P.G. Ortega, D.R. Entem, F. Fernández, Phys. Rev. D **93**, 074027 (2016)

[143] W. Lucha, F.F. Schoberl, Int. J. Mod. Phys. C **10**, 607 (1999)

Table 5.7: E1 transition widths of bottomonia (in keV).

Decays	Ours	Ref.[86]	PDG[18]	Ref.[80]	Ref. [139]	Ref. [131]	Ref. [134]
$2^3S_1 \to 1^3P_0$	1.38000	2.370	1.220	1.09	1.15	1.65	1.67
$2^3S_1 \to 1^3P_1$	3.87511	5.689	2.210	2.17	1.87	2.57	2.54
$2^3S_1 \to 1^3P_2$	5.84652	8.486	2.290	2.62	1.88	2.53	2.62
$2^3S_0 \to 1^1P_1$	10.3487	10.181	-	3.41	4.17	3.25	6.10
$3^3S_1 \to 2^3P_0$	1.44755	3.330	1.200	1.21	1.67	1.65	1.83
$3^3S_1 \to 2^3P_1$	4.10768	7.936	2.560	2.61	2.74	2.65	2.96
$3^3S_1 \to 2^3P_2$	6.29319	11.447	2.660	3.16	2.80	2.89	3.23
$3^3S_1 \to 1^3P_0$	6.89619	0.594	0.055	0.097	0.03	0.124	0.07
$3^3S_1 \to 1^3P_1$	2.54430	1.518	0.018	0.0005	0.09	0.307	0.17
$3^3S_1 \to 1^3P_2$	3.91653	2.354	0.200	0.14	0.13	0.445	0.15
$3^1S_0 \to 1^1P_1$	6.96943	3.385	-	0.67	0.03	0.770	1.24
$3^3S_0 \to 2^1P_1$	11.39010	13.981	-	4.25	-	3.07	11.0
$1^3P_2 \to 1^3S_1$	37.69970	57.530	34.380	31.8	31.2	29.5	38.2
$1^3P_1 \to 1^3S_1$	34.72050	54.927	32.544	31.9	27.3	37.1	33.6
$1^3P_0 \to 1^3S_1$	32.70690	49.530	-	27.5	22.1	42.7	26.6
$1^1P_1 \to 1^1S_0$	38.71140	72.094	35.770	35.8	37.9	54.4	55.8
$2^3P_2 \to 2^3S_1$	11.05290	28.848	15.100	15.5	16.8	18.8	18.8
$2^3P_1 \to 2^3S_1$	10.07620	26.672	19.400	15.3	13.7	15.9	15.9
$2^3P_0 \to 2^3S_1$	9.43571	23.162	-	14.4	9.90	11.7	11.7
$2^1P_1 \to 2^1S_0$	11.01620	35.578	-	16.2	-	23.6	24.7
$2^3P_2 \to 1^3S_1$	9.41195	29.635	9.800	12.5	7.74	8.41	13.0
$2^3P_1 \to 1^3S_1$	9.20092	28.552	8.900	10.8	7.31	8.01	12.4
$2^3P_0 \to 1^3S_1$	9.05706	28.552	-	10.8	6.69	7.36	11.4
$2^1P_1 \to 1^1S_0$	9.44253	26.769	-	5.4	-	9.9	15.9
$1^3D_1 \to 1^3P_0$	16.24530	34.815	-	16.1	-	24.2	23.6
$1^3D_1 \to 1^3P_1$	11.27790	9.670	-	19.8	-	12.9	12.3
$1^3D_1 \to 1^3P_2$	0.67091	0.394	-	13.3	-	0.67	0.65
$1^3D_2 \to 1^3P_1$	20.36500	11.489	-	1.02	19.3	24.8	23.8
$1^3D_2 \to 1^3P_2$	6.05832	3.583	-	7.23	5.07	6.45	6.29
$1^3D_3 \to 1^3P_2$	24.12070	14.013	-	32.1	21.7	26.7	26.4
$1^1D_2 \to 1^1P_1$	25.03720	14.821	-	30.3	-	30.2	42.3

Table 5.8: M1 transition widths of bottomonia (in eV).

Decays	Ours	Ref.[87]	Ref.[80]	PDG[18]	Ref. [139]	Ref. [140]	Ref. [141]
$1^3S_1 \rightarrow 1^1S_0$	0.01436	37.668	10.00	-	4.00	5.8	15.36
$2^3S_1 \rightarrow 2^1S_0$	0.01601	5.619	0.59	-	0.05	1.4	1.82
$2^3S_1 \rightarrow 1^1S_0$	1.25374	77.173	66.00	12.5 ± 4.9	-	6.4	-
$3^3S_1 \rightarrow 3^1S_0$	0.01629	2.849	3.90	-	-	0.8	-
$3^3S_1 \rightarrow 2^1S_0$	3.12243	36.177	11.00	< 14	-	1.5	-
$3^3S_1 \rightarrow 1^1S_0$	1.72572	76.990	71.00	10 ± 2	-	10.5	-

Table 5.9: Leptonic decay widths of bottomonia (in keV).

$n^{2S+1}L_j$	$\Gamma_{l^+l^-}$	$\Gamma^C_{l^+l^-}$	Ref.[82]	PDG[18]	Ref.[87]	Ref. [138]	Ref. [81](eV)	Ref. [142]
1^3S_1	0.91227	0.59379	0.7700	1.340 ± 0.018	0.582	1.300	1.65	0.71
2^3S_1	0.65325	0.42526	0.5442	0.612 ± 0.011	0.197	0.760	0.821	0.37
3^3S_1	0.57278	0.37288	0.4288	0.443 ± 0.008	0.149	0.450	0.569	0.27
4^3S_1	0.48505	0.34039	0.3549	0.272 ± 0.029	0.129	0.260	0.431	0.21
5^3S_1	0.48505	0.31578	0.3035	0.310 ± 0.07	0.117	0.180	0.348	0.18
1^3D_1	10.96020 (eV)	7.13748 (eV)	0.0050	-	1.65	0.106 (eV)	1.880 (eV)	1.40 (eV)
2^3D_1	12.69930 (eV)	8.26971 (eV)	0.0058	-	2.42	0.078 (eV)	2.810(eV)	2.50(eV)
3^3D_1	18.73760 (eV)	12.2004 (eV)	0.0059	-	3.19	0.051 (eV)	3.000(eV)	-
4^3D_1	24.99260 (eV)	16.2709 (eV)	0.0058	-	3.97	0.042(eV)	3.000(eV)	-
5^3D_1	32.20100 (eV)	20.9611 (eV)	0.0057	-	-	0.028 (eV)	0.003(eV)	-

Table 5.10: Digamma decay widths of S and P-waves bottomonia (in keV) without and with QCD corrections.

$n^{2S+1}L_j$	$\Gamma_{\gamma\gamma}$	$\Gamma^C_{\gamma\gamma}$	Ref.[86]	Ref.[82]	Ref.[129]	Ref. [87]	Ref. [81]	Ref. [134]
1^1S_0	0.30499	0.23719	0.3870	0.3035	0.940	0.2361	1.050	0.527
2^1S_0	0.24568	0.19106	0.2630	0.2122	0.410	0.0896	0.489	0.263
3^1S_0	0.23729	0.18454	0.2290	0.1668	0.290	0.0726	0.323	0.172
4^1S_0	0.23624	0.18372	0.2120	0.1378	0.200	0.0666	0.237	0.105
5^1S_0	0.23739	0.18462	0.2010	0.1176	0.170	0.0636	0.192	0.121
1^3P_0	0.08412	0.08522	0.0196	0.1150	0.150	0.0168	0.199	0.037
1^3P_2	0.07952	0.01467	0.0052	0.0147	0.093	0.0024	0.011	0.007
2^3P_0	0.07959	0.08056	0.0195	0.1014	0.150	0.0172	0.205	0.037
2^3P_2	0.08078	0.01386	0.0052	0.0131	0.012	0.0024	0.013	0.006
3^3P_0	0.08216	0.08063	0.0194	0.0875	0.130	0.0192	0.180	0.037
3^3P_2	0.02252	0.01387	0.0051	0.0114	0.013	0.0027	0.004	0.006
4^3P_0	0.02128	0.08184	0.0192	0.0768	0.130	-	0.157	-
4^3P_2	0.02129	0.01408	0.0051	0.0100	0.015	-	0.014	-
5^3P_0	0.02162	0.08323	0.0191	0.0686	-	-	0.146	-
5^3P_2	0.02198	0.01431	0.0050	0.0090	-	-	0.014	-

Table 5.11: Trigamma decay widths of bottomonia (in unit of 10^{-3} eV) without QCD corrections.

$n^{2S+1}L_j$	$\Gamma_{\gamma\gamma\gamma}$	Ref.[86]	Ref.[81]	Ref.[129]	Ref. [87]	Ref. [142]	Ref.[83]
1^3S_1	30.36900	33.560	19.40	17.0	33.560	19.40	16
2^3S_1	24.46270	12.670	10.90	9.8	12.670	10.90	3
3^3S_1	23.62710	10.261	8.04	7.6	10.261	8.04	1
4^3S_1	23.52240	9.400	6.36	6.0	9.400	6.36	-
5^3S_1	23.63810	8.979	5.43	-	8.979	5.43	-

Table 5.12: Digluon decay widths of bottomonia (in MeV) without and with QCD corrections.

$n^{2S+1}L_j$	Γ_{gg}	Γ_{gg}^C	Ref.[86]	Ref.[82]	Ref.[129]	Ref. [87]	Ref. [81]	Ref. [142]
1^1S_0	4.33520	5.58201	5.448	6.8520	16.600	8.219	17.9	20.180
2^1S_0	3.49207	4.49639	3.710	5.2374	7.200	3.121	8.33	10.640
3^1S_0	3.37280	4.34282	3.229	4.3182	4.900	2.529	5.51	7.940
4^1S_0	3.35785	4.32357	2.985	3.6829	3.400	2.317	4.03	-
5^1S_0	3.37436	4.34483	2.832	3.2196	2.900	2.214	3.26	-
1^3P_0	1.20151	0.10870	0.276	1.4297	2.600	0.721	3.37	2.000
1^3P_2	0.32040	0.31831	0.073	0.2370	0.147	0.192	0.165	0.084
2^3P_0	1.13537	0.08409	0.275	1.2358	2.600	0.741	3.52	2.370
2^3P_2	0.30276	0.30078	0.073	0.2064	0.207	0.198	0.220	0.104
3^3P_0	1.13611	0.07036	0.273	1.0539	2.200	0.828	3.10	2.460
3^3P_2	0.30296	0.30098	0.072	0.1767	0.227	0.221	0.243	0.112
4^3P_0	1.15308	0.06057	0.271	0.9175	2.100	-	-	-
4^3P_2	0.30749	0.30547	0.072	0.1543	0.248	-	-	-
5^3P_0	1.17255	0.05283	0.269	0.8127	-	-	-	-
5^3P_2	0.31268	0.31063	0.071	0.1370	-	-	-	-
1^1D_2	5.93167 (keV)	-	-	-	1.800 (keV)	0.489 (keV)	0.657 (keV)	0.370 (keV)
2^1D_2	7.53656 (keV)	-	-	-	1.530 (keV)	0.764 (keV)	1.22 (keV)	0.670 (keV)
3^1D_2	12.10030 (keV)	-	-	-	1.839 (keV)	1.0006 (keV)	1.59 (keV)	-
4^1D_2	17.45940 (keV)	-	-	-	-	1.380 (keV)	1.86 (keV)	-
5^1D_2	24.21910 (keV)	-	-	-	-	-	2.13 (keV)	-

Chapter 6

Summary and Future Outlook

The theoretical studies of excited spectra of heavy-light mesons become intensive in light of the recent finding of heavier hadrons, such as pentaquarks, tetraquarks, baryons, and mesons. With recent upgrades in accelerators and detectors, heavy mesons and baryons are focused more and have become observable phenomena. The spectroscopy of these heavy hadrons can be studied using experimental data and available phenomenological models. These experimental facilities and theoretical studies are continuously improving our understanding of hadrons and their dynamics.

We presented a thorough investigation of heavy-light and heavy-heavy mesons in the framework of phenomenological approaches. This thesis describes strong decays of excited charm and bottom mesons to the ground state with the emission of light pseudoscalar mesons in the framework of leading order approximation of heavy quark effective theory. Also, in this thesis, mass spectra and decay properties of bottomonia are explored in the framework of the phenomenological potential model.

The framework "Heavy Quark Effective Theory" is an effective QCD theory describing the dynamics of heavy-light hadron systems. The mass of heavy quark $m_Q (Q = c, b)$ is defined as $m_Q \gg \Lambda_{QCD}$, where Λ_{QCD} is a non-perturbative scale of 0.2 GeV. The masses of c, b, t quarks are substantially larger than Λ_{QCD}. So, the physics of hadrons containing one of these quarks is thus substantially simplified by switching to an effective theory built by taking the limit of QCD when the masses of such heavy quarks go to infinity with their four velocities fixed. In this limit, new symmetries of strong interactions emerge, which can be used to predict many aspects of such hadrons. In limit $m_Q \to \infty$, the dynamics of light quark remain invariant of spin and flavor of heavy quark (c or b). This is called heavy quark spin-flavor symmetry. For N heavy quarks, this effective theory exhibits $SU(2N)$ heavy quark spin-flavor symmetries. These symmetries play a crucial role in determining various properties of heavy-light hadrons like masses, strong decay widths, branching fractions, branching ratios, coupling constants, etc. Thus, this theory provides us a unique opportunity to explore the understanding of low energy QCD physics and the associated properties like color confinement and chiral symmetry breaking.

Our next framework is the phenomenological "Potential Model," through which we studied the mass spectra of heavy mesons and their decay properties. For studying hadron spectroscopy, there are various types of phenomenological potential models available, like coulomb potential, Cornell potential, power law, Song and Lin potential, Screened coulomb potential, Yukawa potential, etc. Basically, potential models are based on the concept that potential can describe the interaction of quarks and antiquarks. Although interquark interaction is a non-Abelian and non-linear theory, it is complicated and still lacks understanding. But, with the help of the potential model, we can grasp interquark interaction to some extent. When the quark mass is large, and the quark velocity is $v << c$, the system can be considered non-relativistic, and solving the Schr$\ddot{o}$dinger equation gives the properties of that system. The Schr$\ddot{o}$dinger wave equation with quark-antiquark potentials can be solved numerically with the Runge -Kutta method using the Mathematica notebook. In this thesis, We have comprehensively studied the mass spectra of bottomonium states and their decay properties in the framework of the phenomenological potential model.

Inspired by the experimental growth of the excitation spectrum of heavy-light mesons, we are motivated to analyze radially excited charm and bottom mesons in the framework of heavy quark effective theory. Specifically, we studied experimentally unseen states $3S$, $3P$, $1F$ charm, and bottom mesons and their strange partners. By exploring non-perturbative parameters Δ_F, λ_F, where Δ_F is spin averaged mass splitting between F states ($F = S, T, X, Y, Z, R$) and lowest-lying states (H) and λ_F is mass splitting between spin partners of the same doublet, we analyzed mass spectra of radially excited $n = 3$, D and B mesons. The heavy quark symmetry implies that these non-perturbative parameters are unaffected by flavor, i.e., $\Delta_F^{(c)} = \Delta_F^{(b)}$; $\lambda_F^{(c)} = \lambda_F^{(b)}$. We exploited this symmetry with available information for $n = 2$ and $n = 3$ bottom mesons to predict the masses and decay widths of the corresponding charm mesons. The obtained mass spectrum for $n = 3$ bottom mesons is consistent with the results of other models. On comparing with the relativistic quark model, our masses differ by $25 - 50$ MeV. our predicted masses are close to the theoretical estimations of T.A Lahde et al., which employed a non-relativistic quark model. To check the authenticity of these predicted masses of charm mesons, we used them as input and calculated masses of bottom mesons for $n = 3$ states. These obtained masses for $n = 3$ bottom mesons are in good agreement with the outcomes of other theoretical models. To complete the understanding of bottom spectra, we have also computed masses for $1F$-wave bottom mesons, which are nicely agreed with other theoretical estimations. Using these predicted masses, we analyzed the strong decays of excited charm and bottom meson to the ground state with the emission of light pseudoscalar mesons in terms of coupling constants. The computed strong decay widths in terms of the square of coupling constants are compared with available theoretical decay widths; we obtained the upper bounds of coupling constants for associated states. The determination of coupling constants is crucial in hadron spectroscopy. They provide the strength of transitions between the fields (H, S, T, X, Y, Z). With sufficient experimental data, values of the coupling constant can be established. The running experimental facilities LHCb, BESIII, KEK-B, and the forthcoming project PANDA are projected to fit such strong couplings and will be able to investigate heavy meson interactions in the near future. We have involved isospin-violating factors while studying strong decays of excited charm and bottom mesons. This factor arises when the mass difference between strange parent heavy-light meson and non-strange daughter heavy-light meson is less than the mass of the kaon particle. In such cases, parent D and B mesons with strangeness decay into daughter D and B mesons without strangeness and neutral pion by $\pi^0 - \eta$ mixing. This isospin-violating factor ϵ is estimated for pseudoscalar mesons within QCD, as discussed in Chapter 3. Hence, this factor is multiplied with the decay widths of associated modes. We plot our mass results for radially excited states $3S, 3P, 1F$ on Regge lines in (M^2, J) and (M^2, n_r) planes. From these Regge lines, by fixing slopes and intercepts, we calculated masses of experimentally missing states ($n = 4$). We also used Regge trajectories for identifying experimentally missing state $D_2^*(3000)$. Using these trajectories and branching ratios, we tentatively identified $D_2^*(3000)$ as 1^3F_2 state. The calculation for masses, decay widths for radially excited states, and corresponding analysis are presented in Chapter 3.

Assigning particular J^P value (spin-parity quantum number) to recently observed experimental states and placing them in spectra is crucial. As we know, when we approach high energy levels, the higher energy levels are more closely spaced than lower energy levels. Consequently, several possible assignments, either radially or orbitally, arise for a single state. A specific position of the state in its mass spectra can help in revealing many other important strong interaction parameters such as hadronic coupling constants, branching ratios, spins and mass splittings, decay widths, and many more. Recently two new excited states $B_{sJ}(6063)$ and $B_{sJ}(6114)$ are observed in B^+K^- mass spectrum by LHCb collaborations. We apply HQET formalism to analyze states $B_{sJ}(6063)$ and $B_{sJ}(6114)$ and assigned their J^P's as 2^3S_1 and 1^3D_1 respectively by examine their several properties like masses, decay widths, branching ratios. To assign J^P values, we predicted masses of $2S, 1P, 1D$ strange bottom mesons with flavor-free parameters Δ_F and λ_F, which are in good agreement with other models estimations. Taking $1/m_Q$ correction to the leading order Lagrangian, modify flavor parameters $\Delta_F^{(b)} = \Delta_F^{(c)} + \delta\Delta_F$ and $\lambda_F^{(b)} = \lambda_F^{(c)}\delta\lambda_F$. Using corrections, the gap from experimental masses is narrowed with our results. Our predicted masses for 1^3P_1 and 1^3P_2 are consistent with observed masses of LHCb, CDF, and DO collaborations (only available experimental states). It is noticed that the effect of such corrections is very small for the higher excited states. While analyzing strong decays for $2S$ bottom strange meson, we found $B^{*+}K^-$ is dominating mode over other modes with contribution of 22.53% and 33.46% to total decay widths for $B(2^1S_0)$ and $B(2^3S_1)$ respectively. Similarly, for 1^3P_0, 1^1P_1, 1^3P_1, 1^3P_2 bottom strange states, dominating decay modes are $B_s\pi$, $B_s^*\pi^0$, $B_s^*\pi^0$, $B_s\pi$ respectively. The natural parity D states 1^3D_1 and 1^3D_3 both are dominant in BK decay mode with branching fractions of 56.73% and 36.67%, respectively, while the unnatural parity states 1^1D_2 and 1^3D_2 shows dominance for B^*K decay channel with branching fractions of 77.51% and 67.02% respectively. On the basis of computed masses and decay widths, we have classified state $B_{sJ}(6063)$ as $B_s(2^3S_1)$ and state $B_{sJ}(6114)$ state as $B_s(1^3D_1)$. The details of the calculations and analyses related to these new states are presented in Chapter 4.

In recent decades, experimental growth toward heavy hadrons has continuously increased and enriched spectra. These recent findings in spectra of heavy mesons have ignited a curiosity to investigate $Q\bar{Q}$ spectroscopy. So, the discovery of these heavy hadrons motivates us to test the authenticity of available theoretical models and make predictions about their properties like J^P values with their decay modes, branching ratios, magnetic moments, form factors, polarization amplitudes, and couplings. Theoretical methods explain these data and provide predictions for future experimental investigation. Motivated by several recent observations, we have explored bottomonia spectra and their decay properties like radiative decays, digluon decays, trigluon decays, dileptonic decays, and weak decays in the framework of the phenomenological potential model. The masses of nS, nP, nD, nF $(n = 1, 2, 3, 4, 5)$-waves of bottomonium mesons are computed with a non-relativistic potential given in Eq. (5.1) and solve the Schrödinger wave equation numerically. We also incorporate spin-dependent terms - spin- spin, spin-orbit, and tensor terms to remove mass degeneracy and obtain excited states Our findings for the masses are consistent with experimentally observed masses and theoretical predictions for respective states. Our calculated masses for 1^3S_1 bottomonium state is 9.44816 GeV, which is very close to experimental value 9.460 ± 0.00026 GeV. By using Van Royen - Weisskopf formula, we investigate leptonic decay constants, di-leptonic, di-gamma, tri-gamma, and di-gluon decay widths and also incorporate first-order radiative corrections, which are very useful in revealing the non-perturbative domain of QCD. We also computed radiative transition widths, which give a better insight into the non-perturbative aspects of QCD. The results for mass spectroscopy and decay properties of bottomonia and their analysis are presented in Chapter 5.

We believe and hope that our predictions for heavy-light mesons and heavy mesons in the framework of heavy quark effective theory and potential model will provide significant insight to experimentalists for the upcoming data. But, We still have a long way to go to understand the Quantum Chromodynamics (QCD) properties of heavy mesons fully, which is our ultimate goal. The investigation of heavy mesons within this thesis has established a solid groundwork. Nevertheless, there is potential for future endeavors to expand upon this research, exploring the intricacies of highly excited spectra in the charm and bottom meson sector. This extension can be achieved by developing an effective Lagrangian with higher-order $1/m_Q$ corrections and implementing this Lagrangian to study heavy-light mesons. Furthermore, the scope of this research can be broadened by investigating strong decays that transition to the ground state, encompassing not only interactions with light pseudo-scalar mesons ($J^P = 0^-$) but also including vector mesons ($J^P = 1^-$). Our research work in the phenomenological potential model can be extended to calculate mass spectra and decay properties of beauty-charmed mesons. This potential model scheme will also be used to study exotic hadrons and is helpful in identifying newly observed states. More details can be studied by including higher-order relativistic corrections and couple channel effects, which may give better insight.